PROPERTY IMPROVEMENT OF ANTIBACTERIAL WOUND DRESSING FROM HYDROXYPROPYL METHYLCELLULOSE AND CARBOXYMETHYL STARCH POLYMER BLEND USING CROSSLINKING AGENT AND ANTIBACTERIAL AGENTS

VIPAWAN PITPISUTKUL

A THESIS SUBMITTED IN PARTIAL FULFILLMENT OF THE REQUIREMENT FOR THE DEGREE OF DOCTOR OF PHILOSOPHY IN APPLIED CHEMISTRY

DEPARTMENT OF CHEMISTRY SCHOOL OF SCIENCE
KING MONGKUT'S INSTITUTE OF TECHNOLOGY LADKRABANG

2024
KMITL--2024-SC-D-012-005

Thesis Title	Property improvement of antibacterial wound dressing from hydroxypropyl methylcellulose and carboxymethyl starch polymer blend using crosslinking agent and antibacterial agents
Student Name	Ms. Vipawan Pitpisutkul
Student ID	60605002
Degree	Doctor of Philosophy (Applied Chemistry)
Department	Chemistry
Year	2024
Thesis Advisor	Assoc. Prof. Dr. Jutarat Prachayawarakorn

Abstract

Because of low swelling degree, water absorption, water vapor transmission rate and no antibacterial activity of HPMC-based film for use in wound dressing application, HPMC film was modified in this research. This research was divided into two parts. The first part was the preparation and characterization of modified hydroxypropyl methylcellulose (HPMC) film by carboxymethyl starch (CMS) (i.e., 10, 20, and 30 wt%) using zinc oxide nanoparticles (ZnONPs) (30 and 50wt%) as an antibacterial agent. The second part was the improvement of 70HPMC-30CMS film, which presented the best overall properties, by using succinic acid (SA) as the crosslinker and gallic acid (GA) as an antibacterial agent (1, 3 and 5 wt%). It was found that the infrared absorption peaks of O-H stretching and O-H bending were shifted to lower wavenumbers in HPMC-CMS films and 70HPMC-30CMS-ZnONPs films, suggesting of the formation of hydrogen bond among HPMC, CMS and ZnONPs. After the incorporation of CMS and ZnONPs, lower crystallinity of HPMC-CMS films and 70HPMC-30CMS-ZnONPs films was observed by x-ray diffraction patterns. In addition, SEM images presented the porous structure of HPMC-CMS films after the addition of CMS. The rough surface of 70HPMC-30CMS-ZnONPs films with porous structure were also observed after the addition of ZnONPs. Comparison of HPMC film, mechanical properties of HPMC-CMS films decreased while water absorption, water vapor transmission rate (WVTR), and swelling degree increased. Moreover, mechanical properties, swelling degree, water absorption and WVTR of 70HPMC-30CMS-ZnONPs

films decreased. The improvement of antibacterial activity against both *S. aureus* and *E. coli* was observed with the addition of ZnONPs. In addition, MTT assay showed that 70HPMC-30CMS-ZnONPs films were not toxic to human (HaCat) cells. Nevertheless, high water solubility of 70HPMC-30CMS film resulted in the reduction of dimensional stability and the ease of disintegration. For Part 2, 70HPMC-30CMS film was selected to investigate due to the best overall properties. It was modified by SA (2.5wt%) as the crosslinker and GA (i.e. 1, 3 and 5wt%) as the antimicrobial agent. It was observed that new IR absorption bands at 1725 cm^{-1} attributed to the C=O stretching of the ester group were identified, confirming the crosslinking reaction. The addition of both SA and GA exhibited no impact on the crystallization ability of 70HPMC-30CMS films. The morphology of 70HPMC-30CMS-2.5SA film and 70HPMC-30CMS-2.5SA-GA films also exhibited the porous structure with the reduced pore size. The tensile strength of 70HPMC-30CMS-2.5SA-GA films also increased after the addition of GA due to the enhancement of hydrogen bonds. Furthermore, the addition of SA to 70HPMC-30CMS film increased swelling degree, whereas water solubility, water absorption and WVTR were reduced. Moreover, the incorporation of GA into 70HPMC-30CMS-2.5SA film provided greater swelling degree, gel fraction, water solubility, water absorption, and WVTR. Additionally, the antibacterial activity of 70HPMC-30CMS-2.5SA-GA films against both *S. aureus* and *E. coli* was improved, and the cytotoxicity study demonstrated that 70HPMC-30CMS-2.5SA-1GA film was not toxic to human (HaCat) cells. In this study, 70HPMC-30CMS-2.5SA-1GA film presented excellent overall properties.

Keywords : Antimicrobial activity; CMS; crosslinking; gallic acid; HPMC; ZnO nanoparticles

Acknowledgements

I'd like to express my gratitude to my advisor, Assoc. Prof. Dr. Jutarat Prachayawarakorn, for her guidance, good motivation during the project and proofreading and editing the English in this thesis. I would also like to thank Assoc. Prof. Dr. Supranee Kaewpirom, Assoc. Prof. Dr. Patchanee Charoenying, Assoc. Prof. Dr. Duangkamol Gleeson and Assoc. Prof. Dr. Panpailin Seeharaj for their helpful suggestions on this thesis work. I am grateful for the financial support provide by KMITL Research Fund (KREF 046108). I would like to thank all friends and staff member in the chemistry department for helping me with technical problems. Finally, I would like to express eternal gratitude to my parents for their support and helpful encouragement.

Vipawan Pitpisutkul

Table of Contents

Table of Contents (continued)

Table of Contents (continued)

Table of Contents (continued)

List of Figures

List of Figures (continued)

List of Tables

List of Tables (continued)

Abbreviations/Symbols

HPMC	: Hydroxypropyl methylcellulose
CMS	: Carboxymethyl starch
ZnONPs	: Zinc oxide nanoparticles
SA	: Succinic acid
GA	: Gallic acid
HCl	: Hydrochloric acid
NaOH	: Sodium hydroxide
WI	: Whiteness index
FT-IR	: Fourier-transform infrared spectroscopy
XRD	: X-ray diffraction
SEM	: Scanning electron microscopy
WVTR	: Water vapor transmission rate
ATR	: Attenuated Total Reflectance

Chapter 1

Introduction

1.1 Research motivation

Wound care is a critical aspect of healthcare, and the development of effective wound dressings is essential for promoting optimal healing and preventing infections. Traditional wound dressings often face challenges such as inadequate antimicrobial properties, slow healing rates, and environmental concerns associated with their production and disposal. In response to these challenges, researchers have turned to natural products as a sustainable and effective source for developing antimicrobial wound dressing films [1]. Cellulosic, also known as cellulose derivatives, have found wide applications over the past few decades in a variety of industries, including the food, cosmetics, biomedical, and pharmaceutical industries as well as the biofuels and petrochemical industries. Because of their many beneficial properties, including biocompatibility, biodegradability, non-toxicity, sustainability, availability, and a reasonable price, cellulose derivatives stand out as the top candidate for the development of wound dressings [2].

The hydrophilic polymer hydroxypropyl methylcellulose (HPMC), a nonionic cellulose ether derivative, is semi-synthetic polymer with high stability at a lower pH. It also has no flavor or odor. This biopolymer has been approved as a food additive, E464, by the American Institute, Food and Drug Administration (FDA), the European Institution, European Parliament, and Council Directive [3]. HPMC is one of the most widely utilized cellulose derivatives in many industries (food, construction, cosmetics, biomedical, and pharmaceutical industries) and has good water solubility with outstanding qualities, including biocompatibility, biodegradability, superior stability, extensive availability, excellent swelling, and mechanical properties. Additionally, HPMC has a remarkable capacity to form films and low toxicity [3].

Also, HPMC have been combined with a variety of biopolymers (collagen, chitosan (CS), xanthan gum and gelatin) and bioactive substances (plant extracts, organic or inorganic compounds, and chemical medicines) to create novel potential wound dressings that have the potential to accelerate the healing of wounds and against

bacteria [4]. It was mentioned that the incorporation of xyloglucan and gentamicin sulfate into HPMC films could improve physicochemical properties, antibacterial effect, and drug release [5]. Moreover, tensile strength, swelling capacity and elongation were increased by adding sodium alginate into HPMC hydrogel [6].

Although HPMC film had some benefits, it also had drawbacks, such as low moisture transfer and swelling degree. Hence, the natural hydrophilic polymer including alginate, CS, starch and agarose can be used to improve the limitation of HPMC film. Recently, the addition of modified starch to synthetic polymers or biopolymers has been studied. For example, LLDPE/modified starch blended films showed an increase in WVP when acetylated starch and oxidized starch were added, compared with LLDPE/native starch blended films. It was observed that due to higher polarity of functional groups of modified starch than native starch [7].

Modified starch is the starch that has been physically and chemically modified to form a new structure or functional group. Numerous studies have demonstrated the potential of modified starch for biomedical uses, including drug delivery systems, tissue engineering scaffolds, substrates for cell seeding, and implants for replacing missing bones [8]. Additionally, the modified starch can be used in the preparation of wound dressing, including cadexamer iodine, oxidized starch, hydroxyethyl starch and carboxymethyl starch (CMS). The introduction of CMS can be converted into a hydrogel via chelation with polyvalent cations [9]. Furthermore, hydrogels based on bioactive CMS decorated with CuO nanoparticles were observed to accelerate wound healing and have antioxidative and antimicrobial properties [10].

An anionic polysaccharide called CMS is one of the hydrophilic polymers made from starch which has a water solubility that is frequently used as an additive. It is non-toxic and biodegradable and is becoming more common in many applications [10-12]. Moreover, it has also been suggested that CMS can combine with other polymers. With an increase in CMS content, hydrophilic films based on starch/CMS demonstrated high swelling degree and moisture uptake [13]. Additionally, swelling in the polyvinyl alcohol/CMS composite gel improved as CMS content increased [12]. As a result of the high water solubility of HPMC and CMS, the dimension stability of the blended film

declines over time. The integrity of the biopolymeric film can be improved by incorporating crosslinking agents with different crosslinking types. According to the type of bond that formed, they can be divided into three categories: ionic bond formation, physically crosslinked by hydrogen and Van der Waals interactions, and well-stabilized covalent crosslinking [14]. The chemical crosslinking method has an appropriate process to provide a biopolymer composed of many reacted functional groups, such as the hydroxyl group.

Most crosslinkers have been used with biodegradable polymers such as boric acid, epichlorohydrin, and glutaraldehyde but these crosslinkers are costly and harmful to people [15]. Hence, natural cross-linking agents like tartaric acid (TA), malic acid (MA), citric acid (CA) and succinic acid (SA) are recommended. These organic acids occur naturally and are produced by microbes during fermentation of vegetables and fruits. They can modify polysaccharides and can be manufactured in huge numbers using biotechnological methods [15].

SA is naturally created by honey fermentation and used in the food, pharmaceutical, and agricultural industries, has a good impact on human metabolism without being at risk of accumulating in the body [16]. SA can serve as both solubilizing and crosslinking agents since they have two carboxyl groups. CS-based hydrogels crosslinked by SA showed the improvement of mechanical properties and the decrease of contact angle [17]. Basil seed mucilage (BSM) films were developed by adding several organic acids (SA, MA, and TA), and their physicochemical properties were enhanced by crosslinking with those acids [18]. However, bio-based wound dressing materials are unable to protect the wound from microorganisms; therefore, antimicrobial treatments must be utilized. The increased use of nanoparticles in nearly all sectors over the past decade has cleared the path for their application as wound dressing materials [19]. Moreover, it is known that certain nanofillers, such as organically modified nanoclays and nano-sized metals or metal oxides, possess potent antibacterial activity against a wide range of gram-positive and gram-negative bacterial and fungal diseases [20]. As a result, various nanostructured particle types have been utilized to create antimicrobial wound dressing materials [21, 22].

Excellent antibacterial ability, low cost, and no cellular toxicity are all characteristics of ZnONPs. It has been used in a variety of everyday products, including medical equipment, cosmetics, and medicine delivery [23]. Additionally, ZnONPs containing hydrogels used as wound dressings on a xanthan matrix provided a strong defense against microbial invasion from the outside [24]. It was shown that the addition of ZnONPs to HPMC bio-nanocomposite films improved the film's mechanical, barrier, antibacterial, and UV-blocking properties [25]. Adding ZnONPs to the PVA/CS hydrogel improved the WVP and swelling and increased the number of pores in the hydrogel's structure. Tests for toxicity and microbiology demonstrated that bio-nanocomposites are non-toxic and antibacterial for wound healing application [26]. However, the wound dressing film incorporating high loading of metal oxide nanoparticles has limitations, such as difficult monitoring of the wound and ineffectiveness in maintaining a moist wound environment. Polyphenols are a type of natural antimicrobial that can stop both Gram-positive and Gram-negative germs from growing [27]. Gallic acid (GA) is used in wound dressing films due to its potent antibacterial properties and potential for wound healing [28]. It was mentioned that carboxylated polyvinyl alcohol (PVA-COOH) composite hydrogel films incorporated GA as antibacterial agent increased swelling ratios, mechanical properties and dimension stability. This film showed biocompatibility with L929 cells and antibacterial efficacy against *E. coli* and *S. aureus* [29]. Moreover, the increase in GA contents on gelatin/CS film improved tensile strength and Young's modulus, while the WVP, swelling degree, and transparency were reduced [30]. The incorporation of GA into active packaging film composed of poly lactide-poly (Butylene Adipate-Co-Terephthalate) composite film demonstrated antibacterial efficacy against *E. coli* and *L. monocytogenes*. Furthermore, an increase in tensile strength was observed as the GA content reached 10% by weight [31].

This study aimed to improve properties of HPMC film for wound dressing application. This research was divided into two parts. The first part was the preparation and characterization of HPMC film by CMS using ZnONPs as an antibacterial agent. The second part was the improvement of 70HPMC-30CMS film, which presented the best overall properties, by using SA as the crosslinker and GA as an antibacterial agent. The

modified HPMC films were characterized by functional group analysis, x-ray diffraction, and morphology. Moreover, mechanical properties, gel fraction, water solubility, moisture uptake, WVTR, swelling degree, whiteness, antibacterial activity, and cytotoxicity were also examined.

1.2 Objectives of the study

1) To prepare a bio-based antibacterial wound dressing films from HPMC and CMS by casting technique.

2) To improve physical properties of HPMC and CMS by crosslinking with SA.

3) To study the effect of antibacterial agents (ZnONPs and GA) on properties of various HPMC-CMS films.

1.3 Scope of the study

1) Study the effect of CMS contents (at 0, 10, 20 and 30wt%) on physicochemical properties of HPMC-based films.

2) Study the effect of SA (at 2.5wt%) as crosslinker on physicochemical properties of HPMC-CMS film.

3) Study the effect of various antibacterial agents (ZnONPs and GA) on the functional groups, morphology, crystallinity, degree of swelling, gel fraction, moisture uptake, water vapor transmission rate, whiteness index, antibacterial activity, cytotoxicity and mechanical properties of HPMC-CMS film.

1.4 Benefits of the study

1) The antibacterial wound dressing film could be prepared based on HPMC with favorable chemical and mechanical properties.

2) The antibacterial wound dressing film incorporated ZnONPs and GA may be used as alternative wound dressings.

3) Locally grown cassava has become more valuable.

Chapter 2

Theory and literature reviews

2.1 Wound dressing

Dressings are used to regenerate and reconstruct dermal and epidermal tissues during the healing phase of wounds. Materials used for wound dressings serve as physical barriers that are permeable to moisture and oxygen and shield the wound mostly from bacteria [19]. Traditionally, materials for treating wounds include beeswax pastes, plant fibers, and animal fats. However, they cannot keep and fabricate a moist environment around the wound, reducing the wound-healing process. Antibiotics and antiseptic techniques received significant advancements, and modern wound dressing was created later in the 20th century [32]. Several researchers have found equipment to assist the skin by protecting the wound and accelerating the healing process through wound dressings.

2.1.1 Classification of Wound Dressings

Due to technological advancement in previous years, several wound dressings have been developed internationally to treat all kinds of tissue wounds. Several classifications for wound dressings have been described as physical form (ointment, film, foam, gels), function on a wound (debridement, antibacterial, occlusive, absorbent, adherent), and material used (hydrocolloid, alginate, collagen) [8].

New biopolymeric materials must be developed to achieve certain features to make the perfect wound dressing, which are discussed in Figure 2.1, in order to create dressings that allow for rapid healing with few scars on the body's surface.

2.1.2 Various types of dressing material

Modern or advanced dressings were designed to cover tissue lesions and in this category are included the hydrogels, hydrocolloids, semi-permeable films and alginate dressing [33]. The biggest difference between traditional and modern dressings is local moisture maintenance. Thus, traditional dressings have a lower capacity to maintain the local moisture on the wound site and modern dressing sustain excellent local moisture

to enhance wound healing. The classification of polymeric wound dressing and their specific characteristic are shown in Table 2.1.

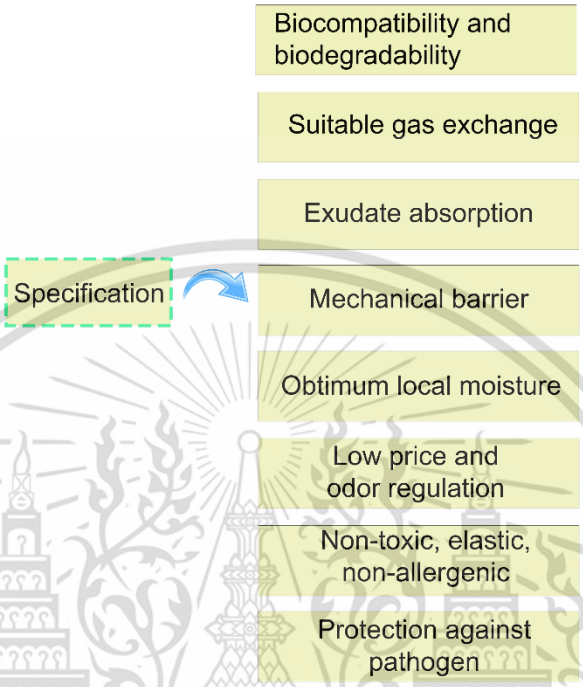

Figure 2.1 Specification of wound dressing [33]

Table 2.1 The unique characteristics of each variety of modern wound dressing [33].

Type of modern wound dressing	Characteristics
Hydrogel	The chemical structure in 3D networks consisting of crosslinked polymeric materials enhances the high capacity to absorb without dissolution in liquid.
Hydrocolloid	They exhibit the capacity to absorb a minimal to moderate content of exudates and exhibit strong biocompatibility, biodegradability, and skin adherence.
Semi-permeable film	The transfer of oxygen and water vapor is permitted via films, which are impervious to pathogens and water. The film is unable to absorb wound fluids fully.
Semi-permeable	Due to their hydrophilic nature, they have a large capacity to absorb a large number of wound fluids. Hence they are indicated for tissue

foam	lesions with a moderate to a high level of wound fluids. Foams have a dehydrating effect, which restricts their usage to dry wounds, and their absolute opacity makes it impossible to monitor the healing process.

2.1.3 Evaluation of the characteristics of wound dressings.

There are various methods for evaluating the qualities of wound dressings. The majority of these tests assess the absorbency of wound dressings. These tests consist of the moisture vapor transmission rate (MVTR), fluid handling capacity, fluid affinity, and water absorption. According to Bolton *et al*. a wound dressing is termed occlusive (moisture retentive) when its moisture retention rate is 840 g/m^2/24 h. Permeable dressings, such as gauzes, have an MVTR of approximately 1,600 g/m^2/24 h, whereas occlusive dressings, such as hydrocolloids, have an MVTR of less than 300 g/m^2/24 h [34].

2.2 Cellulose

Cellulose is the most common carbohydrate on the planet and the primary structural component of plants and trees. It is composed of repeated D-anhydroglucose units connected by -1-4 glycosidic linkages. Figure 2.2 depicts the structure of cellulose [35]. Each anhydroglucose unit possesses a hydroxyl group at positions 2, 3, and 5 on the ring. In addition, cellulose is defined by its reducing and non-reducing ends, which contain one and two hydroxyl groups.

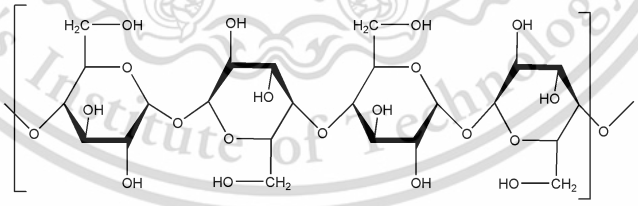

Figure 2.2 Molecular structure of cellulose [35]

It has recently been demonstrated to have diverse applications in the paper, textile, and pharmaceutical industries. As an excipient, cellulose meets the criteria of the Food and Drug Administration (FDA) for pharmaceutical or chemical excipients, including greater stability, being an eco-friendly resource, being easily renewable, and being non-toxic for the manufacture of traditional dosage forms [36].

Cellulose is a one-of-a-kind polymeric material that possesses a number of characteristics, including a fine cross-section, the capacity to absorb moisture, high strength and durability, high thermal stability, strong biocompatibility, low cost, low density, and outstanding mechanical qualities [36]. Nonetheless, cellulose has intrinsic disadvantages. These include poor solubility in common solvents, poor crease resistance, poor dimensional stability, lack of thermoplasticity, excessive hydrophilicity (undesirable for a number of composite applications), and absence of antibacterial characteristics. In order to overcome these disadvantages, controlled physical and/or chemical modification of the cellulose structure is required [37].

2.2.1 Cellulose derivative

Chemically treating or "functionalizing" cellulose has led to the creation of many cellulose derivatives with the goal of increasing its value or making it more useful. Generally, etherification and esterification are included in the chemical derivatization of cellulose based on the hydroxyl group. The derivatives may have different essential properties, such as chemical structure, ability to absorb water, interaction with water, surface activity, and ability to dissolve.

2.2.1.1 Cellulose ether

Cellulose ethers are high-molecular-weight compounds generated by substituting alkyl or substituted alkyl groups for the hydrogen atoms of hydroxyl groups in the anhydroglucose units of cellulose. Commercially significant features of cellulose ethers are governed by their molecular weights, chemical structure, distribution of substituent groups, degree of substitution, and molar substitution (where applicable). In general, these properties include solubility, solution viscosity, surface activity, thermoplastic film characteristics, and resistance to biodegradation, heat, hydrolysis, and oxidation. The viscosity of solutions of cellulose ether is directly proportional to their molecular weights [38]. Some common cellulose ethers include methyl cellulose, ethyl cellulose, hydroxyethyl cellulose, hydroxypropyl cellulose, hydroxypropyl methyl cellulose, carboxymethyl cellulose (CMC), and sodium carboxymethyl cellulose (NaCMC).

2.2.1.2 Cellulose ester

Cellulose esters are typically insoluble in water and have excellent film-forming properties. Pharmaceutical controlled release preparations, such as osmotic and enteric coated drug delivery systems, make extensive use of cellulose esters. These polymers are frequently combined with cellulose ethers to create microporous delivery membranes. Cellulose esters classified as organic or inorganic. Organic cellulose esters are more essential in pharmaceutical applications [38].

In commercial products and medicinal research, organic cellulose esters such as cellulose acetate, cellulose acetate phthalate, cellulose acetate butyrate, cellulose acetate trimellitate, and hydroxypropyl methylcellulose phthalate have been utilized.

2.2.2 Hydroxypropyl methylcellulose (HPMC)

In the pharmaceutical industry, cellulose derivatives play a crucial role as pharmaceutical excipients that are widely used in the production of current medications, the creation of novel dosage forms, and trimming pharmaceutical manufacturing techniques. One of the most widely utilized hydrophilic cellulose derivatives is HPMC, often known as Hypromellose or Methocel™.

The chemical structure of HPMC as well as its physical-chemical qualities

HPMC is a nonionic cellulose ether which their structure is displayed in Figure 2.3. Chemically, HPMC is a semi-synthetically manufactured partly O-methylated and O-(2-hydroxypropylated) cellulose derivative and is made by treatment of natural cellulose with sodium hydroxide. The hydroxyl groups found in natural cellulose can be specifically alkylated by adding methyl and hydroxypropyl groups to increase the water solubility of HPMC.

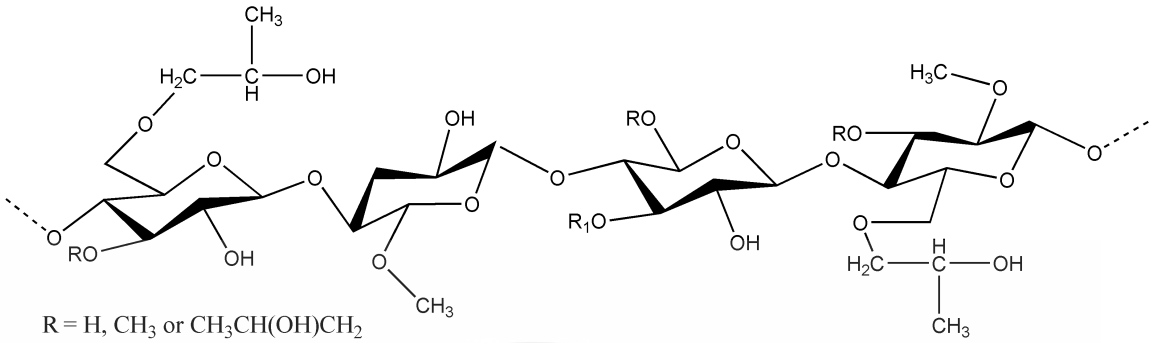

Figure 2.3 chemical structure of HPMC [39].

Various types of HPMC are distinguished according to the 4-digit code given behind the non-commercial name. Various types of HPMC are distinguished according to the 4-digit code given behind the non-commercial name, such as HPMC 2208, HPMC 2906, HPMC 2910. The first two digits represent the average percentage of methoxy-groups (-OCH_3), and the last two digits represent the average percentage of hydroxypropyl-groups (-$OCH_2CH(OH)CH_3$), determined on a dry weight basis [39]. Different molecular weights and substitution ratios of methoxyl and hydroxypropyl have different effects on qualities such as thermal gelation temperature, organic solubility, swelling, powder flow, compactness, diffusion, and drug release [40].

2.2.1.2 Thermal properties

Aqueous HPMC solutions display inverted thermally-induced reversible behavior (sol-gel transitions at relatively high temperatures), frequently accompanied by solution cloudiness. This phenomenon is due to hydrophobic interactions between methoxyl groups of HPMC during subsequent dehydration of the polymer at high temperature [41].

At low temperatures, the polymer completely hydrates. The temperature at which a colloidal solution solidifies into a gel (solidification temperature or gelation point) depends on the number of methoxy-groups present in the HPMC molecule and the ionic strength of the solution. The gelation temperature is around 50 to 90 °C, depending on the polymer type and concentration. [42]. The visible precipitation of polymer molecules can accompany the reversible gelation that occurs upon increasing the temperature. The cloud point and gelation point of the HPMC polymer are not

necessarily identical. Electrolytes can decrease the cloud point and gelation point of HPMC solutions [43].

2.2.3 cellulose derivatives for use in the manufacture of wound dressings

Using derivatives of cellulose as wound dressings over the past few decades, the usage of cellulosic materials has increased significantly in a range of industries, including petrochemicals, biofuels, food, cosmetics, biomedicine, and the pharmaceutical industry. The creation of wound dressings should start with cellulose derivatives since these semi-synthetic biopolymers have a number of favorable properties, including biocompatibility, biodegradability, non-toxicity, sustainability, abundance, and a reasonable price [44].

2.3 Modified starch

The preparation of modified starch, also known as starch derivatives, involves physically, enzymatically, or chemically altering the properties of original starch [45]. Practically all starch applications utilize modified starches, such as in food goods as a thickener, stabilizer, or emulsifier; in pharmaceuticals as a disintegrant; and as a binder in coated paper. Modifications are made to starches to improve their performance in various applications. Starches may be modified to improve their resistance to extreme heat, acid, shear, time, cooling, or freezing; to alter their texture; to decrease or increase their viscosity; to lengthen or shorten their gelatinization time; or to improve their viscosity.

2.3.1 The categorization of modified starch

2.3.1.1 Physical modification

Starch possesses the physical qualities of solubility, gelatinization, retrogradation, and glass transition. As a result of chemical processes, which usually include the breaking and production of new bonds, the chemical characteristics of starch fluctuate. Starch undergoes chemical processes such as hydrolysis, oxidation, esterification, and etherification. The molecular weight and branching properties of starch, which play key roles in the shape and size of granules, may be used to predict its functionality, including texture, pasting, and retrogradation. Amylose has a stronger correlation with

pasting and gel-like textural properties, but amylopectin, which is found in common and waxy maize starches, has a stronger association with rigidity [46].

1. Pre-gelatinized starch

Pregelatinized type is particularly useful in instant gravies, instant pudding and in dry cake mixes for freshness retention. The inherent lumping tendency of these materials is usually reduced by shipping them in form of coarse powder from which fines have been removed. Another method involves incorporation of small amounts of additives such as orthophosphate salts or polyphosphate salts is claimed to be helpful, probably by sequestering with heavy metal ions. Pregelatinized starch is used in many industrial applications wherever cooking facilities are not available or rapid hydration is desired. The properties of the cold water swelling product depend greatly on the pregelatinizing process and equipment used.

2. Heat-treatment starch

Heat-treatment procedure involving heat–humidity, both of which result in a physical alteration of starch without gelatinization, granular integrity disruption, or birefringence destruction.

3. Annealing

Annealing modification is the heating of starch granules in water below the gelatinized temperature and above the glass transition temperature. Annealing induces changes in the structure of starch granules, an increase in granular stability, interactions between the amorphous and crystalline phases of the starch granule, the creation of crystals, the packing of double helices, and a decrease in swelling behavior.

4. Enzymatically modified starch

Enzymatic modification is the one of method type, which is used to hydrolysis of some part of starch into a low molecular weight of starch using enzymes. Enzymatically modified starch is extensively utilized for food and pharmaceutical industries.

2.3.1.2 Chemical modification

The chemical properties of starch are determined by the polyhydroxyl functional groups present in its constituent glucose monomers. The hydroxyl groups at C-2, C-3, and C-6, which lack glycosidic bond connections and pyranose ring formation, are typically accessible for substitution reactions involving the connected hydrogen or the whole hydroxyl group. The OH at carbon six is a primary alcoholic hydroxyl group, whereas those at carbons two and three are secondary. Therefore, starch can be esterified and etherified through hydrolytic breaking of its chains at glycosidic bonds, oxidative interactions with the OH or CC bond to form carbonyl groups, and other reactions with various functional and multifunctional compounds. Most reactions in acidic or basic environments need activation of the hydroxyl group of glucose molecules. The following are some of the chemical reactions and characteristics of starch [46]:

1. Hydroxypropylated starch

Under extremely alkaline conditions, modified starch is created by reacting propylene oxide with a high pH to introduce a hydroxypropyl group on the starch. Due to its capacity to function as a surfactant and emulsifier, hydroxypropyl starch is frequently utilized in cosmetics and beauty goods.

2. Acetylated starch

Under alkaline conditions, they are produced by reacting aqueous suspensions of starch granules with acetic anhydride or vinyl acetate. After the reaction is complete, the starch slurry is neutralized, rinsed, and dehydrated to eliminate the majority of by-products. In water, acetic anhydride is exceedingly unstable. When acetic anhydride reacts with starch, it is hydrolyzed into acetic acid and water. The vinyl acetate hydrolyzed easily as well. The achieved features of acetylated starch include lower gelatinization temperatures, decreased retrogradation and tendency to form gels, and enhanced paste clarity.

3. Acid-modifed starch

These are produced by hydrolyzing aqueous suspensions of starch granules with hydrochloric and/or sulfuric acids at temperatures much below the gelatinization temperature. Due to the fact that these treatments are often applied to aqueous solutions, the level of conversion is restricted so as not to degrade the starch to the point where it begins to swell due to solubilization. The fundamental reaction is the hydrolysis of -D-(1,4) or -D-(1,6) bonds. Thus, acid-modified starch is chemically identical to unmodified starch, with the exception of a decreased molecular weight.

4. Crosslinked starch

Cross-linking is accomplished with cross-linking agents such as sodium trimetaphosphate, sodium tripolyphosphate, epichlorohydrin (EPI), and phosphoryl chloride, etc [47]. EPI is a popular cross-linking modification of a starch reagent. By applying chemical reagents that generate ether or ester links between hydroxyl groups in the starch molecule [48], cross-linking is hypothesized to increase intra- and inter-molecular bonds at multiple sites in the starch molecule, resulting in granule stability [49].

5. Oxidized starch

Starch oxidation is a chemical transformation in which the hydroxyl groups of starch molecules are first oxidized to carbonyl groups and subsequently, as the primary end result, to carboxyl groups [50]. The amount of starch oxidation is indicated by the number of carbonyl and carboxyl groups on the oxidized starch. Oxidized starches have low viscosity, excellent heat stability, low retrogradation, paste transparency, film forming, and adhesion capabilities [51]. Among several oxidizing reagents, sodium hypochlorite is the most often employed modifying agent.

6. Carboxymethyl starch

Under alkaline conditions, carboxymethyl starch is generated by modifying starch with monochloroacetic acid. Carboxylation of starch enhances water solubility as the degree of substitution (DS) increases; at higher substitutions, they are soluble in cold

water and the solution is colored. In many applications, carboxymethyl starch becomes a waste product in textile sizing and desizing operations. Carboxymethyl starch is also compatible with numerous hydrophilic sizing agents, such as polyvinyl alcohol used in paper sizing, to which oil resistance and water insolubility (multivalent-ion salt form) contribute significantly.

2.3.1.3 Modified starch in wound dressing application

Most commercially available starches have received some kind of physical or chemical modification to fulfill the challenges of food and other industries. Examples of modification processes in the food industry include gelatinization, monoester, cross-linked phosphorylation, hydroxypropylation, and so on. Cadexomer iodine [52], oxidized starch [53], hydroxyethyl starch [54] and carboxymethyl starch [22] are among the modified starches utilized in wound dressing preparation [55].

2.3.2 Carboxymethyl starch (CMS)

CMS is typically produced by reacting starch with monochloroacetic acid or its sodium salt after activating the polymer with aqueous NaOH in an aqueous organic solvent, frequently ethanol. The foundation of this procedure is Williamson's ether synthesis as shown in Figure 2.4. Generally, the reaction is carried out in the absence of strong bases to increase the nucleophilicity of the hydroxyl group and aid in the swelling of the starch particles. However, a side reaction could also occur with sodium hydroxide, resulting in sodium glycolate instead of starch glycolate [56].

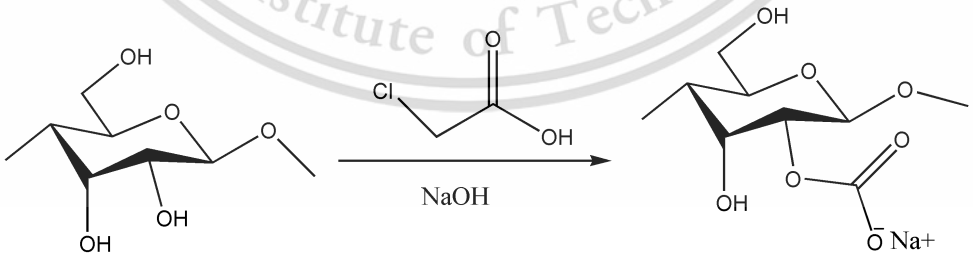

Figure 2.4 Williamson's ether synthesis of starch [56]

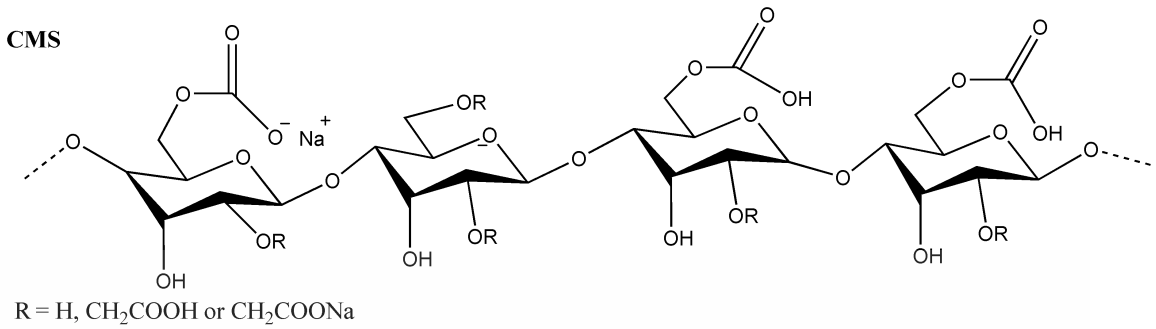

Figure 2.5 Chemical structure of CMS [56]

The degree of substitution, or DS, provides an indication of the quantity of carboxymethyl group that has been generated on the starch molecule. DS is defined technically as the average number of substituents per anhydroglucose unit (AGU). The DS can be determined by means of titrimetry. The CMS's functional qualities depend on the DS. Such qualities include the solution's viscosity, film-forming properties, interaction with cations, supramolecular aggregation formation, and rheological properties. According to the literature, industrially applied carboxymethylation of starch in ethanol results in C-2, C-6, and C-3 replacement [56].

2.4 Plasticizer

Plasticizers improve polymer flexibility and processability. Plasticizers reduce intermolecular secondary bond pressures, making plastic more flexible. Plasticizer functions as an internal lubricant to allow polymers to pass. In free volume theories, a plasticizer increases a polymer's free volume, which is the same at glass transition temperature (Tg). Plasticizers widen the lower temperature range for using materials because they inhibit polymer chain associative behavior and stimulate segmental flexibility, increasing rotational freedom and decreasing Tg. Internal and external plasticizers are classified. External plasticization involves adding plasticizers to polymers. By copolymerizing the parent monomer with flexible copolymers, internal plasticization can be produced.

2.4.1 Glycerol

The empirical chemical formula for glycerol is $C_3H_5(OH)_3$, which indicates that it is a trihydric alcohol. Propanol-1,2,3-triol is the name given to it by IUPAC (Figure 2.6). It has no obvious color or flavor, a mildly sweet taste, and an extremely thick and

absorbent consistency. Because of its polar structure, which includes three separate hydroxyl groups, it dissolves very quickly in water. Glycerol is produced as a consequence of a process that separates fatty acid molecules that are linked to other molecules. This is the primary constituent of fats and oils, and it is found in a variety of organisms, including plants and animals. In the metabolism of both carbohydrates and lipids, glycerol functions as an intermediary. Plasticizers, emulsifiers, sweeteners, and medicinal agents are some of the uses for this substance [38].

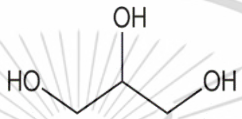

Figure 2.6 Chemical structure of glycerol [57]

2.5 Crosslinking strategies

Crosslinking is the technique of interconnecting polymer chains through covalent or noncovalent bonding to build three-dimensional networks. These processes are recommended to generate bonds between intermolecular and intramolecular polymer chains in order to reinforce the structure of the material. Cross-linking is caused by the reaction of efficient bond-forming multifunctional reagents as a crosslinkers [14]. Three crosslinking strategies are shown in Figure 2.7.

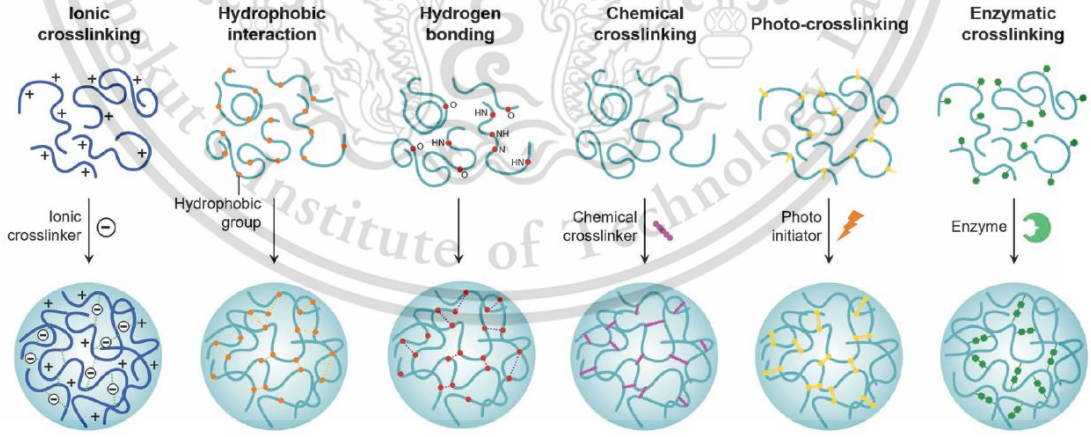

Figure 2.7 Crosslinking method for generating biopolymer [14]

Forming films from biopolymers through cross-linking.

Films are probably the simplest biomaterial structure to produce; hence, most natural and synthetic polymers have been fabricated into films for tissue engineering,

controlled release, and other medical uses [58]. Films composed mostly of biopolymers, such as collagen, one of the most extensively used proteins in medical applications, have very poor mechanical properties, are fragile, and decompose rapidly in water or aqueous solutions. Therefore, the key necessity of crosslinking is the capacity to enhance mechanical characteristics and, as a result, resistance to degradation [14].

Table 2.2 Evaluation of the developed crosslinkers, crosslinking techniques, and biomaterials for biomedical applications – cytotoxicity, mechanical characteristics, and water stability [14]

	Proteins						Carbohydrates				
	Gelatin	BSA	Collagen	Zein	Soy protein	Keratin	Cellulose	Starch	HA	Alginate	Chitosan
Glutaraldehyde	✓	✓	✓	✓	✓	✓	✓	✓	✓	✓	✓
EDC/NHS	✓	✓	✓	–	✓	✓	–	–	✓	✓	✓
Epichlorohydrin	✓	✓	✓	–	–	–	✓	–	✓	–	✓
STMP	–	–	–	–	–	–	✓	✓	–	–	✓
Citric acid	✓	–	✓	✓	–	–	✓	–	–	–	–
Dextran dialdehyde	–	–	✓	–	–	–	✓	✓	✓	–	✓
Genipin	✓	–	✓	–	✓	–	–	–	–	✓	✓
PA	–	–	✓	–	–	–	–	–	–	–	✓
Glyoxal	✓	✓	✓	–	✓	–	–	✓	✓	✓	✓
Chemical	✓	✓	✓	✓	✓	✓	✓	✓	✓	✓	✓
Physical (UV)	✓	✓	✓	–	✓	–	–	✓	–	–	✓
Enzymatic	✓	–	✓	✓	–	✓	–	–	✓	✓	✓
Films	✓	✓	✓	✓	✓	✓	✓	✓	✓	✓	✓
Sponges, porous scaffolds	✓	✓	✓	✓	✓	✓	✓	✓	✓	✓	✓
Micro, nanoparticles	✓	✓	✓	✓	✓	✓	–	✓	✓	–	✓
Hydrogels	✓	✓	✓	–	✓	–	–	✓	✓	✓	✓
Electrospun fibers	✓	–	✓	✓	✓	✓	–	–	–	–	✓
Micro fibers	✓	–	✓	–	✓	–	–	–	–	–	✓
In vitro cytotoxicity	✓	✓	✓	✓	✓	✓	✓	✓	✓	✓	✓
In vivo cytotoxicity	–	–	✓	✓	–	✓	–	–	–	✓	✓
Mechanical properties	Weak	Weak	Weak	Weak	Acceptable	Acceptable	Good	Weak	Weak	Weak	Acceptable
Stability	Poor	Poor	Poor	Poor	Weak	Good	Good	Poor	Weak	Weak	Weak

[a]This table is based on widely reported literature specifically on developing biomaterials for medical applications and is by no means exhaustive.

2.5.1 Chemical crosslinking

The chemical crosslinking of polysaccharides is a flexible technique with excellent mechanical stability. During crosslinking, counterions spread into the polymeric material, and the crosslinking agent reacts with polysaccharides to produce intermolecular or intramolecular bonds. Chemical crosslinking is affected by crosslinking agent concentration and crosslinking time. The high crosslinking agent concentration produces rapid crosslinking. As with physical crosslinking, a large counterion concentration would require longer exposure times for complete polysaccharide crosslinking [15].

2.5.2 Succinic acid (SA)

SA is a dicarboxylic acid with the chemical formula $C_4H_6O_4$. It plays a vital part in the metabolism of microorganisms, and it is widely dispersed in the tissues of plants,

animals, and other organisms. Acid has a melting point that is in the range of 185-187°C. SA is a crystalline, colorless, acidic substance that is soluble in water [16].

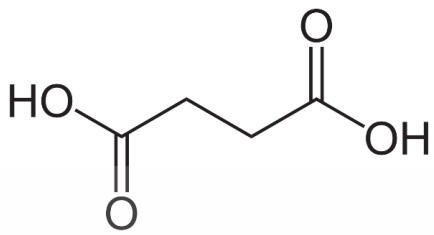

Figure 2.8 Chemical of SA [59]

2.5.2.1 Application of SA

Due to its saturated linear structure, SA can be utilized to synthesize several industrially important compounds. SA is an attractive industry building block since it may be utilized to produce various beneficial derivatives. SA is utilized in pharmaceuticals, lacquers, and perfume esters. It's also utilized as a sequestrant, buffer, and neutralizer. SA promotes plant growth. After protracted illnesses and injuries, succinates (calcium, potassium, and sodium) are beneficial as sedatives, antispasmodics, and contraceptives. By esterifying SA, a solvent called dimethyl succinate can be created in automotive water-cooling systems. SA molecules are also salt-substitute flavoring agents. Succinate salts boost rumen propionate production. It's glycogenic and a protein-synthesis precursor. The succinate salts can be utilized as feed supplements for animals [16].

2.6 Antibacterial agents

Antibacterial agents are a category of substances that combat harmful bacteria. Therefore, by eliminating or lowering the metabolic activity of bacteria, their toxic effect on biological surroundings can be reduced [60].

2.6.1 Zinc oxide nanoparticles

Materials with dimensions as small as 100 nm are the focus of nanotechnology, which focuses on their production and their uses. They have many practical uses in fields as diverse as material science, agriculture, the food industry, cosmetics, medicine, and diagnostics [61]. Because of their unusual chemical and physical properties and large surface area in relation to their volume, nanoscale inorganic compounds have demonstrated exceptional antibacterial activity at extremely low concentrations [62]. Some of them are safe to consume since they provide minerals necessary for human

health. Silver, gold, copper, titanium oxide, and zinc oxide, among others, have all been cited as among the most effective antibacterial inorganic minerals [63].

Zinc oxide nanoparticles are one such inorganic metal oxide that satisfies all of the characteristics and can therefore be used properly as a pharmaceutical, package preservative, and antibacterial agent. It easily diffuses into the food material, kills microorganisms, and prevents human illness. According to European Union regulations 1935/2004/EC and 450/2009/EC, active packaging is defined as material in contact with food that has the power to alter the composition of the food or the surrounding atmosphere [64]. In vitro, nanoparticles of zinc oxide have been utilized as an antibacterial agent against *S. typhi* and *S. aureus*. Zinc oxide nanoparticles displayed the highest toxicity against bacteria among all the metal oxide nanoparticles investigated thus far. Zinc oxide nanoparticles are an example of an inorganic metal oxide that has all of these properties and can be used as a drug, a way to keep packages fresh, and an antibacterial agent [65].

2.6.1.1 Antibacterial mechanism of ZnO nanoparticles

Nanotoxicity is fundamentally linked to microbial cell membrane disruption, which allows nanoparticles to enter the cytoplasm and accumulate [66]. The effect of nanoparticles on the growth of bacteria and viruses is highly dependent on particle size, shape, concentration, agglomeration, colloidal formation, and media pH. Figure 2.9 depicts the mechanism of zinc oxide nanoparticles' antibacterial action.

Induction of intercellular reactive oxygen species (ROS), a potent oxidant that is toxic to bacterial cells, may be one of the causes of antibacterial activity. ZnONP is known to produce hydrogen peroxide, which damages the bacterial cell membrane. In addition, these nanoparticles may produce Zn^{2+} ions, which may permeate the bacterial cell wall and react with internal components, affecting cell viability [66].

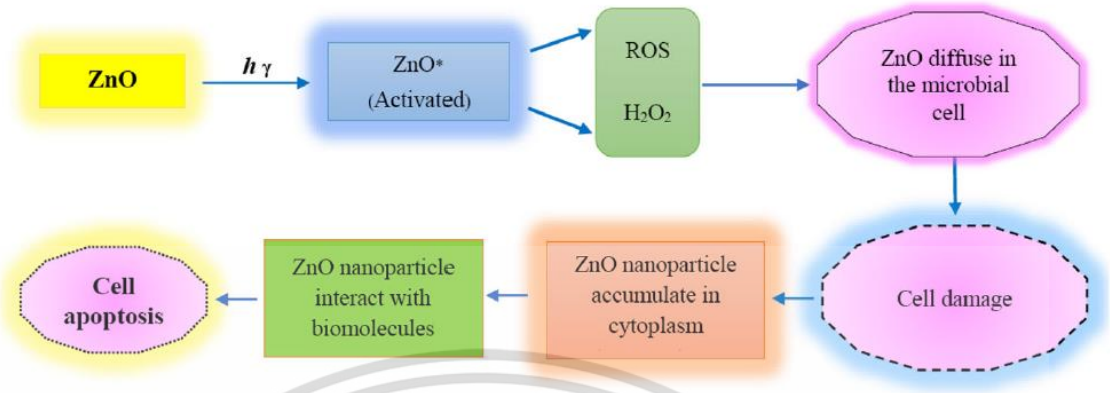

Figure 2.9 Mechanisms of ZnONPs antimicrobial activity [66].

2.6.2 Gallic acid (GA)

GA, a naturally occurring organic compound, is a polyphenolic compound with diverse biological activities and potential therapeutic applications. It belongs to the family of polyphenols and is classified as a trihydroxybenzoic acid derivative. GA is found in various plant-based foods, including fruits, nuts, tea leaves, and certain medicinal herbs. Its chemical structure comprises a benzene ring with three hydroxyl (-OH) groups attached at positions 3, 4, and 5. Its prevalence in traditional herbal remedies and medicinal plants further emphasizes its significance in natural pharmacology. The biological activities of GA include its antioxidant properties, which neutralize free radicals, mitigating oxidative stress and cellular damage. This antioxidant activity is implicated in various health benefits, including potential anti-inflammatory effects and protection against oxidative-induced diseases. Additionally, GA demonstrates antimicrobial properties, demonstrating efficacy against bacteria and fungi, making it a promising natural agent in infection control and wound healing.

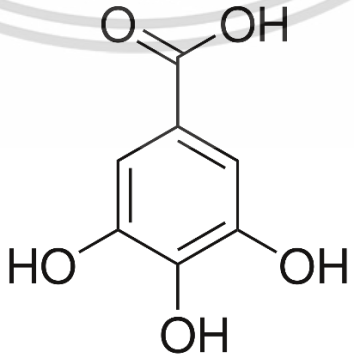

Figure 2.10 Chemical structure of GA

2.6.2.1 Antibacterial mechanism of GA

GA exhibits antibacterial activity through a variety of mechanisms, influencing multiple cellular processes in bacteria. Here are some key antibacterial mechanisms of GA:

1. Cell Membrane Disruption:

GA can disrupt bacterial cell membranes by interacting with lipids. The hydroxyl groups in GA can penetrate the lipid bilayer, leading to changes in membrane permeability and integrity. This disruption can cause the leakage of cellular contents, disturb ion balance, and ultimately lead to cell death [67].

2. Enzyme Inhibition:

GA has been shown to inhibit crucial bacterial enzymes, interfering with various metabolic pathways. For example, it can inhibit DNA gyrase, an enzyme involved in DNA replication. Inhibiting this enzyme disrupts the bacterial DNA replication process, leading to bacteriostatic or bactericidal effects [67].

3. Protein Denaturation:

GA interacts with bacterial proteins, leading to their denaturation. This interference with protein structure and function can affect the normal functioning of enzymes and other proteins essential for bacterial survival [67].

4. Oxidative Stress Induction:

While GA is known for its antioxidant properties, it can paradoxically induce oxidative stress in bacterial cells. GA can promote the generation of ROS, overwhelming the bacterial antioxidant defense mechanisms. This oxidative stress leads to DNA damage, lipid peroxidation, and disruption of cellular redox balance, contributing to bacterial cell death [67].

5. Interference with Biofilm Formation:

GA has been reported to inhibit the formation of bacterial biofilms. Biofilms are protective structures formed by bacteria that enhance resistance to antibiotics. GA disrupts biofilm formation by interfering with the adhesion of bacteria to surfaces and inhibiting the synthesis of extracellular polymeric substances [68].

It's important to note that the antibacterial mechanisms of GA can vary depending on the specific bacterial species, the concentration of GA, and other factors. Additionally, the fact that GA interacts on multiple cellular components and has a complex action mechanism provides it with an excellent antibacterial agent.

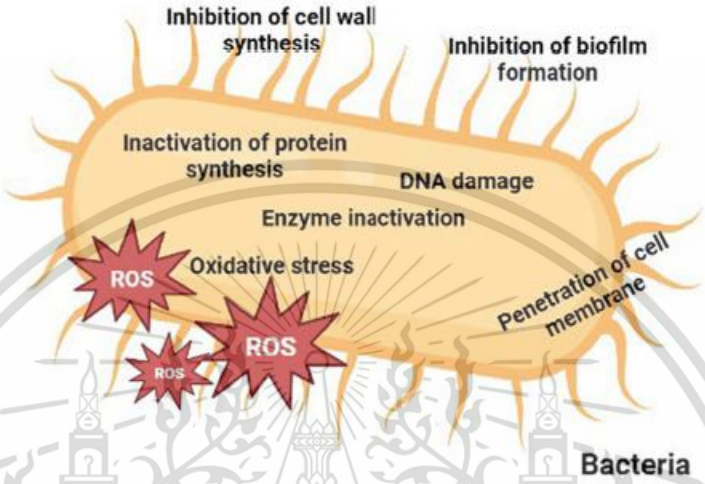

Figure 2.11 Schematic description of antibacterial mechanisms of GA [69].

2.7 Literature Reviews

C. Y. Basch *et al.* (2013) studied the physical and antimicrobial properties of tapioca starch/HPMC edible films incorporated with nisin and/or potassium sorbate. The blended biopolymer-based films with the increase of HPMC contents exhibited an increase of stress at break and elastic modulus, but strain at break decreased. The water solubility of films increased when the HPMC contents rose. On the other hand, the incorporation of HPMC produced no difference in the water vapor permeability of films. These films maintained a suitable behavior as packaging material [70].

M. P. Tedesco *et al.* (2016) studied polymer interactions between gelatin and HPMC for oral disintegrating films. Different concentrations of HPMC on gelatin-based film were studied. Smooth surfaces were found in gelatin and HPMC films, while the blended films displayed heterogeneous surfaces with the presence of continuous areas. The excellent hydrophilic character of HPMC provided a short time of disintegration and good extensibility of film. The decreased contact angle of gelatin/HPMC films indicated that HPMC showed more hydrophilic properties than gelatin [71].

C. Ding *et al.* (2015) prepared and characterized the HPMC/collagen blended film with the ratio of 1:1 by weight. The factor of polyethylene glycol (PEG) as a plasticizer that affects the films' properties was studied. The addition of PEG and collagen into HPMC film exhibited the IR shifted peak position from 3400 to 3376 cm^{-1} caused by the existence of hydrogen bonding between PEG and collagen or HPMC molecules. The morphology of the blended film showed a more homogeneous and compact structure. Thermal and mechanical properties were also improved by the incorporation of HPMC into collagen film [72].

K. Wilpiszewska *et al.* (2020) prepared hydrophilic films based on CMS (DS 0.8) and potato starch for use in the food or agriculture industries. 3 g of CMS/CMC dry powder mixture (with CMS to CMC ratio: 0/100, 20/80, 40/60, 50/50, 60/40, 80/20, or 100/0 wt%) was studied. A remarkable swelling degree of starch/CMS films at around 500% was observed when CMS contents increased. Moreover, the tensile strength and Young's modulus of the blended films decreased with the increment of CMS while the elongation at break enhanced. The moisture absorption and water solubility increased with an increase in CMS contents. The decrease of Tg with a higher CMS amount was due to steric repulsion interaction resulting in high chain mobility of molecules [13].

K. Wilpiszewska *et al.* (2015) studied the effect of calcium montmorillonite (MMT-Ca) on CMS-based nanocomposite films for controlled delivery systems and seed tape production. The improvement of mechanical properties, moisture uptake, and water solubility was obtained in CMS-based films incorporating several amounts of MMT-Ca (1-7wt%). The hydrophobic property of films with the addition of MMT-Ca increased as corresponded to the contact angle results. However, the most efficient clay platelets dispersion was founded for CMS/MMT-Ca_5 film [73].

C. Zhang *et al.* (2020) prepared an intelligent film made from CMS/kappa-carrageenan reinforced by mulberry anthocyanin (MAE) as an indicator. The IR band at 1410 cm^{-1} expanded, and the band at 845 cm^{-1} shifted as a result of the electrostatic force between the anthocyanins, CMS, and carrageenan, revealing that the anthocyanins were bonded to the CMS and carrageenan by electrostatic interaction in the film. The mechanical properties and WVP were improved by adding MAE, whereas the thermal

properties of the film with MAE obtained no difference on the heat stability of the film [74].

A. Ounkaew *et al.* (2020) synthesized bio-based CMS/PVA hydrogels containing AgNPs. The IR shifted absorption bands of nanocomposite hydrogels at 3280–3309 cm^1 confirmed the formation of hydrogen bonding. Due to the hybridization of CA and AgNPs generated under acidulation to create chelation, these hydrogels exhibit synergistic antibacterial activity against *S. aureus* and *E. Coli*. Synthesized hydrogels presented low cytotoxicity and could be utilized as dressings for wounds. The addition of AgNPs enhances the storage modulus and swelling index of hydrogels. The swelling index increased from 194% to 243% with increasing AgNPs content after 24 h of immersion [11].

A. I. Raafat *et al.* (2018) fabricated Xanthan/PVA/ZnO nanocomposite hydrogel, which was used as an active wound dressing. Gamma radiation has been used as an environmentally friendly source for crosslinking and sterilization processes. The dressings made of various contents of zinc oxide (0.5-5wt%) exhibit the improvement of swelling, fluid absorption, water retention, and water vapor transfer characteristics. The nanocomposite dressings exhibited effective defense against microbial invasion and broad-spectrum antibacterial action such as *S. aureus* (Gram positive), *E. Coli*. (Gram negative) and *C. albicans* (fungal) [24].

S. Kondaveeti (2017) studied and characterized HPMC/xyloglucan (XG)/gentamicin (GS) films with antimicrobial properties. The CA (at a concentration of 0.5 g/L) was used as a crosslinker in the blend films of HPMC and XG formed by solution casting. HPMC and XG blended films displayed good mechanical and antibacterial performance. The 50:50 HPMC/XG blended films had the maximum tensile strength (25 MPa) and Young's modulus (689 MPa). As a result of their remarkable antibacterial activity against *S. aureus* and *E coli*, the crosslinked films of HPMC, XG, and their blends loaded with GS revealed their potential for innovative biomedical applications [5].

Z. Abdollahi *et al.* (2021) prepared a bioactive CMS-based hydrogel containing CuO nanoparticles for use in wound healing applications. CA at the contents of 10-20wt% was used as a crosslinking agent during the fabrication of the hydrogels using a

solution-casting method. The 20wt% of CA provided the highest swelling degree. CuO nanoparticles (2 and 4wt%) were added to the hydrogel, which increased its antibacterial abilities, antioxidant activity, and swelling capacity. The hydrogel containing 2% CuO nanoparticles demonstrated good biocompatibility and low toxicity to human dermal fibroblasts (HDFs) [22].

P. Klangmuang and R. Sothornvit (2016) studied the barrier and mechanical properties of HPMC nanocomposite films with antimicrobial activity. These films were fabricated by casting method. Essential oil (15 g/L) from finger root incorporated in HPMC film showed antibacterial efficacy against *S. aureus* and *E. coli*. Furthermore, the gas barrier of the film was improved by combining beeswax and modified montmorillonite nanoclay. In films containing essential oils, it was found that elongation increased and that the elastic modulus and tensile strength decreased [75].

L. Zhang *et al.* (2013) developed capsule materials from HPMC and hydroxypropyl starch (HPS) by casting and capsule manufacture and studied the different ratios of HPMC/HPS. The morphology of blended films was observed, and the compatibility between HPMC and HPS was improved. The contact angle and transparency of films decreased when starch content rose. The IR shifting and overlapping peak positions around (3309 cm^{-1} to 3435 cm^{-1}) were observed and indicated that there was a certain degree of formation of intermolecular hydrogen bonding. Under different shear speeds, the viscosity of solutions with a lower concentration of HPS (50%) was close to that of pure HPMC. This gives a large operating window for making capsules when the dipping process is done at a low shear rate [76].

K. Dharmalingam and R. Anandalakshmi (2019) fabricated sodium carboxymethylcellulose and HPMC using CA as a crosslinker in hydrogel wound healing films. The hydrogel film was prepared by casting method, and the various contents of CA were studied (5-20 wt%). The tensile strength, crystallinity, contact angle, and swelling degree of samples decreased with an increase of CA contents. Moreover, the highly interconnected nanoporous network in hydrogel films was observed from FE-SEM, and a decrease in initial decomposition temperature from TGA and DSC techniques was observed for increasing CA [77].

M. Belay *et al.* (2020) investigated the interaction between SA crosslinking and bacterial cellulose reinforcement on the characteristics of agar films. The addition of SA at the content of 10 wt% showed the enhancement of tensile strength on agar/bacterial cellulose composite film, while the acid contents above 10 wt% obtained a significant decrease in tensile strength and swelling ratio. The cytocompatibility exhibited that the synergistic approach of reinforcement and crosslinking of the films resulted in the development of viability cells (78%) compared to films that were subjected to crosslinking with SA only (65%), respectively [78].

N. Thessrimuang and J. Prachayawarakorn (2019) designed the new biodegradable film from basil seed mucilage and developed the physicochemical properties by adding various types of organic acid (SA, MA, and TA). All of the essential characteristics of BSM films, including stress and strain at maximum load, barrier capability and thermal properties, were enhanced by crosslinking with the dicarboxylic acids. These films thus demonstrated excellent capability for use as biodegradable films, particularly for food packaging. The films with SA showed the greatest efficiency in the crosslinked process of the film sample [18].

K. S. Linn (2022) examined PVA-based films with an antioxidant activity using pectin extracted from *Cissampelos pareira* leaves. The pectin/PVA films were prepared by casting solution and using glycerol as a plasticizer. Various contents of SA (0-64 wt%) were added to the polymer blend at a mass ratio of 1:1. The water contact angle revealed that thicker pectin/PVA films with a higher surface hydrophobicity were formed when SA amounts were increased. The film with 16 wt% of SA had the highest tensile strength and antioxidant activity. For the results, these films can be used as biodegradable food packaging with antioxidant properties [79].

X. Yang *et al.* (2021) studied and produced PVA-COOH through the modification of PVA with succinic anhydride. Subsequently, poly(hexamethylene guanidine) was introduced as a cross-linker, and GA was incorporated as an antibacterial agent, resulting in the formation of PVA-based composite hydrogel films. The films exhibited high swelling ratios, low water solubility, and favorable mechanical properties. The antibacterial efficacy of these substances was 99.999% against *E. coli* and *S. aureus* at a

concentration of 107 CFU/mL. The cytotoxicity test demonstrated favorable biocompatibility with L929 cells; however, the addition of GA led to a decrease in cell viability. The films showed remarkable antioxidant efficacy by scavenging 70% of the 1,1-diphenyl-2-picryhydrazyl free radical [29].

F. Luzi *et al.* (2019) prepared PVA films those incorporated by active constituents such as quercetin (QC) and GA. This study examined the impact of active constituent contents (5 and 10 wt%) on the morphological characteristics, thermal resistance, optical, mechanical, and release properties of PVA. Antioxidant properties and migration with food stimulants were also evaluated. Stress at break, Young's modulus and strain at break increased with the addition of GA and QC. Thermal stability of PVA films with the incorporation of GA and QC was improved. The homogeneity and uniformity of modified PVA films characterized by SEM were also influenced by the addition of GA and QC at concentrations of 5 and 10 wt%. GA is effectively distributed in polymer matrices produced by solvent casting owing to its high hydrophilic nature and solubility in water solution. [80].

L. Rui *et al.* (2017) produced composite films by incorporating or conjugating GA with Tween 20, CS, gelatin, and glycerol. In addition to the microstructures, the physical and functional properties of the films were examined. The increased concentration of GA resulted in diminished water vapor permeability, swelling degree, elongation at break, and transmittance, while water solubility, tensile strength, and Young's modulus increased. Additionally, the antimicrobial and radical scavenging efficacy increased when the GA contents increased [30].

S. Sharma *et al.* (2022) prepared the biodegradable polymer composite poly lactide-poly (butylene adipate-co-terephthalate) with the addition of tannic acid (TA) and GA, it showed that it could be used for active packaging. The UV blocking capability of TA and GA (10 wt%) composite coatings increased by 65–66%. The tensile strength increased after the addition of 10 wt% of TA and GA. Overall, *E. coli* and *L. monocytogenes* growth were reduced. In conclusion, significant UV blocking properties, surface hydrophobicity, and antibacterial properties were confirmed for TA and GA composite film, demonstrating its potential as an active packaging film [31].

A. Naeem et al. (2022) created a hydrogel membrane for the treatment of superficial wounds composed of sodium alginate, polyvinyl alcohol, acrylic acid, and GA. FTIR, TGA, DSC, SEM, XRD, sol-gel fraction, porosity, mechanical strength, swelling, drug release, biodegradation, antioxidation and antimicrobial activity were determined. These hydrogel membranes were successfully synthesized using ethylene glycol dimethacrylate as a crosslinking agent and exhibited excellent thermal stability, high drug loading, increased mechanical strength, and outstanding biodegradability. In addition, the swelling ability and porosity of the surface facilitated a controlled release of the encapsulated drug (GA), with 70.34% release observed at pH 1.2, 70.10% release at pH 5.5 (normal skin pH), and 86.24% release at pH 7.4 (wounds pH) in 48 hours. GA-loaded hydrogel membranes exhibited large area of inhibition against *P. aeruginosa*, *S. aureus*, and *E. coli* [81].

G. K. Malik and J. Mitra (2021) studied the effect of HPMC as a capping material in order to prevent the agglomeration of ZnONPs. The HPMC-ZnO bio-nanocomposite films with various plasticizers (glycerol, sorbitol and polyethylene glycol) were prepared by incorporating capped ZnONPs (at 0, 0.5 and 1 wt%) in HPMC biopolymer, demonstrating that the introduction of ZnONPs enhanced the mechanical, barrier, antibacterial, and UV-blocking capabilities of HPMC film. Minimum inhibitory concentration (MIC) for food application was determined for ZnONPs. *S. aureus* has a MIC of 0.5 mg/mL. On the 12 days, for all ZnONPs, a concentration of 1 mg/mL inhibited around 80% of *Penicillium expansum*, whereas a concentration of 2 mg/mL inhibited 95%. The HPMC-ZnO nanocomposite films provided great potential for active food packaging. [25]

K. M. Amin *et al*. (2020) synthesized ZnONPs-doped PVA/Pluronic acid blended films for active food packaging films. Different contents of ZnO (5-25 wt%) in blended films were studied. The intensity and position of bands between 510 and 750 cm^{-1} confirmed the incorporation of ZnO in PVA/PLUR/ZnO films, and the slight change in band widening at 3200–3400 cm^{-1} implied stronger hydrogen bonding between PVA/PLUR and ZnONPs. Moreover, ZnONPs loading at 25 wt% deposited in the polymer matrix appeared spherical and uniformly distributed, as confirmed by transmission

electron microscopy. Blended film showed an OTR of 1230 mL m^{-2} per day, while that of nanocomposite film was 710 mL m^{-2} per day. The concentration of ZnONPs in the PVA/PLUR/ZnO samples significantly impacted their ability to prevent the growth of all of the tested microbial strains (*S. aureus, B. subtili, P. aeruginosa, E.coli and C. albicans*) with the highest concentration (25 wt%) [82].

M. T. Khorasani *et al.* (2018) developed Heparinized (anticoagulant and anti-inflammation agent) PVA/CS/hydrogels containing ZnONPs for wound dressing and prepared by freeze-thaw technique to form porous bio-nanocomposites material. Adding ZnO improved WVP and swelling characteristics, increasing the number of pores in the hydrogel structure. The addition of ZnONPs (at 0, 0.5, and 1 wt%) increased the rate of sustained heparin release from hydrogel samples. Toxicity and microbiological testing showed that bio-nanocomposite materials had nontoxic and antibacterial properties. After 24 and 48 h, all samples had cell viability >70% and 80%. The antibacterial efficacy against *S. aureus* and *E. coli* exhibited more than 70% compared to the sample without ZnO (60%). PVA/CS/ZnO/Heparin hydrogel bio-nanocomposites can protect wounds against dehydration, exudate accumulation, bacteria growth, and infection and accelerate wound healing [83].

S. Tantiwatcharothai and J. Prachayawarakorn (2020) investigated and evaluted an antibacterial wound dressing derived from basil seed (*O. basilicum L.*) mucilage (BSM) - ZnO nanocomposite through borax crosslinking. Different amount of crosslinker added in BSM wound dressing (0, 5, 10 and 20 wt%) was studied. The wound dressing made from basil seed mucilage demonstrated significant swelling and water retention. The mechanical and thermal properties, as well as the dimensional stability, were improved using borax crosslinking. Antibacterial activity was observed against both *S. aureus* and *E. coli.* Hydrogel sponges made from crosslinked BSM were not harmful to HaCat cells [84].

Chapter 3

Research methodology

3.1 Chemicals

1. Cassava starch; from Chaopraya Phuchrai 1999 Co., Ltd., Thailand.

Table 3.1 The components of cassava starch

Component	Weight percentage (%)
Amylose	16.4±3
Amylopectin	83.6±2
Lipid	0.25±0.1
Protein	6.50-7.50
Humidity	<13
Ash	0.23±0.1
Size	<160 μm
pH	6-7

Remark: Data of the manufacturer.

2. HPMC; food grade from Union Chemical 1986 Co., Ltd., Thailand.

Table 3.2 Specification of HPMC

Details	Lower limit	Upper limit	Value
Methoxy	27.0	30.0	27.8
Hydroxypropyl	4.0	7.5	5.4
Sodium chloride	-	1.5	0.5
Moisture	-	5.0	3.0
Viscosity, 2% in water	3500	5600	4543

Table 3.2 Specification of HPMC (continue)

Details	Lower limit	Upper limit	Value
Particle size, thru 40 U.S. std sieve	99.0	-	100.0

Remark: Data of the manufacturer.

3. Monochloroacetic acid (MCA); ACS reagent ≥ 99.0% from Italmar Co., Ltd., Thailand.

4. Glycerol; food grade from Krungthepchemi Co., Ltd., Thailand.

5. Succinic acid; AR grade 99% from Acros organics Co., Ltd., Pennsylvania.

Table 3.3 Specification of SA

Physical Properties	Value
Appearance	White
Melting point	180-195 °C
Boiling point	235 °C
Flash point	206 °C
Molecular weight	118.09 g/mol
Solubility	Solubility in water: 80 g/L (20°C)

Remark: Data of the manufacturer.

6. Phenolphthalein; analysis grade from Carlo Erba Co., Ltd., France.

7. ZnONPs (20-40 nm); food grade from Nano materials technology, Co. Ltd., Thailand.

Table 3.4 Information of ZnONPs

Data	Identification
Appearance	White, powder
%ZnO	99.76
%Pb	0.0053
%Cd	0.0006
%Al	Not identified
%Moisture	0.02
Particle size	40-80 nm

Remark: Data of the manufacturer.

8. Sodium hydroxide; analysis grade from Carlo Erba Co., Ltd., France.
9. Hydrochloric solution; analysis grade from Carlo Erba Co., Ltd., France.
10. Ethanol 95%; analysis grade from Chemipan Co., Ltd., Thailand.
11. GA; AR grade from Italmar Co., Ltd., Thailand.

Table 3.5 Specification of GA

Physical Properties	Value
Appearance (Color)	white to beige
Appearance (Form)	powder
Solubility (Color)	Colorless to faint yellow
Solubility (Turbdity) 50 mg/ml, EtOH	Clear to slightly cloudy
Molecular weight	170.12 g/mol
Purity (%)	≥98.5

Remark: Data of the manufacturer.

12. Distilled water.

3.2 Instruments

1. Beaker; 50, 250 and 500 ml
2. Hot plate stirrer; CMAG HS7 5000 from IKA Co., Ltd., Thailand.
3. Mechanical stirrer; RW 20 D from IKA Co., Ltd., Thailand
4. Water bath; WNP22 from Memmert Co., Ltd., U.S.A.
5.. Analytical balance; MS204TS/00 from Mettler-Toledo Co., Ltd., Thailand.
6. Vacuum filter; A35 from Eyela Co., Ltd. U.S.A.
7. Hot air oven; UF110 from Memmert Co., Ltd. U.S.A.
8. Blender; EM 44A from SHARP Co., Ltd. Thailand.
9. Universal testing machine; LR 5 K from Lloyd Instrument Co., Ltd., UK.
10. UV-Vis spectrophotometer; UV 9100 from Lab Tech, Inc. USA.
11. Scanning Electron Microscopy (SEM); Quanta 250 from Philips/FEI Co., Ltd., USA.
12. ATR spectrophotometer; IRTracer-100 from Shimadzu Co., Ltd., Japan.
13. X-ray diffractometer (XRD); SmartLab SE from Rigaku Co., Ltd., Japan.

3.3 Procedures

3.3.1 CMS preparation

First, 12.5 g of cassava starch was mixed in a 300-mL solution of 90% isopropanol. Continuous swirling at room temperature added 7.7 mM NaOH to the suspension. At 50 °C, 10.93 g of MCA was added and mixed for 45 mins. After 3 h, the starch suspension was neutralized with glacial acetic acid and then vacuum-filtered. The solid filtrate was rinsed with 85% ethanol until the $AgNO_3$ test showed no chloride ion. The obtained CMS was then filtered and dried at 60 °C for 24 h. To determine the degree of substitution (DS) of the prepared CMS. CMS powder (5g, Na-CMS form) was dissolved in acetone (150 ml), 5 M aqueous HCl (15 ml) was added, and Na-CMS was converted to H-CMS by stirring. After ethanol washing, the neutral dispersion was filtered and dried. H-CMS (0.5 g) was dissolved in an aqueous solution of 0.2 M NaOH. Using a phenolphthalein indicator, the mixture was back-titrated with 0.05 M HCl [85]. The

calculated degree of substitution of the prepared CMS was 0.85±0.07**.** The mean value of the replicates in each titration was measured to obtain the average value of HCl volume A blank was also titrated. The *n*COOH and DS were calculated by Equation (1) and (2), respectively:

$$n\text{COOH} = (V_b\text{-}V) \times c_{HCl} \times 4 \qquad \text{Equation (1)}$$

where: *V*b (ml) was the volume of HCl used for titration of blank; *V* (ml) was volume of HCl used for titration of sample; c_{HCl} (mol/dm^3) was the HCl concentration and 4 was the ratio of the total solution volume (100 cm^3) and the volume taken for titration (25 cm^3)

$$DS = ((162 \times \text{nCOOH})/m_{ds} - 58 \times \text{nCOOH}) \times 100 \qquad \text{Equation (2)}$$

$$m_{ds} = \left(1\text{-}\frac{W_{water}}{100}\right) \times m_s \qquad \text{Equation (3)}$$

where: 162 g/mol was the molar mass of an anhydroglucose unit (AGU); *n*COOH (mol) was quantity of HCl used (mol); 58 g/mol was molar mass of carboxymethyl residue, and m_{ds} (g) was corrected mass of CMS calculated from weight of CMS taken m_s (g) and the water content, w_{water} (%) which was used to calculate in Equation 3.

3.3.2 The preparation of modified HPMC films with CMS and ZnONPs and modified 70HPMC-30CMS films with SA and GA

3.3.2.1 A flowchart of the preparation and characterization of HPMC-CMS blended films incorporating ZnONPs is shown in Figure 3.1.

1. HPMC (2.1 g) and glycerol (30 wt% of the total polymer matrix) were dissolved in 65 ml of hot water (at 85 °C). (Remark: the total weight polymer was 3 g.)

2. Different amounts of CMS (0, 10, 20, and 30 wt% of the total polymer matrix) were separately dissolved in 65 ml distilled water and added to the HPMC solution.

3. The suspension of ZnONPs (in an aqueous medium of 20 ml) after being sonicated for 10 min was added at 30 and 50 wt% based on the weight of the total polymer matrix.

4. The solution of 70HPMC-30CMS with different contents of ZnONPs was agitated magnetically for 15 min at 85 °C.

5. Approximately 150 ml of the solution was poured into a polypropylene tray (21.5 cm x 14.5 cm) and dried for 16 h at 60 °C.

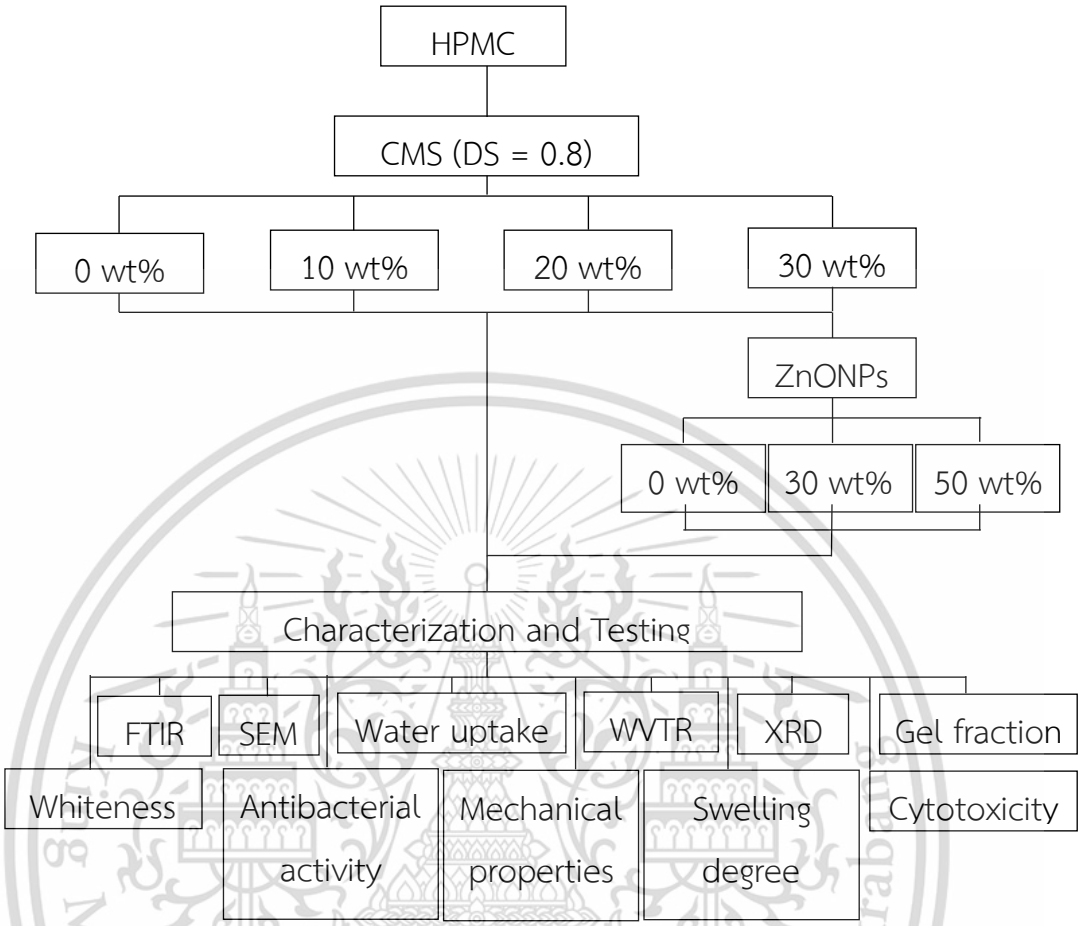

Figure 3.1 A flowchart of the preparation and characterization of HPMC-CMS blended films incorporating ZnONPs.

Table 3.6 Compositions of different modified HPMC films

Sample	HPMC (g)	Glycerol 30 wt% (g)	Distilled water (mL)	CMS		ZnONPs	
				g	wt %	g	wt %
100HPMC-0CMS	3	0.9	150	-			
90HPMC-10CMS	2.7	0.9	150	0.3	10	-	-
80HPMC-20CMS	2.4	0.9	150	0.6	20	-	-
70HPMC-30CMS	2.1	0.9	150	0.9	30	-	-
70HPMC-30CMS-30ZnONPs	2.1	0.9	150	0.9	30	0.9	30
70HPMC-30CMS-50ZnONPs	2.1	0.9	150	0.9	30	1.5	50

3.3.2.2 Figure 3.2 depicts a flowchart of the fabrication and characterization of 70HPMC-30CMS-2.5SA films containing GA.

1. HPMC (2.1 g) and glycerol (30 wt% of the total polymer matrix) were dissolved in 65 ml of hot water (at 85 °C). (Note: the polymer's total weight is 3 g.)

2. In 65 mL of distilled water and 30 wt% of CMS were dissolved and added to the HPMC solution.

3. The mixture was continuously stirred and maintained at 85 °C for 30 min.

4. The aqueous solution of SA, at 2.5 wt% of the total weight of the polymer (10 ml), was slowly dropped into CMS-HPMC mixture and then mixed for 15 min.

5. Different concentrations of GA (0, 1, 3, and 5 wt% of total weight polymer) were dissolved in 10 ml of a 10% ethanol solution and stirred magnetically until a completely homogeneous solution was obtained.

4. The solution of 70HPMC-30CMS-2.5SA with various contents of GA was agitated magnetically for 15 min at 50 °C.

5. Approximately 150 ml of the solution was poured into a polypropylene tray (21.5 cm x 14.5 cm) and dried in the oven for 19 h at 60 °C.

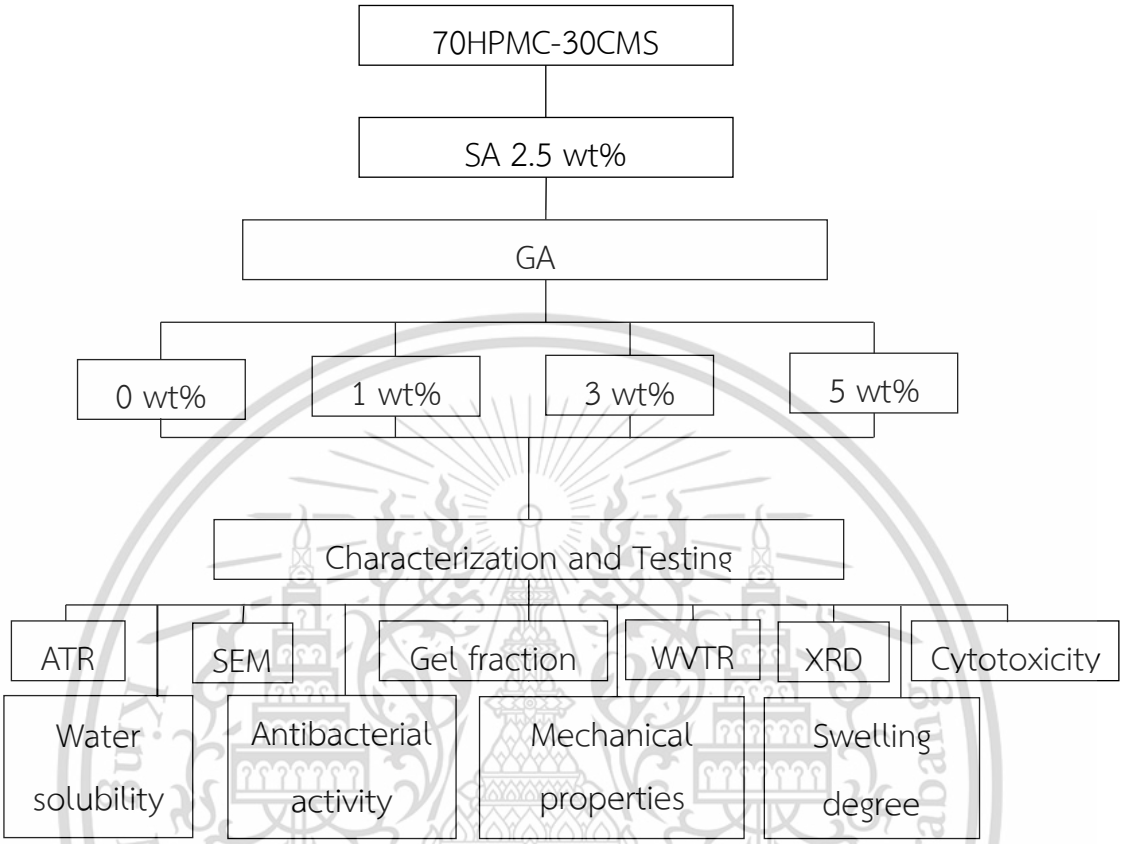

Figure 3.2 A flowchart of the fabrication and characterization of 70HPMC-30CMS-2.5SA films containing GA.

Table 3.7 Compositions of different 70HPMC-30CMS-2.5SA films containing GA.

Sample	HPMC (g)	CMS (g)	SA 2.5 wt% (g)	Glycerol 30 wt% (g)	Distilled water (mL)	GA	
						g	wt %
70HPMC-30CMS	2.1	0.9	-	0.9	150	-	
70HPMC-30CMS-2.5SA	2.1	0.9	0.075	0.9	150		
70HPMC-30CMS-2.5SA-1GA	2.1	0.9	0.075	0.9	150	0.03	1
70HPMC-30CMS-2.5SA-3GA	2.1	0.9	0.075	0.9	150	0.09	3
70HPMC-30CMS-2.5SA-5GA	2.1	0.9	0.075	0.9	150	0.15	5

3.4 Characterizations

3.4.1 Attenuated total reflection spectroscopy (ATR) and Fourier-transform infrared spectroscopy (FT-IR)

Both ATR and FTIR were used in this study.

IRTracer-100 from Shimadzu Co., Ltd., Japan, ATR spectroscopic investigations was utilized. Film samples were chopped into squares of 1 cm^2 in area. In the range 4000-700 cm^{-1}, ATR spectra were acquired with a resolution of 4 cm^1 and 45 successive scans per sample.

The FT-IR spectroscopic studies were conducted using KBr pellets with a Spectrum 2000 GX spectrometer (PerkinElmer, USA). FT-IR spectra were obtained within the frequency range of 4000-400 cm^{-1}, using a resolution of 4 cm^{-1} and conducting 10 consecutive scans for each sample.

3.4.2 Scanning electron microscopy (SEM)

Scanning electron microscope (SEM) (Quanta 250, Philips/FEI, USA) operated at 15 kV was used to investigate the cross-sectional morphology of a film. The sample film was fractured under liquid nitrogen, fixed to a stub, and coated with a thin gold layer.

3.4.3 X-ray diffraction (XRD)

Utilizing equipment from Smart lab SE (Rigaku, Japan), we were able to record a diffractogram using CuKα (=1.54) radiation with an operating voltage of 40 kV and a current of 30 mA over an angular range of 2 = 5–60°. The following equation was utilized in the determination of the crystallinity level:

$$\text{Crystallinity (\%)} = \frac{A_c}{A_c+A_a} \times 100 \qquad \text{Equation (4)}$$

where A_c was the area corresponding to the crystalline region (2θ = 5-30°) and A_a was the amorphous region (2θ = 5-60°) on the X-ray diffractogram.

3.4.4 Mechanical properties

Using a Universal testing machine (Lloyd LR 5K) with a 100 N load cell and 50 mm/min crosshead speed, the mechanical characteristics of a film were determined (ASTM D-882). The film was chopped into 100 x 15 mm^2 squares with an average thickness of 0.09 to 0.10 mm. The film was conditioned with a saturated ammonium nitrate solution at 60±2%RH. All mechanical testing were done at a temperature of 23±1°C and a relative humidity of 60±2%RH.

3.4.5 Water absorption

A film was dried at 105°C for 3 h and then stored in a container with a relative humidity of 99±1%. Ten days were used to determine the water content absorbed by the film (ASTM D-570). The proportion of water absorption was determined using Equation (2):

$$\text{Moisture uptake} = \frac{W_2-W_1}{W_1} \times 100 \qquad \text{Equation (5)}$$

where W_2 and W_1 were the wet and the dried weights of the sample, respectively.

3.4.6 WVTR

WVTR was determined using the gravimetric modified cup technique (the desiccant technique) (ASTM E96). A sealed cup containing the film test (with a surface

area of 32.15 cm^2) was weighed and placed in a chamber with a saturated solution of sodium chloride and a constant relative humidity of 75%. WVTR was determined every 24 hours for seven days. Using the following formulae, the WVTR was computed:

$$WVTR = \frac{\Delta m}{(\Delta t.\ A)} \qquad \text{Equation (6)}$$

where **Δ**m/**Δ**t and A were the weight gain of film samples per day (g/day) and permeative surface area of film samples (cm^2), respectively.

3.4.7 Swelling degree

A film (25.4×25.4 mm^2) was dried at 105°C for 2 h and immersed in distilled water at room temperature for 24 h. The weight of the wet film (W_2) was measured after water removal from the surface. Percentage of swelling was calculated as followed:

$$\text{Swelling (\%)} = \frac{W_2 - W_1}{W_1} \times 100 \qquad \text{Equation (7)}$$

where W_2 and W_1 were the wet and the dried weights of the sample, respectively.

3.4.8 Water solubility

The water solubility was determined using the method described by Y. Ma, R. Yang, and W. Zhao [86]. The dried film was agitated in 50 mL of deionized water for 1 h using magnetic stirring at a speed of 200 rpm. The insoluble film was isolated using centrifugation at a speed of 6000 rpm for 10 minutes. Subsequently, it was subjected to drying at a temperature of 105 °C until its weight reached a constant value, denoted as M_f. The water solubility was determined using the equation (8):

$$\text{Water solubility (\%)} = \frac{M_i - M_f}{M_i} \times 100 \qquad \text{Equation (8)}$$

where M_f and M_i were the constant weight of the insoluble dry film after drying and the initial weight of the sample, respectively.

3.4.9 Gel fraction

The film sample was cut into 25.4×25.4 mm^2 and kept in a desiccator before testing. The film was wrapped with 400 mesh sieve stainless steel and then weighed (M_1). After that, the sieve containing a film was immersed in 100 mL of deionized water in an Erlenmeyer flask and shaken with a shaker (at a speed of 70 rpm) at room temperature for 24 hours. After immersing the film overnight, the sieve containing a film

was dried in an oven at 60 °C for 24 hours and re-weighed (M_2). The gel fraction was determined with an equation (9).

$$\text{Gel fraction (\%)} = \frac{M_2}{M_1} \times 100 \qquad \text{Equation (9)}$$

where M_2 and M_1 were the weight of the insoluble dry film and the initial weight of the sample, respectively.

3.4.10 Whiteness

Each sample's surface color was evaluated with a colorimeter (HunterLab, MiniScan XE Plus). The whiteness index (WI) of the films was determined using Equation (10):

$$WI = 100-\sqrt{(100-L^*)^2+(a^{*2}+b^{*2})} \qquad \text{Equation (10)}$$

where; L*, a*, and b* referred the film color values, the colorimetric parameters of the dry films including L* (lightness), a*(red–green) and b* (yellow–blue) [87].

3.4.11 Antibacterial activity

The method used in this study was agar diffusion and bacterial reduction percentage. The agar diffusion method was used to analyze the inhibition zones against *S. aureus* and *E. coli*. Before the incubation (37°C, 24h), sample discs with a diameter of 10 mm were placed on an agar plate containing gram-positive and gram-negative bacteria. In order to evaluate the antibacterial properties of the sample, the diameter of the inhibition zone was measured.

Furthermore, the JIS Z 2801 test method [88] was used to determine the antibacterial efficacy of the material by evaluating the reduction in viable bacterial count of the treated samples as compared to the control samples. For 24 hours, the sample was subjected to 37 °C and 90% RH, the condition that was considered optimal for bacterial proliferation. Following contact with the test material, the bacteria were subsequently extracted from the sample and quantified. The quantity of bacteria at the beginning was compared to the quantity of bacteria that survived. As shown in Equation (11), the difference between the initial and final count of microorganisms was calculated as a percentage or log reduction.

$$\text{\% Bacterial reduction} = ((B-A) \times 100)/B \qquad \text{Equation (11)}$$

3.4.12 In vitro cytotoxicity

For cytotoxicity testing, human keratinocytes (HaCat) were utilized in an MTT experiment. The sample was incubated in phosphate-buffered saline, filtered, and then Dulbecco's Modified Eagle Condition was added. The combination was incubated for 24 hours at 37 ℃ and supplemented with 10% fetal bovine serum. In a 96-well plate, 100 µl (1 x 10^5 cells/ml) of HaCaT cells were planted and incubated at 37 ℃, 24 h in each well. The incubated filtrate mixture and 10 µl of the MTT solution (5 mg/mL) were then added, followed by a 4-hour incubation at 37 ℃. Then, the solution resulting from the dissolution of formazan was added to the well. The resultant mixture's absorbance at 570 nm was measured using a Biochrom microtiter plate reader. Images of cell morphology were studied using an optical microscope. Using the following equations, percentages of cytotoxicity and cell viability were computed.

$$\%\text{Cytotoxicity} = (A\text{-}B/A) \times 100 \qquad \text{Equation (12)}$$

$$\%\text{Cell viability} = 100 - \text{Cytotoxicity} \qquad \text{Equation (13)}$$

where; A and B were the absorbances of the control and test wells, respectively.

3.4.13 Statistical Analysis

Statistical analysis was carried out by using the analysis of variance (ANOVA) procedure with IBM SPSS statistics 25 software. Tukey's test was used to determine differences among the means. ($p < 0.05$).

Chapter 4

Main results and discussion

This study aimed to study the antibacterial wound dressing films based on HPMC. The films were blended with CMS, modified by SA crosslinking agent and incorporated with the antibacterial agents (ZnONPs and GA).

This chapter is divided in two parts;

(1) the effect of modified starch (CMS) on the physicochemical properties of HPMC-based films and the effect of ZnONPs as antibacterial agent on the physicochemical properties of 70HPMC-30CMS blended film.

(2) the effect of SA and GA as crosslinker and antibacterial agent on the physicochemical properties of 70HPMC-30CMS blended film.

The characterization techniques included FT-IR, XRD and SEM. Furthermore, swelling degree, gel fraction, water solubility, water absorption and WVTR as well as mechanical properties and whiteness were determined. The antibacterial activity and cytotoxicity of the films were also determined. Table 4.1 displays the abbreviations and symbols of the terms used in this study.

Table 4.1 Abbreviations and symbols

No.	Abbreviation	Samples
1	CMS	Carboxymethyl starch film
2	HPMC	Hydroxypropyl methylcellulose film
3	SA	Succinic acid
4	ZnONPs	Zinc oxide nanoparticles
5	GA	Gallic acid

6	HPMC-CMS	HPMC-CMS blended film with all contents of CMS
7	90HPMC-10CMS	HPMC-CMS blended film with 90:10 by %weight
8	80HPMC-20CMS	HPMC-CMS blended film with 80:20 by %weight
9	70HPMC-30CMS	HPMC-CMS blended film with 70:30 by %weight
10	70HPMC-30CMS-ZnONPs	70HPMC-30CMS blended film with all contents of zinc oxide nanoparticles
11	70HPMC-30CMS-30ZnONPs	70HPMC-30CMS blended film incorporated zinc oxide nanoparticles at 30 wt%
12	70HPMC-30CMS-50ZnONPs	70HPMC-30CMS blended film incorporated zinc oxide nanoparticles at 50 wt%
13	70HPMC-30CMS-2.5SA	70HPMC-30CMS blended film crosslinked with succinic acid (2.5wt%)
14	70HPMC-30CMS-2.5SA-GA	70HPMC-30CMS blended film crosslinked with succinic acid (2.5wt%) and incorporated all contents of gallic acid
15	70HPMC-30CMS-2.5SA-1GA	70HPMC-30CMS blended film crosslinked with succinic acid (2.5wt%) and incorporated gallic acid at 1 wt%
16	70HPMC-30CMS-2.5SA-3GA	70HPMC-30CMS blended film crosslinked with succinic acid (2.5wt%) and incorporated gallic acid at 3 wt%
17	70HPMC-30CMS-2.5SA-5GA	70HPMC-30CMS blended film crosslinked with succinic acid (2.5wt%) and incorporated gallic acid at 5 wt%

CMS is a water-soluble polysaccharide that is extensively used as an additive product and is discovered in a variety of applications, such as in the food industry, drug delivery, textile printing, and wound dressing. Because of the limitations of native starch, such as its insolubility in water, turbidity, high viscosity, and gelatinization. The carboxymethylation process (Williamson's ether synthesis) produced a CMS that was substituted with a carboxyl group in starch molecules [56]. This modification generated starch with a low gelatinization temperature and high solubility.

In this study, CMS was synthesized by using a mole ratio between NaOH and MCA that was used in the reaction at 2:1.5, and the degree of substitution of CMS was 0.8±0.07 which is classified as high DS value [73] with the presence of the negatively charged functional groups (CH_2COO^-) in the structure.

4.1 Characterization of modified HPMC film with the addition of CMS and ZnONPs

The objective of this section was to improve properties of HPMC-based film by blending with CMS (100HPMC-0CMS, 90HPMC-10CMS, 80HPMC-20CMS and 70HPMC-30CMS). An investigation was conducted to determine the effect of CMS contents and the use of ZnONPs as the antibacterial agent on 70HPMC-30CMS film. The physicochemical properties of modified HPMC films were characterized by FTIR, SEM, XRD, mechanical properties, whiteness and water absorbed properties including water absorption, WVTR, swelling degree and gel fraction. Moreover, the antibacterial activity and cytotoxicity were studied by agar disk diffusion and MTT assay techniques.

4.1.1 Possible macromolecular interaction between HPMC, CMS and ZnONPs

A schematic representation of possible interactions that may occur between biopolymers (HPMC and CMS) and ZnONPs is illustrated in Figures 4.1(a) and 4.1(b). The methoxyl ($-OCH_3$), hydroxypropoxyl ($-CH_2(CH)CH_3OH$), and hydroxyl (-OH) groups presented in HPMC can form hydrogen bonds with the polar carboxyl and hydroxyl groups of CMS. In the case of 70HPMC-30CMS-ZnONPs films, HPMC was able to perform electrostatic interaction with ZnONPs and hydrogen bonding with CMS and ZnONPs.

Carboxylate groups of CMS (COO^-) are capable of forming electrostatic interactions with Zn^{2+} ions. Similar interaction was reported for chitosan/ZnO nanocomposite films [89]. The CMC/ZnO nanocomposite hydrogel exhibited both electrostatic interaction and hydrogen bonding through the process of crosslinking with Zn^{2+} ions [90].

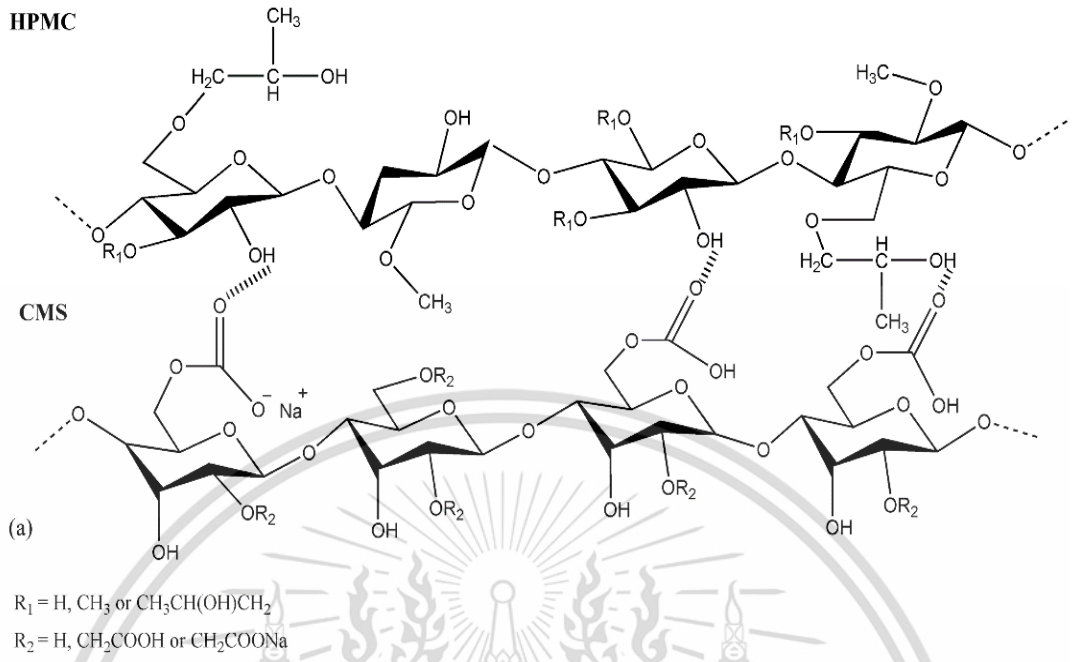

Figure 4.1 Schematic representation of the chemical interactions between HPMC and CMS.

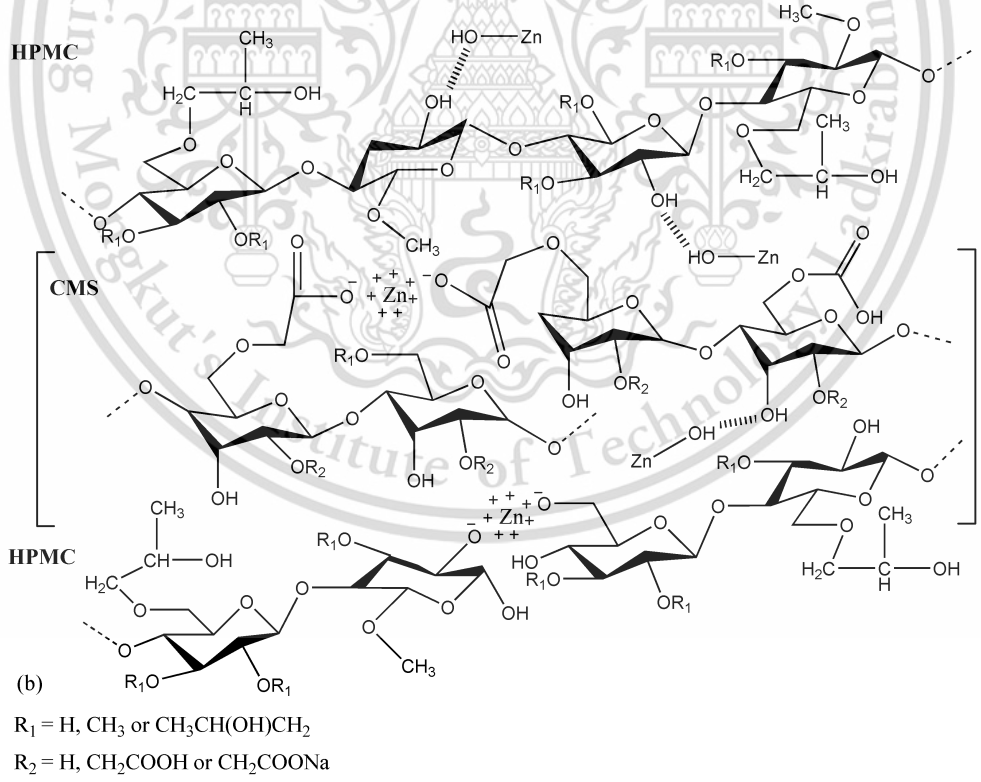

Figure 4.2 Schematic representation of the chemical interactions between HPMC, CMS and ZnONPs

4.1.2 FTIR

Functional group identification can typically be achieved by FTIR. The peak assignments of the characteristic bands in the FT-IR spectra of HPMC and CMS are summarized in Table 4.2.

Table 4.2 Peak identification of the characteristic bands in the FT-IR spectrum of HPMC and CMS [91].

HPMC		CMS	
Band (cm^{-1})	Assignment	Band (cm^{-1})	Assignment
3500-3200	O-H stretching	3700-3100	O-H stretching
2900	C-H stretching of methyl and hydroxy propyl group	3000-2800	Alkane C-H stretching
1650-1600	C-O stretching of six membered cyclic	1750-1735	C=O stretching of carboxylic group
1500-1450	Asymmetric bending of methyl group	1612-1590	C=O stretching of carboxylate group
1400-1350	C-O-C stretching and symmetric bending of -OCH3 and O-H bending	1460-1420	O-H bending
1300-1250	C-O-C stretching of cyclic epoxide	1300-1100	C-O-C stretching
1100-1000	C-O-C stretching	1200-1100	C-O-H bending
1000-950	Pyranose ring	1000-950	C-O stretching Skeletal vibrations of α-1,4-glycosidic bonds
850-800	Rocking mode of CH_2	851-800	C-H bending of CH_2

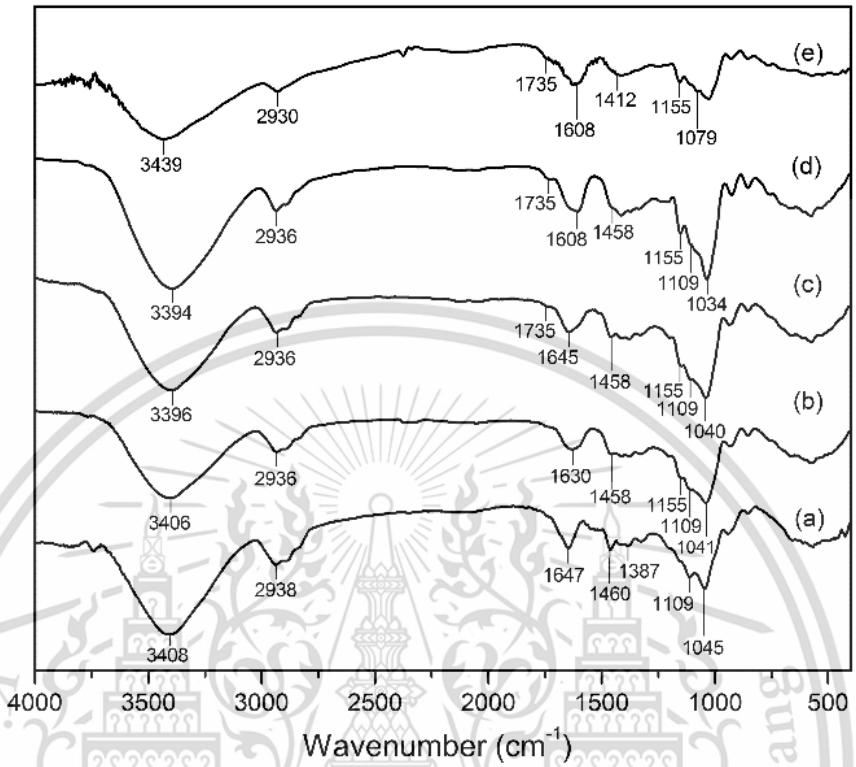

Figure 4.3 FT-IR spectra of HPMC and various HPMC-CMS samples incorporated with different contents of CMS (a) HPMC (b) 90HPMC-10CMS (c) 80HPMC-20CMS (d) 70HPMC-30CMS and (e) CMS.

The FTIR spectra of CMS, HPMC and HPMC-CMS films was shown in Figure 4.3. The FTIR spectrum of CMS exhibited the peak position observed at 1608 cm^{-1}, which was attributed to the asymmetric stretching of the carboxylate group (COO^-). The peak positions at 1412, 1155, and 1079 cm^{-1} were found to correspond to the C-O symmetric stretching of carboxylate groups, C-H bending, and C-C stretching vibrations, respectively [92].

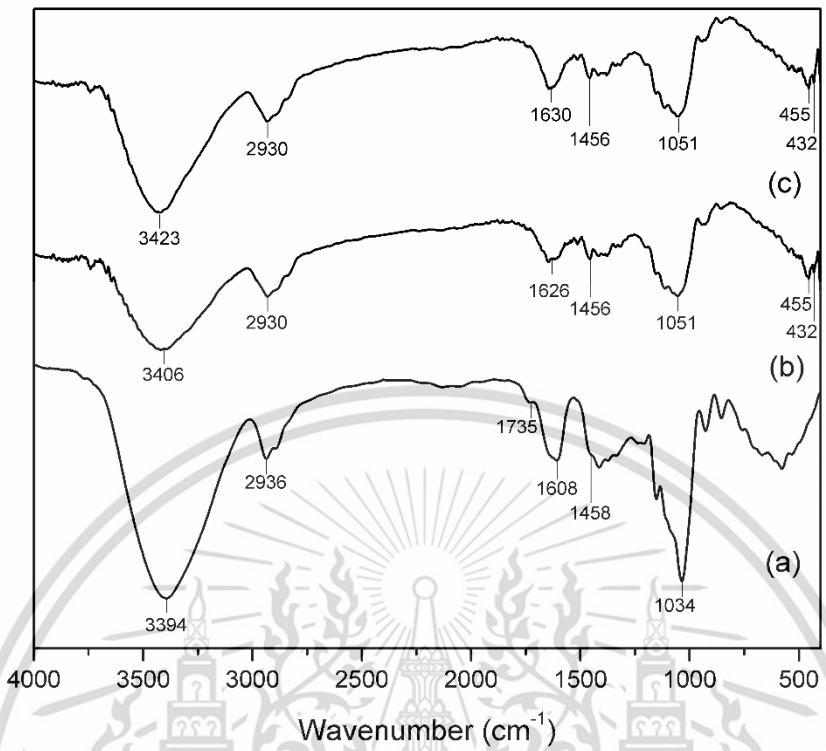

Figure 4.4 FT-IR spectra of 70HPMC-30CMS incorporated with different contents of ZnONPs (a) 70HPMC-30CMS, (b) 70HPMC-30CMS-30ZnONPs and (c) 70HPMC-30CMS-50ZnONPs.

The FTIR spectrum of HPMC (Figure 4.3(a)) revealed that the main wavenumbers associated with O-H stretching, O-H bending, and C-H bending were 3408 cm^{-1}, 1460 cm^{-1}, and 1387 cm^{-1}, respectively. A wavenumber at 1045 cm^{-1} was attributed to C-O stretching, while the medium-intensity bands at 1109 cm^{-1} were attributed to C-O-C asymmetric stretching [76].

For HPMC-CMS blended films, the broad vibrational peak at 1630, 1645, and 1608 cm^{-1} observed in composite films containing HPMC and CMS demonstrated the characteristic overlapped peak between the two components. Additionally, new absorption bands at 1155 cm^{-1} were detected, which corresponded to the C-H bending of CMS. Figure 4.3 and IR spectra of (a) to (d) showed that the shifted peak position of O-H stretching and O-H bending to lower wavenumbers from 3408 and 1460 cm^{-1} to

3394 and 1458 cm^{-1} was observed due to hydrogen bonding between HPMC and CMS [73].

For the 70HPMC-30CMS-ZnONPs nanocomposite films (as presented in Figure 4.4), the FTIR spectra of two concentrations of ZnONPs in 70HPMC-30CMS films (30 and 50%) as shown in Figures 4.4(b)-4.4(c) exhibited characteristic bands comparable to those observed for HPMC-CMS films (Figure (a)). In the 70HPMC-30CMS-ZnONPs films; however, the O-H bending peak position at 1456 cm^{-1} was observed to shifted to lower wavenumber. This result was caused by the formation of new hydrogen bonds between HPMC, CMS, and ZnONPs. In addition, two new absorption wavenumbers at approximately 455 and 432 cm^{-1} were observed and attributed to Zn-O stretching vibration [24].

4.1.3 X-ray diffraction

X-ray diffraction patterns and the degree of crystallinity of various HPMC-CMS films were evaluated using the XRD technique, as shown in Figures 4.5–4.6. The degrees of crystallinity of various HPMC-CMS films were presented in Table 4.3 and were calculated in the crystalline region at 2θ of 5 - 30°.

Figures 4.5 and 4.6 depicted the XRD patterns of various 70HPMC-30CMS-ZnONPs films incorporated ZnONPs. The semi-crystalline structure of HPMC (Figure 4.5 (a)) exhibited the diffracted peaks at 2θ of 7.6° and 20.8°. The main diffracted peaks of CMS at 2θ of 17.1° and 21.7° indicated an amorphous domain resulting from the Williamson's ether synthesis (Figure 4.5(e)) [93]. A similar spectrum for carboxymethyl sago starch (CMSS) was also reported, with a distinctive peak between 10° and 25°, and the main peaks were observed at 2θ of 15.2°, 17.21°, 17.9°, and 23.1°. When the DS of CMSS increased from 0.4 to 0.8, the spectrum became gradually broad, resulting from the extinction of the crystalline structure of native starch after carboxymethylation process [93].

For various HPMC-CMS films, the XRD peaks were also located at 2θ of 7.6° and 20.8°, but the decreased intensity of the diffracted peak at 2θ of 20.8° and percentage of crystallinity (Table 4.3) were clearly observed for HPMC-CMS films, particularly for 70HPMC-30CMS film, because of the addition of CMS. Due to intermolecular interactions between HPMC and CMS, the molecular chain rearrangement of HPMC was restricted, resulting in a decrease in the ordered structure of HPMC-CMS composite films. Dharmalingam and Anandalakshmi [77] reported a similar result for HPMC-CMC films with a decrease in crystallinity degree of HPMC caused by hydrogen bond formation between HPMC and CMC, which provided incomplete orientation of HPMC molecule to form a crystalline domain. Figures 4.6(b) and 4.6(c) display the characteristic diffracted peaks of ZnONPs consisting of distinct peaks at 2θ values of 32.3°, 34.9°, 36.7°, 48.0°, and 58.0° for various 70HPMC-30CMS-ZnONPs nanocomposite films. These peaks corresponded to the (100) (002) (101) (102) and (110) lattice planes of the hexagonal wurtzite structure, respectively [94]. It should be noted that the percentage of crystallinity of the nanocomposite films decreased drastically when compared to 70HPMC-30CMS film. This can be explained by the possible chemical interactions occurring between nanoparticles and polymer matrix (as shown in Figure 4.2) which restricting the mobility of polymer chains to form crystalline structure. Nevertheless, the difference in ZnONPs content did not impact the crystallinity percentage in various 70HPMC-30CMS-ZnONPs films.

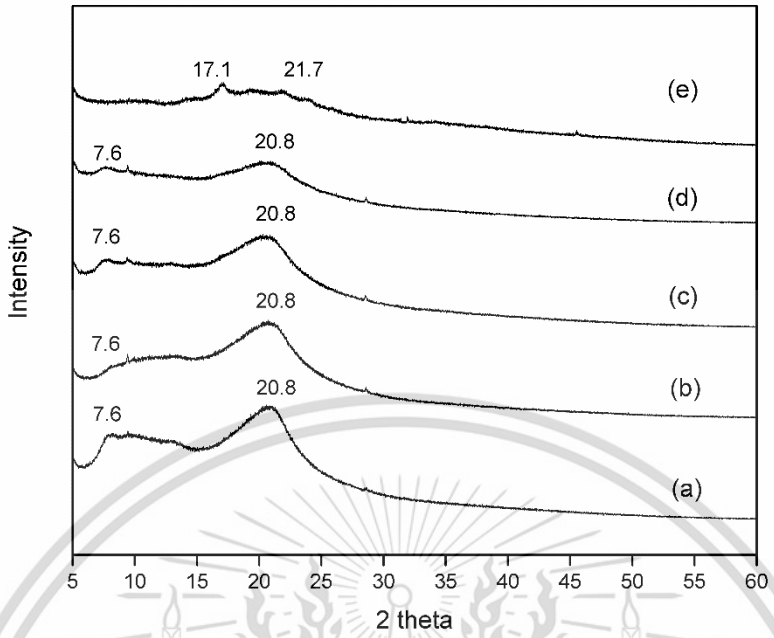

Figure 4.5 XRD patterns of HPMC and various HPMC-CMS samples incorporated with different contents of CMS (a) HPMC (b) 90HPMC-10CMS (c) 80HPMC-20CMS (d) 70HPMC-30CMS and (e) CMS.

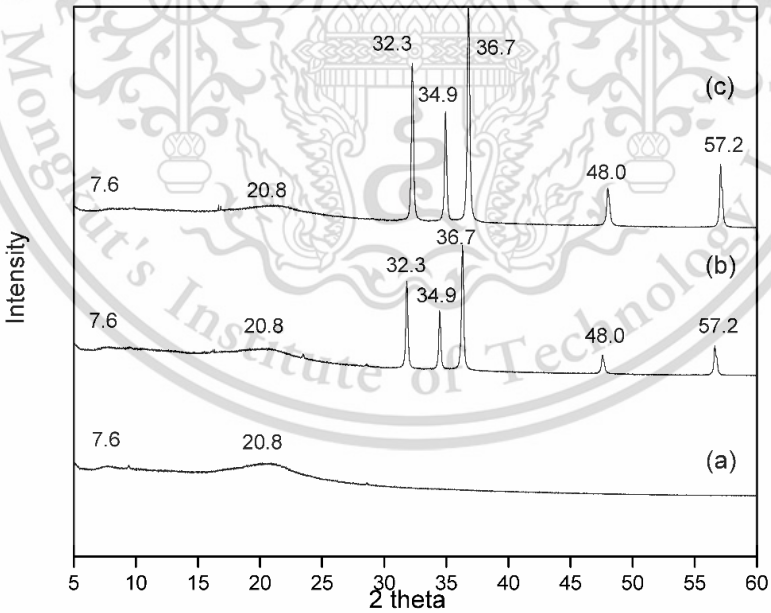

Figure 4.6 XRD patterns of 70HPMC-30CMS incorporated with different contents of ZnONPs (a) 70HPMC-30CMS, (b) 70HPMC-30CMS-30ZnONPs and (c) 70HPMC-30CMS-50ZnONPs.

Table 4.3 Percentage of crystallinity of HPMC films with different contents of CMS and ZnONPs.

Films	Crystallinity (%)
CMS	2.42
HPMC	15.05
90HPMC-10CMS	14.00
80HPMC-20CMS	10.99
70HPMC-30CMS	7.52
70HPMC-30CMS-30ZnONPs	5.61
70HPMC-30CMS-50ZnONPs	5.42

4.1.4 Morphology

SEM is frequently employed for the purpose of examining the cross-sectional surface morphology of cast films. As shown in Figures 4.7(a) and 4.7(b), the HPMC film showed a relatively rough surface with good phase continuity, whereas the CMS film exhibited a smooth surface. This was because of the amorphous structure of CMS produced by the carboxymethylation process as related to XRD analysis with the lowest crystallinity of CMS. On the other hand, the films composed of HPMC-CMS with different contents of CMS (as shown in Figures 4.7(b)–4.7(d)) displayed remarkable porosity characteristics. One possible explanation for the occurrence of pore formation might be attributed to the salting-out phenomenon of sodium salts of CMS components in HPMC solution. According to Zhang *et al.* (2021) [95], the inclusion of sodium salts of CMS in HPMC solution might potentially enhance the solid-liquid phase separation process during drying . This, in turn, led to the development of microporous films composed of HPMC upon the evaporation of water. The elongation of the pore shape was appeared when the content of CMS was increased.

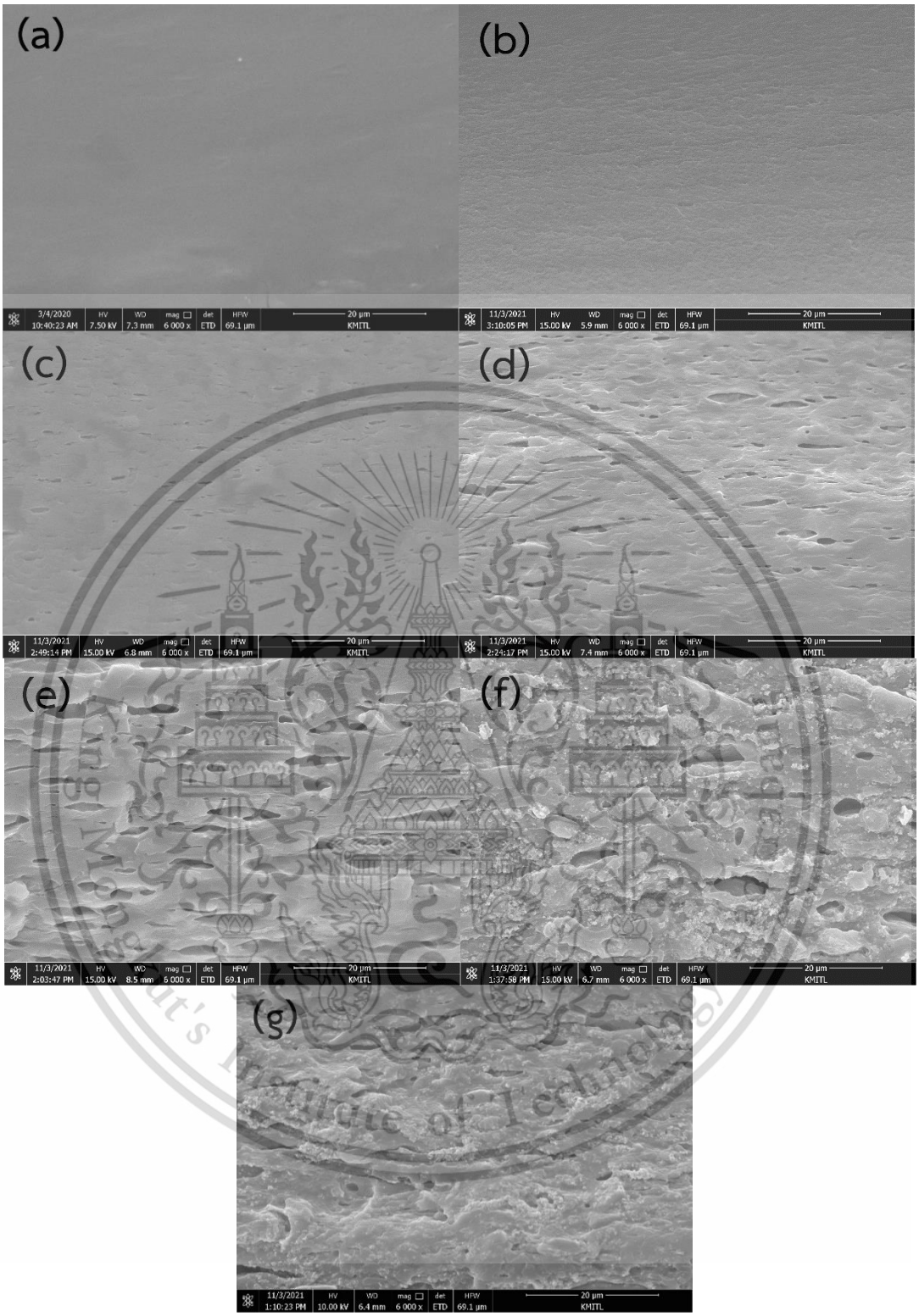

Figure 4.7 SEM micrographs at 6000X of modified HPMC films (a) CMS, (b) HPMC, (c) 90HPMC-10CMS, (d) 80HPMC-20CMS, (e) 70HPMC-30CMS, (f) 70HPMC-30CMS-30ZnONPs, and (g) 70HPMC-30CMS-50ZnONPs.

Furthermore, the surface morphology of different 70HPMC-30CMS-ZnONPs films (as seen in Figures 4.7(e)–(f)) exhibited good dispersion of ZnONPs into the polymer matrix and observed some areas of agglomeration, particularly at higher nanoparticle concentrations. Moreover, the morphological analysis of the film composed of 70HPMC30CMS-50ZnONPs revealed rougher surface compared to the 70HPMC-30CMS-30ZnONPs film. This might be attributed to the increased concentration of ZnONPs, which resulted in enhanced agglomeration of ZnONPs.

4.1.5 Mechanical properties

Table 4.4 displays the mechanical properties of CMS, HPMC, HPMC-CMS, and 70HPMC-30CMS-ZnONPs films. The HPMC film exhibited the highest stress at maximum load and Young's modulus, while the CMS film showed the lowest stress at maximum load and Young's modulus due to higher crystallinity of HPMC than CMS (as shown in Table 4.3). The stress at maximum load, Young's modulus, and strain at maximum load of HPMC-CMS films all decreased significantly as the CMS content increased. As confirmed by SEM and XRD analysis, the primary cause was the porous morphology (Figure 4.7) and the decrease in crystallinity (Table 4.3 and Figure 4.7).

The addition of ZnONPs in 70HPMC-30CMS film showed the decrease of stress at maximum load and Young's modulus of the nanocomposite films as related to the decreased crystallinity percentage. According to the mechanical properties of poly(vinyl alcohol)/chitosan/ZnONPs films decreased when ZnONPs was added [96]. This phenomenon may be ascribed to the aggregation of ZnO particles within the polymer matrix, which disrupted the chemical bonding between polymer matrix and ZnONPs, leading to decreased tensile strength.

Moreover, the similar stress at maximum load and Young's modulus of 70HPMC-30CMS-30ZnONPs and 70HPMC-30CMS-50ZnONPs films were observed, which corresponded to the similar crystallinity of HPMC-CMS-ZnONPs films, as shown in Table 4.3, while the strain at maximum load decreased. This may be due to the fact that the

agglomeration of ZnONPs increased when ZnONPs content increased, which decreased phase continuity (Figures 4.7(e)–(f)).

Table 4.4 Mechanical properties of HPMC films with different contents of CMS and ZnONPs

Films	Stress at maximum load (MPa)	Young's modulus (MPa)	Strain at maximum load (%)
CMS	1.80 ± 0.01^{e}	11.20 ± 0.75^{f}	145.00 ± 0.57^{e}
HPMC	38.74 ± 3.03^{a}	346.66 ± 4.50^{a}	77.33 ± 2.08^{a}
90HPMC-10CMS	35.62 ± 1.15^{a}	333.33 ± 2.51^{b}	77.00 ± 1.32^{a}
80HPMC-20CMS	28.25 ± 1.08^{b}	269.00 ± 4.58^{c}	65.33 ± 0.57^{b}
70HPMC-30CMS	23.67 ± 0.13^{c}	251.66 ± 1.15^{d}	53.33 ± 1.52^{c}
70HPMC-30CMS-30ZnONPs	18.72 ± 0.69^{d}	251.67 ± 3.21^{d}	40.66 ± 1.15^{d}
70HPMC-30CMS-50ZnONPs	16.60 ± 1.03^{d}	220.66 ± 1.52^{e}	40.66 ± 0.57^{d}

Different superscript letters in the same column are significantly different ($p < 0.05$), based on Tukey's test.

4.1.6 Water absorption, WVTR, swelling degree and gel fraction.

The effect of CMS and ZnO-NP on water absorption, WVTR, swelling degree and gel fraction of modified HPMC films were shown in Table 4.5. Usually, the best wound covering film keeps the wound moist, lets gases exchange with the environment, and gets rid of extra fluid. For the water absorption, HPMC film provided the lowest water absorption while CMS film showed the highest water absorption. This may be due to high polarity of CMS including carboxylic and carboxylate groups enhancing the water absorbed capacity. The HPMC-CMS films clearly showed an increase in water absorption when CMS contents increased, and the 70HPMC-30CMS film gave the highest water absorption, resulting from the presence of a high charge of anionic CMS and the porous

structure of the film. Moreover, 70HPMC-30CMS-ZnONPs nanocomposite films exhibited less water absorption than 70HPMC-30CMS film. This might be because the hydrophilic groups in HPMC and CMS were partially lost when they formed hydrogen bonds and electrostatic interactions with ZnONPs. Moreover, this reason also caused the decrease of water absorption in nanocomposite film when ZnONPs contents increased, especially at ZnONPs content of 50 wt%.

The WVTR of a wound dressing is crucial since it directly controls and regulates the moisture content of the wound. The WVTR value for commercial wound dressings can range from 76 to 9360 g/m^2 days [97]. Higher WVTR value of CMS film than HPMC film was due to the amorphous structure of CMS providing increased free volume, which enhanced the water vapor transmission through the film. Furthermore, CMS molecule composed of highly polar groups, such as carboxylate and carboxylic groups, which were capable of interacting with water molecules. These water molecules acted as plasticizers among polymer chains and led to the increase of free volume caused by reduced hydrogen bonds, promoting the water absorption capacity of film. [98]. The lowest WVTR of HPMC film was observed due to the highest crystalline percentage (as confirmed by XRD analysis), resulting in the inhibition of water vapor transfer.

Additionally, the WVTR of HPMC-CMS films increased as CMS content increased. This is due to the presence of more polar group of CMS and the porous structure, as confirmed by SEM. 70HPMC-30CMS-ZnONPs films revealed the reduction of WVTR value that may be due to the nanoparticles generating a tortuous pathway that inhibited the movement of water molecules through the film. Moreover, the possible interaction between ZnONPs and polymers may decrease hydrophilicity of the film after the incorporation of ZnONPs, leading to lower water vapor transfer through the nanocomposite film. Although, the crystallinity of 70HPMC-30CMS film was higher than 70HPMC-30CMS-ZnONPs films but the WVTR value of 70HPMC-30CMS film was higher

than nanocomposite films, suggesting that water vapor transmission capacity was not only depend on the crystallinity of film but also influenced by film porosity.

Furthermore, the WVTR value of 70HPMC-30CMS-ZnONPs films obviously decreased when ZnONPs contents increased. The result indicated that the number of possible interactions among HPMC, CMS, and ZnONPs (as shown in Figure 4.2) increased with the increased ZnONPs content, resulting in the loss of hydrophilic groups to absorb water molecules. Another reason was the reduction of porous structure (as confirmed by SEM in Figure 4.7(e)-4.7(g)) when compared to 70HPMC-30CMS film, which was due to the compact structure resulting from more interactions between polymer chains and ZnONPs.

The swelling degree of different HPMC-CMS films was investigated by immersing a sample in distilled water at 25±5°C for 24 h and weighing the swollen sample at 100% RH. These degrees of swelling are shown in Table 4.5. CMS film exhibited the highest swelling degree, while HPMC film showed the lowest swelling degree. This result was due to the negative charge of CMS in amorphous structure, which led to electrostatic repulsion causing higher swelling degree than HPMC. The HPMC-CMS films exhibited a greater degree of swelling compared to the HPMC film, as indicated by higher percentage values. This may be attributed to porous structure and a reduction in crystallinity, as shown in Figure 4.7 and Table 4.3. These reasons provided the increased free volume within the polymer system, related to higher swelling behavior. Furthermore, the carboxylate groups (COO^-) of CMS are capable of creating vacant spaces between polymer chains through the repulsion of negative charges. The addition of ZnONPs in 70HPMC-30CMS film exhibited the decrease of swelling degree. This result may be attributed to the appearance of hydrogen bonding and electrostatic interactions between ZnONPs and the HPMC-CMS matrix. These interactions led to the reduction in the available space inside the polymer system. Moreover, the swelling level of 70HPMC-30CMS-ZnONPs nanocomposite films decreased as the content of ZnONPs raised. As a

result, the increase of chemical interactions between ZnONPs and HPMC-CMS matrix (hydrogen bond and electrostatic interaction) caused the loss of free volume and free hydroxyl group of these components to absorb water molecules.

Gel fraction is a technique used to measure the extent of bridging (physical interaction including hydrogen bond and electrostatic attraction) or crosslinking (chemical bonding) in a polymer complex. Hence, the evaluation of the gel fraction is valuable in determining the extent of crosslinking. From the results (Table 4.5), the gel fraction of pure HPMC and HPMC-CMS films was below 2% resulting from high water solubility of HPMC. These films were composed of many free hydroxyl and bulky groups (methoxy and hydroxypropyl groups), making water molecules easy to diffuse into the polymer structure. However, the gel fraction of CMS film was higher than that of HPMC. This may be due to the lower water solubility of CMS than HPMC, resulting from a higher capacity to form hydrogen bonds between CMS chains than HPMC chains. Moreover, the addition of CMS enhanced gel fraction of various HPMC-CMS blended films, especially, 70HPMC-30CMS film. The result may be due to good phase compatibility resulting from hydrogen bonding and chain entanglement between HPMC and CMS.

The incorporation of ZnONPs into 70HPMC-30CMS film exhibited an obvious increase in gel fraction. This was because of the appearance of hydrogen bonding and electrostatic interactions between ZnONPs and the HPMC-CMS matrix. Furthermore, the gel fraction of 70HPMC-30CMS-ZnONPs nanocomposite films increased when the ZnONPs content was raised. The result was due to the high loading of ZnONPs, which enhanced electrostatic interaction, leading to an increased gel fraction.

Table 4.5 Water absorption, WVTR, swelling degree and gel fraction of modified HPMC films with different contents of CMS and ZnONPs

Films	Water absorption (%)		WVTR	Swelling	Gel fraction
	Day 4	Day 10	(g m^{-2} day^{-1})	degree (%)	(%)
CMS	43.63±1.89^{a}	57.53±4.76^{a}	208.53±0.34^{b}	304.21±9.66^{a}	12.00±1.15^{c}
HPMC	10.86±2.08^{d}	13.89±2.37^{d}	165.81±0.87^{d}	165.66±4.50^{cd}	0.28±0.06^{d}
90HPMC-10CMS	16.89±1.53^{c}	22.18±2.24^{c}	170.71±1.70^{cd}	168.33±8.02^{cd}	0.59±0.48^{d}
80HPMC-20CMS	19.35±1.58^{bc}	25.88±1.90^{bc}	172.48±2.01^{cd}	183.00±2.64^{bc}	1.18±0.34^{d}
70HPMC-30CMS	20.51±1.53^{b}	28.39±2.52^{b}	222.68±4.73^{a}	200.33±9.33^{ba}	5.57±1.65^{cd}
70HPMC-30CMS-30ZnONPs	18.84±1.02^{b}	25.51±0.53^{bc}	203.62±1.19^{b}	180.33±2.30^{bc}	20.05±5.94^{b}
70HPMC-30CMS-50ZnONPs	17.76±3.60^{bc}	20.14±0.59^{c}	178.05±4.36^{c}	157.33±2.08^{d}	36.78±5.57^{a}
Control (without film)			555.23±6.40		

Different superscript letters in the same column are significantly different ($p < 0.05$), based on Tukey's test.

4.1.7 Whiteness index (WI)

The WI values for all films were displayed in Table 4.6. The HPMC film showed the most transparent appearance with the WI value of 0.86%. However, the introduction of CMS resulted in a gradual increase in WI when CMS contents increased. The results may be due to the porous morphology, which resulted from the difference in refractive index between the polymer phase and the air phase in these materials as corresponded to HPMC microporous photophobic film [99]. As expected, the incorporation of ZnONPs into the 70HPMC-30CMS blended film resulted in an obvious rise in WI compared to the control film (7 0 HPMC-3 0 CMS). This is due to high whiteness properties of ZnONPs, particularly in the case of the film containing 70HPMC-30CMS-50ZnONPs.

Table 4.6 WI of various HPMC films with different contents of CMS and ZnONPs

Samples	WI
HPMC	10.86
90HPMC-10CMS	12.72
80HPMC-20CMS	12.71
70HPMC-30CMS	13.77
70HPMC-30CMS-30ZnONPs	77.46
70HPMC-30CMS-50ZnONPs	86.58

4.1.8 Antibacterial activity

For various HPMC-based films, the antibacterial activity against both Gram-positive *S. aureus* and Gram-negative *E. coli* bacteria was evaluated. Inhibition zones for various HPMC films are illustrated in Table 4.7 and Figure 4.8.

The antibacterial activity of HPMC, 90HPMC-10CMS, 80HPMC-20CMS and 70HPMC-30CMS films revealed non-inhibition zones against both *S. aureus* and *E. coli* bacteria indicating no antibacterial activity. Furthermore, the incorporation of ZnONPs into the 70HPMC-30CMS film enhanced its antibacterial effectiveness against *S. aureus* and *E. coli.* The 70HPMC-30CMS-30ZnONPs and 70HPMC-30CMS-50ZnONPs films exhibited a zone of inhibition against *S. aureus* and *E. coli* with respective diameters of 22.3 and 17.7 mm and 23.5 and 19.1 mm, respectively. As the concentration of ZnONPs in the 70HPMC-30CMS composite film increased, it was observed that the antibacterial activity of the 70HPMC-30CMS-ZnONPs films was enhanced. Additionally, when considering antibacterial efficacy, the *S. aureus* strain exhibited a more obvious inhibition zone when compared to the *E. coli* strain. The obtained results can be attributed to differences in the structures of bacterial cell walls. The cell walls of Gram-positive bacteria are made up of dense peptidoglycans, while the cell walls of Gram-negative bacteria are more

complicated and make it harder for antimicrobial agents to get into the bacterial cell [100]. Other studies have also reported significant findings concerning bionanocomposite hydrogels composed of PVA, CMC and ZnONPs [101]. It was possible to note that the interaction between nanoparticles and the cell membrane led to membrane damage and resulted in cell death.

Table 4.7 *S. aureus* and *E. coli* inhibition zones for HPMC, various HPMC-CMS, 70HPMC-30CMS-30ZnONPs and 70HPMC-30CMS-50ZnONPs films.

Samples	Zone of inhibition (mm)	
	S. aureus	*E. coli*
HPMC	Inactive	Inactive
90HPMC-10CMS	Inactive	Inactive
80HPMC-20CMS	Inactive	Inactive
70HPMC-30CMS	Inactive	Inactive
70HPMC-30CMS-30ZnONPs	22.3	17.7
70HPMC-30CMS-50ZnONPs	23.5	19.1

Films	HPMC	90HPMC-10CMS	80HPMC-20CMS	70HPMC-30CMS
S. aureus	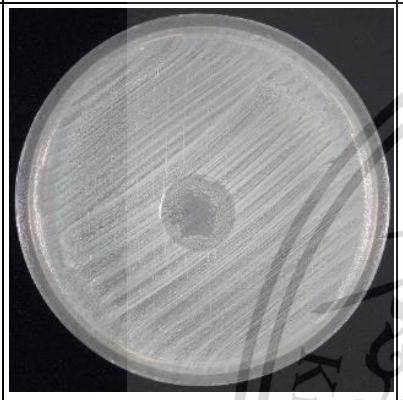			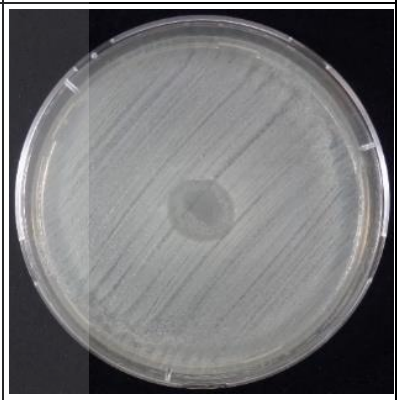
E. coli	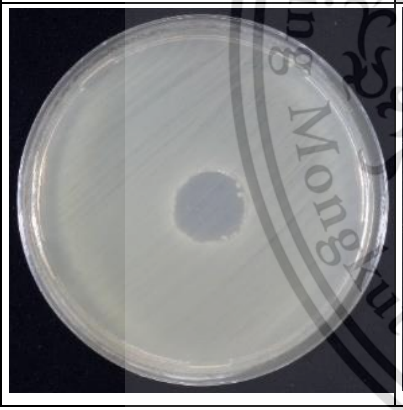			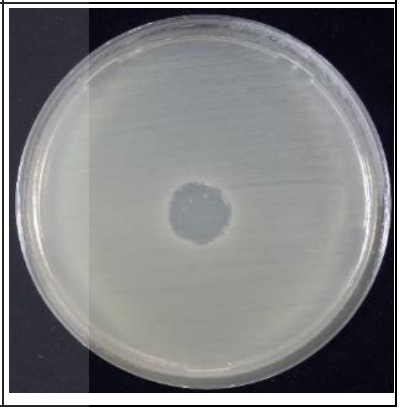

Figure 4.8 Inhibition zones of HPMC, 90HPMC-10CMS, 80HPMC-20CMS and 70HPMC-30CMS films.

Films	70HPMC-30CMS -30ZnONPs	70HPMC-30CMS -50ZnONPs
S. aureus	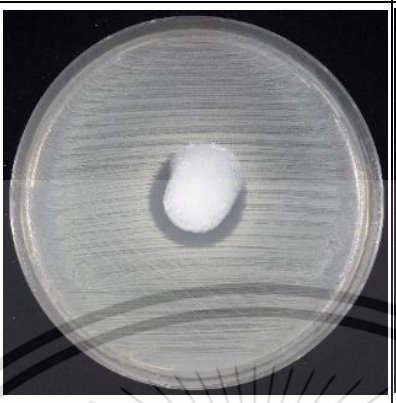	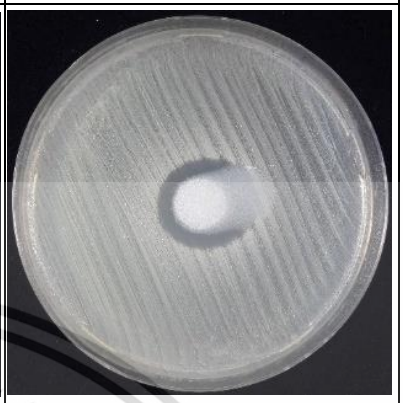
E. coli		

Figure 4.9 Inhibition zones of 70HPMC-30CMS-30ZnONPs and 70HPMC-30CMS-50ZnONPs films.

4.1.9 Cytotoxicity assay

The addition of ZnONPs at high content into dressing material may be to affect cause toxic to human cell so the 70HPMC-30CMS-ZnONPs nanocomposite films were evaluated the cell cytotoxicity by using the standard ISO 10993-5 method. The cytotoxicity and cell viability assays of control, HPMC, 70HPMC-30CMS, 70HPMC-30CMS-30ZnONPs, and 70HPMC-30CMS-50ZnONPs films were evaluated. HaCat cells were used in this study in order to determine the cytotoxicity of nanocomposite films. Cytotoxicity and cell viability were shown in Table 4.8 and Figure 4.9.

Generally, the standard values of cell viability provided over 80%, between 80% and 60%, between 60% and 40%, and below 40% indicated non-toxicity, slight toxicity, moderate toxicity, and severe toxicity to human cells, respectively [102]. Control (without film sample), HPMC and 70HPMC-30CMS films exhibited percentages of cytotoxicity at values of 5.52, 2.37, and 6.79, while percentages of cell viability showed values of 94.45, 97.59, and 93.21, respectively. The incorporation of ZnONPs, the cytotoxicity and the cell viability of 70HPMC-30CMS-ZnONPs films revealed that they were non-toxic to human cells, as evidenced by cell viability values exceeding 80% and cytotoxicity values falling below 20%. The results indicated that the nanocomposite films with high content of ZnONPs didn't cause cell toxicity.

Figure 4.10 Optical microscopy images (200X magnification) of the control, HPMC, 70HPMC-30CMS, 70HPMC-30CMS-30ZnONPs and 70HPMC-30CMS-50ZnONPs films.

Table 4.8 MTT assay results of HPMC, 70HPMC-30CMS, 70HPMC-30CMS-30ZnONPs and 70HPMC-30CMS-50ZnONPs films.

Samples	Cytotoxicity (%)	Cell viability (%)
HPMC	2.37±0.04^{c}	97.59
70HPMC-30CMS	6.79±0.10^{b}	93.21
70HPMC-30CMS-30ZnONPs	7.61±0.14^{b}	92.39
70HPMC-30CMS-50ZnONPs	13.08±0.51^{a}	86.92
Control	5.52±0.43	94.45

Different superscript letters in the same column are significantly different ($p < 0.05$), based on Tukey's test.

4.2 Characterization of modified 70HPMC-30CMS film with the addition of SA and GA.

The objective of this section was to enhance the properties of films composed of HPMC and CMS. An investigation was carried out to examine the impact of SA as the crosslinker and GA as the antibacterial agent on 70HPMC-30CMS film. The physicochemical properties of the modified 70HPMC-30CMS films were characterized by FTIR, SEM, XRD, water absorption, water solubility, WVTR, degree of swelling, gel fraction, mechanical properties. Moreover, antibacterial activity and cell cytotoxicity were also studied.

4.2.1 Possible interactions between HPMC, CMS, SA and GA

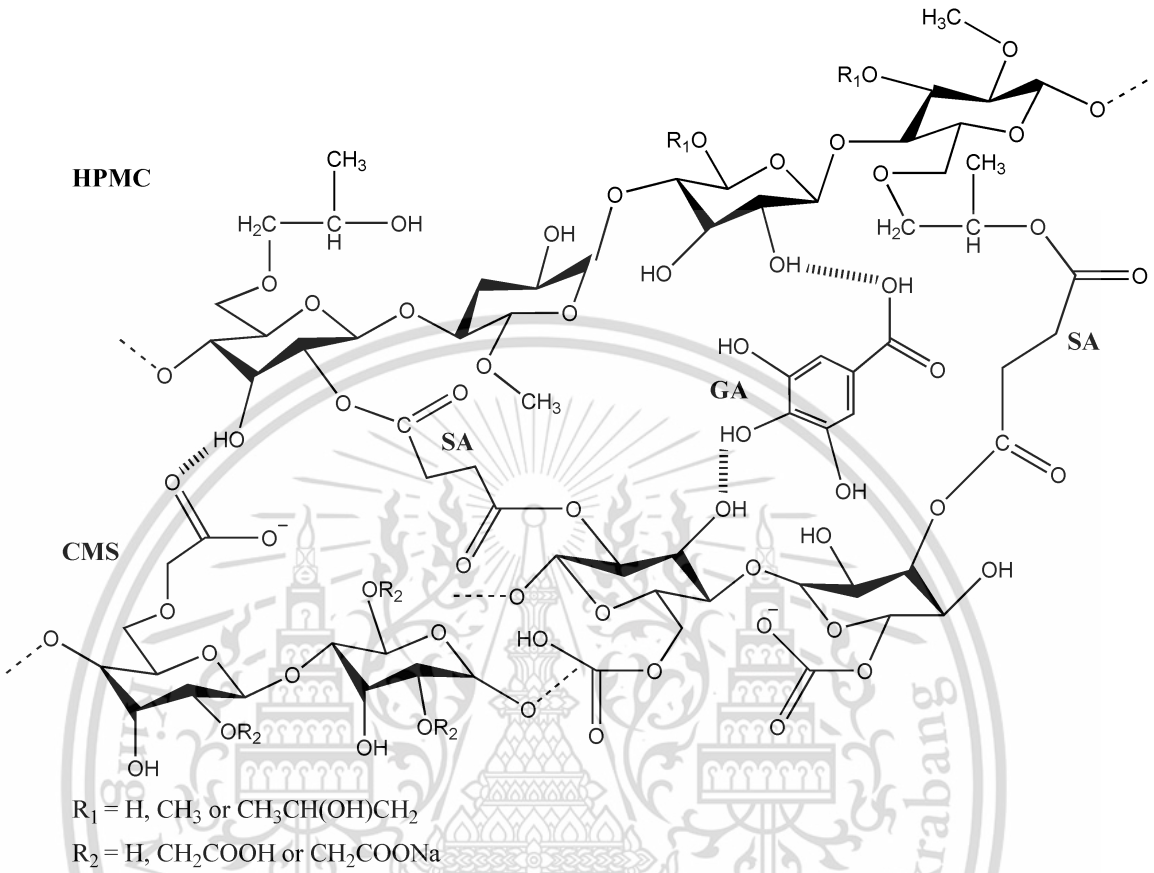

Figure 4.11 The schematic representation of possible interaction/reaction between HPMC, CMS, SA and GA.

Figure 4.10 is a schematic diagram illustrating the possible interaction or reaction occurred among HPMC, CMS, SA, and GA components. The HPMC and CMS functional groups contain many hydroxyl groups that can establish intermolecular interactions through hydrogen bonding. The formation of a covalent bond between the HPMC and CMS components of the film can be created through undergoing an esterification reaction with SA molecules, resulting in crosslinking process. In addition, GA has the ability to form hydrogen bonds with components of HPMC and CMS because the GA molecule contains several polar groups, including three hydroxyl groups and one carboxylic group.

4.2.2 FTIR-ATR

ATR spectrophotometer was used to examine the functional groups of different 70HPMC-30CMS porous films (Figure 4.11(a)). The ATR spectra of 70HPMC-30CMS exhibited strong peaks at 3374 cm^{-1}, 1597 cm^{-1}, and 1453 cm^{-1}. These peaks corresponded to the stretching of the O-H bond, the asymmetric stretching of the C=O bond, and the bending of the O-H bond, respectively [103]. They also exhibited the appearance of the characteristic overlapped peak between HPMC and CMS components.

The 70HPMC-30CMS-2.5SA film exhibited bands with comparable characteristics to those detected in the 70HPMC-30CMS film. An absorption peak at 1725 cm^{-1}, resulting from C=O stretching, was detected, indicating the possibility of a chemical interaction occurring between the acid and starch. The detected absorption band was caused by the creation of an ester bond as a consequence of the cross-linking reaction [104, 105]. The band characteristic of SA, which was identified at approximately 1679 cm^{-1} (Figure 4.11(d)), was ascribed to the C=O stretching of carboxylic groups. The band shifted to a higher wavenumber at 1725 cm^{-1} after the completion of the reaction; this corresponded to SA crosslinking on the agar/bacterial cellulose composite film, which introduced a new band at 1727 cm^{-1}, assigned to C=O stretching of the ester bond [32]. Furthermore, the detection of the shifted peaks of O-H stretching and O-H bending at 3374 cm^{-1} and 1453 cm^{-1} to lower wavenumbers of 3358 cm^{-1} and 1451 cm^{-1} was attributed to the formation of new hydrogen bonds between the two components [73].

The spectra of various 70HPMC-30CMS-2.5SA-GA films exhibited bands that were similar to those observed in 70HPMC-30CMS-2.5SA film. The primary unique peak positions of GA (Figure 4.11(d)) were identified at 3269, 1680, and 1605 cm^{-1}, corresponding to O-H stretching, C=O stretching, and C=C stretching, respectively [106]. The typical peak positions of GA may disappear due to overlap between the presence of antibacterial crosslinked films and GA bands.

Furthermore, the presence of the GA component in the 70HPMC-30CMS-2.5SA-GA films was confirmed by the detection of the C=O stretching band at 1710 cm^{-1} in Figures 2(a)-2(b) [107]. Additionally, it was found that the utilization of GA resulted in the appearance of the characteristic peak position at around 1238 cm^{-1} (Figure 4.11(c)). This peak was attributed to the C-O stretching vibration of the GA.

Moreover, the intensity of the bands at around 1710 and 1238 cm^{-1}, exhibited an increase as the GA contents, were raised. In addition, the shift of the observed peak towards lower wavenumber at around 3348 cm^{-1} in 70HPMC-30CMS-2.5SA-GA films with different GA concentrations might be due to the occurrence of new hydrogen bonding interactions between the polymer matrix and GA molecule.

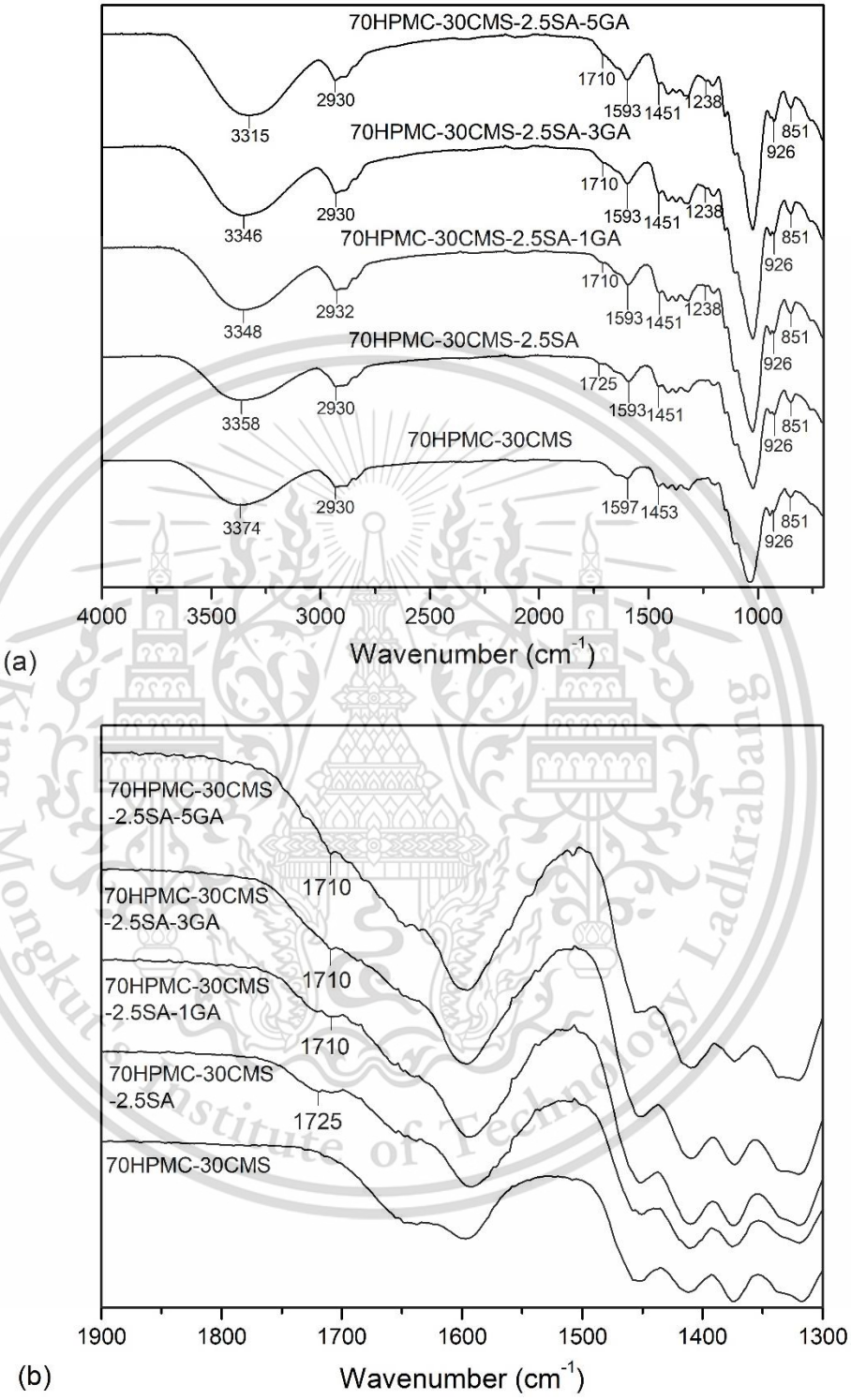

Figure 4.12 FT-IR spectra of 70HPMC-30CMS, 70HPMC-30CMS-2.5SA and various 70HPMC-30CMS-2.5SA-GA films incorporated with different contents of GA.

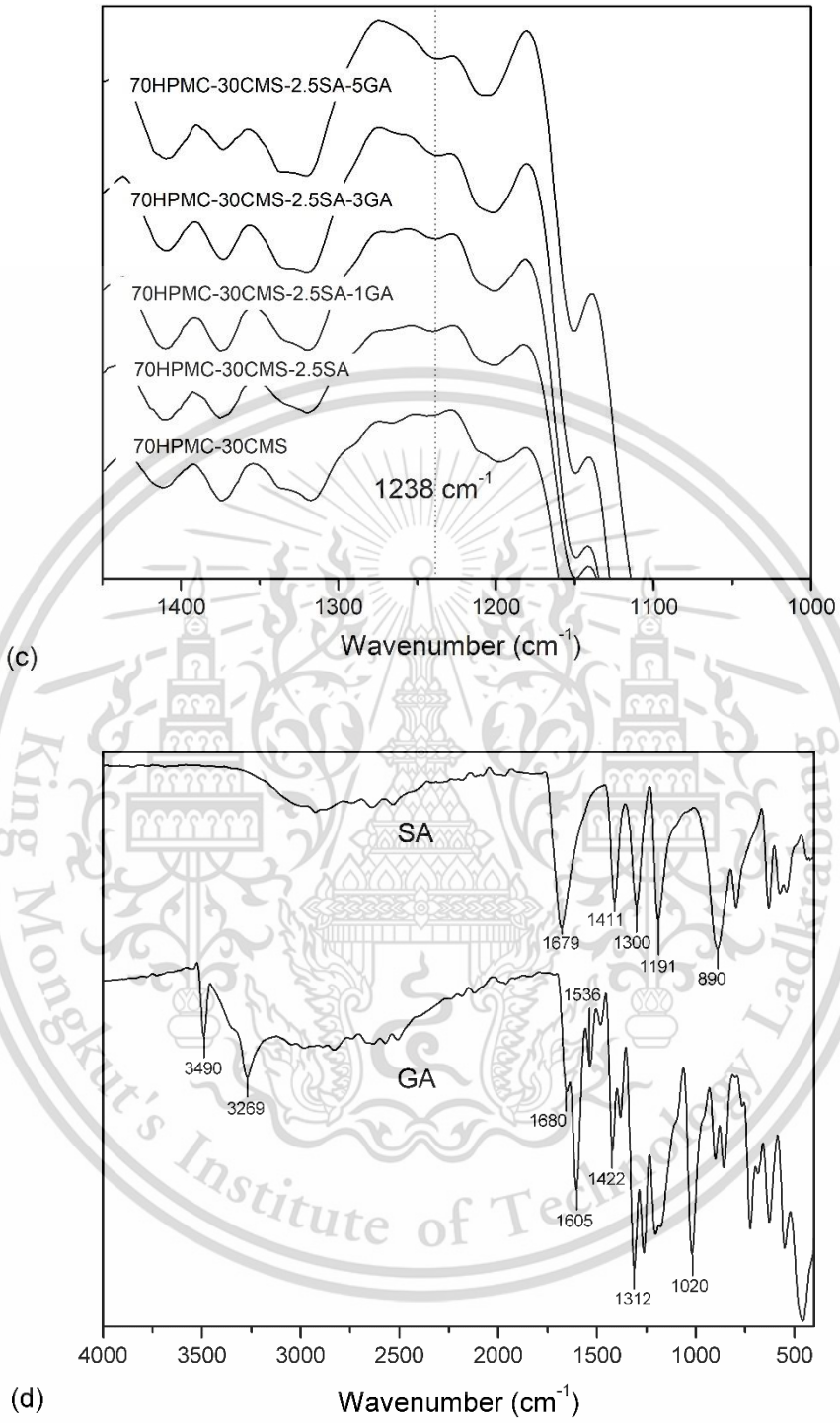

Figure 4.12 (continued) FT-IR spectra of 70HPMC-30CMS 70HPMC-30CMS-2.5SA and various 70HPMC-30CMS-2.5SA-GA films incorporated with different contents of GA.

4.2.3 X-ray diffraction

The XRD patterns and crystallinity percentages for 70HPMC-30CMS, 70HPMC-30CMS-2.5SA, and 70HPMC-30CMS-2.5SA-GA films with different amounts of GA can be observed in Figure 4.12 and Table 4.9. The XRD diffractograms of the different samples revealed the existence of broad peaks at 2θ values of 7.6° and 20.5°, which related to the semi-crystalline nature of HPMC [77].

Specifically, the use of SA as a crosslinking agent for 70HPMC-30CMS-2.5SA film showed no variation in the degree of crystallinity when compared to 70HPMC-30CMS film. The result can be attributed to low content of SA, which exhibited no impact on the crystallization ability of HPMC. Various 70HPMC-30CMS-2.5SA-GA films also exhibited two wider peaks at 2θ = 7.6° and 20.5°, without the diffracted peak caused by the GA molecule. [107]. The obtained result was consistent with the XRD pattern of PVA-based films including tannic acid (TA), as it revealed the absence of the characteristic peak of TA. This suggests that TA is uniformly dispersed within the PVA matrix and that there are strong interactions between PVA and TA [108]. The XRD pattern of ferulic acid (FA)-loaded polycaprolactone and collagen hydrolysate nanofibers also showed that FA was in the amorphous state, resulting in the loss of characteristic peak of FA [109].

By comparison between 70HPMC-30CMS-2.5SA-GA films and 70HPMC-30CMS-2.5SA film, it was found that the addition of GA led to no difference in percentage of crystallinity (Table 4.9). Furthermore, the 70HPMC-30CMS-2.5SA-GA films exhibited a similar amount of crystallinity as the GA content was raised. The observed results may be due to the crystalline structure of GA did not affect the crystallization process of HPMC.

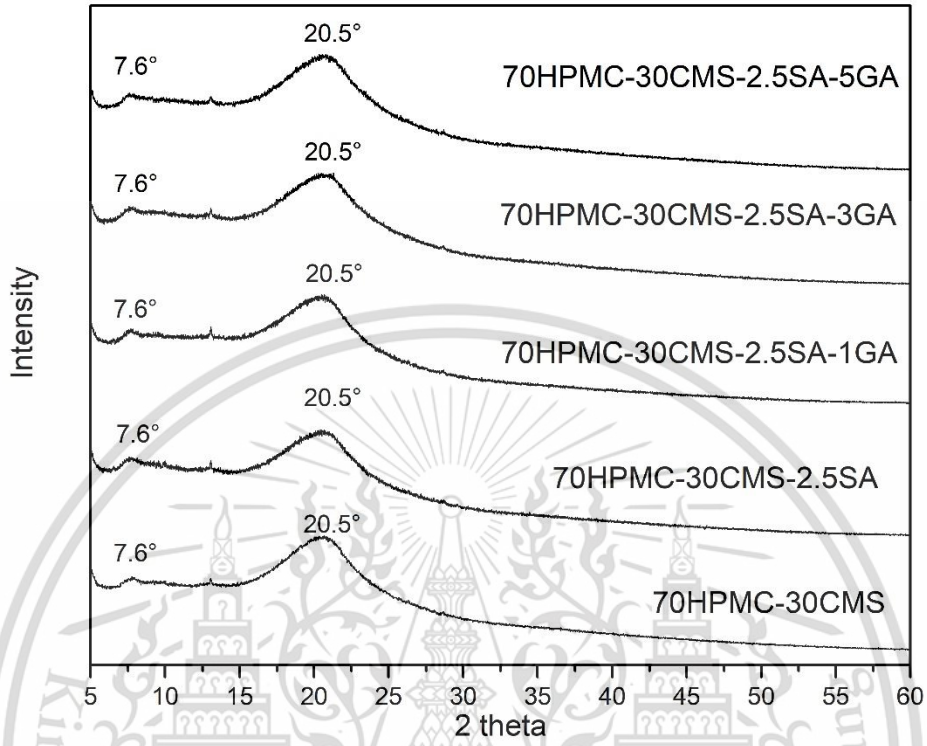

Figure 4.13 XRD patterns of 70HPMC-30CMS 70HPMC-30CMS-2.5SA and various 70HPMC-30CMS-2.5SA-GA films incorporated with different contents of GA.

Table 4.9 Percentage of crystallinity of 70HPMC-30CMS, 70HPMC-30CMS-2.5SA and various 70HPMC-30CMS-2.5SA-GA films incorporated with different contents of GA.

Films	Crystallinity (%)
70HPMC-30CMS	9.21
70HPMC-30CMS-2.5SA	9.19
70HPMC-30CMS-2.5SA-1GA	8.17
70HPMC-30CMS-2.5SA-3GA	8.45
70HPMC-30CMS-2.5SA-5GA	8.86

4.2.4 Morphology

The morphology of different cast films was analyzed using SEM. The 70HPMC-30CMS film, depicted in Figure 4.13(a), exhibited a porous structure with a smooth surface. The presence of pores could be attributed to the salting-out phenomenon of sodium salts of CMS components from HPMC solutions [103, 110]. When the addition of SA, 70HPMC-30CMS-2.5SA film (Figure 4.13(b)) exhibited the remained porous structure with the reduced pore sizes. The result may be due to the esterification between CMS and HPMC by SA crosslinker, resulting in more compact structure and lesser pore size than 70HPMC-30CMS film.

In addition, the cross-sectional microstructure of various 70HPMC-30CMS-2.5SA-GA films (Figures 4.13(c)-4.13(e)) displayed a porous structure without the appearance of GA particles. The cross-sectional morphology of the 70HPMC-30CMS-2.5SA-5GA film (Figure 4(e)) exhibited the reduced pore size in comparison to the 70HPMC-30CMS-2.5SA-1GA and 70HPMC-30CMS-2.5SA-3GA films. It may have been caused by the hydrophilic nature of GA molecules, which improved the phase compatibility of HPMC, CMS, and GA constituents.

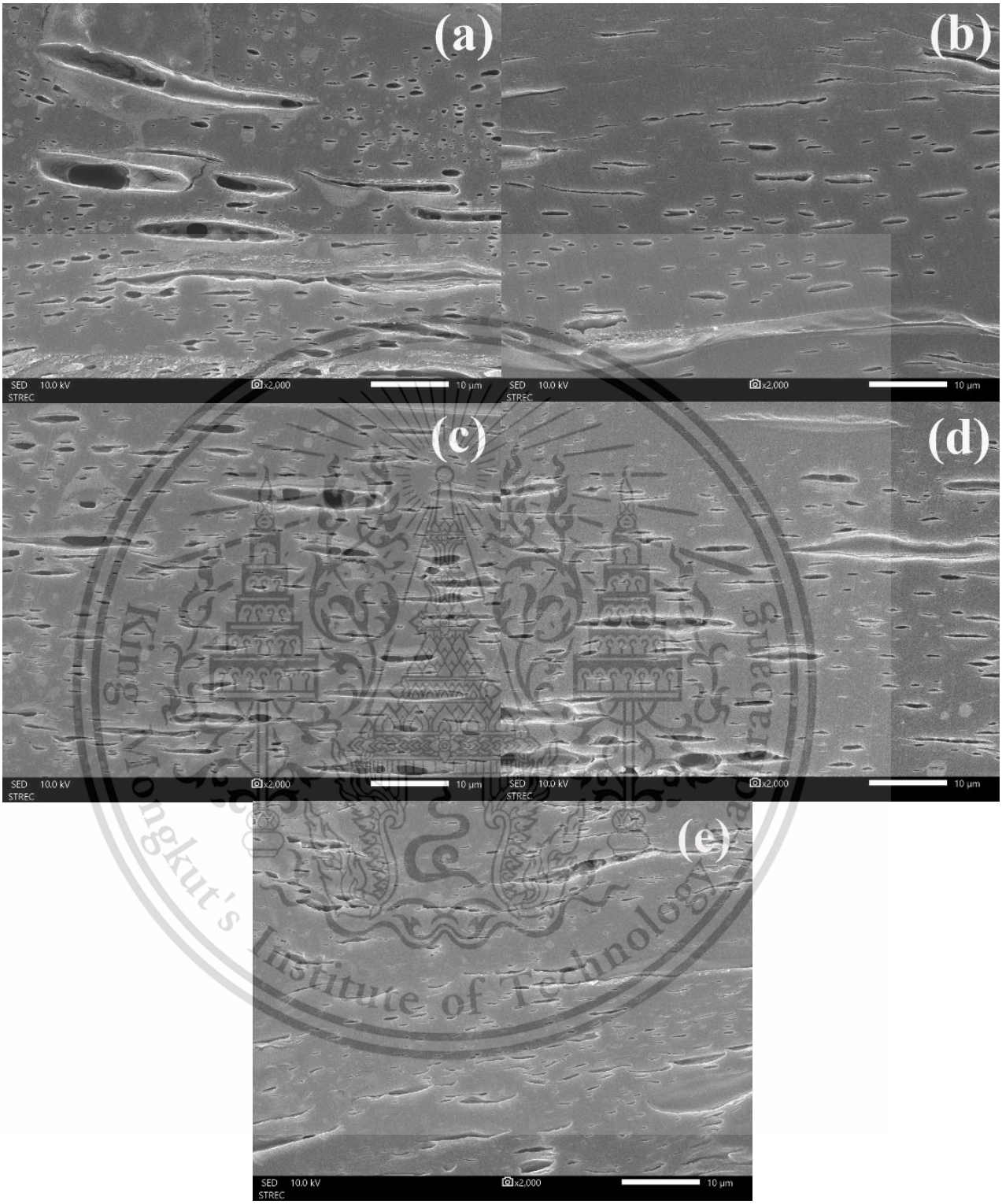

Figure 4.14 SEM micrographs at 2000X of modified 70HPMC-30CMS films (a); 70HPMC-30CMS (b), 70HPMC-30CMS-2.5SA (c), 70HPMC-30CMS-2.5SA-1GA (d), 70HPMC-30CMS-2.5SA-3GA, and (e) 70HPMC-30CMS-2.5SA-5GA.

4.2.5 Mechanical properties

Mechanical properties of 70HPMC-30CMS, 70HPMC-30CMS-2.5SA and different 70HPMC-30CMS-2.5SA-GA films with various contents of GA are shown in Table 4.10. Figure 4.13 (a) shows that the porous structure of blended film caused the lowest stress at maximum load, Young's modulus, and strain at maximum load (Table 4.10).

The stress at maximum load and Young's modulus for 70HPMC-30CMS-2.5SA film was similar to those of 70HPMC-30CMS film, whereas the strain at maximum load showed a significant increase. It may be due to the diminished intermolecular interaction between HPMC and CMS following the crosslinking reaction, as indicated by the presence of an ester bond in the FTIR analysis. Another possible explanation is the plasticizing impact of SA or the partial crosslinking, which increases the mobility of the polymer chains. A similar observation was reported regarding potato starch/chitosan films that were crosslinked with citric acid. This crosslinking decreased the interaction between the macromolecules, leading to the increase of elongation at break [111].

Furthermore, in comparison to 70HPMC-30CMS-2.5SA film, a significant rise in both stress at maximum load and Young's modulus was observed in 70HPMC-30CMS-2.5SA-GA films. These films exhibited a significantly reduced strain at maximum load in comparison to 70HPMC-30CMS-2.5SA film. As verified by FTIR analysis, this may be the result of an increase in hydrogen bonds between HPMC, CMS, and GA components and chemical structure of benzene ring in GA (Figure 4.10), which decreased chain mobility. Similarly, the inclusion of GA in the PVA/poly (hexamethylene guanidine)/GA composite hydrogel film resulted in the enhancement of tensile strength. This improvement can be attributed to the increased hydrogen bonding between the hydrophilic groups presented in both PVA and GA [29].

Moreover, the inclusion of the aromatic ring of the GA molecule in the thermoplastic cassava starch film can potentially improve the mechanical strength of starch film by acting as a reinforcing filler [112]. The impact of increasing GA content did

not produce a statistically significant difference in the mechanical properties of 70HPMC-30CMS-2.5SA-GA films due to the similar crystallinity percentage of 70HPMC-30CMS-2.5SA-GA films (Table 4.9).

Table 4.10 Mechanical properties of 70HPMC-30CMS, 70HPMC-30CMS-2.5SA and various 70HPMC-30CMS-2.5SA-GA films incorporated with different contents of GA.

Films	Stress at maximum load (MPa)	Young's modulus (MPa)	Strain at maximum load (%)
70HPMC-30CMS	5.03±0.52^{a}	78.60±7.16^{a}	8.89±1.28^{a}
70HPMC-30CMS-2.5SA	5.55±0.43^{a}	78.64±7.20^{a}	11.32±1.63^{b}
70HPMC-30CMS-2.5SA-1GA	9.31±0.64^{b}	156.65±11.24^{b}	10.21±1.61^{ab}
70HPMC-30CMS-2.5SA-3GA	9.46±0.63^{b}	167.37±15.45^{b}	10.66±1.06^{ab}
70HPMC-30CMS-2.5SA-5GA	9.61±0.73^{b}	168.60±14.93^{b}	10.27±1.59^{ab}

Different superscript letters in the same column are significantly different ($p < 0.05$), based on Tukey's test

4.2.6 Swelling degree, gel fraction, water solubility, water absorption and WVTR

The efficacy of the wound dressing films was evaluated by analyzing swelling degree, gel fraction, water solubility, water absorption, and WVTR. Typically, a wound dressing film should facilitate the maintenance of moisture at the site, allow for the passage of air, and absorb excess exudate. The hydrophilic properties of 70HPMC-30CMS, 70HPMC-30CMS-2.5SA and various 70HPMC-30CMS-2.5SA-GA films are shown in Table 4.11.

When comparing 70HPMC-30CMS and 70HPMC-30CMS-2.5SA films, the 70HPMC-30CMS-2.5SA film showed a greater swelling degree and gel fraction compared to the

70HPMC-30CMS film. This can be attributed to the loss of hydroxyl groups during esterification, which caused the formation of a crosslinked structure with increased molecular spacing. This crosslinked structure enhanced the water absorbency of the film.

Similarly, the chemical crosslinking of carboxyl-modified PVA/CS showed an increase in the extent of swelling [113]. This was probably because of the increased molecular spacing and decreased hydrogen bonding between polymer structure caused by the crosslinking reaction. As a result, the process of esterification crosslinking led to a reduction in the water solubility, water absorption, and WVTR of the 70HPMC-30CMS-2.5SA film.

The decrease of water absorption capacity was observed in 70HPMC-30CMS-2.5SA film when compared to 70HPMC-30CMS film. This was due to the reduction in porous structure after esterification reaction (as shown in Figure 4.13), leading to a decrease in water absorption capacity. The nanocomposite scaffolds made from carboxymethyl cellulose and crosslinked by CA showed the same outcome [114].

In addition, the 70HPMC-30CMS-2.5SA-GA films exhibited greater swelling degree, gel fraction, water solubility, water absorption, and WVTR compared to 70HPMC-30CMS-2.5SA film. This can be attributed to the increased hydrophilicity of GA, which contains a significant number of hydroxyl and carboxylic groups in its molecular structure. It is worth noting that hydrogen bond formation was also observed.

For 70HPMC-30CMS-2.5SA-GA films incorporated with different contents of GA, it was observed that the increase in GA content resulted in a decrease in swelling degree, gel fraction, water solubility, water absorption, and WVTR. It was possibly because the increase in GA content resulted in the enhancement of hydrogen bonds among HPMC, CMS, and GA.

It was mentioned that the incorporation of GA into PVA/tragacanth gum blend films resulted in the reduction of WVTR due to the formation of denser structure in the

composite films. An increase in GA concentration resulted in the decrease in hydrophilicity [115]. Furthermore, WVP of chitosan/gelatin, caseinate/guar gum, and corn starch/pullulan films decreased when GA was added. This decrease was caused by the creation of hydrogen bonds between the polymer matrix and GA, which led to a reduction in the amount of free space inside the polymer matrix [30, 116, 117].

Table 4.11 Swelling degree, gel fraction, water solubility, water absorption and WVTR of various 70HPMC-30CMS films.

Films	Swelling degree (%)	Gel fraction (%)	Water solubility (%)	Water absorption (%)	WVTR (g m^{-2} day^{-1})
Control (without film)					559.58±10.00
70HPMC-30CMS	119.33±9.86^{a}	5.67±1.65^{a}	89.00±2.00^{a}	129.33±1.15^{a}	426.91±6.13^{a}
70HPMC-30CMS-2.5SA	200.33±10.26^{b}	28.18±1.52^{b}	62.33±4.72^{c}	93.33±4.72^{c}	367.28±7.46^{d}
70HPMC-30CMS-2.5SA-1GA	231.00±7.21^{c}	38.16±1.41^{c}	72.00±1.00^{b}	124.00±2.00^{ab}	407.38±4.40^{b}
70HPMC-30CMS-2.5SA-3GA	222.00±8.71^{bc}	29.89±1.77^{b}	64.67±5.13^{bc}	119.00±1.00^{b}	393.38±1.97^{bc}
70HPMC-30CMS-2.5SA-5GA	218.00±4.35^{bc}	26.90±0.46^{b}	63.00±3.61^{c}	98.33±2.08^{c}	384.39±4.87^{c}

Different superscript letters in the same column are significantly different ($p < 0.05$), based on Tukey's test

4.2.7 Antibacterial activity

Figure 4.14 displays the bacterial growth plate, while Table 4.12 presents the bacterial reduction percentage for the control, 70HPMC-30CMS, 70HPMC-30CMS-2.5SA, and 70HPMC-30CMS-2.5SA-GA films. The results assessed the antibacterial efficacy of the films against Gram-positive bacteria *S. aureus* and Gram-negative bacteria *E. coli*. As expected, both the control (distilled water) and 70HPMC-30CMS film showed a decrease in antibacterial efficacy, with reduction values of -12.88, -9.28, -8.07, and -5.55 against *S. aureus* and *E. coli*, respectively, after 24 hours of incubation. This result indicated that these films had no antibacterial effect. However, the 70HPMC-30CMS-2.5SA film (Figure 4.14(a)) demonstrated strong antibacterial activity against gram-positive and gram-negative bacteria, with a bacterial reduction of 100% against *S. aureus* and a reduction of 59.91% against *E. coli*. Huang, S. observed that SA suppressed the antibacterial efficacy against *S. aureus* and *P. fluorescens* (gram-negative bacteria), explaining that the two bacteria were damaged by the release of nucleic acids and proteins from their cells. Furthermore, SA exhibited antibacterial properties against gram-positive bacteria such as *M. luteus*, as well as gram-negative bacteria including *L. hongkongensis* and *E. coli* [118-120].

It was observed that the antibacterial effectiveness was significantly greater against gram-positive bacteria (*S. aureus*) than against gram-negative bacteria (*E. coli*). This variation was related to the different cell wall compositions of the two types of bacteria. Gram-positive bacteria consisting of complex peptidoglycan exhibited a greater capacity for cell penetration, whereas complex gram-negative bacteria possessed more versatile cell walls [121].

As shown in Table 4.11, it was evident that the number of viable cells in 70HPMC-30CMS-2.5SA-GA films containing various quantities of GA decreased after 24 hours of contact time. The disc plate analysis, as illustrated in Figures 4.14(a)-4.14(b) exhibited no bacterial growth for both gram-positive and gram-negative bacteria. This

indicated that the 70HPMC-30CMS-2.5SA-GA films exhibited remarkable antimicrobial activity and were suitable for use as wound dressings.

Table 4.12 Bacterial reduction percentage of the control and various 70HPMC-30CMS films against *S.aureus* and *E.coli*.

Films	*S. aureus*			*E. coli*		
	Surviving cells (Log CFU/ml) after 0 h	Surviving cells (Log CFU/ml) after 24 h	Bacterial reduction (%)	Surviving cells (Log CFU/ml) after 0 h	Surviving cells (Log CFU/ml) after 24 h	Bacterial reduction (%)
Control (Distilled water)	6.52±0.04	7.36±0.05	-12.88	6.69±0.05	7.23±0.05	-8.07
70HPMC-30CMS	6.51±0.01	7.12±0.06	-9.28	6.70±0.01	7.07±0.06	-5.55
70HPMC-30CMS-2.5SA	5.77±0.02	0.00±0.00	100	6.15±0.04	2.47±0.01	59.91
70HPMC-30CMS-2.5SA-1GA	6.40±0.03	0.00±0.00	100	6.44±0.02	0.00±0.00	100
70HPMC-30CMS-2.5SA-3GA	6.39±0.06	0.00±0.00	100	6.43±0.04	0.00±0.00	100
70HPMC-30CMS-2.5SA-5GA	6.39±0.06	0.00±0.00	100	6.16±0.03	0.00±0.00	100

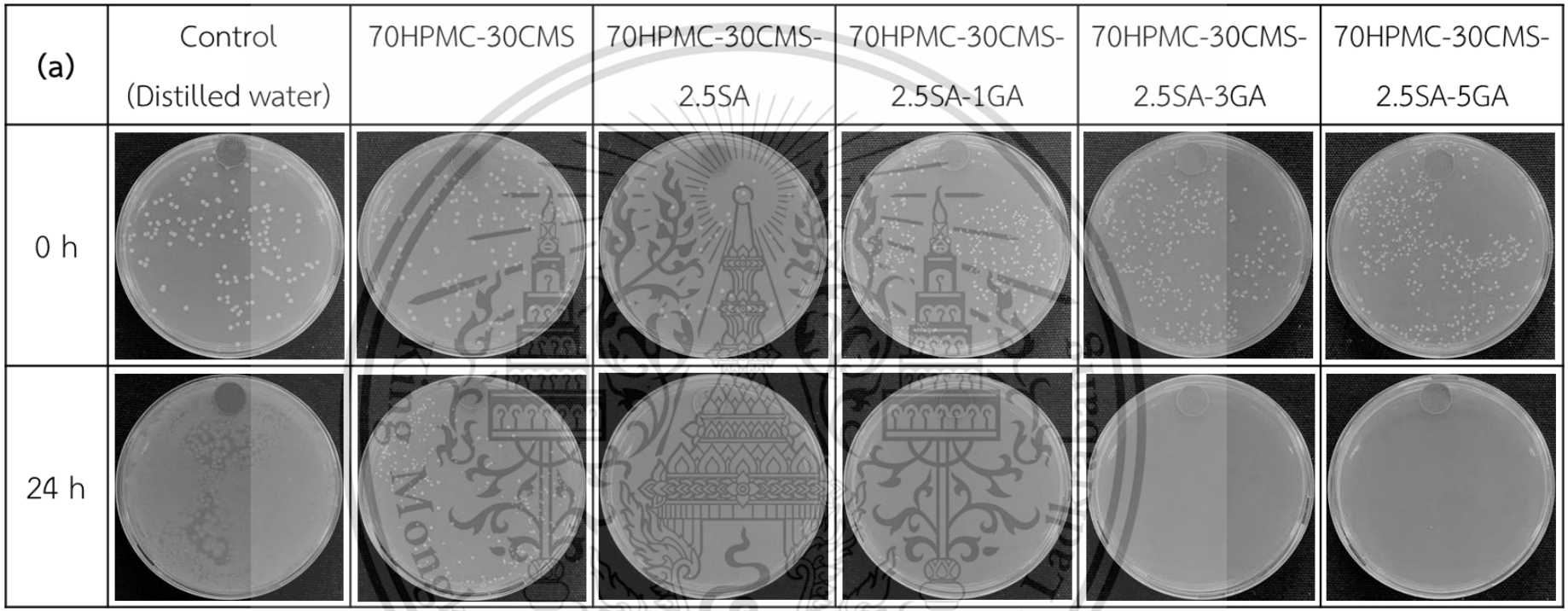

Figure 4.15 Antibacterial activity of the control and various 70HPMC30CMS films total bacterial colonies counting for (a) *S. aureus* and (b) *E. coli* after the contacting time at 0 and 24 hours

(b)	Control (Distilled water)	70HPMC-30CMS	70HPMC-30CMS-2.5SA	70HPMC-30CMS-2.5SA-1GA	70HPMC-30CMS-2.5SA-3GA	70HPMC-30CMS-2.5SA-5GA
0 h	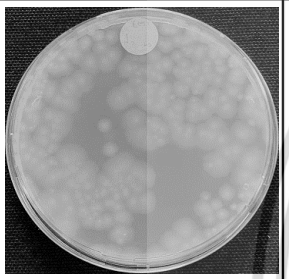		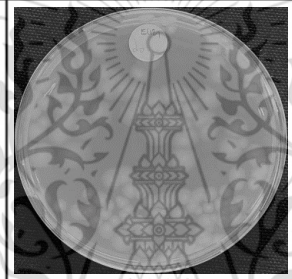		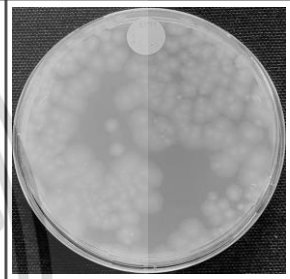	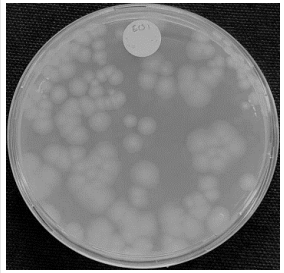
24 h	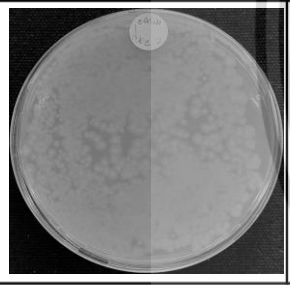	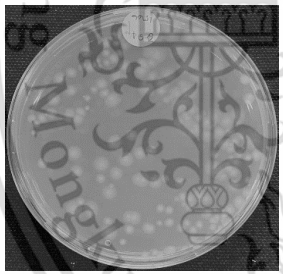		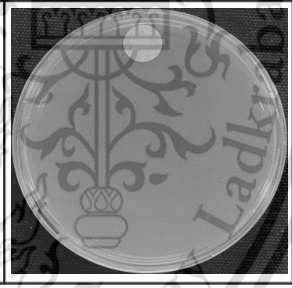	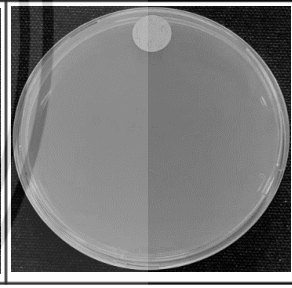	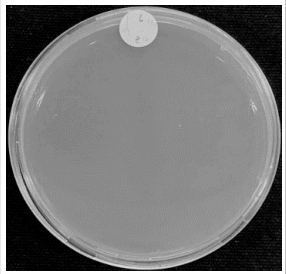

Figure 4.15 (Continued) Antibacterial activity of the control and various 70HPMC30CMS films total bacterial colonies counting for (a) *S. aureus* and (b) *E. coli* after the contacting time at 0 and 24 hours

4.2.8 Cytotoxicity assay

The MTT assay was used to investigate the cytotoxicity of various 70HPMC-30CMS-2.5SA-GA films, with HaCat cells. The cytotoxicity and cell viability values for the control, 70HPMC-30CMS-2.5SA, and 70HPMC-30CMS-2.5SA-1GA films were similar (Table 4.13 and Figure 4.15), which showed that these films were not harmful to human cells. The cytotoxicity values of the control, 70HPMC-30CMS-2.5SA, and 70HPMC-30CMS-2.5SA-1GA films were 3.55%, 0.42%, and 3.31%, respectively.

Nevertheless, the 70HPMC-30CMS-2.5SA-GA films with GA contents of 3 and 5 wt% exhibited significant cytotoxicity values of 31.16 and 62.47%, respectively. As to the ISO 10993-5 standard, cell viability values over 80%, between 80% and 60%, between 60% and 40%, and below 40% indicated non-toxicity, slight toxicity, moderate toxicity, and severe toxicity to human cells, respectively [102]. The 70HPMC-30CMS-2.5SA-3GA film showed a cell viability value of 68.84%, indicating the slight harm to human cells. However, the use of 5wt% GA resulted in a reduced cell viability value of 37.53%, suggesting moderate harm to human cells. All findings indicated that 70HPMC-30CMS-2.5SA-1GA film was appropriate for the application of wound dressing.

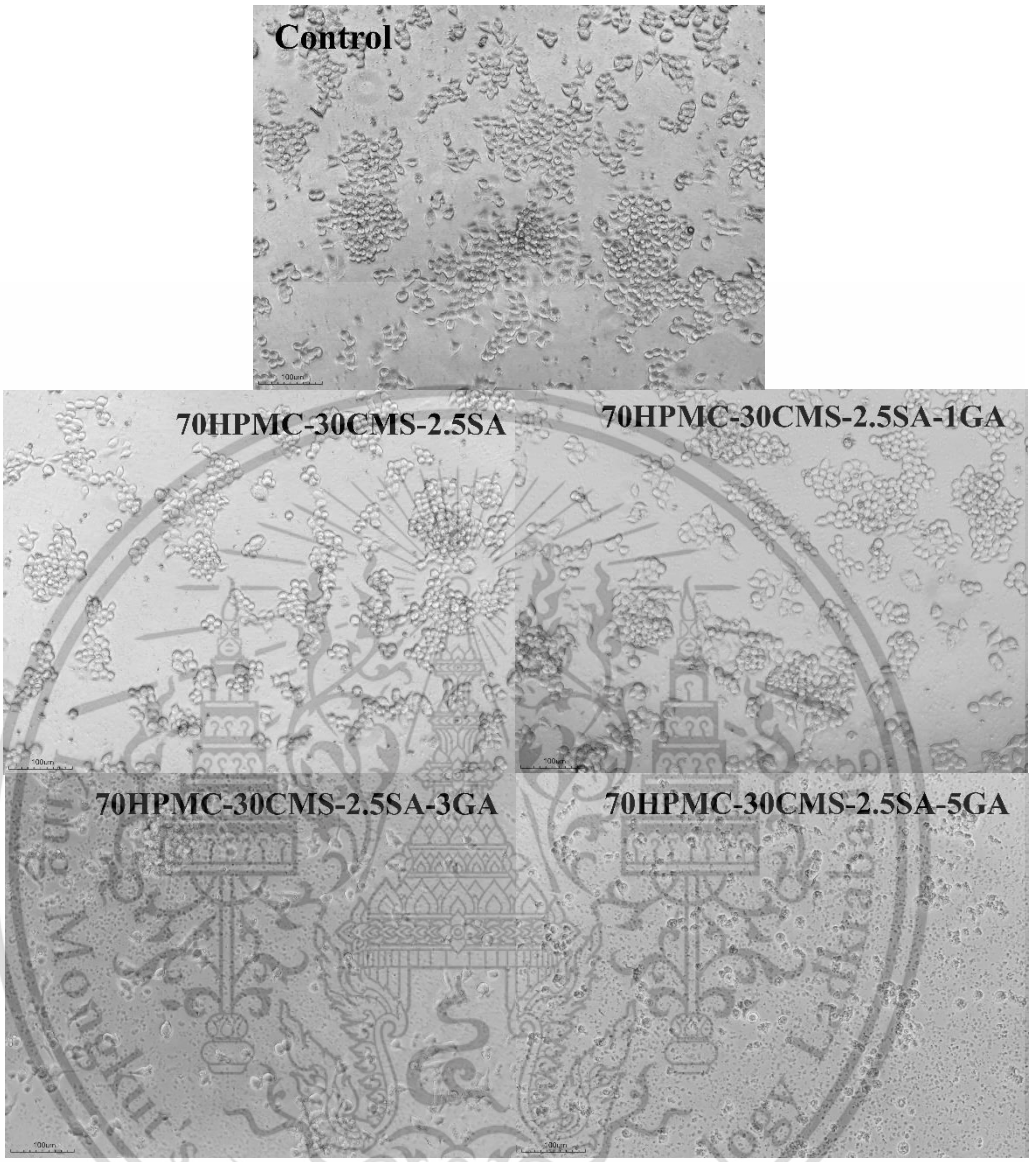

Figure 4.16 Optical microscopy images (100X magnification) of HaCat cells incubated after 4 h of 70HPMC-30CMS-2.5SA and various 70HPMC-30CMS-2.5SA-GA films.

Table 4.13 MTT assay results of the control and different 70HPMC-30CMS films.

Samples	Cytotoxicity (%)	Cell viability (%)
Control	5.52	94.45
70HPMC-30CMS	6.79	93.21
70HPMC-30CMS-2.5SA	0.42	99.58
70HPMC-30CMS-2.5SA-1GA	3.31	96.69
70HPMC-30CMS-2.5SA-3GA	31.16	68.84
70HPMC-30CMS-2.5SA-5GA	62.47	37.53

Chapter 5

Conclusions and suggestions

5.1 Conclusions

This research was divided into two parts. The first part was the preparation and characterization of modified HPMC film with the addition of CMS (i.e., 10, 20, and 30wt%) using ZnONPs (30 and 50wt%) as the antibacterial agent. The second part was the improvement of 70HPMC-30CMS film, using SA (2.5wt%) as the crosslinker and GA (1, 3 and 5wt%) as the antibacterial agent.

5.1.1 Modification of HPMC film by CMS and ZnONPs

5.1.1.1 For HPMC-CMS blended films, the new IR absorption bands at 1155 cm^{-1} was found, confirmed the presence of CMS. The FTIR spectra of blended HPMC-CMS films showed the shifted peak position of O-H stretching and O-H bending to lower wavenumbers. For 70HPMC-30CMS-ZnONPs nanocomposite films, the O-H bending peak was also shifted to lower wavenumbers.

5.1.1.2 For XRD analysis, the addition of CMS caused the reduction of percentage of crystallinity, especially in 70HPMC-30CMS film. The percentage of crystallinity of the 70HPMC-30CMS-ZnONPs nanocomposite films also decreased drastically compared to 70HPMC-30CMS film, while the difference in ZnONPs contents did not affect the crystallinity percentage.

5.1.1.3 For morphology, HPMC film showed rough surface, while CMS film presented smooth surface. However, HPMC-CMS films with different CMS contents displayed remarkable pore characteristics. The surface morphology of 70HPMC-30CMS-30ZnONPs and 70HPMC-30CMS-50ZnONPs films showed rough surface and porous structure with good ZnONPs dispersion into the polymer matrix. The increased concentration of ZnONPs also caused more rough surface.

5.1.1.4 HPMC film exhibited the highest stress at maximum load and Young's modulus. However, HPMC-CMS blended films showed the significant decrease in stress

at maximum load, Young's modulus, and strain at maximum load, especially when CMS content increased. The addition of ZnONPs to 70HPMC-30CMS film also showed the decrease of stress at maximum load and Young's modulus.

5.1.1.5 HPMC film demonstrated the lowest water absorption and WVTR, whereas the addition of CMS resulted in the increase of water absorption and WVTR. Moreover, the water absorption and WVTR of HPMC-CMS blended films increased when CMS content increased. Nevertheless, the reduction of water absorption and WVTR was detected in 70HPMC-30CMS-ZnONPs nanocomposite films, especially when ZnONPs concentration was increased.

5.1.1.6 HPMC film revealed the lowest swelling degree while the addition of CMS into HPMC film exhibited the increase of swelling degree and gel fraction. The decrease of swelling degree was observed in 70HPMC-30CMS-ZnONPs nanocomposite films, especially when ZnONPs concentration was raised. The addition of ZnONPs in 70HPMC-30CMS-30ZnONPs and 70HPMC-30CMS-50ZnONPs films exhibited the increase of gel fraction.

5.1.1.7 The lowest WI was observed for HPMC film. However, the incorporation of CMS into HPMC film revealed a gradual increase in WI while higher WI was observed for HPMC-CMS films with the addition of ZnONPs.

5.1.1.8 HPMC-CMS films demonstrated no antibacterial activity. The films exhibited excellent antibacterial activity against both *S. aureus* and *E. coli* after the inclusion of ZnONP. Antibacterial activity was found to be significantly greater against *S. aureus* than *E. coli.*

5.1.1.9 From cytotoxicity test, 70HPMC-30CMS-ZnONPs nanocomposite films were not toxic to human (HaCat) cells.

5.1.1.10 In this investigation, 70HPMC-30CMS-30ZnONPs film exhibited the most favourable characteristics in terms of overall performance. These characteristics included the greatest WVTR, water absorption, swelling degree, mechanical strength, and antimicrobial properties.

5.1.2 Modification of 70HPMC-30CMS film with SA and GA.

5.1.1.1 For 70HPMC-30CMS films, the new IR absorption bands at 1725 cm^{-1} was found, confirming crosslinking reaction among HPMC, CMS and SA. The FTIR spectra of 70HPMC-30CMS-2.5SA film with the addition of GA also showed the shifted peak position of O-H stretching to lower wavenumbers.

5.1.1.2 For XRD analysis of 70HPMC-30CMS-2.5SA film, the addition of both SA and GA caused no impact on the crystallization of HPMC.

5.1.1.3 For the incorporation of SA, the surface morphology of 70HPMC-30CMS-2.5SA film also showed the porous structure with the reduced pore sizes. 70HPMC-30CMS-2.5SA-GA films with different GA contents also displayed porous structures with smaller pore sizes than 70HPMC-30CMS film, especially 70HPMC-30CMS-2.5SA-5GA film.

5.1.1.4 70HPMC-30CMS and 70HPMC-30CMS-2.5SA films exhibited similar stress at maximum load and Young's modulus values. The addition of GA into 70HPMC-30CMS-2.5SA film showed significant increase in stress at maximum load, Young's modulus while strain at maximum load decreased.

5.1.1.5 The addition of SA exhibited the increase of swelling degree and gel fraction, whereas the reduction of water absorption, WVTR, and water solubility was observed for 70HPMC-30CMS-2.5SA film. The incorporation of GA into 70HPMC-30CMS-2.5SA film provided greater swelling degree, gel fraction, water solubility, water absorption, and WVTR. The reduction of swelling degree, gel fraction, water solubility, water absorption, and WVTR was detected in 70HPMC-30CMS-2.5SA-GA films when GA content increased.

5.1.1.6 70HPMC-30CMS film showed no antibacterial activity while 70HPMC-30CMS-2.5SA film exhibited strong antibacterial activity against *S. aureus*. After the inclusion of GA, 70HPMC-30CMS-2.5SA-1GA, 70HPMC-30CMS-2.5SA-3GA and 70HPMC-30CMS-2.5SA-5GA films exhibited the excellent antibacterial activity against both *S. aureus* and *E. coli*.

5.1.1.7 From cytotoxicity test, 70HPMC-30CMS, 70HPMC-30CMS-2.5SA and 70HPMC-30CMS-2.5SA-1GA films were not toxic to human cells while the incorporation of GA at 3wt% and 5wt% revealed the slight to moderate harm to HaCat cells.

5.1.1.8 In this study, 70HPMC-30CMS-2.5SA-1GA films represented the best overall properties by considering these following properties: the greatest water absorption, WVTR, swelling degree and mechanical properties. Moreover, 70HPMC-30CMS-2.5SA-1GA film also provided excellent antibacterial activity and presented no toxicity to HaCat cells.

5.2 Suggestions

The present research focused on improving the physicochemical properties of modified HPMC films by blending with CMS. The dimensional stability and antibacterial activity of 70HPMC-30CMS film were improved using SA crosslinkers and antibacterial agents (ZnONPs and GA) for wound dressing applications. However, the modified HPMC films can be further improved by the following suggestions:

5.2.1 To study the effect of salting out on HPMC matrix, blending with other types of anionic polymers such as CMC, xylan, pullulan, and agarose was interesting. This is because the carboxylate ion of anionic polymers that may induce the porous structure of HPMC film for the enhancement of swelling degree, water absorption and WVTR [122].

5.2.2 The other types of natural antibacterial agents with healing properties (i.e. sericin and aloe vera extract) are suggested to enhance the effectiveness of modified HPMC for wound dressing application [123-125].

5.2.3 High water solubility of the obtained film in this study was the limitation when compared to commercial film used for wound dressing applications. High water solubility of HPMC film could be improved by blending with other polymers that showed lower water solubility than CMS such as alginate, due to the similarity of carboxylate group and higher water resistant than CMS [126, 127].

References

[1] Boateng, J. S. Matthews, K. H. Stevens, H. N. E. and Eccleston, G. M. 2008. "Wound Healing Dressings and Drug Delivery Systems: A Review." *Journal of Pharmaceutical Sciences*, 97(8), 2892-2923.

[2] Liu, K. Du, H. Zheng, T. Liu, H. Zhang, M. Zhang, R. and Si, C. 2021. "Recent advances in cellulose and its derivatives for oilfield applications." *Carbohydrate Polymers*, 259, 117740.

[3] Ghadermazi, R. Hamdipour, S. Sadeghi, K. Ghadermazi, R. and Khosrowshahi Asl, A. 2019. "Effect of various additives on the properties of the films and coatings derived from hydroxypropyl methylcellulose—A review." *Food Science & Nutrition*, 7(11), 3363-3377.

[4] Jiang, Q. zhou, W. Wang, J. Tang, R. Zhang, D. and Wang, X. 2016. "Hypromellose succinate-crosslinked chitosan hydrogel films for potential wound dressing." *International Journal of Biological Macromolecules*, 91, 85-91.

[5] Kondaveeti, S. Damato, T. C. Carmona-Ribeiro, A. M. Sierakowski, M. R. and Petri, D.F.S. 2017. "Sustainable hydroxypropyl methylcellulose/xyloglucan/gentamicin films with antimicrobial properties." *Carbohydrate Polymers*, 165, 285-293.

[6] Prabu, D. Majdalawieh, A. F. Abu-Yousef, I. A. Inbasekaran, K. Balasubramaniam, T. Nallaperumal, N. and Gunasekar, C. J. 2016. "Preparation and characterization of gatifloxacin-loaded sodium alginate hydrogel membranes supplemented with hydroxypropyl methylcellulose and hydroxypropyl cellulose polymers for wound dressing." *International journal of pharmaceutical investigation*, 6(2), 86-95.

[7] Panrong, T. Karbowiak, T. and Harnkarnsujarit, N. 2020. "Effects of acetylated and octenyl-succinated starch on properties and release of green tea compounded starch/LLDPE blend films." *Journal of Food Engineering*, 284, 110057.

[8] Torres, F. G. Commeaux, S. and Troncoso, O. P. 2013. “Starch-based biomaterials for wound-dressing applications.” Starch - Stärke, 65(7-8), 543-551.

[9] Wilpiszewska, K. Spychaj, T. and Pazdzioch, W. 2016. “Carboxymethyl starch/montmorillonite composite microparticles: Properties and controlled release of isoproturon.” *Carbohydrate Polymers*, 136, 101-106.

[10] Abdollahi, Z. Zare, E. N. Salimi, F. Goudarzi, I. Tay, F. R. and Makvandi, P. 2021. “Bioactive Carboxymethyl Starch-Based Hydrogels Decorated with CuO Nanoparticles: Antioxidant and Antimicrobial Properties and Accelerated Wound Healing In Vivo.” *International Journal of Molecular Sciences*, 22(5), 2531.

[11] Ounkaew, A. Kasemsiri, P. Jetsrisuparb, K. Uyama, H. Hsu, Y.-I. Boonmars, and Chindaprasirt, P. 2020. “Synthesis of nanocomposite hydrogel based carboxymethyl starch/polyvinyl alcohol/nanosilver for biomedical materials.” *Carbohydrate Polymers*, 248, 116767.

[12] Gong, G. Zhang, F. Cheng, Z. and Zhou, L. 2015. “Facile fabrication of magnetic carboxymethyl starch/poly(vinyl alcohol) composite gel for methylene blue removal.” *International Journal of Biological Macromolecules*, 81, 205-211.

[13] Wilpiszewska, K. 2019. “Hydrophilic films based on starch and carboxymethyl starch.” *Polish Journal of Chemical Technology*, 21, 26-30.

[14] Reddy, N. Reddy, R. and Jiang, Q. (2015). “Crosslinking biopolymers for biomedical applications.” *Trends in Biotechnology*, 33(6), 362-369.

[15] Alavarse, A. C. Frachini, E. C. G. da Silva, R. L. C. G. Lima, V. H. Shavandi, A. and Petri, D. F. S. 2022. “Crosslinkers for polysaccharides and proteins: Synthesis conditions, mechanisms, and crosslinking efficiency, a review.” *International Journal of Biological Macromolecules*, 202, 558-596.

[16] Saxena, R. K. Saran, S. Isar, J. and Kaushik, R. 2017. 27 - Production and Applications of Succinic Acid. In A. Pandey, S. Negi, & C. R. Soccol (Eds.), Current Developments in Biotechnology and Bioengineering (pp. 601-630): Elsevier.

[17] Tsao, C. T. Chang, C. H. Li, Y. D. Wu, M. F. Lin, C. P. Han, J. L. and Hsieh, K. H. 2011. "Development of chitosan/ dicarboxylic acid hydrogels as wound dressing materials." *Journal of Bioactive and Compatible Polymers*, 26(5), 519-536.

[18] Thessrimuang, N. and Prachayawarakorn, J. 2019. "Development, modification and characterization of new biodegradable film from basil seed (*Ocimum basilicum L.*) mucilage." *Journal of the Science of Food and Agriculture*, 99(12), 5508-5515.

[19] Shalaby, M. A. Anwar, M. M. and Saeed, H. 2022. "Nanomaterials for application in wound Healing: current state-of-the-art and future perspectives." *Journal of Polymer Research*, 29(3), 91.

[20] Mohammadzadeh-Vazifeh, M. Hosseini, S. M. Mohammadi, A. Jahanfar, M. and Maleki, H. 2020. "Investigation of the antimicrobial properties of nanoclay and chitosan based nanocomposite on the microbial characteristics of Gouda cheese." *Iranian journal of microbiology,* 12(2), 121-126.

[21] Krishnan, P. D. Banas, D. Durai, R. D. Kabanov, D. Hosnedlova, B. Kepinska, M. and Kizek, R. 2020. "Silver Nanomaterials for Wound Dressing Applications." *Pharmaceutics*, 12(9), 821.

[22] Abdollahi, Z. Zare, E. N. Salimi, F. Goudarzi, I. Tay, F. R. and Makvandi, P. 2021. "Bioactive Carboxymethyl Starch-Based Hydrogels Decorated with CuO Nanoparticles: Antioxidant and Antimicrobial Properties and Accelerated Wound Healing In Vivo." Int J Mol Sci, 22(5).

[23] Medina Cruz, D. Mostafavi, E. Vernet-Crua, A. Barabadi, H. Shah, V. Cholula-Díaz, J. L. and Webster, T. J. 2020. "Green nanotechnology-based zinc oxide (ZnO)

nanomaterials for biomedical applications: a review." *Journal of Physics: Materials*, 3(3), 034005.

[24] Raafat, A. I. El-Sawy, N. M. Badawy, N. A. Mousa, E. A. and Mohamed, A. M. 2018. "Radiation fabrication of Xanthan-based wound dressing hydrogels embedded ZnO nanoparticles: In vitro evaluation." *International Journal of Biological Macromolecules*, 118, 1892-1902.

[25] Malik, G. K. and Mitra, J. 2021. "Zinc Oxide Nanoparticle Synthesis, Characterization, and Their Effect on Mechanical, Barrier, and Optical Properties of HPMC-Based Edible Film." *Food and Bioprocess Technology*, 14(3), 441-456.

[26] Gutha, Y. Pathak, J. L. Zhang, W. Zhang, Y. and Jiao, X. 2017. "Antibacterial and wound healing properties of chitosan/poly(vinyl alcohol)/zinc oxide beads (CS/PVA/ZnO)." *International Journal of Biological Macromolecules*, 103, 234-241.

[27] Dong, Q. L. Barker, G. C. Gorris, L. G. M. Tian, M. S. Song, X. Y. and Malakar, P. K. 2015. "Status and future of Quantitative Microbiological Risk Assessment in China." *Trends in Food Science & Technology*, 42(1), 70-80.

[28] Zhang, D. Nie, S. Xie, M. and Hu, J. 2020. "Antioxidant and antibacterial capabilities of phenolic compounds and organic acids from Camellia oleifera cake." *Food Science and Biotechnology*, 29(1), 17-25.

[29] Yang, X. Wang, B. Sha, D. Liu, Y. Liu, Z. Shi, K. and Ji, X. 2021a. "PVA/Poly(hexamethylene guanidine)/Gallic Acid Composite Hydrogel Films and Their Antibacterial Performance." *ACS Applied Polymer Materials*, 3(8), 3867-3877.

[30] Rui, L. Xie, M. Hu, B. Zhou, L. Yin, D. and Zeng, X. 2017. "A comparative study on chitosan/gelatin composite films with conjugated or incorporated gallic acid." *Carbohydrate Polymers*, 173, 473-481.

[31] Sharma, S. Perera, K. Y. Pradhan, D. Duffy, B. Jaiswal, A. K. and Jaiswal, S. 2022. "Active Packaging Film Based on Poly Lactide-Poly (Butylene Adipate-Co-Terephthalate) Blends Incorporated with Tannic Acid and Gallic Acid for the Prolonged Shelf Life of Cherry Tomato." *Coatings*, 12(12), 1902.

[32] Shah, J. B. 2011. "The history of wound care." *The journal of the American College of Certified Wound Specialists*, 3(3), 65-66.

[33] Tudoroiu, E.-E. Dinu-Pirvu, C.-E. Albu Kaya, M. G. Popa, L. Anuta, V. Prisada, R. M. and Ghica, M. V. 2021. "An Overview of Cellulose Derivatives-Based Dressings for Wound-Healing Management." *Pharmaceuticals* (Basel, Switzerland), 14(12), 1215.

[34] Bolton, L. L. Monte, K. and Pirone, L. A. 2000. "Moisture and healing: beyond the jargon." Ostomy Wound Manage, 46(1A Suppl), 51S-62S; quiz 63S-64S.

[35] Kamide, K. 2005. "2 - Characterization of Molecular Structure of Cellulose Derivatives. In K. Kamide (Ed.), *Cellulose and Cellulose Derivatives* (pp. 25-188). Amsterdam: Elsevier.

[36] Roy, D. Semsarilar, M. Guthrie, J. T. and Perrier, S. 2009. "Cellulose modification by polymer grafting: a review." *Chemical Society Reviews*, 38(7), 2046-2064.

[37] Hebeish, A. and Guthrie, T. J. 2012. **The Chemistry and Technology of Cellulosic Copolymers**: Springer Berlin Heidelberg.

[38] Javad, S. and Khosro, A. 2013. ***Application of Cellulose and Cellulose Derivatives in Pharmaceutical Industries.*** In V. Theo van de & G. Louis (Eds.), Cellulose (pp. Ch. 3). Rijeka: IntechOpen.

[39] Wen, H. and Park, K. 2011. ***Oral controlled release formulation design and drug delivery***: theory to practice: John Wiley & Sons.

[40] Sarkar, N. 1979. "Thermal gelation properties of methyl and hydroxypropyl methylcellulose." *Journal of Applied Polymer Science*, 24(4), 1073-1087.

[41] Haque, A. Richardson, R. K. Morris, E. R. Gidley, M. J. and Caswell, D. C. 1993. "Thermogelation of methylcellulose. Part II: effect of hydroxypropyl substituents." *Carbohydrate Polymers*, 22(3), 175-186.

[42] Rowe R. C. Sheskey P. J. and Weller P. J. 2003. ***Handbook of pharmaceutical excipients*** (4th ed. / edited by Raymond C. Rowe Paul J. Sheskey Paul J. Weller). Pharmaceutical Press ; American Pharmaceutical Association.

[43] Mitchell, K. Ford, J. L. Armstrong, D. J., Elliott, P. N. C., Rostron, C., and Hogan, J. E. 1990. "The influence of additives on the cloud point, disintegration and dissolution of hydroxypropylmethylcellulose gels and matrix tablets." *International Journal of Pharmaceutics*, 66(1), 233-242.

[44] Seddiqi, H. Oliaei, E. Honarkar, H. Jin, J. Geonzon, L. C. Bacabac, R. G. and Klein-Nulend, J. 2021. "Cellulose and its derivatives: towards biomedical applications." *Cellulose*, 28(4), 1893-1931.

[45] Vaclavik, V. A. and Christian, E. W. 2007. ***Essentials of Food Science***: Springer New York.

[46] Umoren, S. A. Solomon, M. M. and Saji, V. S. 2022. "Chapter 12 - Starch and its derivatives. In S. A. Umoren, M. M. Solomon, & V. S. Saji (Eds.), Polymeric Materials in Corrosion Inhibition (pp. 287-302): Elsevier.

[47] Ratnayake, W. S. and Jackson, D. S. 2008. "Phase transition of cross-linked and hydroxypropylated corn (Zea mays L.) starches." *LWT - Food Science and Technology*, 41(2), 346-358.

[48] Singh, J. Kaur, L. and McCarthy, O. J. 2007. "Factors influencing the physico-chemical, morphological, thermal and rheological properties of some chemically modified starches for food applications—A review." *Food Hydrocolloids*, 21(1), 1-22.

[49] Runtenberg, M. W. and Solarek, D. 1984. Starch derivatives: Production and uses Starch: Chemistry and technology (pp. 311-388): Elsevier.

[50] Zhou, F. Liu, Q. Zhang, H. Chen, Q. and Kong, B. 2016. "Potato starch oxidation induced by sodium hypochlorite and its effect on functional properties and digestibility." *International Journal of Biological Macromolecules*, 84, 410-417.

[51] Sánchez-Rivera, M. M. García-Suárez, F. J. L. Velázquez del Valle, M. Gutierrez-Meraz, F. and Bello-Pérez, L. A. 2005. "Partial characterization of banana starches oxidized by different levels of sodium hypochlorite." *Carbohydrate Polymers*, 62(1), 50-56.

[52] Woo, K. Dowsett, C. Costa, B. Ebohon, S. Woodmansey, E. J. and Malone, M. 2021. "Efficacy of topical cadexomer iodine treatment in chronic wounds: Systematic review and meta-analysis of comparative clinical trials." *International wound journal*, 18(5), 586-597.

[53] Wang, W. Jiang, S. Jiang, S. Zhai, L. and Jiang, Q. 2011. "Poly(vinyl alcohol)/Oxidized Starch Fibres via Electrospinning Technique: Fabrication and Characterization." *Iranian Polymer Journal* (English Edition), 20.

[54] Mo, X. Iwata, H. and Ikada, Y. 2010. "A tissue adhesives evaluated in vitro and in vivo analysis." *Journal of Biomedical Materials Research Part A*, 94A(1), 326-332.

[55] Waliszewski, K. N. Aparicio, M. A. Bello, L. S. A. and Monroy, J. A. 2003. "Changes of banana starch by chemical and physical modification." *Carbohydrate Polymers*, 52(3), 237-242.

[56] Yanli, W. Wenyuan, G. and Xia, L. 2009. "Carboxymethyl Chinese yam starch: synthesis, characterization, and influence of reaction parameters." *Carbohydrate Research*, 344(13), 1764-1769.

[57] Gull, M. and Pasek, M. A. 2021. "The Role of Glycerol and Its Derivatives in the Biochemistry of Living Organisms, and Their Prebiotic Origin and Significance in the Evolution of Life." *Catalysts*, 11(1), 86.

[58] Rault, I. Frei, V. Herbage, D. Abdul-Malak, N. and Huc, A. 1996. "Evaluation of different chemical methods for cross-linking collagen gel, films and sponges." *Journal of Materials Science: Materials in Medicine*, 7(4), 215-221.

[59] Wang, H. C. Huang, H. B. Huang, X. M. and Hu, Z. Q. 2006. "Sugar and acid compositions in the arils of Litchi chinensis Sonn.: cultivar differences and evidence for the absence of succinic acid." *The Journal of Horticultural Science and Biotechnology*, 81(1), 57-62.

[60] Kenawy, E.-R. 2001. "Biologically active polymers. IV. Synthesis and antimicrobial activity of polymers containing 8-hydroxyquinoline moiety." *Journal of Applied Polymer Science*, 82(6), 1364-1374.

[61] Siddiqi, K. S. Rahman, A. and Husen, A. 2018. "Properties of Zinc Oxide Nanoparticles and Their Activity Against Microbes." *Nanoscale Research Letters*, 13(1), 141.

[62] Rai, M. Yadav, A. and Gade, A. 2009. "Silver nanoparticles as a new generation of antimicrobials." *Biotechnology Advances*, 27(1), 76-83.

[63] Chaudhry, Q. Scotter, M. Blackburn, J. Ross, B. Boxall, A. Castle, L. and Watkins, R. 2008. "Applications and implications of nanotechnologies for the food sector." *Food Additives & Contaminants: Part A*, 25(3), 241-258.

[64] Restuccia, D. Spizzirri, U. G. Parisi, O. I. Cirillo, G. Curcio, M. Iemma, F. and Picci, N. 2010. "New EU regulation aspects and global market of active and intelligent packaging for food industry applications." *Food Control*, 21(11), 1425-1435.

[65] Hu, X. Cook, S. Wang, P. and Hwang, H.-m. 2009. “In vitro evaluation of cytotoxicity of engineered metal oxide nanoparticles”. *Science of The Total Environment*, 407(8), 3070-3072.

[66] Zhang, L. Jiang, Y. Ding, Y. Povey, M. and York, D. 2007. “Investigation into the antibacterial behaviour of suspensions of ZnO nanoparticles (ZnO nanofluids).” *Journal of Nanoparticle Research*, 9(3), 479-489.

[67] Borges, A. Abreu, A. C. Ferreira, C. Saavedra, M. J. Simões, L. C. and Simões, M. 2015. “Antibacterial activity and mode of action of selected glucosinolate hydrolysis products against bacterial pathogens.” *Journal of Food Science and Technology, 52*(8), 4737-4748.

[68] Tian, Q. Wei, S. Su, H. Zheng, S. Xu, S. Liu, M. and Li, J. 2022. “Bactericidal activity of gallic acid against multi-drug resistance Escherichia coli.” *Microbial Pathogenesis*, 173, 105824.

[69] Keyvani-Ghamsari, S. Rahimi, M. and Khorsandi, K. 2023. “An update on the potential mechanism of gallic acid as an antibacterial and anticancer agent.” *Food Science & Nutrition*, 11(10), 5856-5872.

[70] Basch, C. Y. Jagus, R. J. and Flores, S. K. 2013. “Physical and Antimicrobial Properties of Tapioca Starch-HPMC Edible Films Incorporated with Nisin and/or Potassium Sorbate.” *Food and Bioprocess Technology*, 6(9), 2419-2428.

[71] Tedesco, M. P. Monaco-Lourenço, C. A. and Carvalho, R. A. 2016. “Gelatin/hydroxypropyl methylcellulose matrices — Polymer interactions approach for oral disintegrating films.” *Materials Science and Engineering: C*, 69, 668-674.

[72] Ding, C. Zhang, M. and Li, G. 2015. “Preparation and characterization of collagen/hydroxypropyl methylcellulose (HPMC) blend film.” *Carbohydrate Polymers*, 119, 194-201.

[73] Wilpiszewska, K. Antosik, A. K. and Spychaj, T. 2015. "Novel hydrophilic carboxymethyl starch/montmorillonite nanocomposite films." *Carbohydrate Polymers*, 128, 82-89.

[74] Zhang, C. Sun, G. Cao, L. and Wang, L. 2020. "Accurately intelligent film made from sodium carboxymethyl starch/k-carrageenan reinforced by mulberry anthocyanins as an indicator." *Food Hydrocolloids*, 108, 106012.

[75] Klangmuang, P. and Sothornvit, R. 2016. "Barrier properties, mechanical properties and antimicrobial activity of hydroxypropyl methylcellulose-based nanocomposite films incorporated with Thai essential oils." *Food Hydrocolloids*, 61, 609-616.

[76] Zhang, L. Wang, Y. Liu, H. Yu, L. Liu, X. Chen, L. and Zhang, N. 2013. "Developing hydroxypropyl methylcellulose/hydroxypropyl starch blends for use as capsule materials." *Carbohydrate Polymers*, 98(1), 73-79.

[77] Dharmalingam, K. and Anandalakshmi, R. 2019. "Fabrication, characterization and drug loading efficiency of citric acid crosslinked NaCMC-HPMC hydrogel films for wound healing drug delivery applications." *International Journal of Biological Macromolecules*, 134, 815-829.

[78] Belay, M. Tyeb, S. Rathore, K. Kumar, M. and Verma, V. 2020. "Synergistic effect of bacterial cellulose reinforcement and succinic acid crosslinking on the properties of agar." *International Journal of Biological Macromolecules*, 165, 3115-3122.

[79] Linn, K. S. Kasemsiri, P. Jetsrisuparb, K. Iamamornphan, W. Chindaprasirt, P. and Knijnenburg, J. T. N. 2022. "Development of Biodegradable Films with Antioxidant Activity Using Pectin Extracted from *Cissampelos pareira* Leaves." *Journal of Polymers and the Environment,* 30(5), 2087-2098.

[80] Luzi, F. Pannucci, E. Santi, L. Kenny, J. M. Torre, L. Bernini, R. and Puglia, D. 2019. "Gallic acid and quercetin as intelligent and active ingredients in poly (vinyl alcohol) films for food packaging." *Polymers*, 11(12), 1999.

[81] Naeem, A. Yu, C. Zhu, W. Chen, X. Wu, X. Chen, L. and Guan, Y. 2022. "Gallic Acid-Loaded Sodium Alginate-Based (Polyvinyl Alcohol-Co-Acrylic Acid) Hydrogel Membranes for Cutaneous Wound Healing: Synthesis and Characterization." *Molecules*, 27(23), 8397.

[82] Amin, K. M. Partila, A. M. Abd El-Rehim, H. A. and Deghiedy, N. M. 2020. "Antimicrobial ZnO Nanoparticle–Doped Polyvinyl Alcohol/Pluronic Blends as Active Food Packaging Films." *Particle & Particle Systems Characterization*, 37(4), 2000006.

[83] Khorasani, M. T. Joorabloo, A. Moghaddam, A. Shamsi, H. and MansooriMoghadam, Z. 2018. "Incorporation of ZnO nanoparticles into heparinised polyvinyl alcohol/chitosan hydrogels for wound dressing application." *International Journal of Biological Macromolecules,* 114, 1203-1215.

[84] Tantiwatcharothai, S. and Prachayawarakorn, J. 2020. "Property improvement of antibacterial wound dressing from basil seed (*O. basilicum L.*) mucilage- ZnO nanocomposite by borax crosslinking." *Carbohydrate Polymers*, 227, 115360.

[85] Stojanović, Ž. Jeremić, K. Jovanović, S. and Lechner, M. D. 2005. "A Comparison of Some Methods for the Determination of the Degree of Substitution of Carboxymethyl Starch." *Starch - Stärke*, 57(2), 79-83.

[86] Ma, Y. Yang, R. and Zhao, W. 2020. "Innovative Water-Insoluble Edible Film Based on Biocatalytic Crosslink of Gelatin Rich in Glutamine." *Foods*, 9(4), 503.

[87] McDonald, R. 1997. ***Colour physics for industry***. Society of Dyes and Colourists, West Yorkshire. Society of Dyers

[88] Association, J. S. 2010. Antibacterial products–Test for antibacterial activity and efficacy. JIS(2801), 10.1111.

[89] Boura-Theodoridou, O. Giannakas, A. Katapodis, P. Stamatis, H. Ladavos, A. and Barkoula, N.-M. 2020. "Performance of ZnO/chitosan nanocomposite films for antimicrobial packaging applications as a function of NaOH treatment and glycerol/PVOH blending." *Food Packaging and Shelf Life*, 23, 100456.

[90] Priyadarshi, R. and Negi, Y. S. 2017. "Effect of Varying Filler Concentration on Zinc Oxide Nanoparticle Embedded Chitosan Films as Potential Food Packaging Material." *Journal of Polymers and the Environment*, 25(4), 1087-1098.

[91] Sahoo, S. Chakraborti, C. Behera, P. and Mishra, S. 2011. "Spectroscopic Investigations of a Controlled Release Mucoadhesive Suspension." *Asian Journal of Pharmaceutical and Clinical Research, 4*, 63-70.

[92] Kaczmarska, K. Grabowska, B. Spychaj, T. Zdanowicz, M. Sitarz, M. Bobrowski, A. and Cukrowicz, S. 2018. "Effect of microwave treatment on structure of binders based on sodium carboxymethyl starch: FT-IR, FT-Raman and XRD investigations". *Spectrochim Acta A Mol Biomol Spectrosc*, 199, 387-393.

[93] Zahib, I. R. Md Tahir, P. Talib, M. Mohamad, R. Alias, A. H. and Lee, S. H. 2021. "Effects of degree of substitution and irradiation doses on the properties of hydrogel prepared from carboxymethyl-sago starch and polyethylene glycol." *Carbohydrate Polymers*, 252, 117224.

[94] Manabeng, M. Mwankemwa, B. S. Ocaya, R. O. Motaung, T. E. and Malevu, T. D. 2022. "A Review of the Impact of Zinc Oxide Nanostructure Morphology on Perovskite Solar Cell Performance." *Processes*, 10(9), 1803.

[95] Zhang, L. Wang, X.-F. Peng, Y.-L. Zhao, Y. Qian, J.-Y. and Ding, X. 2021. "Effect of different ionic liquids acting as plasticizers on the multi-scale structures and physical

properties of hydroxypropyl methylcellulose/monosodium phosphate photophobic film." *International Journal of Biological Macromolecules*, 179, 466-474.

[96] Hezma, A. M. Rajeh, A. and Mannaa, M. A. 2019. "An insight into the effect of zinc oxide nanoparticles on the structural, thermal, mechanical properties and antimicrobial activity of Cs/PVA composite." *Colloids and Surfaces A: Physicochemical and Engineering Aspects*, 581, 123821.

[97] Wu, P. Fisher, A. C. Foo, P. P. Queen, D. and Gaylor, J. D. S. 1995. "In vitro assessment of water vapour transmission of synthetic wound dressings." *Biomaterials*, 16(3), 171-175.

[98] Akhtar, M.-J. Jacquot, M. Jamshidian, M. Imran, M. Arab-Tehrany, E. and Desobry, S. 2013. "Fabrication and physicochemical characterization of HPMC films with commercial plant extract: Influence of light and film composition." *Food Hydrocolloids*, 31(2), 420-427.

[99] Zhang, L. Lu, Y.-Q. Qian, J.-Y. Yue, L.-N. Li, Q. Xiao, L.-X. and Guan, C.-R. 2020. "Microstructures, physical and sustained antioxidant properties of hydroxypropyl methylcellulose based microporous photophobic films." *International Journal of Biological Macromolecules*, 152, 1002-1009.

[100] Izgis, H. Ilhan, E. Kalkandelen, C. Celen, E. Guncu, M. M. Turkoglu Sasmazel, H. and Constantinescu, G. 2022. "Manufacturing of Zinc Oxide Nanoparticle (ZnO NP)-Loaded Polyvinyl Alcohol (PVA) Nanostructured Mats Using Ginger Extract for Tissue Engineering Applications." *Nanomaterials*, 12(17), 3040.

[101] Joorabloo, A. Khorasani, M. T. Adeli, H. Mansoori-Moghadam, Z. and Moghaddam, A. 2019. "Fabrication of heparinized nano ZnO/poly(vinylalcohol)/carboxymethyl cellulose bionanocomposite hydrogels using artificial neural network for wound dressing application." *Journal of Industrial and Engineering Chemistry*, 70, 253-263.

[102] Zepon, K. M. Martins, M. M. Marques, M. S. Heckler, J. M. Dal Pont Morisso, F. Moreira, M. G. and Kanis, L. A. 2019. "Smart wound dressing based on k–carrageenan/locust bean gum/cranberry extract for monitoring bacterial infections." *Carbohydrate Polymers*, 206, 362-370.

[103] Pitpisutkul, V. and Prachayawarakorn, J. 2022. "Hydroxypropyl methylcellulose/carboxymethyl starch/zinc oxide porous nanocomposite films for wound dressing application." *Carbohydrate Polymers*, 298, 120082.

[104] Gebresas, G. A. Szabó, T. and Marossy, K. 2023. "A comparative study of carboxylic acids on the cross-linking potential of corn starch films." *Journal of Molecular Structure*, 1277, 134886.

[105] Ghorpade, V. S. Dias, R. J. Mali, K. K. and Mulla, S. I. 2019. "Citric acid crosslinked carboxymethylcellulose-polyvinyl alcohol hydrogel films for extended release of water soluble basic drugs." *Journal of Drug Delivery Science and Technology*, 52, 421-430.

[106] Lam, P.-L. Lee, K. K.-H. Kok, S. H.-L. Cheng, G. Y.-M. Tao, X.-M. Hau, D. K.-P. and Wong, R. S.-M. 2012. "Development of formaldehyde-free agar/gelatin microcapsules containing berberine HCl and gallic acid and their topical and oral applications." *Soft Matter*, 8(18), 5027-5037.

[107] Yu, C. Chen, X. Zhu, W. Li, L. Peng, M. Zhong, Y. and Guan, Y. 2022. "Synthesis of Gallic Acid-Loaded Chitosan-Grafted-2-Acrylamido-2-Methylpropane Sulfonic Acid Hydrogels for Oral Controlled Drug Delivery: In Vitro Biodegradation, Antioxidant, and Antibacterial Effects." *Gels*, 8(12), 806.

[108] Dai, H. Huang, Y. and Huang, H. 2018. "Enhanced performances of polyvinyl alcohol films by introducing tannic acid and pineapple peel-derived cellulose nanocrystals." *Cellulose*, 25(8), 4623-4637.

[109] Kumar, C. S. Soloman, A. M. Thangam, R. Perumal, R. K. Gopinath, A. and Madhan, B. 2020. "Ferulic acid-loaded collagen hydrolysate and polycaprolactone nanofibres for tissue engineering applications." *IET Nanobiotechnology*, 14(3), 202-209.

[110] Zhang, L. Yue, L.-N. Sui, Y.-L. Zhao, Y. Ding, X. Li, Q. and Qian, J.-Y. 2021. "Regulating the mechanical properties and microporous structures of hydroxypropyl methylcellulose based microporous photophobic films by adjusting the l-ethyl-3-methylimidazolium acetate content." *Progress in Organic Coatings*, 155, 106226.

[111] Wu, H. Lei, Y. Lu, J. Zhu, R. Xiao, D. Jiao, C. and Li, M. 2019. "Effect of citric acid induced crosslinking on the structure and properties of potato starch/chitosan composite films." *Food Hydrocolloids*, 97, 105208.

[112] Promsorn, J. and Harnkarnsujarit, N. 2022. "Oxygen absorbing food packaging made by extrusion compounding of thermoplastic cassava starch with gallic acid." *Food Control*, 142, 109273.

[113] Zhang, D. Zhou, W. Wei, B. Wang, X. Tang, R. Nie, J. and Wang, J. 2015. "Carboxyl-modified poly(vinyl alcohol)-crosslinked chitosan hydrogel films for potential wound dressing." *Carbohydrate Polymers*, 125, 189-199.

[114] Štiglic, A. D. Gürer, F. Lackner, F. Bračič, D. Winter, A. Gradišnik, L. and Mohan, T. 2022. "Organic acid cross-linked 3D printed cellulose nanocomposite bioscaffolds with controlled porosity, mechanical strength, and biocompatibility." *iScience*, 25(5), 104263.

[115] Goudar, N. Vanjeri, V. N. Dixit, S. Hiremani, V. Sataraddi, S. Gasti, T. and Chougale, R. B. 2020. "Evaluation of multifunctional properties of gallic acid crosslinked Poly (vinyl alcohol)/Tragacanth Gum blend films for food packaging applications." *International Journal of Biological Macromolecules*, 158, 139-149.

[116] Khan, M. R. Volpe, S. Salucci, E. Sadiq, M. B. and Torrieri, E. 2022. "Active caseinate/guar gum films incorporated with gallic acid: Physicochemical properties and release kinetics." *Journal of Food Engineering*, 335, 111190.

[117] Zhang, M. Yang, B. Yuan, Z. Sheng, Q. Jin, C. Qi, J. and Xiong, G. 2023. "Preparation and performance testing of corn starch/pullulan/gallic acid multicomponent composite films for active food packaging." *Food Chemistry: X*, 19, 100782.

[118] Yang, X. Wang, B. Sha, D. Liu, Y. Liu, Z. Shi, K. and Ji, X. 2021. "PVA/poly (hexamethylene guanidine)/gallic acid composite hydrogel films and their antibacterial performance." *ACS Applied Polymer Materials*, 3(8), 3867-3877.

[119] Yang, L. H. Lau, S. C. K. Lee, O. O. Tsoi, M. M. Y. and Qian, P. Y. 2007. "Potential roles of succinic acid against colonization by a tubeworm." *Journal of Experimental Marine Biology and Ecology*, 349(1), 1-11.

[120] Kumar, R. Chandar, B. and Parani, M. 2018. "Use of succinic & oxalic acid in reducing the dosage of colistin against New Delhi metallo-β-lactamase-1 bacteria." *Indian J Med Res*, 147(1), 97-101.

[121] Gutiérrez, T. J. Seligra, P. G. Jaramillo, C. M. Jaramillo, C. M. Famá, L. and Goyanes, S. "Effect of Filler Properties on the Antioxidant Response of Thermoplastic Starch Composites." Handbook of Composites from Renewable Materials (pp. 337-369).

[122] Hay, W. T. Fanta, G. F. Peterson, S. C. Thomas, A. J. Utt, K. D. Walsh, K. A. and Selling, G. W. 2018. "Improved hydroxypropyl methylcellulose (HPMC) films through incorporation of amylose-sodium palmitate inclusion complexes." *Carbohydrate Polymers*, 188, 76-84.

[123] Siritientong, T. and Aramwit, P. 2015. "Characteristics of carboxymethyl cellulose/sericin hydrogels and the influence of molecular weight of carboxymethyl cellulose." *Macromolecular Research*, 23(9), 861-866.

[124] Zhao, Y. Li, H. Chen, J. and Wang, Y. 2023. "A novel high water-soluble antibacterial films-based guar gum incorporated with Aloe vera gel and **ε**-polylysine." *Food Chemistry*, 427, 136686.

[125] Singh, S. Gupta, A. and Gupta, B. 2018. "Scar free healing mediated by the release of aloe vera and manuka honey from dextran bionanocomposite wound dressings." *International Journal of Biological Macromolecules*, 120, 1581-1590.

[126] Rangel-Marrón, M. Montalvo-Paquini, C. Palou, E. and López-Malo, A. 2013. "Optimization of the moisture content, thickness, water solubility and water vapor permeability of sodium alginate edible films using experimental design." *Proceedings of the 4th WSEAS International Conference in Recent Advances on Chemical Engineering, Biochemistry and Computational Chemistry*, 72-78.

[127] Marangoni Júnior, L. Rodrigues, P. R. da Silva, R. G. Vieira, R. P. and Alves, R. M. V. 2021. "Sustainable Packaging Films Composed of Sodium Alginate and Hydrolyzed Collagen: Preparation and Characterization." *Food and Bioprocess Technology*, 14(12), 2336-2346.

Appendices

Appendix A

FT-IR study

FTIR-ATR spectra of CMS, HPMC and various modified HPMC films

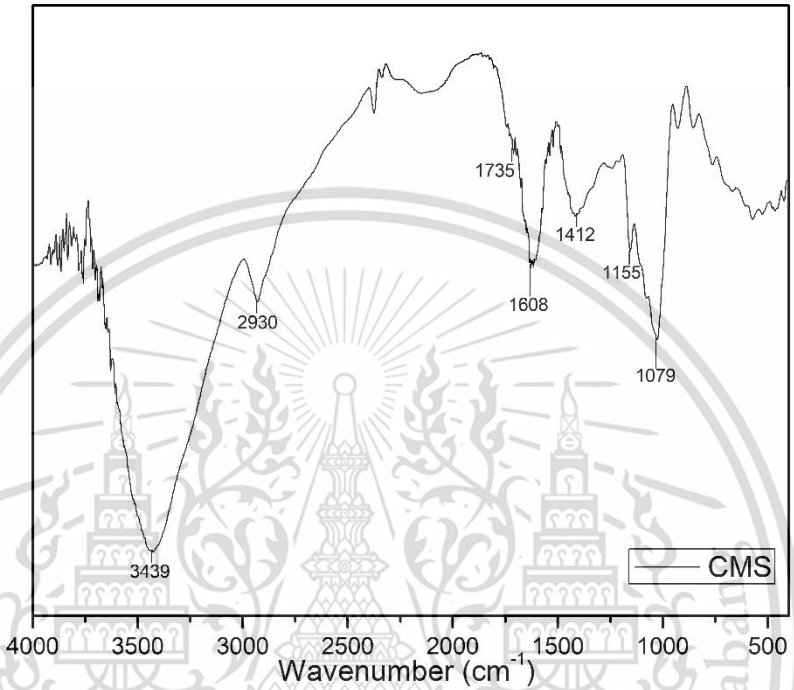

Figure A-1 FT-IR spectrum of CMS

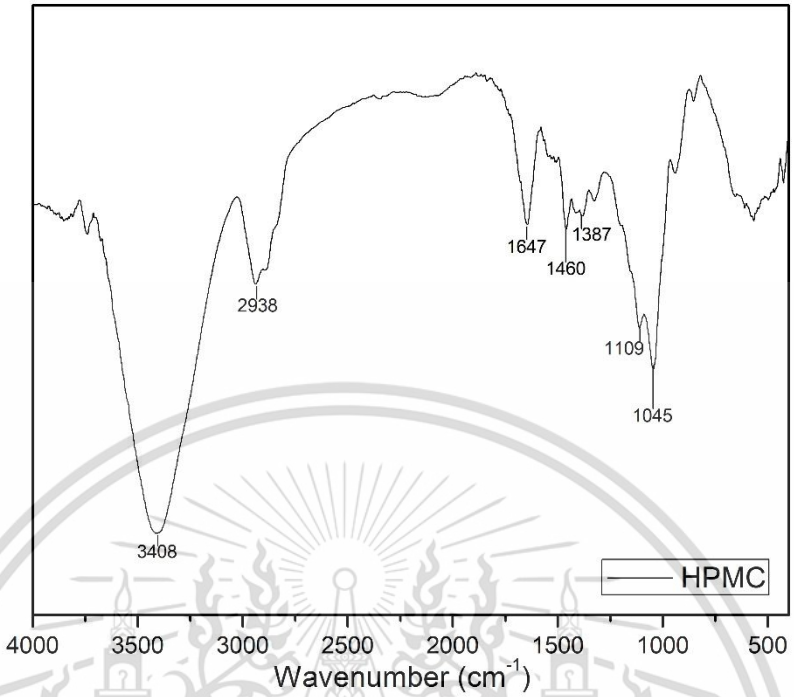

Figure A-2 FT-IR spectrum of HPMC

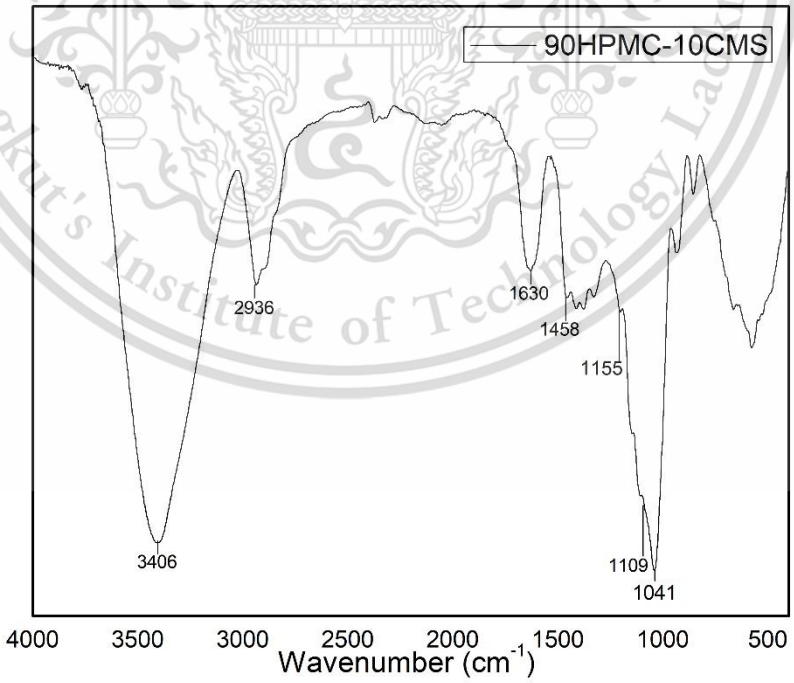

Figure A-3 FT-IR spectrum of 90HPMC-10CMS

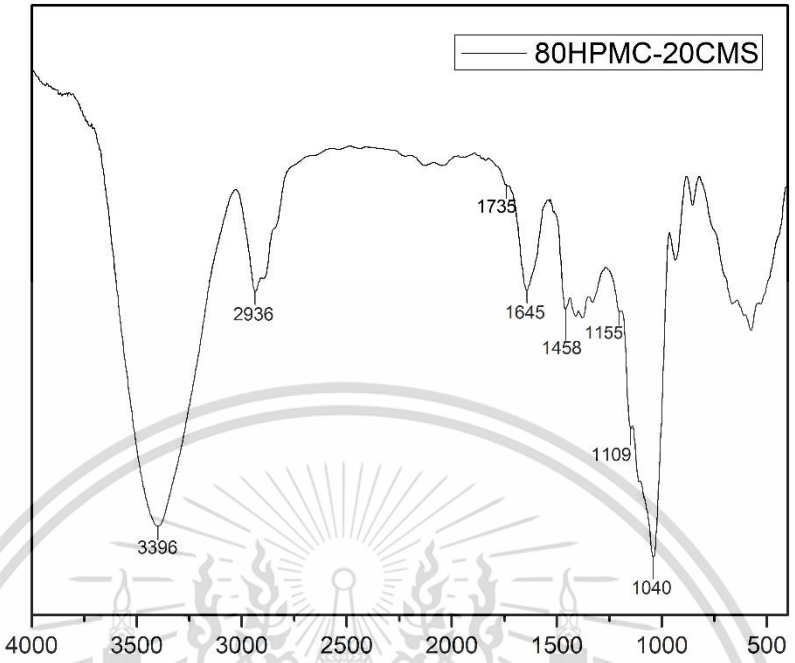

Figure A-4 FT-IR spectrum of 80HPMC-20CMS

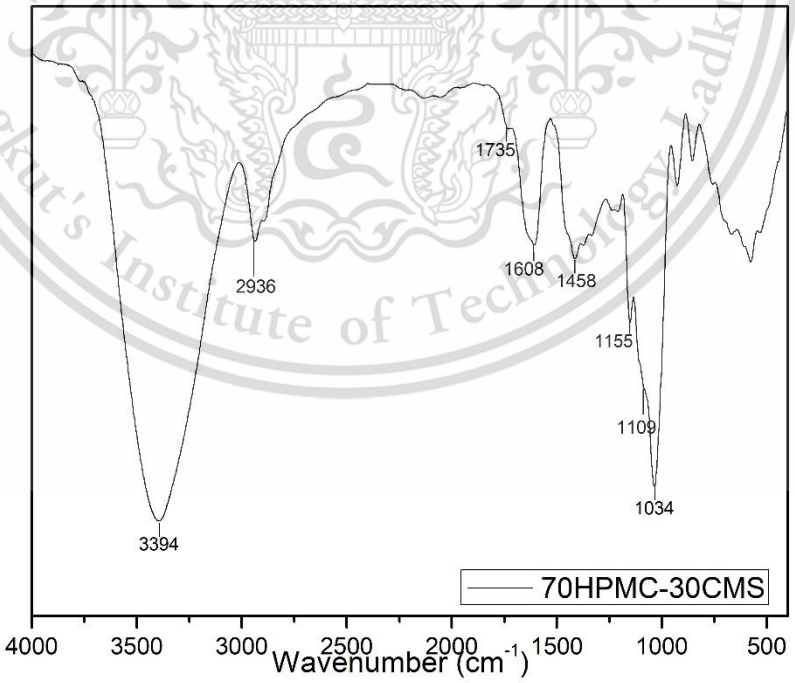

Figure A-5 FT-IR spectrum of 70HPMC-30CMS

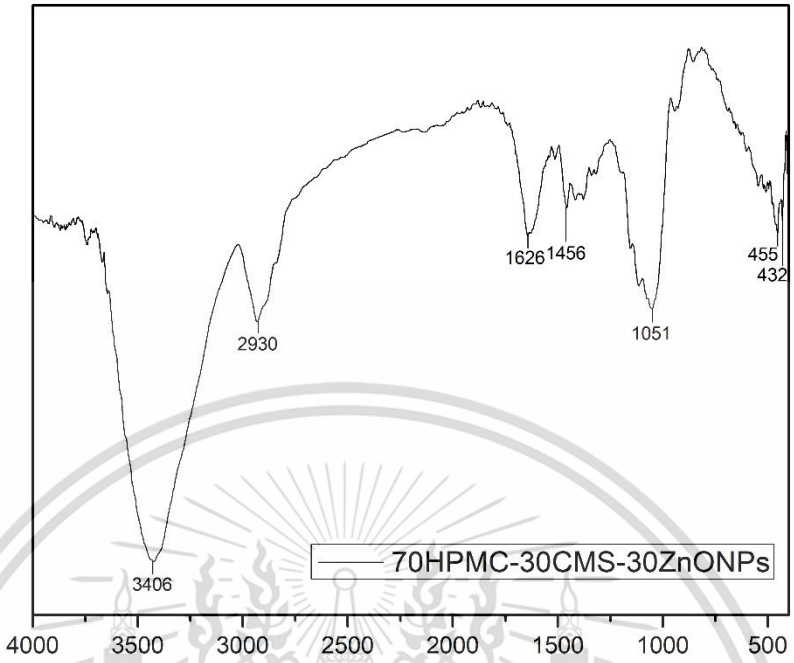

Figure A-6 FT-IR spectrum of 70HPMC-30CMS-30ZnONPs

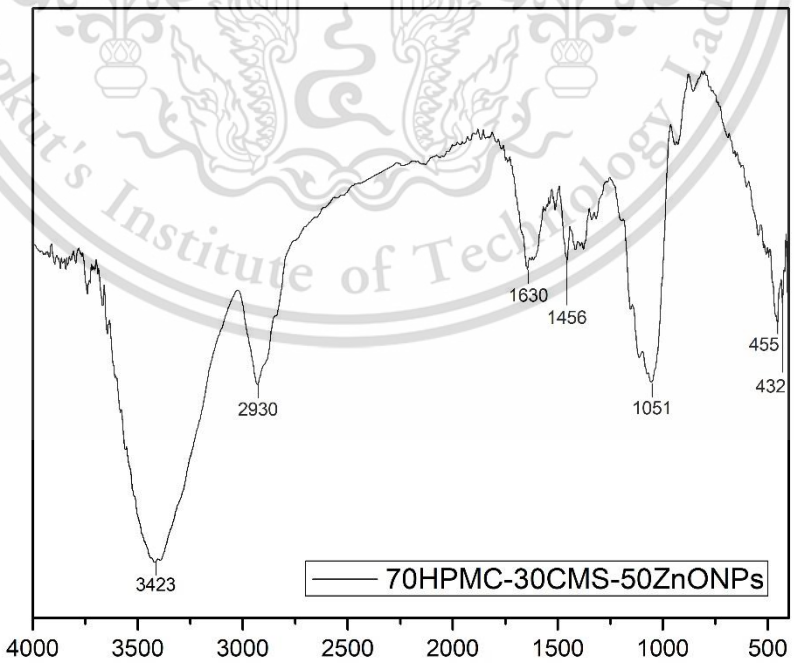

Figure A-7 FT-IR spectrum of 70HPMC-30CMS-50ZnONPs

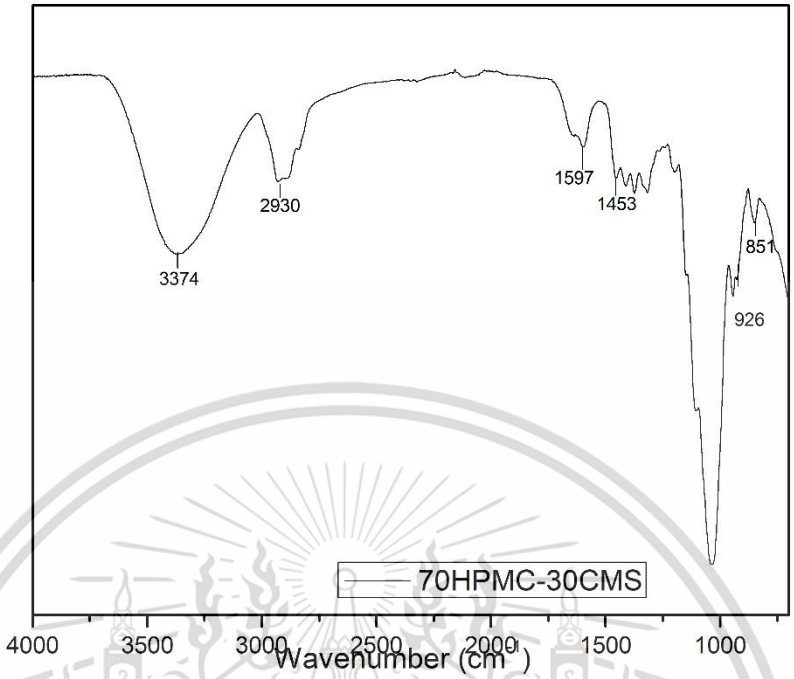

Figure A-8 ATR spectrum of 70HPMC-30CMS

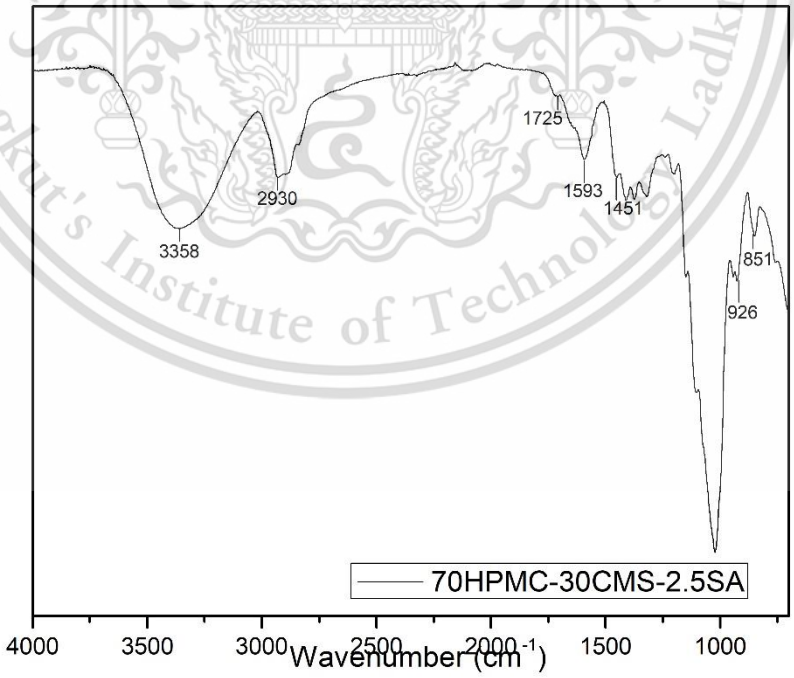

Figure A-9 ATR spectrum of 70HPMC-30CMS-2.5SA

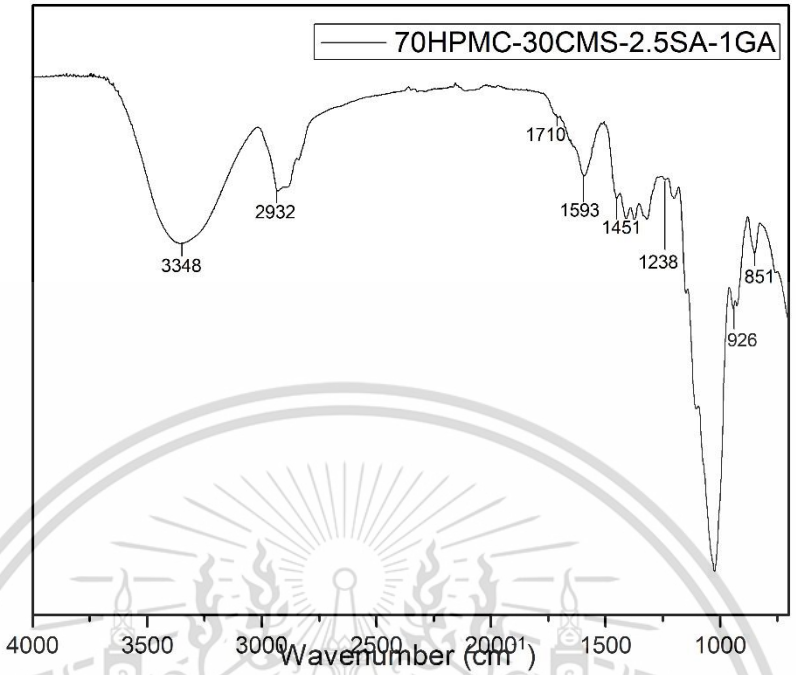

Figure A-10 ATR spectrum of 70HPMC-30CMS-2.5SA-1GA

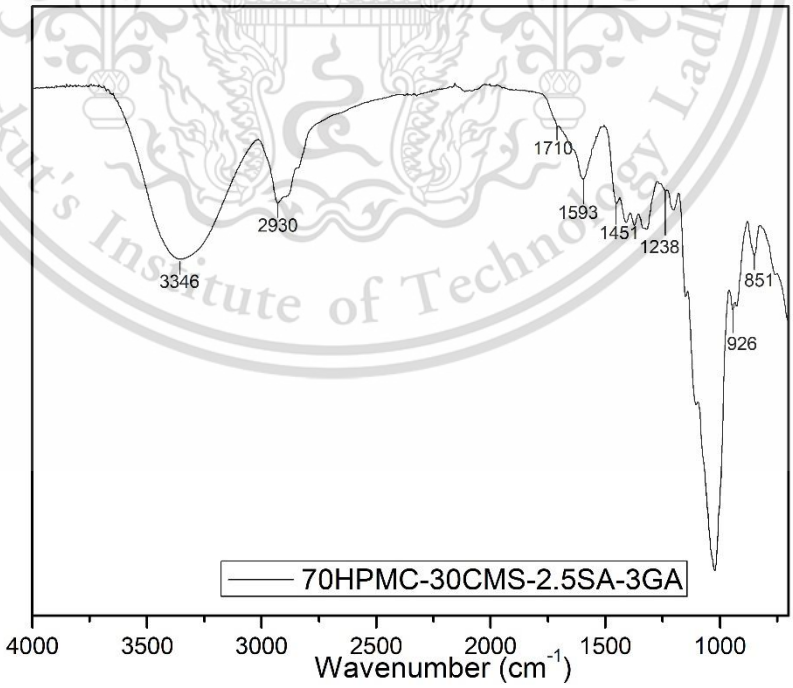

Figure A-11 ATR spectrum of 70HPMC-30CMS-2.5SA-3GA

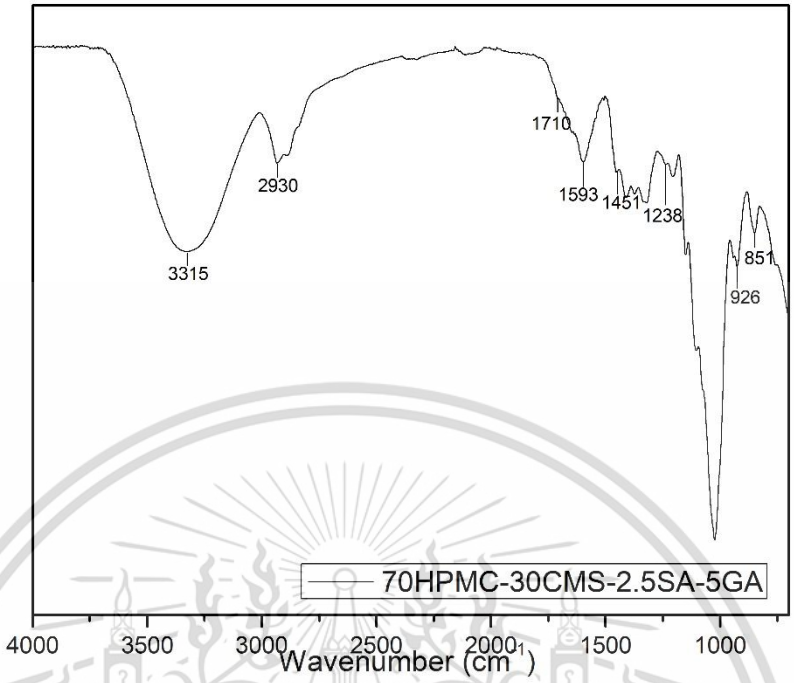

Figure A-12 ATR spectrum of 70HPMC-30CMS-2.5SA-5GA

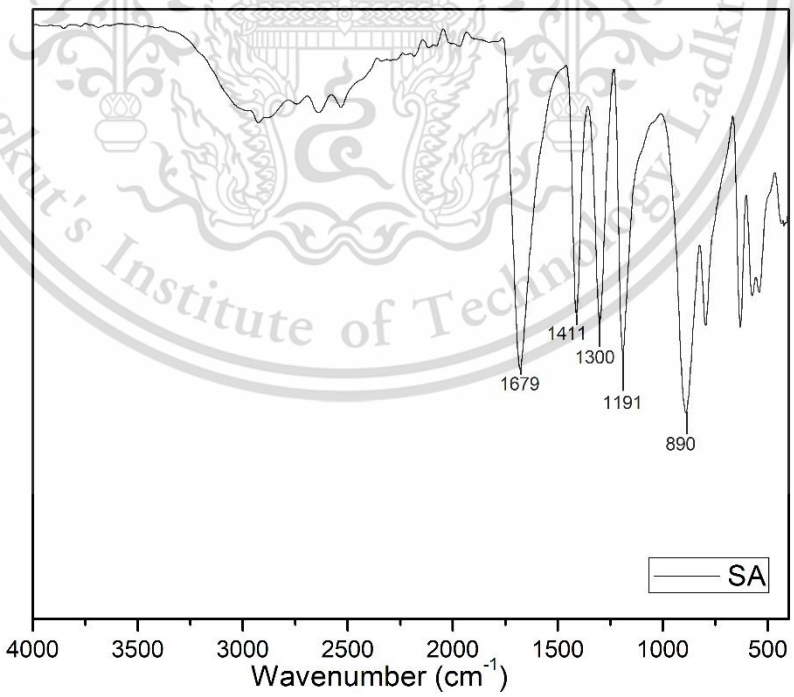

Figure A-13 ATR spectrum of SA

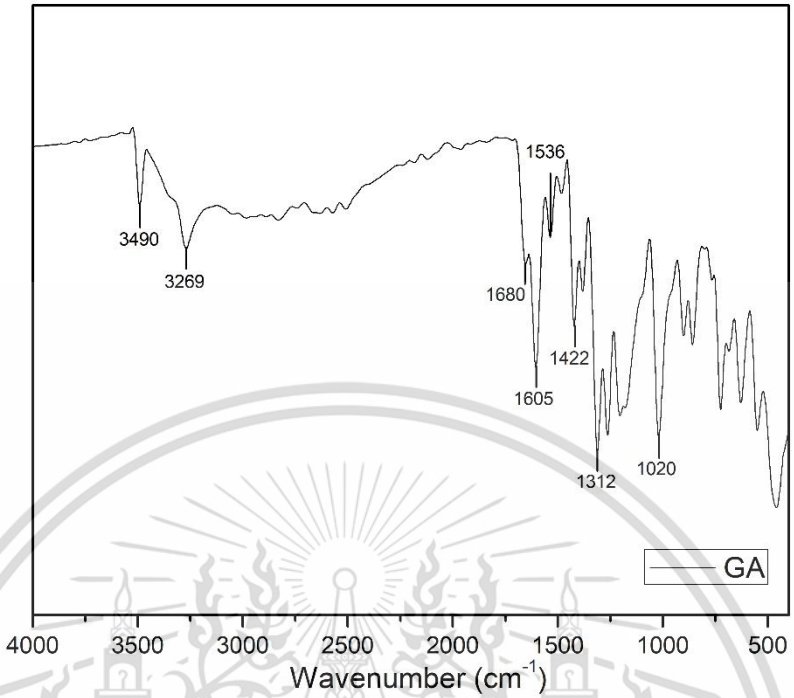

Figure A-14 ATR spectrum of GA

Appendix B

X-ray diffraction (XRD) study

X-ray diffractograms of CMS, HPMC and various modified HPMC films

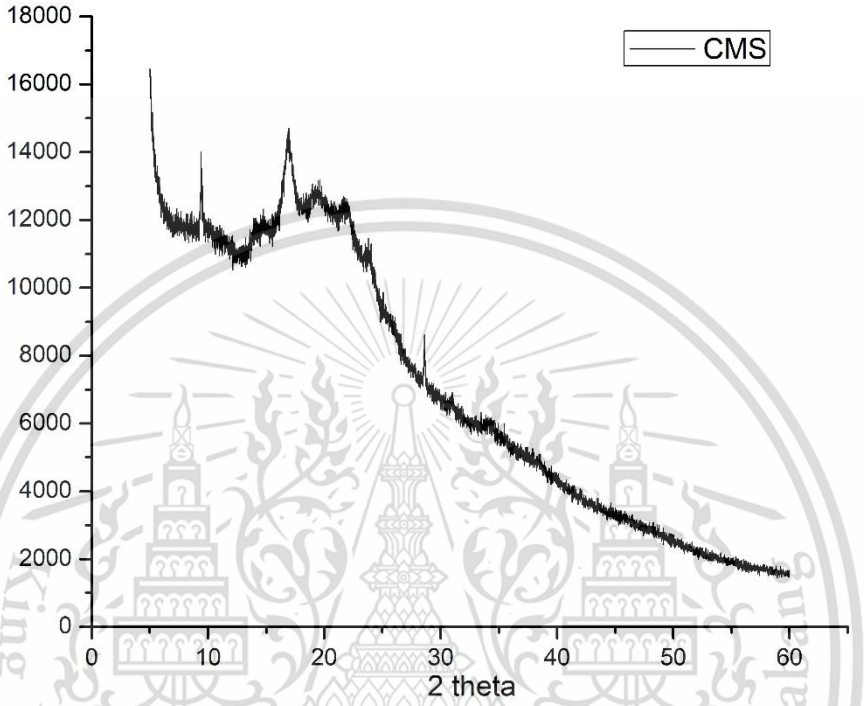

Figure B-1 X-ray diffractogram of CMS film

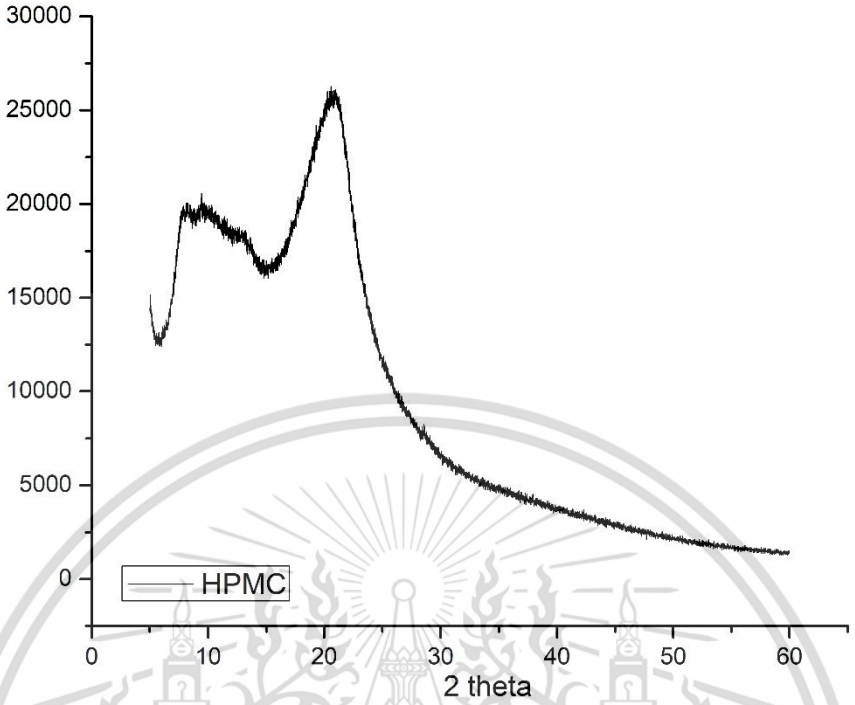

Figure B-2 X-ray diffractogram of HPMC film

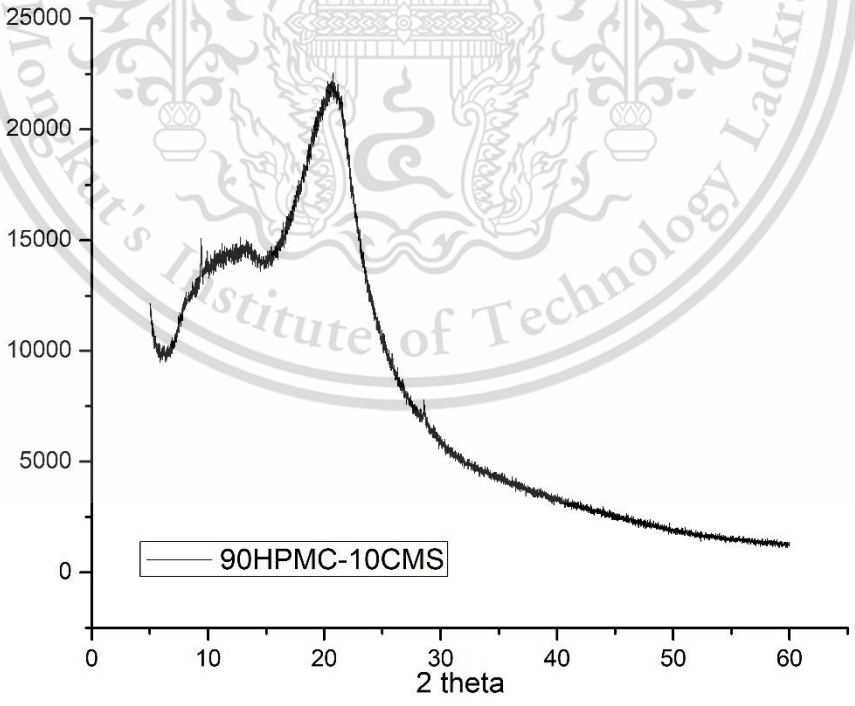

Figure B-3 X-ray diffractogram of 90HPMC-10CMS film

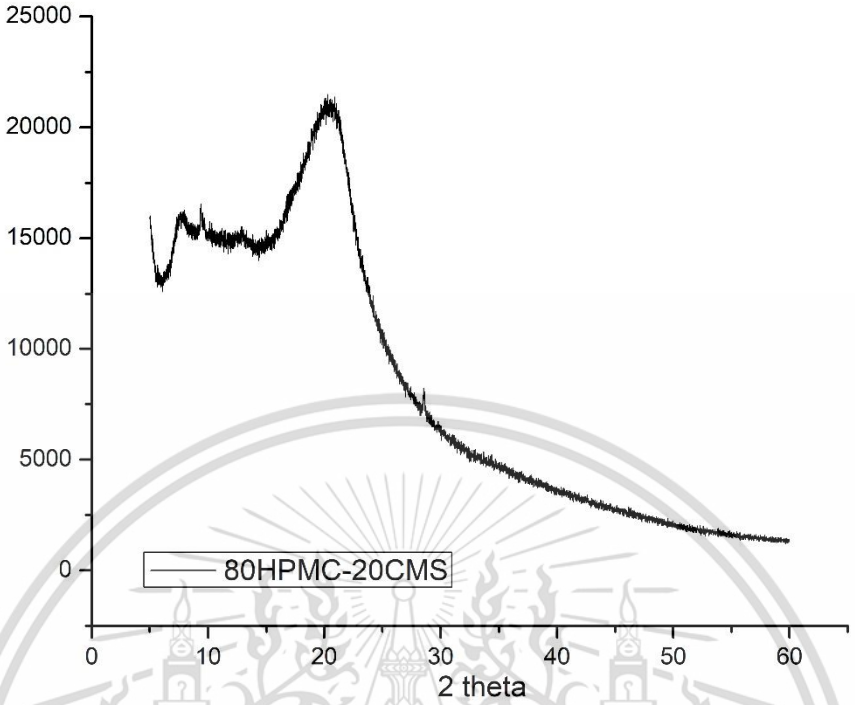

Figure B-4 X-ray diffractogram of 80HPMC-20CMS film

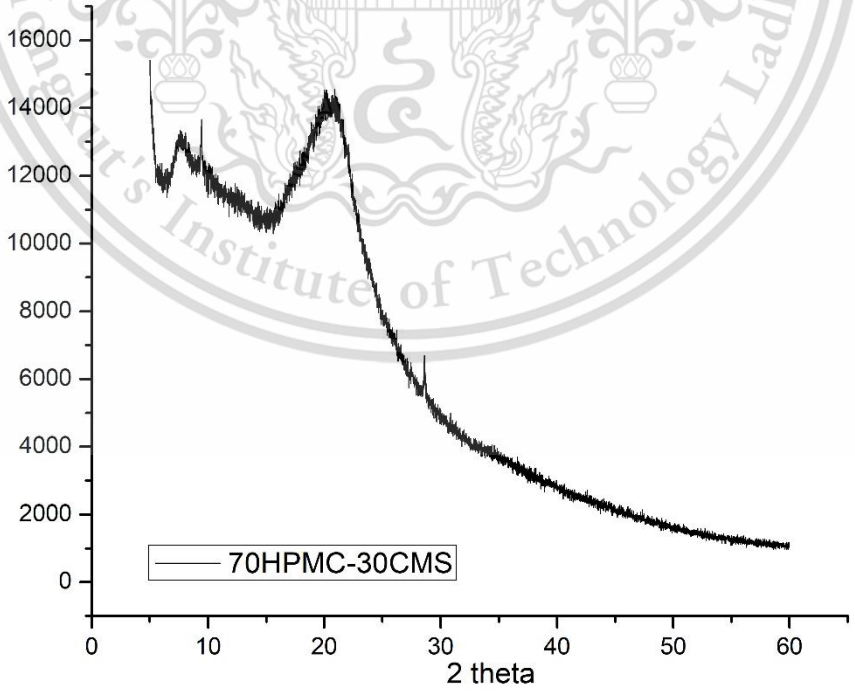

Figure B-5 X-ray diffractogram of 70HPMC-30CMS film

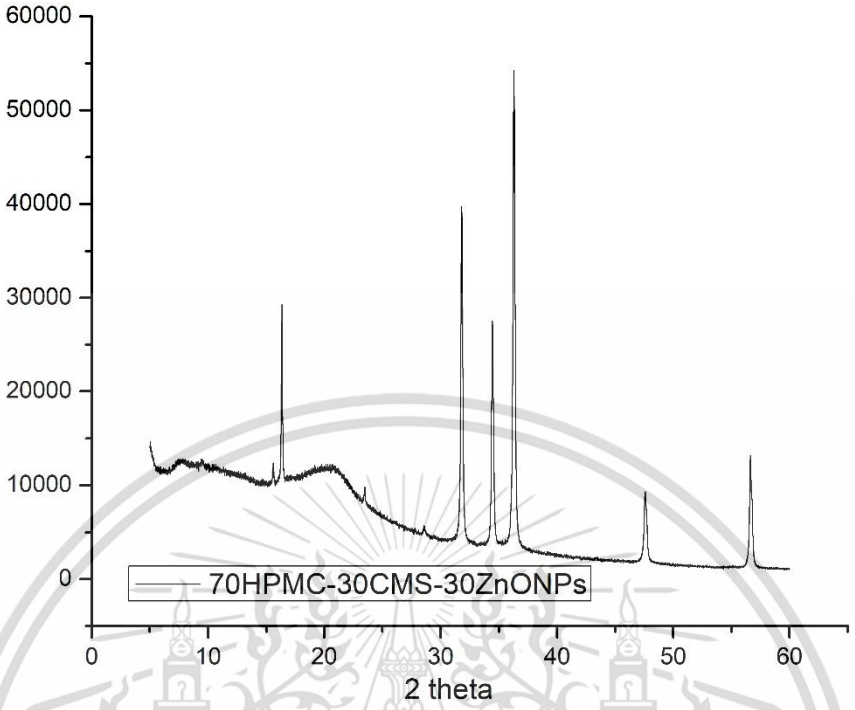

Figure B-6 X-ray diffractogram of 70HPMC-30CMS-30ZnONPs film

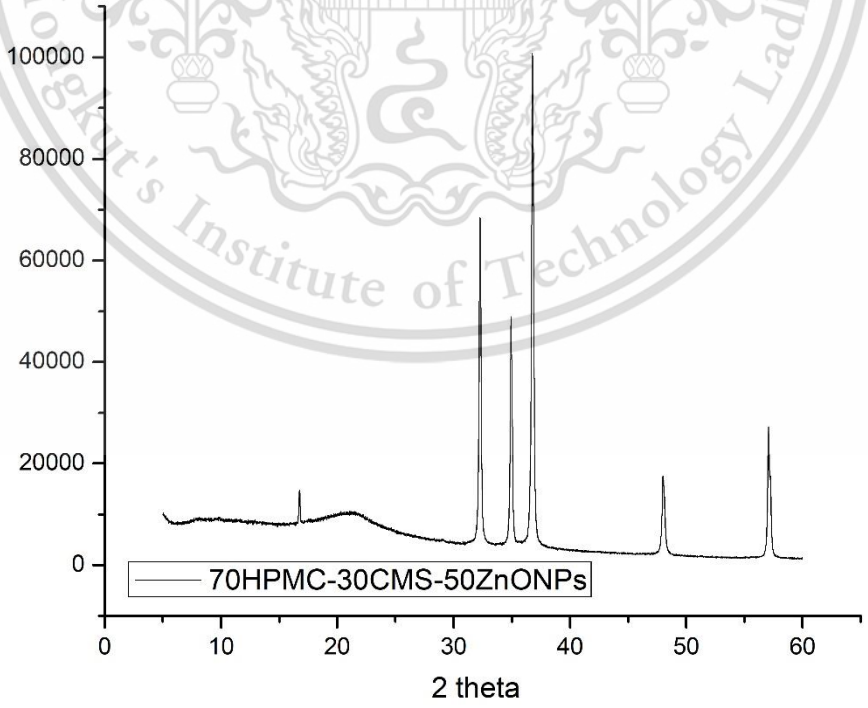

Figure B-7 X-ray diffractogram of 70HPMC-30CMS-50ZnONPs film

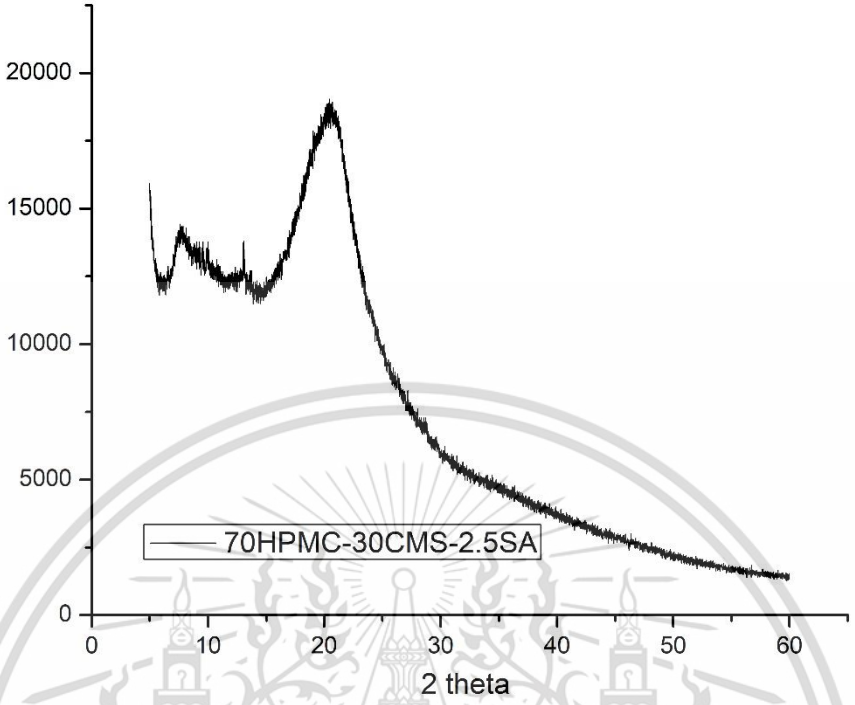

Figure B-8 X-ray diffractogram of 70HPMC-30CMS-2.5SA film

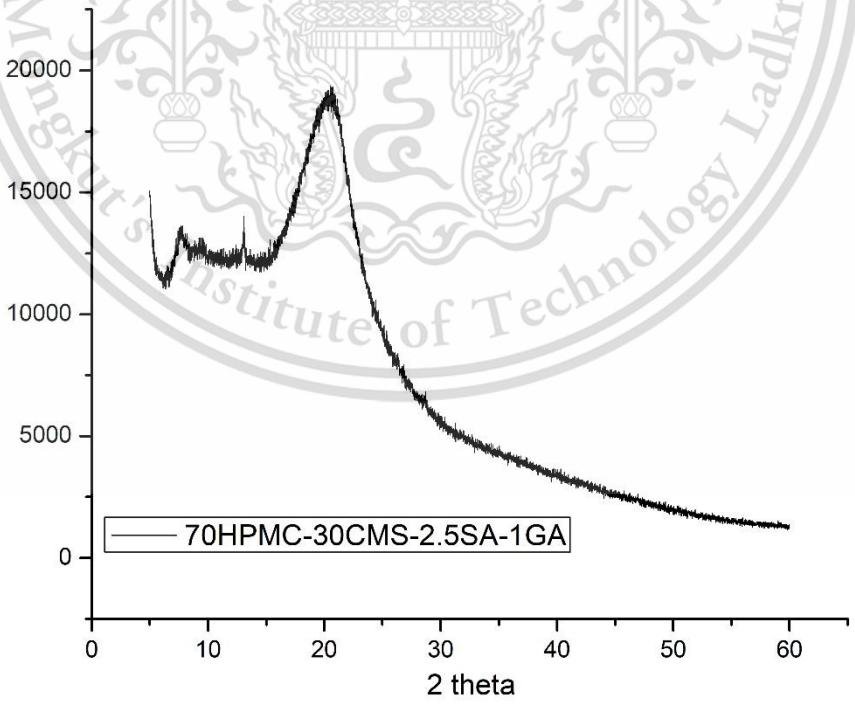

Figure B-9 X-ray diffractogram of 70HPMC-30CMS-2.5SA-1GA film

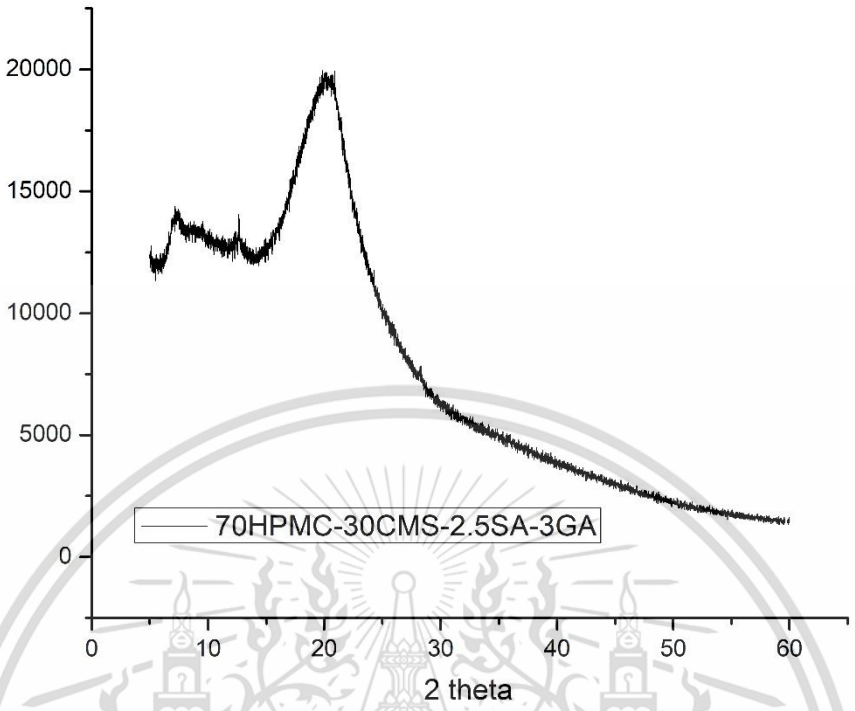

Figure B-10 X-ray diffractogram of 70HPMC-30CMS-2.5SA-3GA film

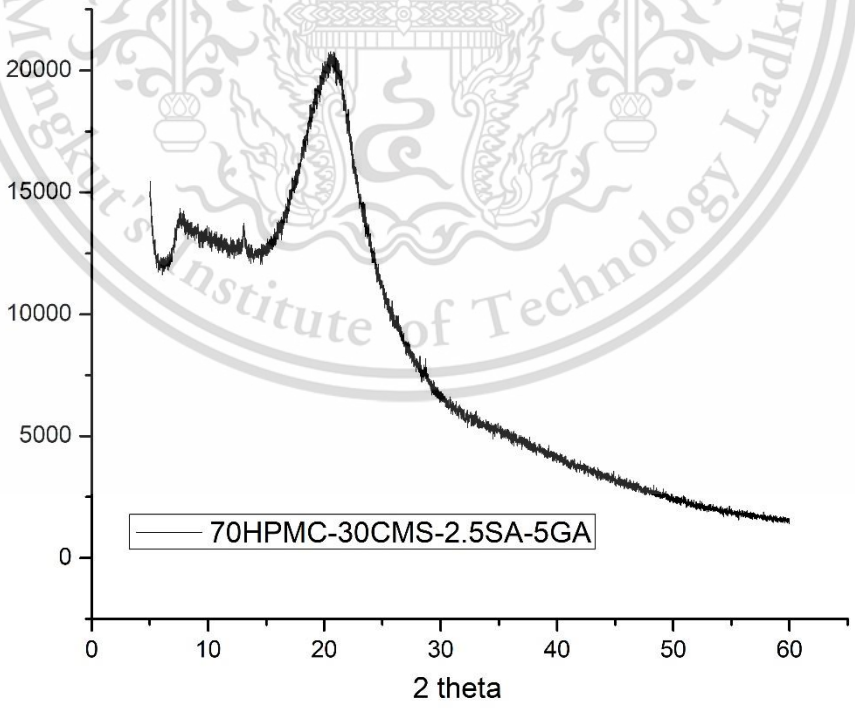

Figure B-11 X-ray diffractogram of 70HPMC-30CMS-2.5SA-5GA film

Appendix C

mechanical properties

Table C-1 Mechanical properties of modified HPMC films with CMS and ZnONPs.

Films	Stress at maximum load (MPa)	Young's modulus (MPa)	Strain at maximum load (%)
CMS	1.80 ± 0.01^{e}	11.20 ± 0.75^{f}	145.00 ± 0.57^{e}
HPMC	38.74 ± 3.03^{a}	346.66 ± 4.50^{a}	77.33 ± 2.08^{a}
90HPMC-10CMS	35.62 ± 1.15^{a}	333.33 ± 2.51^{b}	77.00 ± 1.32^{a}
80HPMC-20CMS	28.25 ± 1.08^{b}	269.00 ± 4.58^{c}	65.33 ± 0.57^{b}
70HPMC-30CMS	23.67 ± 0.13^{c}	251.66 ± 1.15^{d}	53.33 ± 1.52^{c}
70HPMC-30CMS-30ZnONPs	18.72 ± 0.69^{d}	251.67 ± 3.21^{d}	40.66 ± 1.15^{d}
70HPMC-30CMS-50ZnONPs	16.60 ± 1.03^{d}	220.66 ± 1.52^{e}	40.66 ± 0.57^{d}

Table C-2 Mechanical properties of modified 70HPMC-30CMS films by SA and GA

Films	Stress at maximum load (MPa)	Young's modulus (MPa)	Strain at maximum load (%)
70HPMC-30CMS	5.03±0.52^{a}	78.60±7.16^{a}	8.89±1.28^{a}
70HPMC-30CMS-2.5SA	5.55±0.43^{a}	78.64±7.20^{a}	11.32±1.63^{b}
70HPMC-30CMS-2.5SA-1GA	9.31±0.64^{b}	156.65±11.24^{b}	10.21±1.61^{ab}
70HPMC-30CMS-2.5SA-3GA	9.46±0.63^{b}	167.37±15.45^{b}	10.66±1.06^{ab}
70HPMC-30CMS-2.5SA-5GA	9.61±0.73^{b}	168.60±14.93^{b}	10.27±1.59^{ab}

Author Biography

Name	Ms. Vipawan Pitpisutkul
Date of Birth	18 October 1990
Address	30 soi suansiam 2 Ramindra road, Kunnayao, Bangkok, 10230
Education	(2012) Bachelor of science in industrial chemistry (King Mongkut's Institute of Technology Ladkrabang) (2015) Master of science in polymer technology (King Mongkut's Institute of Technology Ladkrabang)
Scholarship	-
Academic Publications	1. V. Pitpisutkul and J. Prachayawarakorn. 2020. "Preparation and physicochemical properties of carboxymethyl starch/hydroxypropyl methylcellulose films. 129-132. In The 10th International Polymer Conference of Thailand, Bangkok 2. V. Pitpisutkul and J. Prachayawarakorn, 2022. "Hydroxypropyl methylcellulose/carboxymethyl starch/zinc oxide porous nanocomposite films for wound dressing application. Carbohydrate Polymers, 298, 120082. 3. V. Pitpisutkul, T. Jamjumras, K. Sawasdee & J. Prachayawarakorn, 2022. Effects of Hydroxypropyl Methylcellulose Fiber Amounts and Aspect Ratios on Properties of Biodegradable Composites Prepared from Thermoplastic Starch. Current Applied Science and Technology, 23. 4. V. Pitpisutkul and J. Prachayawarakorn, 2024. "Porous antimicrobial crosslinked film of hydroxypropyl methylcellulose/carboxymethyl starch incorporating gallic acid for wound dressing application. International Journal of Biological Macromolecules, 256, 128231.

Carbohydrate Polymers 298 (2022) 120082

Contents lists available at ScienceDirect

Carbohydrate Polymers

journal homepage: www.elsevier.com/locate/carbpol

Hydroxypropyl methylcellulose/carboxymethyl starch/zinc oxide porous nanocomposite films for wound dressing application

Vipawan Pitpisutkul [a], Jutarat Prachayawarakorn [a,b,*]

[a] Department of Chemistry, School of Science, King Mongkut's Institute of Technology Ladkrabang (KMITL), Bangkok 10520, Thailand
[b] Advanced Materials Research Unit, School of Science, King Mongkut's Institute of Technology Ladkrabang (KMITL), Bangkok 10520, Thailand

ARTICLE INFO

Keywords:
Starch
Cellulose
Zinc oxide
Wound dressing

ABSTRACT

Because of low moisture uptake, water vapor transmission rate, oxygen transmission rate, swelling capacity and no antibacterial activity of hydroxypropyl methylcellulose (HPMC) film, carboxymethyl starch (CMS) and zinc oxide nanoparticles (ZnO-NPs) were incorporated in order to improve its limitations for wound dressing application. The infrared shifted peak of O—H stretching and O—H bending in HPMC/CMS blended films was detected due to hydrogen bond formation between HPMC and CMS. Scanning electron images of HPMC/CMS blended films exhibited porous structure. In addition, swelling degree, moisture uptake, water vapor transmission rate and oxygen transmission rate of HPMC/CMS blended films with various contents of CMS clearly increased compared to HPMC film. Moreover, HPMC/CMS nanocomposite films loaded with ZnO-NPs showed good antibacterial activity against *Staphylococcus aureus* and *Escherichia coli*, revealing their potential for wound dressing application. Percentage of crystallinity, cytotoxicity, mechanical and thermal properties were also examined.

1. Introduction

Nowadays, research development of biocompatible materials for biomedical applications is a challenging work to modify different chemical structures of natural polymers for multi-functional properties in biofilms. An ideal wound dressing should have the following characteristics: biocompatibility, high fluid absorption capacity, sufficient water vapor transmission rate (WVTR) and antimicrobial behavior. Wound dressings can be produced from a variety of natural polysaccharides, including cellulose and starch (Savencu, Iurian, Porfire, Bogdan, & Tomuță, 2021).

Hydroxypropyl methylcellulose (HPMC), white powder, is non-ionic cellulose ether and commonly used in food and pharmaceutical formulations (Burdock, 2007). The cellulose ether has several important properties such as high tensile strength, biodegradability and good biocompatibility with natural biopolymers (Seddiqi et al., 2021). Typically, hydrogen bonding between polar groups (hydroxypropyl and hydroxyl groups) and hydrophobic interaction between non-polar (methyl) group allow HPMC to generate intermolecular and intramolecular interactions within HPMC structure. However, HPMC films show limited swelling degree, moisture retention and gas exchange with the environment.

HPMC has been reported to blend with several natural biopolymers such as pectin, protein, κ-carrageenan, xanthan gum or chitosan. It was mentioned that HPMC film showed the lowest WVP value and the increase of WVP was detected by the addition of pectin (Peng et al., 2021). The addition of HPMC into corn starch-based films reduced retrogradation of native starch and increased starch film permeability (Jiménez, Fabra, Talens, & Chiralt, 2012). In addition, the improvement of elongation, oxygen permeability and swelling in κ-carrageenan/HPMC film was observed (Sun, Liang, Tan, & Wang, 2018).

One interesting method to improve properties of HPMC film is to blend with chemically-modified starch such as carboxymethyl starch (CMS). CMS is a polysaccharide-based polymer, commonly used in drug delivery, wound treatment and food processing. (Antosik, Piątek, & Wilpiszewska, 2019). CMS can be produced from native starch by etherifying hydroxyl groups with chloroacetic acid resulting in carboxylate group in the starch backbones.

CMS has also been mentioned to mix with other polymers. Hydrophilic films from starch/CMS showed high swelling degree and moisture uptake with the increase of CMS contents (Wilpiszewska, 2019). High moisture uptake was observed in CMS/carboxymethyl cellulose (CMC)

* Corresponding author at: Department of Chemistry, School of Science, King Mongkut's Institute of Technology Ladkrabang (KMITL), Bangkok 10520, Thailand.
E-mail address: jutarat.si@kmitl.ac.th (J. Prachayawarakorn).

https://doi.org/10.1016/j.carbpol.2022.120082
Received 17 May 2022; Received in revised form 31 August 2022; Accepted 2 September 2022
Available online 7 September 2022

blended film as CMS concentration increased (Antosik et al., 2019). The enhancement of swelling degree in polyvinyl alcohol/CMS composite gel was also observed when CMS contents increased (Gong, Zhang, Cheng, & Zhou, 2015).

Interestingly, the blending of both hydrophilic polymers, i.e., HPMC and CMS has never been reported. It is expected that swelling degree, moisture uptake and WVTR of HPMC will be improved with the incorporation of CMS. Since both HPMC and CMS show no antibacterial activity; therefore, zinc oxide nanoparticles (ZnO-NPs) antibacterial agent was added. ZnO-NPs have been applied in several daily products such as drug delivery, cosmetics, and medical devices. The increased contents of ZnO-NPs in the wound dressing prepared from basil seed (*O. basilicum* L.) mucilage-ZnO nanocomposite caused the improvement of water retention, mechanical properties and antibacterial activity (Tantiwatcharothai & Prachayawarakorn, 2020). Tensile properties and antibacterial performance against *S. aureus* of chitosan-based film were found to increase when hydroxyapatite was added (Cunha et al., 2020). Because HPMC film shows low swelling degree and water vapor transfer, anionic CMS could be added to improve its limitations. Moreover, antibacterial activity of the blend could be solved by the addition of ZnO-NPs. To best of our knowledge, HPMC/CMS blended films modified by ZnO-NPs have not been mentioned.

This study aimed to improve the properties of HPMC film for wound dressing application by blending it with different contents of CMS and ZnO-NPs. Various HPMC/CMS/ZnO-NPs films were characterized by functional group analysis, X-ray diffraction and morphology. Moreover, mechanical properties, thermal stability, moisture uptake, WVTR, oxygen transmission rate, swelling degree, whiteness, antibacterial activity and cytotoxicity were also examined.

2. Experimental

2.1. Materials

HPMC (Methocel F4M) was obtained from Union Chemical 1986 Co., Ltd. (Bangkok, Thailand) with 27.9 % methoxy group, 7.4 % hydroxypropoxy group and an averaged viscosity value of 4021 mPa·s. Cassava starch (16.4 % amylose and 83.6 % amylopectin) was received from Chaopraya Phuchrai 1999 Co., Ltd. (Kamphaengphet, Thailand). Glycerol (Food grade $\geq$ 99.7 %) and monochloroacetic acid (MCA, ACS reagent $\geq$ 99.0 %) were purchased from Chemipan Co., Ltd (Bangkok, Thailand) and Italmar Co., Ltd (Bangkok, Thailand), respectively. ZnO-NPs (20–40 nm) were supplied from Nano Materials Technology, Co. Ltd. (Chonburi, Thailand). Silver nitrate and sodium hydroxide were AR grade.

2.2. CMS preparation

CMS was prepared according to Wilpiszewska, Antosik, and Spychaj (2015). Briefly, cassava starch (12.5 g) was suspended in 300 mL isopropanol solution 90 % (v/v) and continuously stirred. NaOH (7.7 M) solution was poured into the suspension with continuous stirring at room temperature. After 45 min, MCA (10.93 g) was added and the mixture was stirred at the temperature of 50 °C. After 3 h, the starch suspension was neutralized with glacial acetic acid and filtered by vacuum filtration. The solid filtrate was washed with 85 % ethanol until no chloride ion could be detected with $AgNO_3$ test. The obtained modified starch was filtered and dried at 60 °C for 24 h.

Degree of substitution of the prepared CMS was determined. CMS powder 5 g, (Na-CMS form) was dispersed in acetone (150 mL), 5 M aqueous HCl (15 mL) was added and then stirred to convert Na-CMS to H-CMS. The neutral dispersion after washing by ethanol was filtered and dried. H-CMS (0.5 g) was dissolved in 0.2 M NaOH aqueous solution. The mixture was back-titrated with 0.05 M HCl using phenolphthalein indicator (Stojanović, Jeremić, Jovanović, & Lechner, 2005). Degree of substitution of the prepared CMS was found to be 0.85 $\pm$ 0.07.

2.3. Preparation of HPMC and modified HPMC films

Several HPMC films were produced by solution casting using glycerol as the plasticizer. Different contents of CMS (0, 10, 20 and 30 wt% were added into HPMC matrix) and two different contents of ZnO-NPs i.e., 30 % and 50 wt% were incorporated into the blend of HPMC and CMS matrix. The concentration of the film forming solutions was maintained at 2 % (w/v) using 30%wt of glycerol. For the nanocomposite films, the solution containing HPMC, CMS and glycerol were prepared and then ZnO-NPs was added. The solution was heated and stirred (85 °C, 1 h). After that, the solution was cool down to room temperature. Finally, the solution was poured into polypropylene trays and dried (60 °C, 16 h).

2.4. Fourier-transform infrared spectroscopy (FT-IR)

FT-IR spectroscopic analysis was used to record IR spectra by using Spectrum 2000 GX spectrometer (PerkinElmer, USA). The scanning range of FT-IR was performed at the wavelength of 4000–400 cm^{-1} with a resolution of 4 cm^{-1} using ten consecutive scans.

2.5. Morphology

Cross-section morphology of a film was examined by a scanning electron microscope (SEM) (LEO 1455VP, ZEISS, Germany) using an accelerating voltage of 15 kV. The sample film was fractured under liquid nitrogen, fixed on a stub and coated with a thin gold layer.

2.6. X-ray diffraction (XRD)

A diffractogram was recorded using Smart lab (Rigaku, Japan) with CuKα (λ = 1.54 Å) radiation operating at 40 kV and 30 mA with the angular range of 2θ = 5–60°. The degree of crystallinity was calculated by Eq. (1):

$$\text{Crystallinity}\ (\%) = \frac{\text{Ac}}{\text{Ac} + \text{Aa}} \times 100 \quad (1)$$

where A_c was the area corresponding to the crystalline region (2θ = 5–30°) and A_a was the amorphous region (2θ = 5–60°) on the X-ray diffractogram.

2.7. Mechanical properties

A universal testing machine (Lloyd LR 5 K) with 100 N load cell and 50 mm/min crosshead speed was used to determine the mechanical properties of a film (ASTM D-882). The film with the averaged thickness of 0.09–0.10 mm. was cut into 100 × 15 mm^2. The film was conditioned at 60 $\pm$ 2 % RH using a saturated ammonium nitrate solution. All the mechanical tests were conducted at 23 $\pm$ 1 °C and 60 $\pm$ 2%RH.

2.8. Moisture uptake, WVTR and oxygen transmission rate (OTR)

A film was dried at 105 °C for 3 h and then kept in a closed container at 99 $\pm$ 1 % RH. The content of water absorbed by the film was determined for 10 days (ASTM D-570). The percentage of moisture uptake was calculated as Eq. (2):

$$\text{Moisture uptake} = \frac{W_2 - W_1}{W_1} \times 100 \quad (2)$$

where W_2 and W_1 were the wet and the dried weights of the sample, respectively.

WVTR was measured with the gravimetric modified cup method (the desiccant method) (ASTM E96). The sealed cup with the film testing (with an area of 32.15 cm^2) was weighted and placed in a chamber at constant 75 % RH by containing a saturated solution of sodium chloride. WVTR was measured every 24 h for 7 days.

The OTR of samples (with an area of 50 cm^2) was measured using a Mocon OX-Tran 2/22(L) (Mocon Inc., USA) according to ASTM D3985 operated at 23 °C and 0 % RH. The WVTR, and OTR were determined using the following equations:

$$WVTR = \frac{\Delta m}{(\Delta t \bullet A)} \quad (3)$$

$$OTR = (dV/dt)/A \quad (4)$$

where $\Delta m/\Delta t$, dV/dt and A were the weight gain of film samples per day (g/day), the volume of permeated oxygen and permeative surface area of film samples (cm^2), respectively.

2.9. Swelling degree

A film (20 × 20 mm^2) was dried at 105 °C for 2 h and immersed in distilled water at room temperature for 24 h. The weight of the wet film (W_2) was measured after water removal from the surface. Percentage of swelling was calculated as followed:

$$\text{Swelling } (\%) = \frac{W_2 - W_1}{W_1} \times 100 \quad (5)$$

where W_2 and W_1 were the wet and the dried weights of the sample, respectively.

2.10. Whiteness

The surface color of each sample was measured using a colorimeter (HunterLab, MiniScan XE Plus). Whiteness index (WI) of the films was calculated using Eq. (6):

$$WI = 100 - \sqrt{(100 - L^*)^2 + (a^{*2} + b^{*2})} \quad (6)$$

where; L*, a*, and b* referred the film color values (McDonald, 1997).

2.11. Thermal properties

A sample of approximately 10–12 mg was tested under nitrogen atmosphere within a temperature range of 30 to 600 °C at the heating rate of 10 °C/min using a thermogravimetric analyzer (TGA/DSC 3+ Mettler Toledo, Switzerland).

2.12. Antibacterial activity

The inhibition zones were examined by the agar diffusion method against *S. aureus* and *E. coli* pathogens. The sample discs with the diameter of 10 mm were placed on an agar plate loaded with Gram-positive and Gram-negative strains before the incubation (37 °C, 24 h). The inhibition zone diameter was determined for the antimicrobial activities of the sample.

2.13. In vitro cytotoxicity

For cytotoxicity test, MTT assay using human keratinocytes (HaCat) cells was utilized. A sample (0.0115 ± 0.0007 g) was immersed in phosphate-buffered saline, and filtered, then, Dulbecco's Modified Eagle Condition was added. The mixture was incubated (37 °C, 24 h) and supplemented with 10 % fetal bovine serum. HaCat cells 100 μL (1 × 10^5 cells/mL) were seeded and incubated (37 °C, 24 h) into each well of a 96-well plate. Then, 100 mL of the incubated filtrate mixture and 10 μL of the MTT solution (5 mg/mL) were added and incubated at 37 °C for 4 h. Then, formazan dissolution and the resultant solution were added to the well. The absorbance at 570 nm of the final mixture was measured using a Biochrom microtiter plate reader. Cell morphology was examined using optical microscope images. Percentages of cytotoxicity and cell viability were calculated by the following equations.

$$\%\text{Cytotoxicity} = (A–B/A) \times 100 \quad (7)$$

$$\%\text{Cell viability} = 100 - \text{Cytotoxicity} \quad (8)$$

where; A and B were the absorbances of the control and test wells, respectively.

2.14. Statistical analysis

Statistical analysis was performed by using the analysis of variance (ANOVA) procedure with IBM SPSS statistics 25 software. Tukey's test was used to measure differences among the means ($p < 0.05$).

3. Results and discussion

A schematic diagram presenting the possible interactions between biopolymers (HPMC and CMS) including ZnO-NPs is shown in Figs. 1(a) and (b). The functional groups of HPMC containing methoxyl groups (–OCH_3), hydroxy proproxyl groups (–$CH_2(CH)CH_3OH$) and hydroxyl group (–OH) which could form hydrogen bonds with polar groups of CMS (carboxyl and hydroxyl groups). For HPMC/CMS/ZnO-NPs films, HPMC could form not only hydrogen bond with CMS and ZnO-NPs but also electrostatic interaction with ZnO-NPs. Carboxylate groups (COO^-) of CMS could interact with Zn^{2+} ions by forming electrostatic interaction. Similar interactions were also reported for the casted chitosan/ZnO nanocomposite films (Boura-Theodoridou et al., 2020). The electrostatic interaction and hydrogen bond were also found in CMC/ZnO nanocomposite hydrogel via crosslinking with Zn^{2+} ions (Priyadarshi, Kumar, & Rhim, 2020).

3.1. FTIR

For FTIR spectrum of HPMC (Fig. 2(a)), the major wavenumbers were at 3408 cm^{-1}, 1460 cm^{-1} and 1387 cm^{-1} ascribed to O—H stretching, O—H bending and C—H bending, respectively. The medium-intensed bands at 1109 cm^{-1} was assigned to C—O—C asymmetric stretching and another wavenumber at 1045 cm^{-1} was corresponded to C—O stretching (Zhang et al., 2013). Additionally, the spectrum of CMS presented the weak peak position at 1735 cm^{-1}, caused by C═O stretching of carboxylic group. Asymmetric stretching of carboxylate group (COO^-) gave a strong absorption peak at 1608 cm^{-1} and the peak positions at 1412, 1155 and 1079 cm^{-1} were corresponded to C—O symmetric stretching of carboxylate groups, C—H bending and C—C stretching vibrations, respectively (Kaczmarska et al., 2018).

For HPMC/CMS blended films, the vibrational broad peak at 1630, 1645 and 1608 cm^{-1} exhibited the characteristic overlapped peak between HPMC and CMS components. The new absorption bands at 1155 cm^{-1}, corresponded to C—H bending of CMS were also observed. In addition, the shifted peak of O—H stretching and O—H bending to lower wavenumbers was detected due to new hydrogen bond formation between the two components (Wilpiszewska et al., 2015).

The spectra of various HPMC/CMS/ZnO-NPs nanocomposite films are shown in Fig. 2(b). FTIR spectra of two contents of ZnO-NPs (30 and 50 %) in the blend films presented the characteristic bands similar to those observed for HPMC/CMS blends. However, the shifted peak of O—H bending to lower wavenumber was observed in the nanocomposite films. This result was due to the new hydrogen bond formation between HPMC, CMS and ZnO-NPs. Moreover, two new absorption wavenumbers were observed at around 455 and 432 cm^{-1}, attributed to Zn—O stretching vibration (Raafat, El-Sawy, Badawy, Mousa, & Mohamed, 2018).

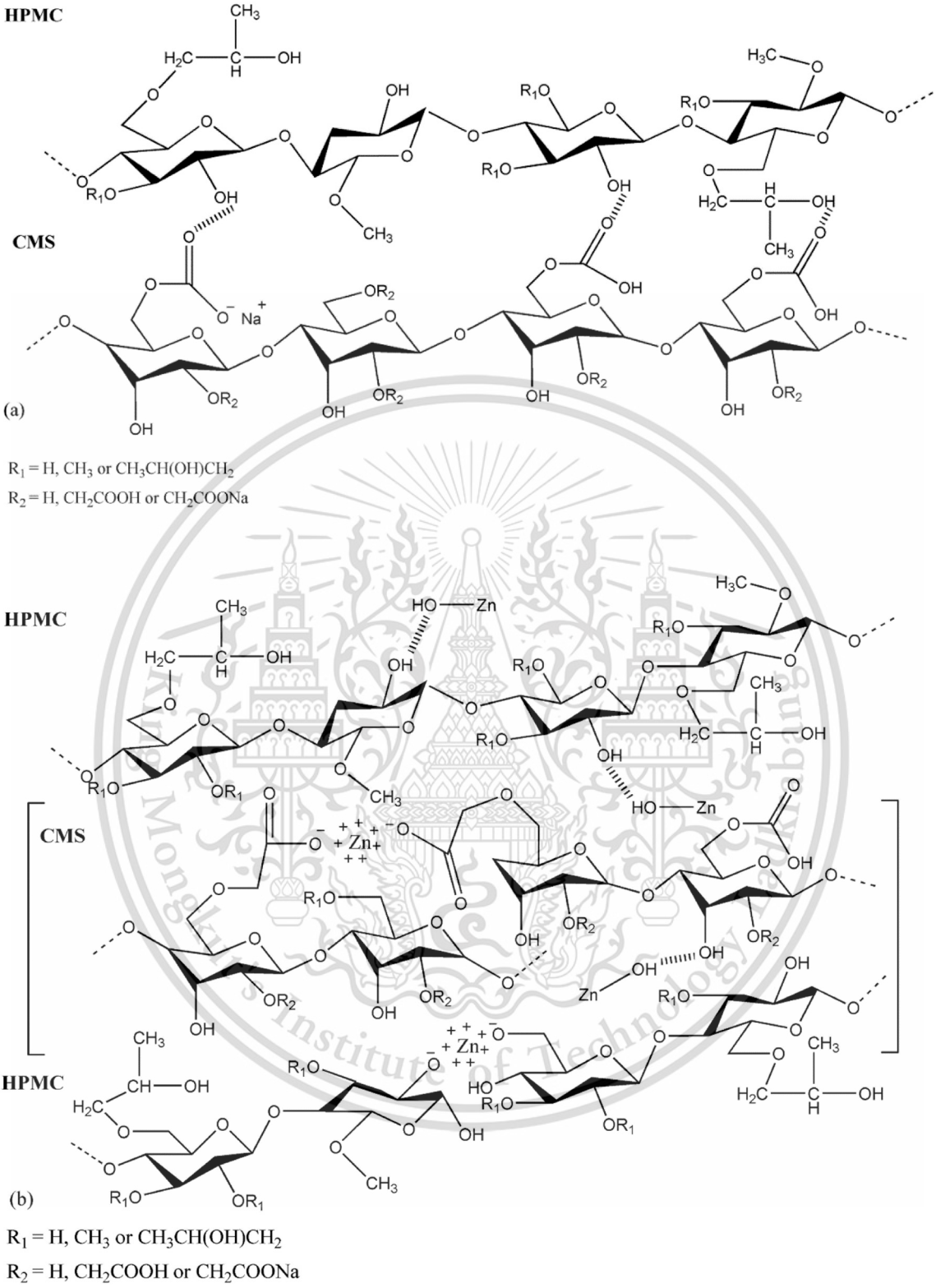

Fig. 1. The schematic representation of different types of interactions for (a) HPMC/CMS and (b) HPMC/CMS/ZnO-NPs. Abbreviations: HPMC—hydroxypropyl methyl cellulose; CMS—carboxymethyl starch.

3.2. XRD

XRD patterns of different HPMC/CMS/ZnO-NPs films are shown in Fig. 3. The semi-crystalline structure of HPMC showed the diffracted peak at 2θ of 7.6° and 20.8°. The diffracted peaks of CMS at 2θ of 17.1° and 21.7° exhibited broad peaks, indicating of amorphous domain from the starch etherification by MCA (Fig. 3(a)). For various HPMC/CMS blended films, the XRD peaks were also located at 2θ of 7.6° and 20.8° but the decreased intensity of the diffracted peak at 2θ of 20.8° and percentage of crystallinity (Table 1) were clearly found for HPMC/CMS films, especially for 70HPMC/30CMS film, resulting from the addition of CMS. The reduction of the crystallinity in HPMC/CMS blended films was

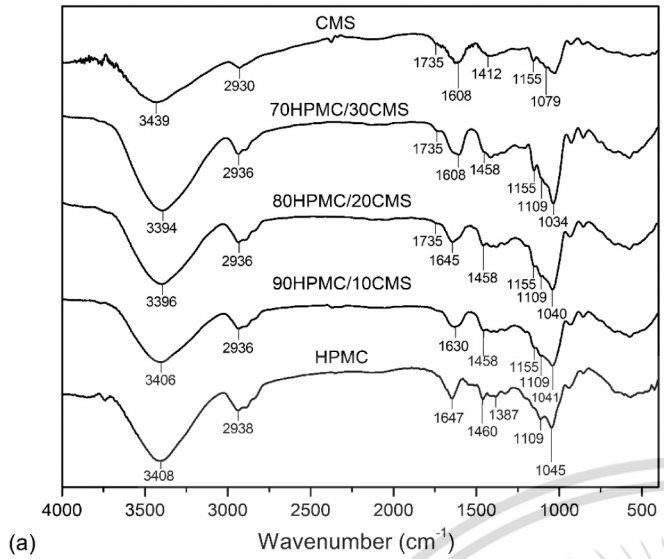

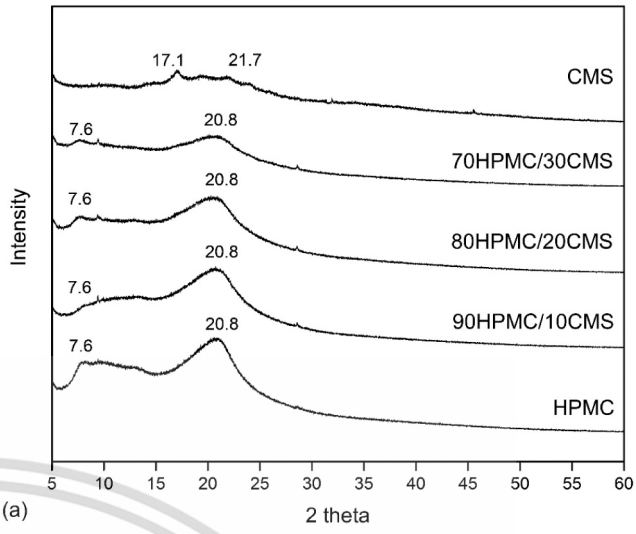

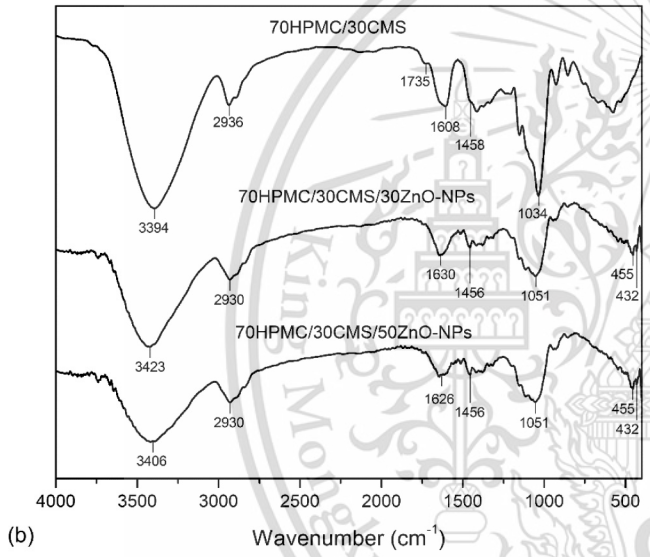

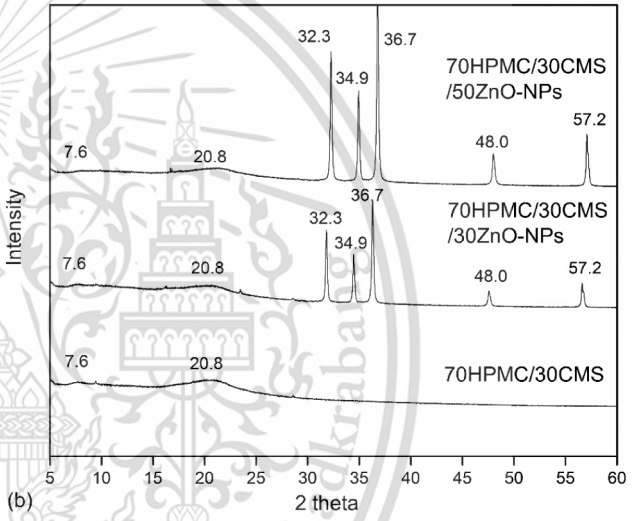

Fig. 2. FTIR spectra of different HPMC films (a) HPMC/CMS and (b) HPMC/CMS/ZnO-NPs.

Fig. 3. X-ray diffractograms of various HPMC films (a) HPMC/CMS and (b) HPMC/CMS/ZnO-NPs.

caused by intermolecular interaction between HPMC and CMS, led to the restriction of molecular chain rearrangement of HPMC (Fig. 1(a)). Similar result was reported for HPMC-CMC film with the drop of HPMC crystalline plane (Dharmalingam & Anandalakshmi, 2019). The diffraction pattern of different HPMC/CMS/ZnO-NPs films (Fig. 3(b)) showed the characteristic diffraction peaks of ZnO-NPs consisting of the sharp peaks at 2θ values of 32.3°, 34.9°, 36.7° 48.0° and 57.2°, corresponded to (100) (002) (101) (102) and (110) lattice planes of hexagonal wurtzite structure, respectively (Kanmani & Rhim, 2014). It should be noted that the percentage of crystallinity of the nanocomposite films was lower than 70HPMC/30CMS. However, the increase in ZnO-NPs contents was not affect the degree of crystallinity of different HPMC/CMS/ZnO-NPs films.

3.3. SEM

It was found that morphology of HPMC film (Fig. 4(a)) was rather rough with good phase continuity. In contrast, HPMC/CMS films (Fig. 4 (b)–(d)) clearly exhibited porous structures. This could be due to salting-out phenomenon of sodium salts of CMS components in HPMC solution. Sodium salts of CMS might facilitate the thermally induced solid-liquid phase separation of HPMC solution during the drying, resulting in HPMC-based microporous films after water evaporation (Zhang et al., 2021). The increasing concentration of CMS-Na introduced HPMC aggregation and the formation of HPMC coagulation phase that enclosed the remaining water phase was induced by further water evaporation (Zhang et al., 2020). Moreover, various types of sodium salt could form microstructure on HPMC films (Zhang et al., 2017). When CMS contents were increased, the pore shape tended to elongate.

Moreover, the surface morphology of various nanocomposite films (Fig. 4(e)–(f)) showed a relatively uniform distribution of ZnO-NPs including some ZnO-NPs agglomeration (red arrows), especially when the nanoparticle contents increased. In addition, the morphology of 70HPMC/30CMS/50ZnO-NPs film was rougher than that of 70HPMC/30CMS/30ZnO-NPs film due to the increased agglomeration of ZnO-NPs.

3.4. Mechanical properties

Mechanical properties of various HPMC films are shown in Table 1 and Fig. 5. The highest stress at maximum load and Young's modulus was found in HPMC film due to the high crystallinity of HPMC (Table 1). With increasing CMS content, HPMC/CMS blended films showed a significant decrease in stress at maximum load, Young's modulus, and

Table 1
Percentage of crystallinity, mechanical properties of various HPMC films.

Films	Crystallinity (%)	Stress at maximum load (MPa)	Young's modulus (MPa)	Strain at maximum load (%)
HPMC	15.05	38.17 ± 6.72^{a}	349.80 ± 28.42^{a}	73.50 ± 12.48^{a}
90HPMC/10CMS	14.00	37.57 ± 6.78^{a}	342.70 ± 19.88^{ab}	68.30 ± 12.58^{ab}
80HPMC/20CMS	10.99	26.63 ± 2.38^{b}	248.10 ± 15.09^{ab}	65.00 ± 4.63^{ab}
70HPMC/30CMS	7.52	24.03 ± 2.25^{b}	250.90 ± 12.79^{b}	59.60 ± 6.74^{b}
70HPMC/30CMS/30ZnO-NPs	6.55	18.23 ± 2.79^{c}	244.86 ± 17.38^{c}	42.20 ± 9.04^{c}
70HPMC/30CMS/50ZnO-NPs	6.15	16.26 ± 4.95^{c}	229.60 ± 12.41^{c}	42.50 ± 13.65^{c}

Different superscript letters in the same column are significantly different ($p < 0.05$), based on Tukey's test.

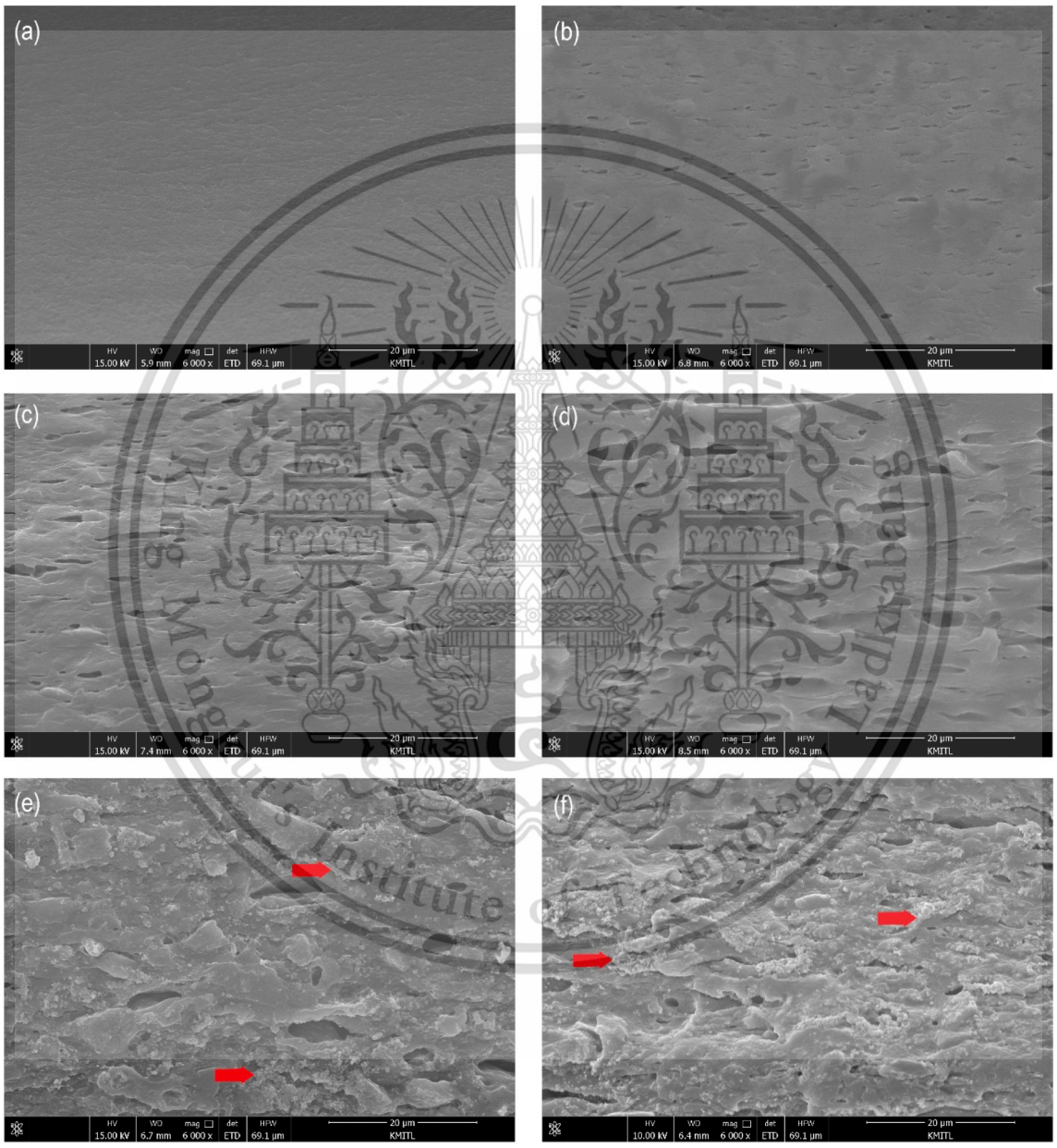

Fig. 4. Cross-section morphology of films (a); HPMC, (b) 90HPMC/10CMS, (c) 80HPMC/20CMS, (d) 70HPMC/30CMS, (e) 70HPMC/30CMS/30ZnO-NPs and (f) 70CMS/30HPMC/50ZnO-NPs.

strain at maximum load. The main reasons were the porous morphology and the decrease in the percentage of crystallinity, as confirmed by SEM and XRD analysis, respectively.

Additionally, it was shown that nanocomposite films showed lower stress at maximum load and Young's modulus than HPMC/CMS films, as related with XRD data (Table 1). This may be due to the presence of ZnO-NPs agglomeration that reduced phase continuity (Fig. 4(e)–(f)). Therefore, stress transfer between HPMC and CMS in the nanocomposite films was inhibited. The decrease in mechanical properties was also reported for poly(vinyl alcohol)/chitosan/ZnO-NPs films due to the nanoparticle agglomeration (Hezma, Rajeh, & Mannaa, 2019). Typically, tensile strength of wound dressing film should be in the range of

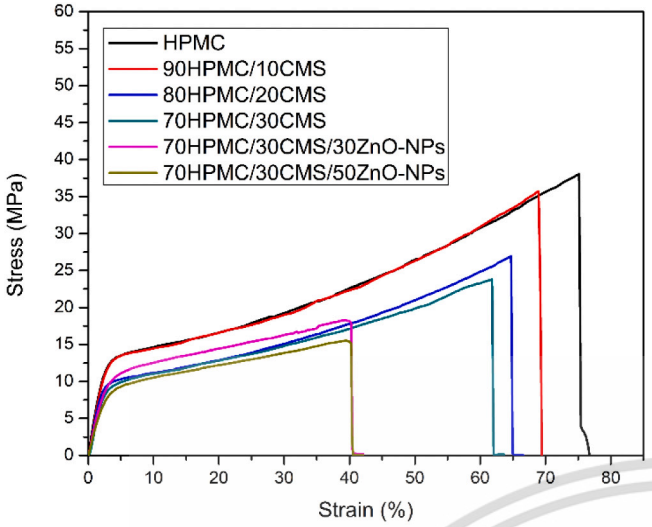

Fig. 5. Stress-strain curve of various HPMC films.

2.5–16 MPa (Savencu et al., 2021) and the stress at maximum load of various porous films obtained from this study was within this range.

3.5. Moisture uptake, WVTR, OTR and swelling properties

The ideal wound dressing film is needed to maintain wound hydration, allow gas exchange and remove excess exudate. It can be seen from Table 2 that HPMC film showed the lowest moisture uptake. The moisture uptake of HPMC/CMS films clearly increased with the increasing contents of CMS and 70HPMC/30CMS blended film presented the highest moisture uptake, especially at day 10. This was attributed to the higher polarity of anionic CMS and to the film porous structure. As expected, 70HPMC/30CMS/ZnO-NPs films showed lower moisture uptake than 70HPMC/30CMS blended film possibly due to the partially disappearance of hydrophilic groups of HPMC and CMS by forming hydrogen bonding and electrostatic interaction with ZnO-NPs.

The WVTR values of different blended films in Table 2 were raised with the increase of CMS contents. The result was related to the decrease of crystallinity including the porous structure as confirmed by XRD and SEM techniques.

However, the reduction of WVTR in 70HPMC/30CMS/ZnO nanocomposite films was observed and the lowest WVTR was detected in 70HPMC/30CMS/50ZnO-NPs film. ZnO-NPs in HPMC/CMS matrix could generate a tortuous pathway that inhibited the movement of water molecules through the film even further. The reduction of WVTR was also founded in chitosan film incorporated ZnO-NPs (Priyadarshi & Negi, 2017). Nevertheless, the WVTR of 70HPMC/30CMS/30ZnO-NPs film was higher than that of 70HPMC/30CMS/50ZnO-NPs and HPMC films. Additionally, when compared to HPMC film, the WVTR data of various film samples increased and demonstrated the acceptable WVTR values of commercial wound dressing materials (Wang, Shih, Hsieh, Huang, & Wang, 2020; Wu, Fisher, Foo, Queen, & Gaylor, 1995). A higher WVTR typically suggests faster wound drying, which leads to scar creation, but a lower WVTR generates slow healing process and raises the risk of bacterial growth.

Essentially, oxygen is required wound healing process. The OTR values of the different films (Table 2) surpassed the instrument testing and were >2000 cm^3 m^{-2} day^{-1}, whereas, the OTR value was <100 cm^3 m^{-2} day^{-1} for HPMC film. Higher OTR values of various HPMC films added by CMS and ZnO-NPs were due to the porous structure of the films. Similar observation was reported for porous chitosan-based films (Chitrattha & Phaechamud, 2016).

Swelling behavior was found to increase when the swelling time raised. All HPMC/CMS blended films presented higher percentage of swelling (Table 2) than HPMC film due to the decrease of crystallinity (Table 1), leading to high free volume of polymer system. Moreover, the carboxylate groups of CMS could establish empty sites between polymer chains by repelling negative charges from each other.

The swelling degree of different HPMC/CMS/ZnO-NPs nanocomposite films was found to decrease significantly when ZnO-NPs contents were increased. This result may be due to new hydrogen bond and electrostatic interaction between ZnO-NPs and HPMC/CMS matrix, resulting in the decrease of free volume in the polymer system.

3.6. WI

WI values of all films were shown in Table 3. HPMC film showed a relative clear film with WI at 11 %, while the addition of CMS indicated the gradual increase of WI. As expected, the addition of ZnO-NPs into HPMC/CMS blended film clearly presented higher WI than the control film (70HPMC/30CMS) due to high whiteness characteristics of ZnO-NPs, especially for 70HPMC/30CMS/50ZnO-NPs.

3.7. Thermal properties

Thermogravimetric (TGA) and derivative thermogravimetric (DTG) thermograms of various HPMC films are shown in Fig. 6 and Table 3. The first decomposition stage was caused by water evaporation. The second step was arisen from the thermal degradation of glycerol including CMS at the temperature of 207–259 °C, with the *overlapping* decomposition *temperature* between CMS and glycerol. The third stage from 349 to 355 °C was due to the thermal degradation of HPMC (Gómez-Carracedo, Alvarez-Lorenzo, Gómez-Amoza, & Concheiro, 2003). It should be noted that HPMC degradation temperatures of various blended films were not significantly changed.

The incorporation of ZnO-NPs into HPMC/CMS matrix led to the reduction of thermal decomposition temperature (Fig. 6(b) and (d)). It was reported that thermal excitation of ZnO was able to form free oxygen and promotes the peroxy radicals to damage the polymer chain (Ma & Zhang, 2009). Moreover, the weight loss at the temperature around 350 °C of HPMC/CMS blended films and HPMC/CMS/ZnO-NPs nanocomposite films decreased when CMS and ZnO-NPs contents

Table 2
Moisture uptake, WVTR, OTR and swelling degree of various HPMC films.

Films	Moisture uptake (%)		WVTR ($g\ m^{-2}\ day^{-1}$)	OTR ($cm^3\ m^{-2}\ day^{-1}$)	Swelling degree (%)	
	Day 4	Day 10			1 h	24 h
HPMC	10.86 ± 2.08^{a}	13.89 ± 2.37^{d}	165.81 ± 0.87^{e}	89.17	99.16 ± 4.36^{b}	165.66 ± 4.50^{bc}
90HPMC/10CMS	16.89 ± 1.53^{b}	22.18 ± 2.24^{c}	170.71 ± 1.70^{de}	–	96.72 ± 6.04^{b}	168.33 ± 8.02^{bc}
80HPMC/20CMS	19.35 ± 1.58^{b}	25.88 ± 1.90^{ab}	172.48 ± 2.01^{cd}	–	106.16 ± 6.30^{b}	183.00 ± 2.64^{ab}
70HPMC/30CMS	20.51 ± 1.53^{b}	28.39 ± 2.52^{a}	222.68 ± 4.73^{a}	>2000	155.66 ± 2.96^{a}	200.33 ± 9.33^{a}
70HPMC/30CMS/30ZnO-NPs	18.84 ± 1.02^{b}	25.51 ± 0.53^{ab}	203.62 ± 1.19^{b}	>2000	77.52 ± 4.17^{c}	180.33 ± 2.30^{b}
70HPMC/30CMS/50ZnO-NPs	17.76 ± 3.60^{b}	20.14 ± 0.59^{c}	178.05 ± 4.36^{c}	>2000	69.34 ± 6.76^{c}	157.33 ± 2.08^{c}
Control (without film)			555.23 ± 6.40			

Different superscript letters in the same column are significantly different ($p < 0.05$), based on Tukey's test.

Table 3
WI, thermal properties, inhibition zones and MTT assay results of various HPMC films.

Films	WI (%)	Degradation temperature (°C)				Zone of inhibition (mm)		Cytotoxicity (%)	Cell viability (%)
		Step 1 (Water)	Step 2 (Glycerol + CMS)	Step 3 (HPMC)	Weight loss (%)	*S. aureus*	*E. coli*		
HPMC	10.86 ± 0.10^{a}	78	207	355	90.62	Inactive	Inactive	2.37 ± 0.04^{c}	97.59
90HPMC/10CMS	12.82 ± 0.29^{b}	98	238	353	88.67				
80HPMC/20CMS	12.71 ± 0.47^{b}	86	243	353	87.62				
70HPMC/30CMS	13.77 ± 0.55^{b}	87	259	353	85.91	Inactive	Inactive	6.79 ± 0.10^{b}	93.21
70HPMC/30CMS/30ZnO-NPs	77.46 ± 1.26^{c}	88	233	350	67.41	22.3	17.7	7.61 ± 0.14^{b}	92.39
70HPMC/30CMS/50ZnO-NPs	86.58 ± 1.30^{d}	85	230	349	57.22	23.5	19.1	13.08 ± 0.51^{a}	86.92
Control								5.52 ± 0.43	94.45

Different superscript letters in the same column are significantly different ($p < 0.05$), based on Tukey's test.

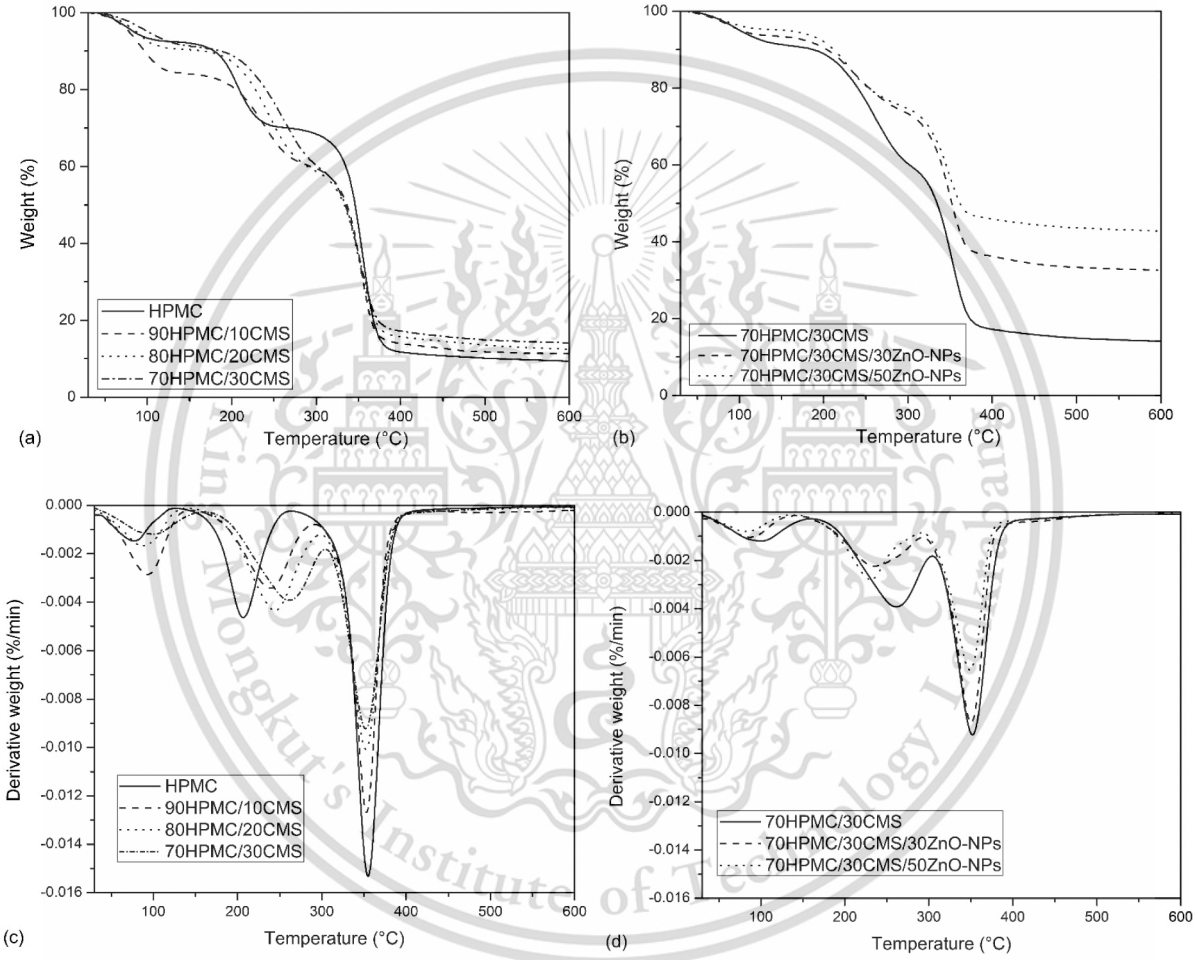

Fig. 6. TGA and DTG of various HPMC films.

increased. The result implied that the addition of CMS and ZnO-NPs into HPMC film led to the improvement of thermal stability. Similar result was also observed in PVA/pluronic/ZnO blends (Amin, Partila, Abd El-Rehim, & Deghiedy, 2020).

3.8. Antimicrobial activities

The effectiveness of antibacterial activity against bacteria in various HPMC films was determined using *S. aureus* (Gram positive) and *E. coli* (Gram negative). The inhibition zones of different HPMC films are shown in Table 3 and Fig. 7(a). It was observed that the addition of ZnO-NPs in 70HPMC/30CMS blended film showed the increase of antibacterial activity when ZnO-NPs contents increased. Furthermore, antibacterial activity against *S. aureus* strain represented more inhibition zone than that of *E. coli* strain. The result was arisen from the differences in bacteria cell wall structures: Gram-positive bacteria composes of the dense cell walls of peptidoglycan; while, Gram-negative bacteria presents more complex cell wall and, thus, caused the difficulty of an antimicrobial agent to penetrate into the bacterial cell (Gutiérrez et al., 2017). Several observations were also mentioned for tragacanth gum-based nanocomposite film and basil seed mucilage-ZnO nanocomposite sponge (Janani, Zare, Salimi, & Makvandi, 2020; Tantiwatcharothai & Prachayawarakorn, 2020).

3.9. In vitro cytotoxicity

MTT test using HaCat cells was carried out to compare the cytotoxicity of the various films to that of a control (no ZnO-NPs). It was

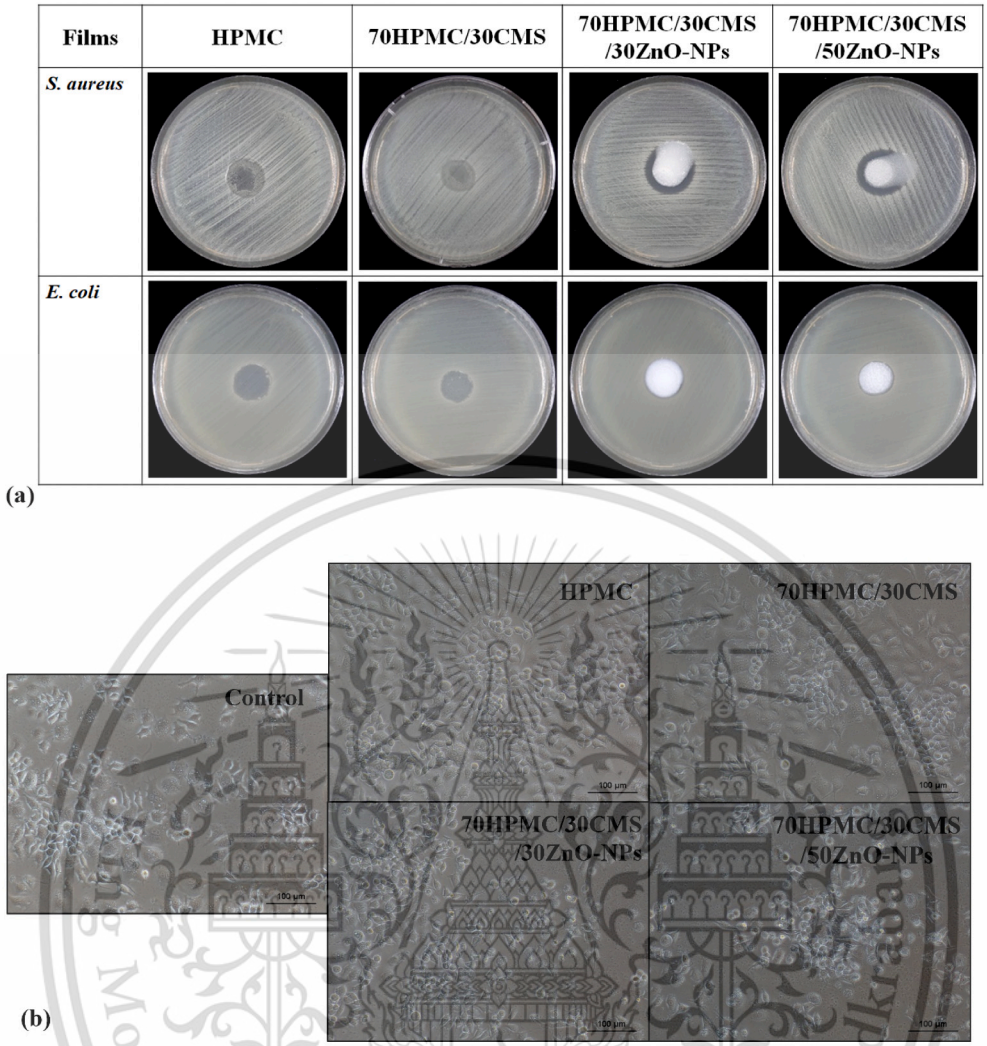

Fig. 7. (a) Inhibition zones of different HPMC films against *S. aureus* and *E. coli* and (b) optical images of HaCat cells incubated after 24 h of various HPMC films.

observed that the cytotoxicity and cell viability of nanocomposite films tended to decrease with the incorporation of ZnO-NPs as shown in Fig. 7 (b) and Table 3. However, the blended and nanocomposite films were non-toxic to human cells since all of the cell viability values were higher than 80 % (Zepon et al., 2019).

4. Conclusion

Various porous HPMC/CMS/ZnO-NPs nanocomposite films were successfully prepared by solution casting technique. When CMS and ZnO-NPs were incorporated into HPMC film, the IR shifted peak of O—H bending was observed, indicating the formation of new hydrogen bonds. The addition of CMS to HPMC film caused the increase of WVTR, OTR and swelling degree; while, crystallinity and mechanical properties reduced. The incorporation of ZnO-NPs improved antibacterial activity against *S. aureus* and *E. coli*. Moreover, HPMC/CMS nanocomposite films were not toxic to human cells (HaCat cells). In this study, the optimal ZnO-NPs loading in nanocomposite films was 30 % ZnO-NPs, which offered a good balance of physicochemical characteristics and antibacterial activity for wound dressing application.

CRediT authorship contribution statement

Vipawan Pitpisutkul: Investigation, Methodology, Validation, Writing – original draft, Formal analysis. **Jutarat Prachayawarakorn:** Validation, Supervision, Funding acquisition, Writing – review & editing.

Declaration of competing interest

The authors declare that they have no known competing financial interests or personal relationships that could have appeared to influence the work reported in this paper.

Data availability

No data was used for the research described in the article.

Acknowledgements

The authors express their sincere appreciation to King Mongkut's Institute of Technology Ladkrabang (Grant No. KREF 046108) for financial support and to School of Science for facility support.

References

Antosik, A. K., Piątek, A., & Wilpiszewska, K. (2019). Carboxymethylated starch and cellulose derivatives-based film as human skin equivalent for adhesive properties testing. *Carbohydrate Polymers, 222*, Article 115014.

Amin, K. M., Partila, A. M., Abd El-Rehim, H. A., & Deghiedy, N. M. (2020). Antimicrobial ZnO nanoparticle-doped polyvinyl alcohol/pluronic blends as active

food packaging films. *Particle & Particle Systems Characterization, 37*(4), Article 2000006.
Boura-Theodoridou, O., Giannakas, A., Katapodis, P., Stamatis, H., Ladavos, A., & Barkoula, N.-M. (2020). Performance of ZnO/chitosan nanocomposite films for antimicrobial packaging applications as a function of NaOH treatment and glycerol/PVOH blending. *Food Packaging and Shelf Life, 23*, Article 100456.
Burdock, G. A. (2007). Safety assessment of hydroxypropyl methylcellulose as a food ingredient. *Food and Chemical Toxicology, 45*(12), 2341–2351.
Chitrattha, S., & Phaechamud, T. (2016). Oxygen transmission of modified natural rubber, poly (lactic acid) and chitosan porous structures for wound dressing. *Asian Journal of Pharmaceutical Sciences, 11*(1), 168–169.
Cunha, C. S., Castro, P. J., Sousa, S. C., Pullar, R. C., Tobaldi, D. M., Piccirillo, C., & Pintado, M. M. (2020). Films of chitosan and natural modified hydroxyapatite as effective UV-protecting, biocompatible and antibacterial wound dressings. *International Journal of Biological Macromolecules, 159*, 1177–1185.
Dharmalingam, K., & Anandalakshmi, R. (2019). Fabrication, characterization and drug loading efficiency of citric acid crosslinked NaCMC-HPMC hydrogel films for wound healing drug delivery applications. *International Journal of Biological Macromolecules, 134*, 815–829.
Gómez-Carracedo, A., Alvarez-Lorenzo, C., Gómez-Amoza, J. L., & Concheiro, A. (2003). Chemical structure and glass transition temperature of non-ionic cellulose ethers. *Journal of Thermal Analysis and Calorimetry, 73*(2), 587–596.
Gong, G., Zhang, F., Cheng, Z., & Zhou, L. (2015). Facile fabrication of magnetic carboxymethyl starch/poly(vinyl alcohol) composite gel for methylene blue removal. *International Journal of Biological Macromolecules, 81*, 205–211.
Gutiérrez, T. J., Seligra, P. G., Jaramillo, C. M., Jaramillo, C. M., Famá, L., & Goyanes, S. (2017). Effect of filler properties on the antioxidant response of thermoplastic starch composites. In K. M. Vijay, K. T. Manju, & R. K. Michael (Eds.), *Handbook of composites from renewable materials* (pp. 337–369). Argentina: Scrivener Publishing LLC.
Hezma, A. M., Rajeh, A., & Mannaa, M. A. (2019). An insight into the effect of zinc oxide nanoparticles on the structural, thermal, mechanical properties and antimicrobial activity of Cs/PVA composite. *Colloids and Surfaces A: Physicochemical and Engineering Aspects, 581*, Article 123821.
Janani, N., Zare, E. N., Salimi, F., & Makvandi, P. (2020). Antibacterial tragacanth gum-based nanocomposite films carrying ascorbic acid antioxidant for bioactive food packaging. *Carbohydrate Polymers, 247*, Article 116678.
Jiménez, A., Fabra, M. J., Talens, P., & Chiralt, A. (2012). Influence of hydroxypropylmethylcellulose addition and homogenization conditions on properties and ageing of corn starch based films. *Carbohydrate Polymers, 89*(2), 676–686.
Kaczmarska, K., Grabowska, B., Spychaj, T., Zdanowicz, M., Sitarz, M., Bobrowski, A., & Cukrowicz, S. (2018). Effect of microwave treatment on structure of binders based on sodium carboxymethyl starch: FT-IR, FT-raman and XRD investigations. *Spectrochimica Acta. Part A, Molecular and Biomolecular Spectroscopy, 199*, 387–393.
Kanmani, P., & Rhim, J.-W. (2014). Properties and characterization of bionanocomposite films prepared with various biopolymers and ZnO nanoparticles. *Carbohydrate Polymers, 106*, 190–199.
Ma, X.-Y., & Zhang, W.-D. (2009). Effects of flower-like ZnO nanowhiskers on the mechanical, thermal and antibacterial properties of waterborne polyurethane. *Polymer Degradation and Stability, 94*(7), 1103–1109.
McDonald, R. (1997). In *Colour physics for industry*. West Yorkshire: Society of Dyers and Colourists.
Peng, X., Yang, G., Yue, Q., Ren, X., Zhou, Y., & Zhang, M. (2021). The film-forming characterization and structural analysis of pectin from sunflower heads. *International Journal of Polymer Science, 2021*, Article 8859108.
Priyadarshi, R., & Negi, Y. S. (2017). Effect of varying filler concentration on zinc oxide nanoparticle embedded chitosan films as potential food packaging material. *Journal of Polymers and the Environment, 25*(4), 1087–1098.
Priyadarshi, R., Kumar, B., & Rhim, J.-W. (2020). Green and facile synthesis of carboxymethylcellulose/ZnO nanocomposite hydrogels crosslinked with Zn2+ ions. *International Journal of Biological Macromolecules, 162*, 229–235.
Raafat, A. I., El-Sawy, N. M., Badawy, N. A., Mousa, E. A., & Mohamed, A. M. (2018). Radiation fabrication of xanthan-based wound dressing hydrogels embedded ZnO nanoparticles: In vitro evaluation. *International Journal of Biological Macromolecules, 118*, 1892–1902.
Savencu, I., Iurian, S., Porfire, A., Bogdan, C., & Tomuță, I. (2021). Review of advances in polymeric wound dressing films. *Reactive and Functional Polymers, 168*, Article 105059.
Seddiqi, H., Oliaei, E., Honarkar, H., Jin, J., Geonzon, L. C., Bacabac, R. G., & Klein-Nulend, J. (2021). Cellulose and its derivatives: Towards biomedical applications. *Cellulose, 28*(4), 1893–1931.
Stojanović, Ž., Jeremić, K., Jovanović, S., & Lechner, M. D. (2005). A comparison of some methods for the determination of the degree of substitution of carboxymethyl starch. *Starch - Stärke, 57*(2), 79–83.
Sun, G., Liang, T., Tan, W., & Wang, L. (2018). Rheological behaviors and physical properties of plasticized hydrogel films developed from κ-carrageenan incorporating hydroxypropyl methylcellulose. *Food Hydrocolloids, 85*, 61–68.
Tantiwatcharothai, S., & Prachayawarakorn, J. (2020). Property improvement of antibacterial wound dressing from basil seed (O. Basilicum L.) mucilage- ZnO nanocomposite by borax crosslinking. *Carbohydrate Polymers, 227*, Article 115360.
Wang, C.-C., Shih, T.-Y., Hsieh, Y.-T., Huang, J.-L., & Wang, J. (2020). L-arginine grafted Poly(Glycerol Sebacate) materials: An antimicrobial material for wound dressing. *Polymers, 12*(7), 1457.
Wilpiszewska, K. (2019). Hydrophilic films based on starch and carboxymethyl starch. *Polish Journal of Chemical Technology, 21*, 26–30.
Wu, P., Fisher, A. C., Foo, P. P., Queen, D., & Gaylor, J. D. S. (1995). In vitro assessment of water vapour transmission of synthetic wound dressings. *Biomaterials, 16*(3), 171–175.
Wilpiszewska, K., Antosik, A. K., & Spychaj, T. (2015). Novel hydrophilic carboxymethyl starch/montmorillonite nanocomposite films. *Carbohydrate Polymers, 128*, 82–89.
Zepon, K. M., Martins, M. M., Marques, M. S., Heckler, J. M., Dal Pont Morisso, F., Moreira, M. G., & Kanis, L. A. (2019). Smart wound dressing based on κ-carrageenan/locust bean gum/cranberry extract for monitoring bacterial infections. *Carbohydrate Polymers, 206*, 362–370.
Zhang, L., Zhao, Y., Qian, J.-Y., Jiang, S., Liu, J., & He, X.-L. (2017). Relationship between multi-scale structures and properties of photophobic films based on hydroxypropyl methylcellulose and monosodium phosphate. *Carbohydrate Polymers, 174*, 572–579.
Zhang, L., Lu, Y.-Q., Qian, J.-Y., Yue, L.-N., Li, Q., Xiao, L.-X., & Guan, C.-R. (2020). Microstructures, physical and sustained antioxidant properties of hydroxypropyl methylcellulose based microporous photophobic films. *International Journal of Biological Macromolecules, 152*, 1002–1009.
Zhang, L., Wang, X.-F., Peng, Y.-L., Zhao, Y., Qian, J.-Y., & Ding, X. (2021). Effect of different ionic liquids acting as plasticizers on the multi-scale structures and physical properties of hydroxypropyl methylcellulose/monosodium phosphate photophobic film. *International Journal of Biological Macromolecules, 179*, 466–474.
Zhang, L., Wang, Y., Liu, H., Yu, L., Liu, X., Chen, L., & Zhang, N. (2013). Developing hydroxypropyl methylcellulose/hydroxypropyl starch blends for use as capsule materials. *Carbohydrate Polymers, 98*(1), 73–79.

International Journal of Biological Macromolecules 256 (2024) 128231

Contents lists available at ScienceDirect

International Journal of Biological Macromolecules

journal homepage: www.elsevier.com/locate/ijbiomac

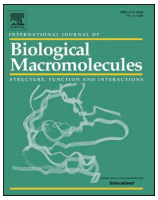

Porous antimicrobial crosslinked film of hydroxypropyl methylcellulose/carboxymethyl starch incorporating gallic acid for wound dressing application

Vipawan Pitpisutkul [a], Jutarat Prachayawarakorn [a,b,*]

[a] Department of Chemistry, School of Science, King Mongkut's Institute of Technology Ladkrabang (KMITL), Bangkok 10520, Thailand
[b] Advanced Materials Research Unit, School of Science, King Mongkut's Institute of Technology Ladkrabang (KMITL), Bangkok 10520, Thailand

ARTICLE INFO

Keywords:
Cellulose
Gallic acid
Starch
Wound dressing

ABSTRACT

Because of weak mechanical qualities and low degree of swelling of hydroxypropyl methylcellulose/carboxymethyl starch (HP/CMS) blended films for wound dressing application, this work prepared a unique antimicrobial crosslinked film utilizing succinic acid (SA) as a non-toxic crosslinker and gallic acid (GAL) as an antibacterial agent. It was observed that the infrared-shifted peak position of O—H stretching and bending in HP/CMS/SA/GAL films was caused by hydrogen bond formation among HP, CMS and GAL components. The antimicrobial crosslinked films considerably enhanced their mechanical properties and swelling degree. After adding SA and GAL, the films retained their porosity structure as observed by scanning electron images. Moreover, GAL-loaded HP/CMS/SA films could inhibit *Staphylococcus aureus* and *Escherichia coli* growth, showing their wound dressing potential. Crystallinity percentage, water vapor transmission rate, gel fraction, water solubility, water uptake and cytotoxicity were also investigated.

1. Introduction

In general, wound dressings should be biocompatible, non-toxic, absorbent, and have a balanced water vapor transmission rate (WVTR) [1]. The antibacterial qualities of the dressing also inhibit microorganism development. Dressing materials, including films, sponges, and hydrogels, can be prepared from natural and synthetic polymers [2]. Natural polymers are beneficial to use as wound dressings because they have good biocompatibility, non-immunogenicity, and non-toxicity [3]. Wound dressings can be fabricated utilizing natural polysaccharides, such as cellulose or starch [4].

Cellulose is regarded as an almost unlimited raw material source for the growing demand for eco-friendly and biocompatible products such as wound dressings and drug capsules. Since cellulose is unable to dissolve in water and is indigestible by the body, it has limited practical applications, especially in pharmaceutical and biomedical industries [5]. The chemical structure of cellulose can be altered to produce cellulose derivatives with adequate physicochemical qualities. Cellulose derivatives are potential semi-synthetic biopolymers with water-soluble properties, biocompatibility, non-toxicity, and cost-effectiveness [6].

The cellulose derivatives such as hydroxypropyl methylcellulose (HP) are widely used in biotechnological applications due to their high water solubility, wide availability, superior film-forming capability, low toxicity, and high biocompatibility [7]. It was reported that degree of substitution of methoxy groups and the molar substitution of hydroxypropyl groups determined the polarity of HP, which influenced its interactions with water and medicines [8]. HP-based composite materials and their blending with bioactive substances have been studied. It was mentioned that HP/xanthan gum foam containing phenytoin and insulin for wound dressing material showed higher porosity, water uptake ability and adhesive performance, as compared with HP foam alone [9]. HP/*Ocimum basilicum L.* (OB) extract exhibited high hydrophilicity along with the increase in swelling degree and water vapor permeability (WVP). The incorporation of OB provided the flexible film with healing process [10]. Edible film made from HP-reinforced silver nanoparticles could extend food shelf life in food packaging, and the decrease of WVP, tensile strength, and Young's modulus was observed [7]. Nevertheless, HP film still exhibits low swelling, high water solubility, and poor gas transfer with the surrounding environment without antibacterial activity. The incorporation of carboxymethyl starch (CMS) or sodium CMS into HP film is; therefore, an interesting method for enhancing the limitations.

* Corresponding author at: Department of Chemistry, School of Science, King Mongkut's Institute of Technology Ladkrabang (KMITL), Bangkok 10520, Thailand.
E-mail address: jutarat.si@kmitl.ac.th (J. Prachayawarakorn).

https://doi.org/10.1016/j.ijbiomac.2023.128231
Received 5 September 2023; Received in revised form 9 November 2023; Accepted 16 November 2023
Available online 21 November 2023

CMS is a chemically modified starch made from polysaccharides and used in medications, wound healing, and food [11]. The process, of transforming hydroxyl groups in native starch into anionic groups, specifically carboxylate group (COO-), is achieved through the application of chloroacetic acid [12]. CMS is soluble in cool water, which enables the casting process [13]. For starch/CMS films, as the concentration of CMS increased in starch/CMS films, the films became more hydrophilic and absorbed more moisture [14]. Additionally, the incorporation of CMS and zinc oxide nanoparticles into HP-based nanocomposite films enhanced its swelling degree, WVTR, and oxygen transmission rate in comparison to HP film [15]. However, low dimensional stability, poor mechanical properties, and low swelling degree of HP/CMS film limit their use as wound dressings [13]. Crosslinking is a common technique used to improve the limitations of these films.

Crosslinking agents such as natural carboxylic acid, namely, citric acid (CA), malic acid, and succinic acid (SA) have been used to improve properties of cellulose, proteins, starch, and protein-based films [16–18]. SA is produced naturally through the fermentation of honey and is utilized in food, pharmaceutical, and agricultural industries [19]. As it contains two carboxyl groups, SA can function as both solubilizing and cross-linking agent [20]. It was mentioned that, chitosan (CS)-based hydrogels crosslinked by SA exhibited the increased mechanical properties and the reduced contact angle [21]. The addition of SA, malic acid, and tartaric acid into basil seed mucilage films improved their physical and chemical properties by crosslinking process [16]. Also, low water-soluble, low WVTR and high tensile strength were obtained by the incorporation of CA into either HP or CS films [22]. In order to improve the antibacterial activity of wound dressing, there have been many types of the antibacterial agents such as antibiotics [23], metal oxide nanoparticles [24] or phenolic compounds [25].

Gallic acid (GAL) is a natural phenolic compound that is present in numerous plant species and fruits [26]. Its notable properties include antioxidant and antimicrobial activity, which have been extensively studied [25,27,28]. Furthermore, GAL has been observed to trigger cell death in cancer cells in a targeted manner, while exhibiting cytocompatibility with normal cells at low concentrations [29]. It was reported that GAL-incorporated CS/gelatin composite films in food packaging exhibited low swelling degree and WVP due to many hydrogen bonds among GAL, gelatin, and CS. On the other hand, tensile strength of CS/gelatin/GAL film increased and provided antibacterial activity [27].

In addition, polyvinyl alcohol (PVA)/poly(hexamethylene guanidine) composite hydrogel films added with GAL exhibited hydrophilic surfaces, high swelling ratio, low water solubility, great mechanical characteristics and good antibacterial activity [25]. Besides, GAL loading at 5 wt% into PVA films for food packaging presented the increase of mechanical properties with antioxidant behavior [28]. As far as current literature is concerned, there has been no report for HP/CMS films crosslinked with SA and modified by GAL.

This research aimed to improve properties of HP/CMS film for use as the wound dressing by crosslinking with SA and improving antibacterial activity with GAL. Functional group analysis, crystallinity, and morphology were examined. In addition, mechanical properties, water uptake, WVTR, swelling degree, gel fraction, water solubility, cytotoxicity and antibacterial activity against *S. aureus* and *E. coli* of several HP/CMS films were evaluated.

2. Experimental

2.1. Materials

HP (Methocel F4M) was received from Union Chemical 1986 Co., Ltd (Bangkok, Thailand) with methoxy group of 27.0–30.0 % and hydroxypropoxy group of 4.0–7.5 %. Cassava starch (16.4 % amylose and 83.6 % amylopectin) was obtained from Chaopraya Phuchrai 1999 Co., Ltd. (Kamphaengphet, Thailand). Monochloroacetic acid (MCA), SA and GAL were purchased from Italmar Co., Ltd (Bangkok, Thailand). Sodium hydroxide (NaOH) and silver nitrate ($AgNO_3$) were AR grade. Glycerol was obtained from Chemipan Co., Ltd (Bangkok, Thailand).

2.2. CMS preparation

CMS was prepared according Wilpiszewska et al. [30]. Briefly, cassava starch (12.5 g) was mixed in 300 mL of isopropanol (90 % v/v) and then stirring at room temperature. Then, NaOH (7.7 M) solution was added to the suspension. After 45 min, MCA (10.93 g) was added and mixed at 50 °C. After 3 h, glacial acetic acid was used to neutralize the suspension and then vacuum-filtered. The solid filtrate was rinsed with 85 % ethanol till $AgNO_3$ test showed no chloride ion. CMS was produced by filtering and drying at 60 °C for 24 h. According to Stojanović et al. [31], the degree of substitution of the prepared CMS was 0.85 ± 0.07.

2.3. Fabrication of different HP/CMS films

HP/CMS, HP/CMS/SA and HP/CMS/SA/GAL films were prepared by solution casting using glycerol as the plasticizer. The concentration of the film-forming solutions (both CMS and HPMC) was maintained at 2 % (w/v), as the concentration of CMS was 30 wt% of the total weight polymer. SA (2.5 wt% of dry-weight polymer) and various contents of GAL (0, 1, 3 and 5 wt% of dry-weight polymer) were utilized. GAL solution was prepared by dissolving and stirring GAL powder in 10 mL of a 10 % ethanol solution, followed at room temperature for 15 min. For HP/CMS film, HP:CMS (70:30 by %weight) were prepared with 30 wt% of glycerol (wt% of total weight polymer) and then dispersed in hot water (85 °C, 30 min) with continuous stirring to complete the dissolution. HP/CMS/SA film and HP/CMS/SA/GAL films were made by mixing HP, CMS, and glycerol with SA for 15 min. After cooling to 50 °C, GAL solution was added and mixed at room temperature for 10 min. All samples were casted onto polypropylene trays and dried (60 °C, 16 h). To complete crosslinking, the dried films were finally preheated at 110 °C for 10 min [32].

2.4. Functional group analysis

Functional groups of a film were identified using attenuated total reflectance spectroscopy instrument (ATR), IRTracer-100 Fourier transform infrared spectrophotometer (Shimadzu, Japan) across 700–4000 cm^{-1} wavenumber range with the resolution of 4 cm^{-1} using 45 consecutive scans performed for each sample.

2.5. Morphology

Cross-section morphology of a film was examined by a scanning electron microscope (SEM) (JSM-IT500HR, JEOL, LA) using an accelerating voltage of 10 kV with 2000× magnification. The film was fractured and sputtered with a thin layer of gold before being mounted on aluminium stub with carbon adhesive tape.

2.6. Crystallinity

X-ray diffraction (XRD) technique was used to determine the degree of crystallinity. At room temperature, a diffractogram was collected using Smart lab (Rigaku, Japan) with CuKα (λ = 1.54 Å) radiation operating at 40 kV and 30 mA with the angular range of 2θ = 5–60°. The degree of crystallinity was determined by Eq. (1):

$$\text{Crystallinity}\ (\%) = \frac{\text{Ac}}{\text{Ac} + \text{Aa}} \times 100 \quad (1)$$

where A_c was the area corresponding to the crystalline region (2θ = 5–30°) and A_a was the amorphous region (2θ = 5–60°) on the X-ray

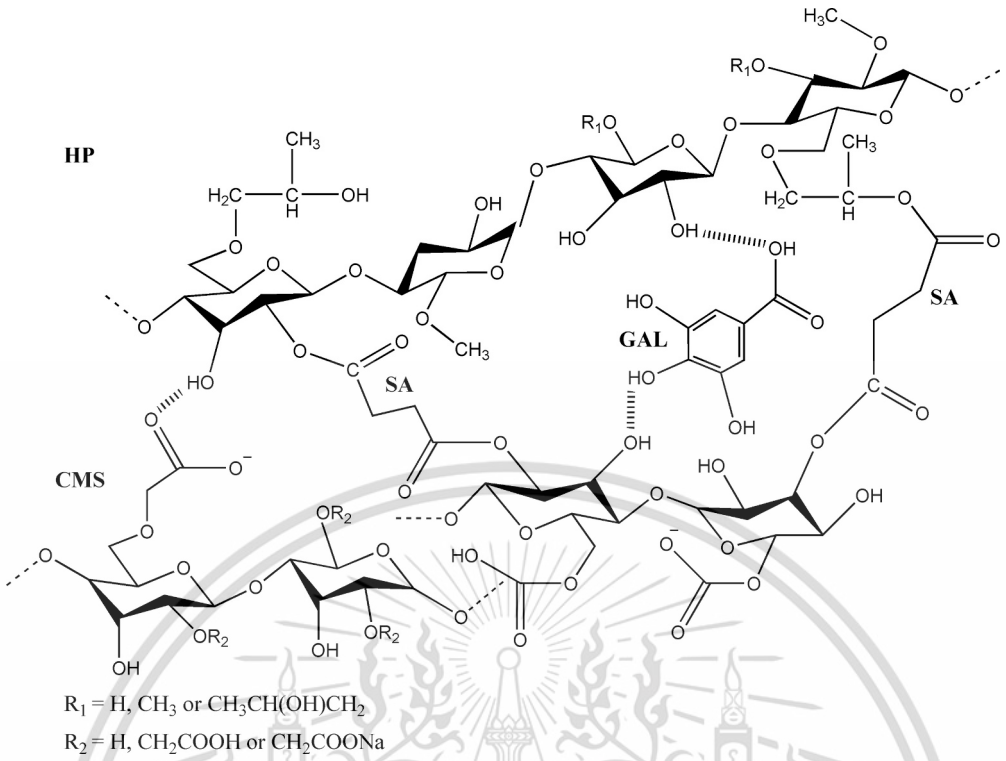

Fig. 1. The schematic representation of possible interaction/reaction for HP/CMS, HP/CMS/SA and HP/CMS/SA/GAL films Abbreviations: HP—hydroxypropyl methyl cellulose; CMS—carboxymethyl starch; SA—succinic acid; GAL—gallic acid.

diffractogram.

2.7. Mechanical properties

A universal testing machine by using Cometech (QC-536M1, Taiwan) with 2 kN load cell and 50 mm/min crosshead speed was applied to determine the mechanical properties of a film according to ASTM D-882 standard. The film with the averaged thickness of 0.14–0.16 mm. was cut into 100 × 15 mm^2 rectangular pieces. The film was placed in a closed container containing solution of ammonium nitrate (60 ± 2 % RH) overnight before the measurement. The test condition was prepared at 23 ± 1 °C and 60 ± 2 % RH. The averaged values of stress at maximum load, Young's modulus, and strain at maximum load were obtained from ten samples.

2.8. Swelling degree, gel fraction, water solubility, water uptake, and WVTR

For swelling degree, a film (20 × 20 mm^2) was first dried at 105 °C for 2 h and then wrapped with 400 mesh sieve stainless steel. The sieve containing a film was immersed in distilled water at room temperature for 24 h. The weight of the wet film (W_2) was measured after water removal from the surface by blotting with a filtered paper. Each film was tested for three times and percentage of swelling was calculated as followed:

$$\text{Swelling } (\%) = \frac{W_2 - W_1}{W_1} \times 100 \quad (2)$$

where W_2 and W_1 were the wet and the dried weights of the sample, respectively.

Gel fraction was determined using a square film with an averaged weight of 0.19 g. The film was dried overnight in an oven (Memmert UF110, Germany) at 60 °C until the sample weight was constant. Then, the dried film was soaked into distilled water at room temperature for 24 h. The gel fraction of sample was determined from the weight ratio of the insoluble dry film (W_1) after soaking in the water for 24 h and the initial weight of dry film (W_0) as shown in Eq. (3).

Water solubility was measured as described by Y. Ma and R. Yang and W. Zhao [33]. The dried film was stirred in 50 mL of deionized water (1 h) with magnetic stirring at 200 rpm. The insoluble film was separated by centrifugation at 6000 rpm for 10 min and then dried (105 °C) until the weight remained constant (W_0). The water solubility was calculated according to Eq. (4):

$$\text{Gel fraction } (\%) = \frac{W_1}{W_0} \times 100 \quad (3)$$

$$\text{Water solubility } (\%) = \frac{W_1}{W_0} \times 100 \quad (4)$$

where W_1 and W_0 were the weight of insoluble dry gel and the initial weight of a dry film, respectively.

Water uptake test was performed in accordance with ASTM D-570 standard technique. A film was dried at 105 °C for 3 h and then placed in a closed container at 99 ± 1 % RH. The content of water absorbed by the film was measured for 4 days. The percentage of water uptake was calculated as Eq. (5):

$$\text{Water uptake } (\%) = \frac{W_2 - W_1}{W_1} \times 100 \quad (5)$$

where W_2 and W_1 were the wet and the dried weights of the sample, respectively.

WVTR was measured according to ASTM E96 with the gravimetric modified cup method (the desiccant method) and the cup was filled with silica gel and then sealed. The sealed cup containing a sample was weighted and placed in a chamber containing a saturated solution of sodium chloride at a constant 75 % RH. The weight gain was collected every 24 h for 7 days and calculated according to Eq. (6):

$$\text{WVTR} = \frac{\Delta m}{(\Delta t.A)} \quad (6)$$

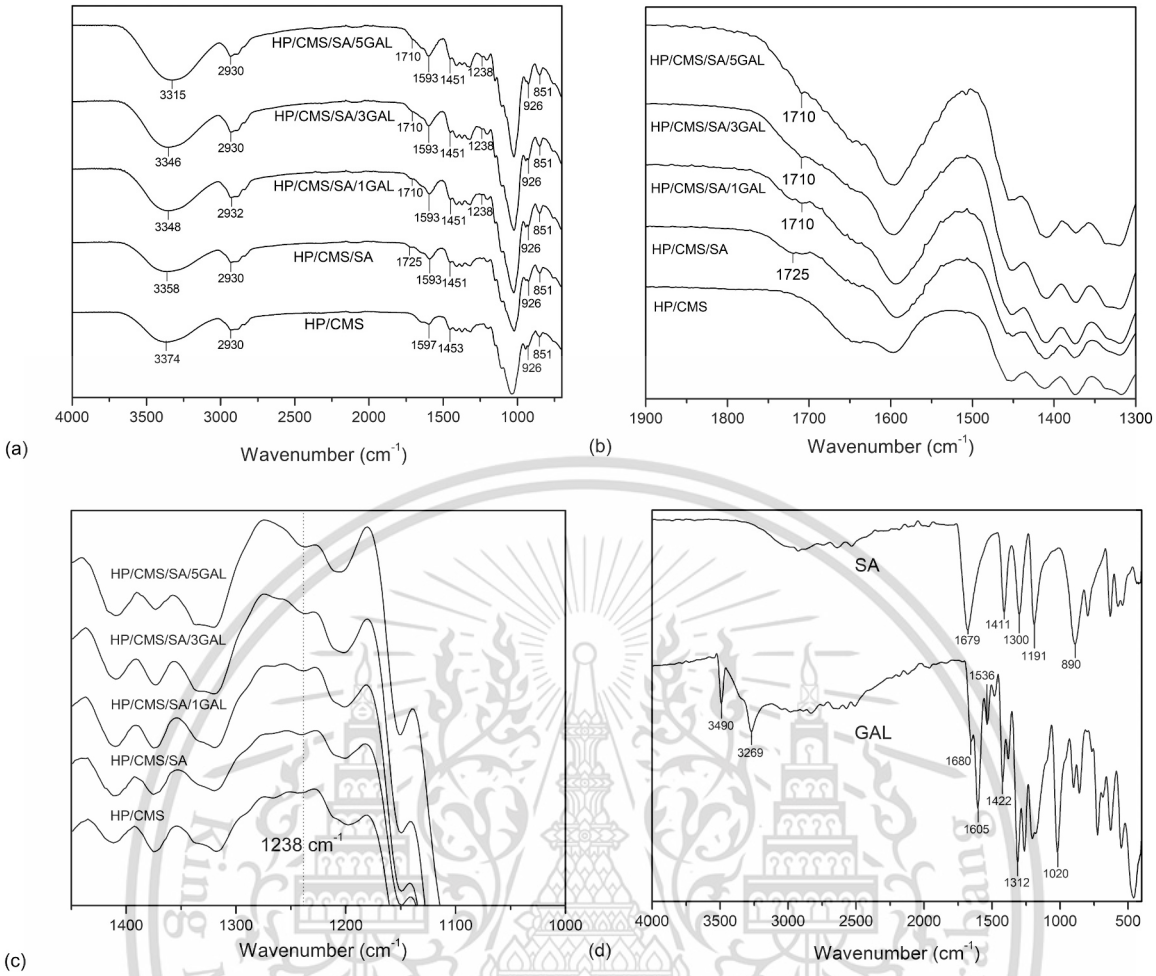

Fig. 2. ATR spectra of HP/CMS, HP/CMS/SA and HP/CMS/SA/GAL films with different contents of GAL.

where Δm was the weight gain (g) of the film sample per day (g/d); Δt was the time variation (days) and A was permeative surface area of the film sample (m^2).

2.9. Antibacterial activity

A film was tested for antibacterial activity following JIS Z 2801 standard [34]. Two different types of bacteria, gram-positive *Staphylococcus aureus* (*S. aureus*) and the gram-negative *Escherichia coli* (*E. coli*), were used for testing the sample. The sample was exposed to the microorganisms for 24 h at 37 °C, 90%RH, the optimal condition for the bacterial growth. After bacteria were exposed to the test material, the bacteria were extracted from the sample and counted. A comparison between the number of surviving bacteria and the initial quantity of bacteria was determined. The difference between the initial and final number of microbes was determined by a percentage or log reduction as shown in Eq. (7).

$$\text{Bacterial reduction } (\%) = ((B - A)*100)/B \quad (7)$$

where A and B were Log CFU per milliliter of bacteria after 24 h and before the testing, respectively.

2.10. Cytotoxicity assay

The MTT assay with human keratinocytes (HaCat) was used for cytotoxicity. After filtering a sample in phosphate-buffered saline, Dulbecco's Modified Eagle Medium was added. The mixture was incubated at 37 °C for 24 h and added with 10 % fetal bovine serum. Each well of a 96-well plate was seeded with 100 μL (1×10^5 cells/mL) of HaCat cells and incubated at 37 °C for 24 h. After adding 100 mL of the filtrate mixture and 10 μL of MTT solution (5 mg/mL), the mixture was incubated at 37 °C for 4 h. Formazan dissolution and the resultant solution were added to the well. The absorbance of the resultant mixture at 570 nm was recorded using a Biochrom microtiter plate reader. Cell morphology was investigated via optical microscopy. Eq. (8) and Eq. (9) determined percentages of cytotoxicity and cell viability:

$$\text{Cytotoxicity } (\%) = (A - B/A) \times 100 \quad (8)$$

$$\text{Cell viability } (\%) = 100 - \text{Cytotoxicity } (\%) \quad (9)$$

where, A and B were the absorbances of the control and test wells, respectively.

2.11. Statistical analysis

Statistical analysis was performed by using the analysis of variance (ANOVA) procedure with IBM SPSS statistics 25 software. Tukey's test was used to measure differences among the means ($p < 0.05$).

3. Results and discussion

Fig. 1 depicts a schematic diagram showing the possible interaction/reaction of various materials, including HP, CMS, SA, and GAL. The functional groups of HP and CMS containing many hydroxyl groups

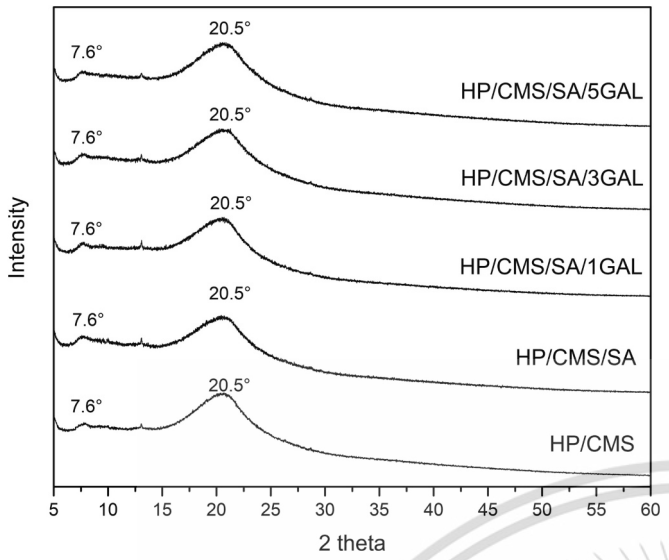

Fig. 3. X-ray diffractograms of HP/CMS, HP/CMS/SA and HP/CMS/SA/GAL films with different contents of GAL.

Table 1
Degree of crystallinity and mechanical properties of HP/CMS, HP/CMS/SA and HP/CMS/SA/GAL films with various contents of GAL.

Films	Crystallinity (%)	Stress at maximum load (MPa)	Young's modulus (MPa)	Strain at maximum load (%)
HP/CMS	9.21	5.03 ± 0.52[a]	78.60 ± 7.16[a]	8.89 ± 1.28[a]
HP/CMS/SA	9.19	5.55 ± 0.43[a]	78.64 ± 7.20[a]	11.32 ± 1.63[b]
HP/CMS/SA/1GAL	8.17	9.31 ± 0.64[b]	156.65 ± 11.24[b]	10.21 ± 1.61[ab]
HP/CMS/SA/3GAL	8.45	9.46 ± 0.63[b]	167.37 ± 15.45[b]	10.66 ± 1.06[ab]
HP/CMS/SA/5GAL	8.86	9.61 ± 0.73[b]	168.60 ± 14.93[b]	10.27 ± 1.59[ab]

Different superscript letters in the same column are significantly different ($p < 0.05$), based on Tukey's test.

which could form intermolecular interaction via hydrogen bonding. For HP/CMS/SA film, covalent bond between HP and CMS components could be created through esterification reaction with SA molecules, led to crosslinking process. Furthermore, the use of GAL could form hydrogen bonding with HP and CMS components due to the presence of multiple polar groups (namely, three hydroxyl groups and one carboxylic group) on GAL molecule.

3.1. Functional group analysis

The functional groups of various HP/CMS porous films were analyzed using ATR spectrophotometer (Fig. 2(a)). For ATR spectrum of HP/CMS, the prominent peak positions were observed at 3374 cm^{-1}, 1597 cm^{-1}, and 1453 cm^{-1}, which were attributed to the stretching of O—H bond, the asymmetric stretching of C═O bond, and the bending of O—H bond, respectively [15]. They also revealed the appearance of the characteristic overlapped peak between HP and CMS components.

HP/CMS/SA film presented the characteristic bands similar to those observed for HP/CMS film. The new absorption peak position at 1725 cm^{-1}, attributed to C═O stretching was observed, suggesting that a chemical reaction could take place between the acid and starch. The observed absorption band was caused by the formation of ester bond resulting from the cross-linking reaction [17,35]. The characteristic band of SA (Fig. 2(d)) was found at around 1679 cm^{-1}, attributed to C═O stretching of carboxylic groups. After the completed reaction, the band was shifted to higher wavenumber at 1725 cm^{-1}, corresponded to SA crosslinking on agar/bacterial cellulose composite film which presented the new band at 1727 cm^{-1}, attributed to C═O stretching of ester bond [32]. Additionally, the shifted peak of O—H stretching and O—H bending at 3374 cm^{-1} and 1453 cm^{-1} to lower wavenumbers at 3358 cm^{-1} and 1451 cm^{-1} was identified due to new hydrogen bond formation between the two components [30].

In the spectra of different HP/CMS/SA/GAL films, the typical bands were comparable to those detected for HP/CMS/SA film. The main characteristic peak positions of GAL (Fig. 2(d)) were found at 3269, 1680 and 1605 cm^{-1}, attributed to O—H stretching, C═O stretching and C═C stretching, respectively [36]. The presence of antibacterial crosslinked films and GAL bands may overlap, leading to the disappearance of the characteristic peak positions of GAL.

Moreover, the C═O stretching band of HP/CMS/SA/GAL films at 1710 cm^{-1} (Fig. 2(a)-(b)) was detected and it indicated the existence of GAL component [37]. It was also found that the use of GAL brought about a new peak position at about 1238 cm^{-1} (Fig. 2(c)), which was assigned for C—O stretching vibration of the GAL [28].

Furthermore, the intensity of the bands at around 1710 and 1238 cm^{-1} increased when the GAL contents increased. Additionally, the observed peak shift towards lower wavenumber at approximately 3348 cm^{-1} in HP/CMS/SA/GAL films with varying GAL concentrations could be attributed to the formation of new hydrogen bonding interaction between the polymer matrix and GAL molecule.

3.2. XRD

XRD patterns and percentage of crystallinity for HP/CMS, HP/CMS/SA and HP/CMS/SA/GAL films with various contents of GAL are shown in Fig. 3 and Table 1. XRD diffractograms of various samples indicated the presence of broad peaks at 2θ of 7.6° and 20.5°, which corresponded to the semi-crystalline structure of HP [8]. However, the weak diffracted peaks arisen from CMS component at 2θ of 17.1° and 21.7° [15] could not be observed in the XRD patterns of different HP/CMS films. This can be attributed to the amorphous characteristics of CMS, which overlapped the diffracted peak of crystalline structure of HP.

In particular, the utilization of SA as a crosslinking agent for HP/CMS/SA film exhibited no difference in degree of crystallinity compared to HP/CMS film. The result could be attributed to low SA concentration, which showed no effect on the ability of HP to crystalize. Different HP/CMS/SA/GAL films also displayed two broader peaks at 2θ = 7.6° and 20.5° without the diffracted peak arisen from GAL molecule [37]. This result corresponded with XRD pattern of PVA-based films that contained tannic acid (TA), which showed the absence of the characteristic peak of tannic acid (TA), indicating their homogeneous dispersion in the PVA matrix and strong interactions between PVA and TA [38]. Similar observation was mentioned for XRD pattern of ferulic acid (FA)-loaded polycaprolactone and collagen hydrolysate nanofibers which indicated that FA was in the amorphous state [39].

By comparison among HP/CMS/SA/GAL films and HP/CMS/SA film, it was found that the addition of GAL led to no difference in percentage of crystallinity (Table 1). In addition, HP/CMS/SA/GAL films showed similar percentage of crystallinity when GAL content increased. These results may be because the crystalline structure of GAL did not affect the crystallization of HP.

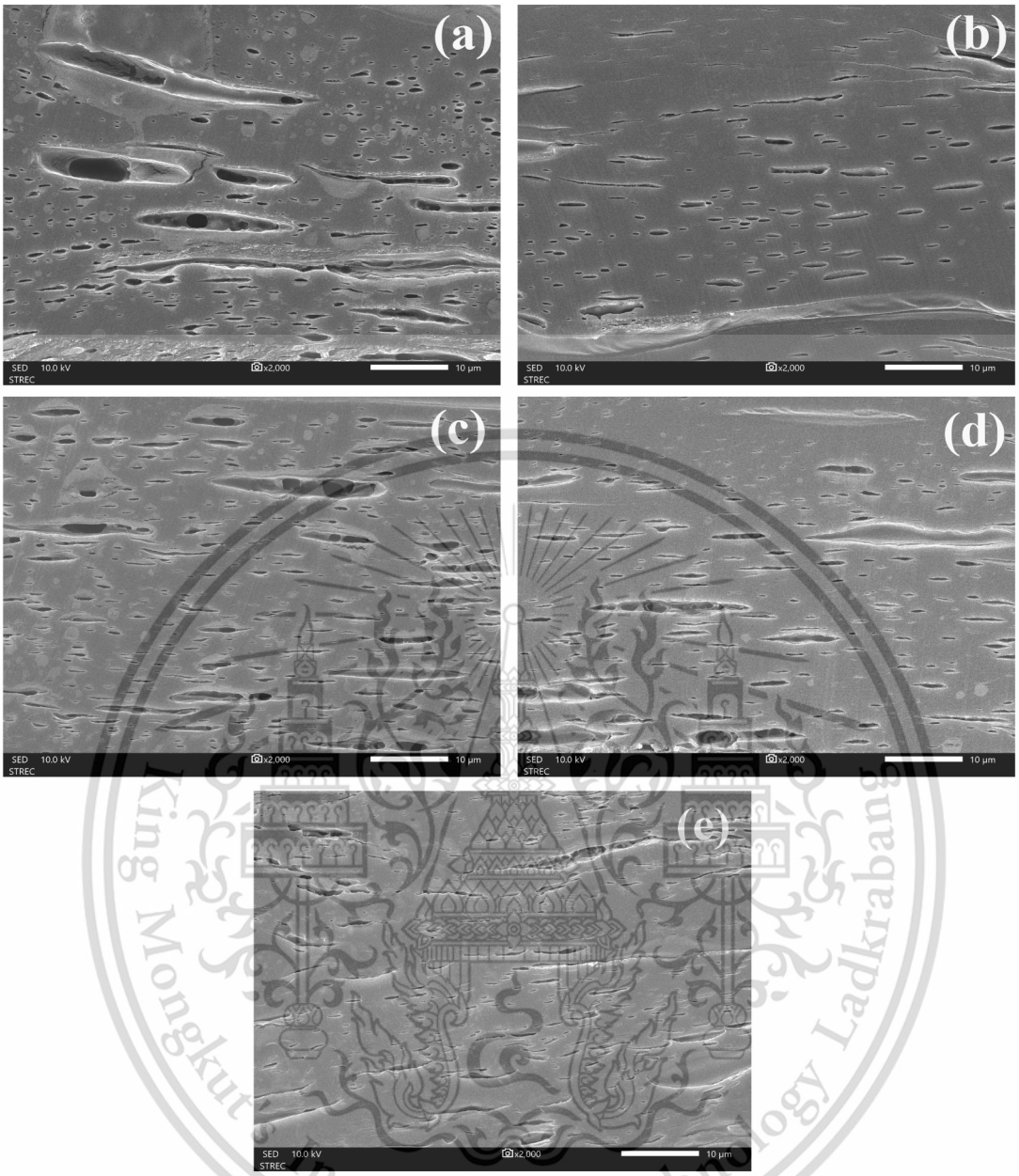

Fig. 4. Cross-section morphology of various HP/CMS films (a); HP/CMS, (b) HP/CMS/SA (c) HP/CMS/SA/1GAL, (d) HP/CMS/SA/3GAL, (e) and HP/CMS/SA/5GAL.

3.3. SEM

Morphology of various casted films was examined using SEM. HP/CMS (as shown in Fig. 4(a)) showed porous structure with smooth surface. The formation of pores could be attributed to the salting-out phenomenon of sodium salts of CMS components from HP solutions [15,40].

Compared to HP/CMS film, the cross-sectional morphology of HP/CMS/SA film revealed the porous structure with significant smaller pore size. The observed result could be ascribed to the crosslinking mechanism between CMS and HP by SA crosslinker, as verified by ester linkage in Fig. 2, leading to denser structure and smaller pore size than HP/CMS film.

Furthermore, the cross-sectional microstructure of several HP/CMS/SA/GAL films (Fig. 4(c)-(e)) also exhibited a porous structure without the presence of GAL particles. Especially, the cross-sectional morphology of HP/CMS/SA/5GAL film (Fig. 4(e)) demonstrated smaller pore size when compared to HP/CMS/SA/1GAL and HP/CMS/SA/3GAL films. It was possibly attributed to hydrophilic of GAL molecules enhancing phase compatibility among HP, CMS, and GAL components.

3.4. Mechanical properties

One of the most important characteristics of wound dressing material is its mechanical properties. Mechanical properties of HP/CMS, HP/CMS/SA and HP/CMS/SA/GAL films with various contents of GAL are shown in Table 1 and Fig. 5. Due to the highly porous structure of blended film (Fig. 4(a)), HP/CMS film presented the lowest stress at maximum load, Young's modulus and strain at maximum load (Table 1).

For HP/CMS/SA film, stress at maximum load and Young's modulus were comparable to those of HP/CMS film, whereas strain at maximum load increased significantly. It could be because of the reduction of intermolecular interaction between HP and CMS after crosslinking reaction as confirmed by FTIR analysis with the occurrence of ester bond.

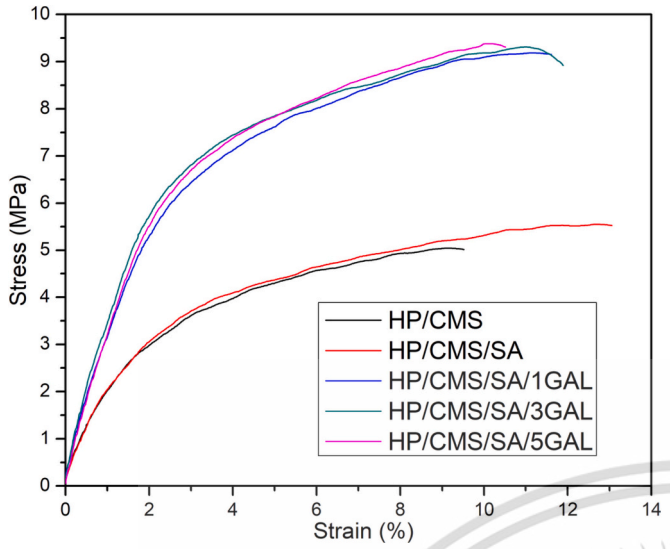

Fig. 5. Stress-strain curve of various HP/CMS films.

Table 2
Swelling degree, gel fraction, water solubility, water uptake and WVTR of HP/CMS, HP/CMS/SA and HP/CMS/SA/GAL films with various contents of GAL.

Films	Swelling degree (%)	Gel fraction (%)	Water solubility (%)	Water uptake (%)	WVTR ($g\ m^{-2}\ day^{-1}$)
Control (without film)					559.58 ± 10.00
HP/CMS	119.33 ± 9.86^{a}	5.67 ± 1.65^{a}	89.00 ± 2.00^{a}	129.33 ± 1.15^{a}	426.91 ± 6.13^{a}
HP/CMS/SA	200.33 ± 10.26^{b}	28.18 ± 1.52^{b}	62.33 ± 4.72^{c}	93.33 ± 4.72^{c}	367.28 ± 7.46^{d}
HP/CMS/SA/1GAL	231.00 ± 7.21^{c}	38.16 ± 1.41^{c}	72.00 ± 1.00^{b}	124.00 ± 2.00^{ab}	407.38 ± 4.40^{b}
HP/CMS/SA/3GAL	222.00 ± 8.71^{bc}	29.89 ± 1.77^{b}	64.67 ± 5.13^{bc}	119.00 ± 1.00^{b}	393.38 ± 1.97^{bc}
HP/CMS/SA/5GAL	218.00 ± 4.35^{bc}	26.90 ± 0.46^{b}	63.00 ± 3.61^{c}	98.33 ± 2.08^{c}	384.39 ± 4.87^{c}

Different superscript letters in the same column are significantly different ($p < 0.05$), based on Tukey's test.

It could also be because of some plasticizing effect of SA or due to partial crosslinking, thereby enhancing the mobility of the polymer chains. Similar report was found for potato starch/CS films added by CA that reduced the interaction between the macromolecules, resulting in the increase of elongation at break [41].

Moreover, the significant increase of both stress at maximum load and Young's modulus in HP/CMS/SA/GAL films was also observed when compared to HP/CMS/SA film. The strain at maximum load of these films was slightly lower than that of SA-crosslinked film. This could be the result from the increase of hydrogen bonds among HP, CMS, and GAL components (Fig. 1), as confirmed by FTIR analysis, which decreased chain mobility. As corresponded to previous research, PVA/poly(hexamethylene guanidine)/GAL composite hydrogel film exhibited the increase of tensile strength with the incorporation of GAL due to the raised hydrogen bonds between the hydrophilic groups existing in both PVA and GAL [25]. In addition, the incorporation of the aromatic ring of GAL molecule into thermoplastic cassava starch film may enhance the mechanical strength of the film through its role as a reinforcing filler [42]. For HP/CMS/SA/GAL films, the effect of GAL content on mechanical properties showed no significant difference when GAL content increased as corresponded to crystallinity percentage of these films. Generally, the optimal range for tensile strength of wound dressing film is between 2.5 and 16 MPa [4]. The porous films analyzed in this study exhibited the stress at maximum load of approximately 9 MPa, revealing the effectiveness of HP/CMS/SA/GAL films for use in wound dressing applications.

3.5. Swelling degree, gel fraction, water solubility, water uptake, and WVTR

Swelling degree, gel fraction, water solubility, water uptake and WVTR were examined to determine the efficiency of the wound dressing films. In general, a wound dressing film should assist in keeping the site moist, letting in air, and absorbing any excess exudate. Table 2 presents hydrophilic properties of HP/CMS, HP/CMS/SA and HP/CMS/SA/GAL films.

For comparison between HP/CMS and HP/CMS/SA films, HP/CMS/SA film exhibited higher swelling degree and gel fraction than those of HP/CMS film due to the loss of hydroxyl groups during esterification, which created a crosslinked structure with the increase of molecular spacing that enhanced the water absorbency of the film. Similarly, an increase in the degree of swelling was observed in the chemical crosslinking of carboxyl-modified PVA/CS [43]. This was likely due to the increased molecular spacing and decreased hydrogen bonding in the polymers caused by the crosslinking reaction. Consequently, the esterification crosslinking caused the decrease of water solubility, water uptake and WVTR of the crosslinked HP/CMS/SA film. According to SEM analysis, the morphology of HP/CMS/SA film showed the decrease of pore size, resulting in low water absorbed capacity. Similar finding was observed for the nanocomposite scaffolds from carboxymethyl cellulose crosslinked by CA [44].

Moreover, HP/CMS/SA/GAL films presented higher swelling degree, gel fraction, water solubility, water uptake and WVTR than those of HP/CMS/SA film due to the enhancement of the hydrophilic property of GAL, which contained numerous hydroxyl and carboxylic groups in its molecular structure; eventhough, hydrogen bond formation could be observed.

For various HP/CMS/SA/GAL films, it was observed that the increase of GAL content resulted in the decrease of swelling degree, gel fraction, water solubility, water uptake and WVTR. It was possibly because the increase of GAL content resulted in the enhancement of hydrogen bonds among HP, CMS and GAL.

For WVTR results, it was related to previous studies that showed the effect of the addition of GAL and GAL content on WVTR testing. The addition of GAL in PVA/tragacanth gum blend films exhibited the decrease of WVTR caused by the compact structure of the composite films. When GAL content increased, the decrease of hydrophilicity was observed [45]. In addition, water vapor permeability (WVP) of chitosan/gelatin, caseinate/guar gum and corn starch/pullulan films dropped with the incorporation of GAL due to hydrogen bonding formation between the polymer matrix and GAL, resulting in the decrease of free volume in the polymer matrix [27,46,47].

3.6. Antimicrobial efficiency

The qualitative evaluation of the antimicrobial efficacy of various films was carried out according to JIS Z 2801 standard [34]. The bacterial growth plate and bacterial reduction percentage for the control, HP/CMS, HP/CMS/SA, and HP/CMS/SA/GAL films are shown in Fig. 6 and Table 3, respectively. The results measured the antimicrobial activity of the films against *S. aureus* (Gram-positive) and *E. coli* (Gram-negative) bacteria.

As expected, the control and HP/CMS film exhibited a decrease in antibacterial efficacy with negative reduction values of −12.88, −9.28 and −8.07, −5.55 against *S. aureus* and *E. coli*, respectively, following 24 h incubation period, indicating no antibacterial activity while HP/CMS/SA film (Fig. 6(a)) presented effective antibacterial activity against gram-positive bacteria. It was found that HP/CMS/SA film showed the

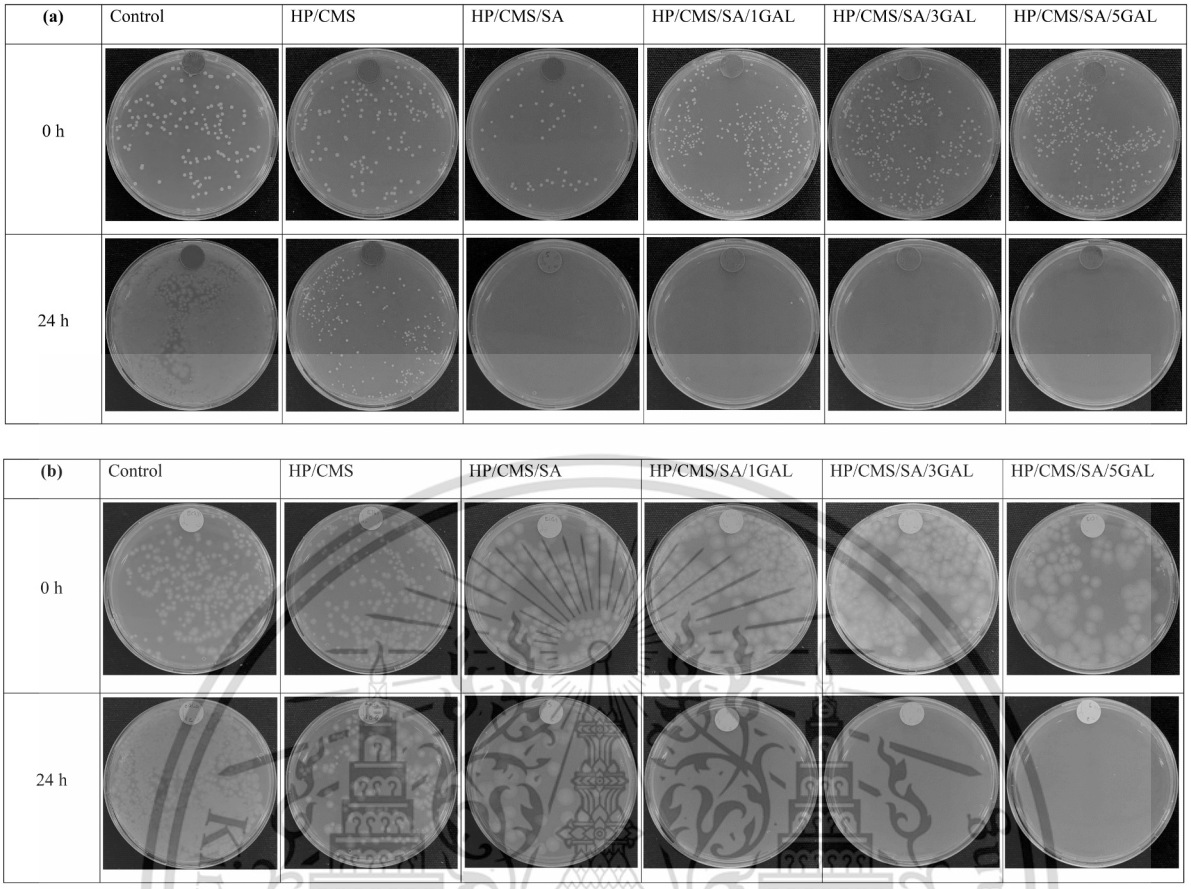

Fig. 6. Antibacterial activity of the control, HP/CMS, HP/CMS/SA, and HP/CMS/SA/GAL films with various contents of GAL; total bacterial colonies counting for (a) *S. aureus* and (b) *E. coli* after the contacting time at 0 and 24 h.

Table 3
Bacterial reduction percentage of the control, HP/CMS, HP/CMS/SA and HP/CMS/SA/GAL films against *S. aureus* and *E. coli* and MTT assay results of various HP/CMS.

Films	*S. aureus*			*E. coli*			Cytotoxicity (%)	Cell viability (%)
	Surviving cells (Log CFU/mL) after 0 h	Surviving cells (Log CFU/mL) after 24 h	Bacterial reduction (%)	Surviving cells (Log CFU/mL) after 0 h	Surviving cells (Log CFU/mL) after 24 h	Bacterial reduction (%)		
Control	6.52 ± 0.04	7.36 ± 0.05	−12.88	6.69 ± 0.05	7.23 ± 0.05	−8.07	3.55	94.45
HP/CMS	6.51 ± 0.01	7.12 ± 0.06	−9.28	6.70 ± 0.01	7.07 ± 0.06	−5.55	[15]	[15]
HP/CMS/SA	5.77 ± 0.02	0.00 ± 0.00	100	6.15 ± 0.04	2.47 ± 0.01	59.91	0.42	99.58
HP/CMS/SA/1GAL	6.40 ± 0.03	0.00 ± 0.00	100	6.44 ± 0.02	0.00 ± 0.00	100	3.31	96.69
HP/CMS/SA/3GAL	6.39 ± 0.06	0.00 ± 0.00	100	6.43 ± 0.04	0.00 ± 0.00	100	31.16	68.84
HP/CMS/SA/5GAL	6.39 ± 0.06	0.00 ± 0.00	100	6.16 ± 0.03	0.00 ± 0.00	100	62.47	37.53

percentage of bacterial reduction of 100 % and 59.91 % against *S. aureus* and *E. coli*, respectively. Huang, S. discovered that SA inhibited antibacterial activity against *S. aureus* and *P. fluorescens* (gram-negative bacteria), explaining that two bacteria were damaged, leading to the leakage of nucleic acids and proteins from the bacterial cells [48]. Moreover, the antibacterial activity of SA was observed against gram-positive bacteria such as *M. luteus* and gram-negative bacteria, including *L. hongkongensis* and *E. coli* [25,49,50].

The antibacterial effectiveness against gram-positive bacteria (*S. aureus*) was greater than that against gram-negative bacteria (*E. coli*) due to the fact that gram-positive bacteria has dense cell walls composed of peptidoglycan, whereas gram-negative bacteria has more complex cell walls, making it more difficult for an antimicrobial agent to penetrate the bacterial cells [51].

After 24 h of contacting time, it was clear that the number of living cells in HP/CMS/SA/GAL films with different amounts of GAL decreased (as shown in Table 3). The disk plate analysis (as shown in Fig. 6(a)-(b)) revealed the absence of bacterial growth for both gram-positive and gram-negative bacteria, presenting excellent antimicrobial activity of HP/CMS/SA/GAL films for wound dressing application.

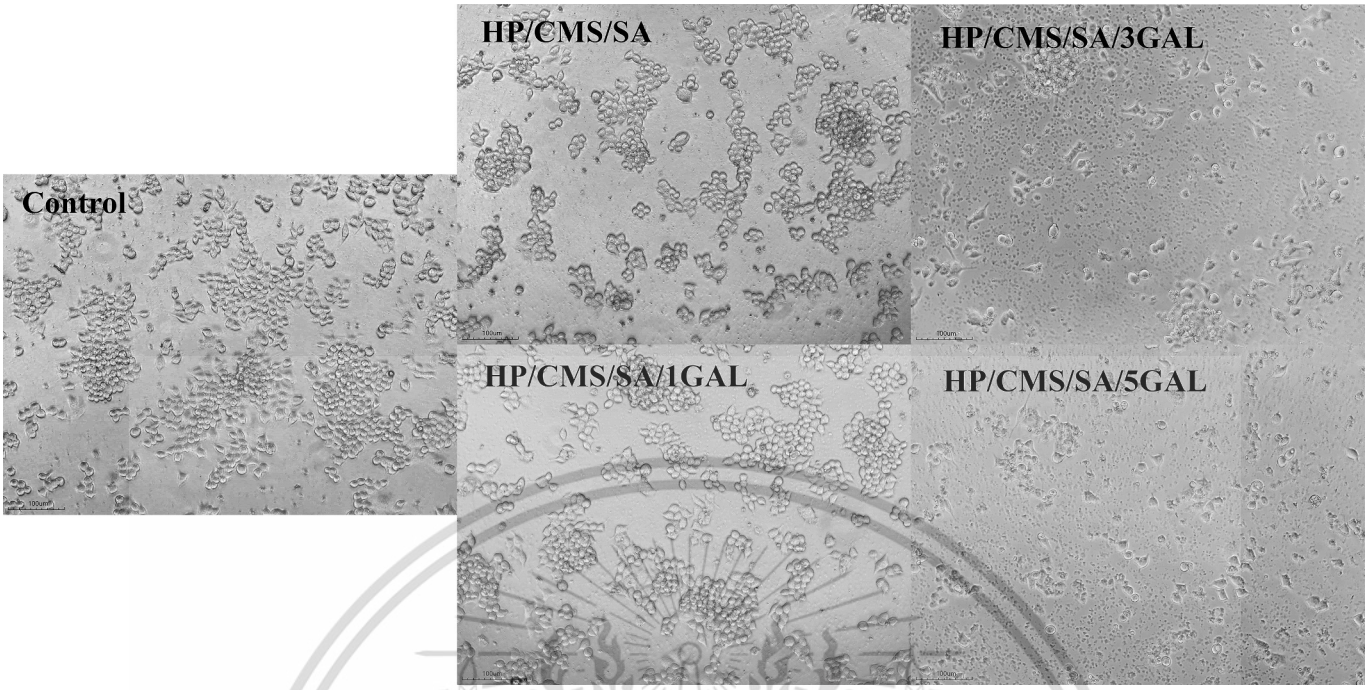

Fig. 7. Optical images of HaCat cells incubated after 4 h of various HP/CMS films.

3.7. Cytotoxicity assay

For cytotoxicity test as determined by the MTT assay, HaCat cells were selected for the evaluation of the cytotoxicity of different HP/CMS/SA/GAL films. It was observed that the cytotoxicity and cell viability values for the control, HP/CMS/SA and HP/CMS/SA/1GAL appeared similar (Table 3 and Fig. 7), indicating that these films are clearly non-toxic to human cells. It was found that, the cytotoxicity values of the control, HP/CMS/SA, and HP/CMS/SA/1GAL films were 3.55, 0.42 and 3.31 %, respectively. However, the HP/CMS/SA/GAL films with GAL contents of 3 and 5 wt% presented high cytotoxicity values of 31.12 and 62.47 %, respectively. According to ISO 10993-5 standard, the values of cell viability above 80 %, 80–60 %, 60–40 %, and below 40 %, represent non-toxicity, slight toxicity, moderate toxicity, and severe toxicity to human cells, respectively [52]. HP/CMS/SA/GAL films with 3 wt% of GAL content exhibited the cell viability value of 68.84 %, indicating of slight harmful to human cells and the use of 5 wt% GAL caused lower cell viability value (37.53 %), presenting severely harmful to human cells. All results suggested that HP/CMS/SA/1GAL was suitable for the use of wound dressing application.

4. Conclusion

Porous HP/CMS, HP/CMS/SA, and HP/CMS/SA/GAL films were successfully prepared by using SA and GAL as the crosslinker and the antibacterial agent, respectively. The incorporation of SA into HP/CMS film resulted in the appearance of IR absorption peak position of 1725 cm^{-1}, suggested the occurrence of crosslinking by the ester bond formation. SEM images exhibited the porous morphology of HP/CMS/SA film with smaller pore size. Comparison with HP/CMS film, swelling degree and gel fraction of HP/CMS/SA film increased, while water solubility, water uptake and WVTR decreased. Moreover, stress at maximum load, Young's modulus, percentage of crystallinity presented no significant difference after the crosslinking reaction. Upon the addition of both SA and GAL, the infrared peak position shift of O—H stretching was observed, indicating the formation of new hydrogen bonds. Moreover, smaller pore size of HP/CMS/SA/GAL films was observed upon the increased concentration of GAL. In addition, the incorporation of both SA and GAL resulted in the increase of stress at maximum load, Young's modulus, water uptake, water solubility, gel fraction, and swelling degree, as well as notable antibacterial efficacy against *S. aureus* and *E. coli*. The current study revealed that HP/CMS/SA/1GAL films exhibited superior physicochemical properties, antibacterial efficacy, and were also non-toxic to HaCat cells, making them a promising candidate for use as a wound dressing material.

Authors' statement

All authors declare that the manuscript is original and has not been published elsewhere. We also confirmed that the revised manuscript has been approved by all authors.

Declaration of competing interest

The authors declare that they have no known competing financial interests or personal relationships that could have appeared to influence the work reported in this paper.

Acknowledgements

The authors express their sincere appreciation to King Mongkut's Institute of Technology Ladkrabang, Thailand (Grant No. 2566-02-05-009) for financial support.

References

[1] D. Archana, J. Dutta, P.K. Dutta, Evaluation of chitosan nano dressing for wound healing: characterization, in vitro and in vivo studies, Int. J. Biol. Macromol. 57 (2013) 193–203, https://doi.org/10.1016/j.ijbiomac.2013.03.002.
[2] G.D. Mogoşanu, A.M. Grumezescu, Natural and synthetic polymers for wounds and burns dressing, Int. J. Pharm. 463 (2) (2014) 127–136, https://doi.org/10.1016/j.ijpharm.2013.12.015.
[3] M. Naseri-Nosar, Z.M. Ziora, Wound dressings from naturally-occurring polymers: a review on homopolysaccharide-based composites, Carbohydr. Polym. 189 (2018) 379–398, https://doi.org/10.1016/j.carbpol.2018.02.003.
[4] I. Savencu, S. Iurian, A. Porfire, C. Bogdan, I. Tomuță, Review of advances in polymeric wound dressing films, React. Funct. Polym. 168 (2021), 105059, https://doi.org/10.1016/j.reactfunctpolym.2021.105059.

[5] E.-E. Tudoroiu, C.-E. Dinu-Pîrvu, M.G. Albu Kaya, L. Popa, V. Anuța, R.M. Prisada, M.V. Ghica, An overview of cellulose derivatives-based dressings for wound-healing management, Pharmaceuticals 14 (12) (2021) 1215, https://doi.org/10.3390/ph14121215.
[6] H. Seddiqi, E. Oliaei, H. Honarkar, J. Jin, L.C. Geonzon, R.G. Bacabac, J. Klein-Nulend, Cellulose and its derivatives: towards biomedical applications, Cellulose 28 (4) (2021) 1893–1931, https://doi.org/10.1007/s10570-020-03674-w.
[7] E.-S. Khater, A. Bahnasawy, B.A. Gabal, W. Abbas, O. Morsy, Effect of adding nano-materials on the properties of hydroxypropyl methylcellulose (HPMC) edible films, Sci. Rep. 13 (1) (2023) 5063, https://doi.org/10.1038/s41598-023-32218-y.
[8] K. Dharmalingam, R. Anandalakshmi, Fabrication, characterization and drug loading efficiency of citric acid crosslinked NaCMC-HPMC hydrogel films for wound healing drug delivery applications, Int. J. Biol. Macromol. 134 (2019) 815–829, https://doi.org/10.1016/j.ijbiomac.2019.05.027.
[9] S. Taymouri, N. Amiri, M. Rabbani, M. Minaiyan, A. Baradaran, Preparation and characterization of a hydroxypropyl methylcellulose based wafer for simultaneous delivery of phenytoin and insulin as wound dressing material, Pharm. Dev. Technol. 27 (3) (2022) 301–312, https://doi.org/10.1080/10837450.2022.2049606.
[10] C. Schmitt, M.C. Jacques, T.T. Andrighetti, A.S. Antunes, C.F.d. Barros, C.M.D. d. Freitas, É.J. Bunhak, I. Angeli de Lima, Hydroxypropyl methylcellulose-based films incorporated with *Ocimum basilicum L.* extract for skin wound healing, Concilium 22 (7) (2022) 583–597, https://doi.org/10.53660/CLM-722-768.
[11] A. Ounkaew, P. Kasemsiri, K. Jetsrisuparb, H. Uyama, Y.-I. Hsu, T. Boonmars, A. Artchayasawat, J.T.N. Knijnenburg, P. Chindaprasirt, Synthesis of nanocomposite hydrogel based carboxymethyl starch/polyvinyl alcohol/nanosilver for biomedical materials, Carbohydr. Polym. 248 (2020), 116767, https://doi.org/10.1016/j.carbpol.2020.116767.
[12] T. Spychaj, K. Wilpiszewska, M. Zdanowicz, Medium and high substituted carboxymethyl starch: synthesis, characterization and application, Starch - Stärke 65 (1–2) (2013) 22–33, https://doi.org/10.1002/star.201200159.
[13] K. Wilpiszewska, A.K. Antosik, M. Zdanowicz, The effect of citric acid on physicochemical properties of hydrophilic carboxymethyl starch-based films, J. Polym. Environ. 27 (2019) 1379–1387, https://doi.org/10.1007/s10924-019-01436-9.
[14] K. Wilpiszewska, Hydrophilic films based on starch and carboxymethyl starch, Pol. J. Chem. Technol. 21 (2019) 26–30, https://doi.org/10.3390/polym12112447.
[15] V. Pitpisutkul, J. Prachayawarakorn, Hydroxypropyl methylcellulose/carboxymethyl starch/zinc oxide porous nanocomposite films for wound dressing application, Carbohydr. Polym. 298 (2022), 120082, https://doi.org/10.1016/j.carbpol.2022.120082.
[16] N. Thessrimuang, J. Prachayawarakorn, Development, modification and characterization of new biodegradable film from basil seed (*Ocimum basilicum L.*) mucilage, J. Sci. Food Agric. 99 (12) (2019) 5508–5515, https://doi.org/10.1002/jsfa.9812.
[17] G.A. Gebresas, T. Szabó, K. Marossy, A comparative study of carboxylic acids on the cross-linking potential of corn starch films, J. Mol. Struct. 1277 (2023), 134886, https://doi.org/10.1016/j.molstruc.2022.134886.
[18] L. Sharma, H.K. Sharma, C.S. Saini, Edible films developed from carboxylic acid cross-linked sesame protein isolate: barrier, mechanical, thermal, crystalline and morphological properties, J. Food Sci. Technol. 55 (2) (2018) 532–539, https://doi.org/10.1007/s13197-017-2962-4.
[19] R. Saxena, S. Saran, J. Isar, R. Kaushik, Production and Applications of Succinic Acid, Current Developments in Biotechnology and Bioengineering, Elsevier Publishing Inc., Amsterdam, Netherlands, 2017, pp. 601–630, https://doi.org/10.1016/B978-0-444-63662-1.00027-0.
[20] C.T. Tsao, C.H. Chang, Y.D. Li, M.F. Wu, C.P. Lin, J.L. Han, S.H. Chen, K.H. Hsieh, Development of chitosan/dicarboxylic acid hydrogels as wound dressing materials, J. Bioact. Compat. Polym. 26 (5) (2011) 519–536, https://doi.org/10.1177/0883911511422627.
[21] F. Gabriele, A. Donnadio, M. Casciola, R. Germani, N. Spreti, Ionic and covalent crosslinking in chitosan-succinic acid membranes: effect on physicochemical properties, Carbohydr. Polym. 251 (2021), 117106, https://doi.org/10.1016/j.carbpol.2020.117106.
[22] H. Möller, S. Grelier, P. Pardon, V. Coma, Antimicrobial and physicochemical properties of chitosan–HPMC-based films, J. Agric. Food Chem. 52 (21) (2004) 6585–6591, https://doi.org/10.1021/jf0306690.
[23] W. Shao, H. Liu, X. Liu, S. Wang, J. Wu, R. Zhang, H. Min, M. Huang, Development of silver sulfadiazine loaded bacterial cellulose/sodium alginate composite films with enhanced antibacterial property, Carbohydr. Polym. 132 (2015) 351–358, https://doi.org/10.1016/j.carbpol.2015.06.057.
[24] S. Tantiwatcharothai, J. Prachayawarakorn, Property improvement of antibacterial wound dressing from basil seed (*O. basilicum L.*) mucilage - ZnO nanocomposite by borax crosslinking, Carbohydr. Polym. 227 (2020), 115360, https://doi.org/10.1016/j.carbpol.2019.115360.
[25] X. Yang, B. Wang, D. Sha, Y. Liu, Z. Liu, K. Shi, W. Liu, C. Yu, X. Ji, PVA/poly (hexamethylene guanidine)/gallic acid composite hydrogel films and their antibacterial performance, ACS Appl. Polym. Mater. 3 (8) (2021) 3867–3877, https://doi.org/10.1021/acsapm.1c00447.
[26] M. Calderón-Oliver, E. Ponce-Alquicira, Chapter 7 - fruits: a source of polyphenols and health benefits, in: A.M. Grumezescu, A.M. Holban (Eds.), Natural and Artificial Flavoring Agents and Food Dyes, Academic Press, Cambridge, United states, 2018, pp. 189–228, https://doi.org/10.1016/B978-0-12-811518-3.00007-7.
[27] L. Rui, M. Xie, B. Hu, L. Zhou, D. Yin, X. Zeng, A comparative study on chitosan/gelatin composite films with conjugated or incorporated gallic acid, Carbohydr. Polym. 173 (2017) 473–481, https://doi.org/10.1016/j.carbpol.2017.05.072.
[28] F. Luzi, E. Pannucci, L. Santi, J.M. Kenny, L. Torre, R. Bernini, D. Puglia, Gallic acid and quercetin as intelligent and active ingredients in poly (vinyl alcohol) films for food packaging, Polymers 11 (12) (2019) 1999, https://doi.org/10.3390/polym11121999.
[29] D.J. Yang, S.H. Moh, D.H. Son, S. You, A.W. Kinyua, C.M. Ko, M. Song, J. Yeo, Y.-H. Choi, K.W. Kim, Gallic acid promotes wound healing in normal and hyperglucidic conditions, Molecules 21 (7) (2016) 899, https://doi.org/10.3390/molecules21070899.
[30] K. Wilpiszewska, A.K. Antosik, T. Spychaj, Novel hydrophilic carboxymethyl starch/montmorillonite nanocomposite films, Carbohydr. Polym. 128 (2015) 82–89, https://doi.org/10.1016/j.carbpol.2015.04.023.
[31] Ž. Stojanović, K. Jeremić, S. Jovanović, M.D. Lechner, A comparison of some methods for the determination of the degree of substitution of carboxymethyl starch, Starch-Stärke 57 (2) (2005) 79–83, https://doi.org/10.1002/star.200400342.
[32] M. Belay, S. Tyeb, K. Rathore, M. Kumar, V. Verma, Synergistic effect of bacterial cellulose reinforcement and succinic acid crosslinking on the properties of agar, Int. J. Biol. Macromol. 165 (2020) 3115–3122, https://doi.org/10.1016/j.ijbiomac.2020.10.144.
[33] Y. Ma, R. Yang, W. Zhao, Innovative water-insoluble edible film based on biocatalytic crosslink of gelatin rich in glutamine, Foods 9 (4) (2020) 503, https://doi.org/10.3390/foods9040503.
[34] Japanese Standards Association, Antibacterial products–test for antibacterial activity and efficacy, JIS 2801 (2010) 10–1111.
[35] V.S. Ghorpade, R.J. Dias, K.K. Mali, S.I. Mulla, Citric acid crosslinked carboxymethylcellulose-polyvinyl alcohol hydrogel films for extended release of water soluble basic drugs, J. Drug Deliv. Sci. Technol. 52 (2019) 421–430, https://doi.org/10.1016/j.jddst.2019.05.013.
[36] P.-L. Lam, K.K.-H. Lee, S.H.-L. Kok, G.Y.-M. Cheng, X.-M. Tao, D.K.-P. Hau, M.C.-W. Yuen, K.-H. Lam, R. Gambari, C.-H. Chui, R.S.-M. Wong, Development of formaldehyde-free agar/gelatin microcapsules containing berberine HCl and gallic acid and their topical and oral applications, Soft Matter 8 (18) (2012) 5027–5037, https://doi.org/10.1039/C2SM07236J.
[37] C. Yu, X. Chen, W. Zhu, L. Li, M. Peng, Y. Zhong, A. Naeem, Z. Zang, Y. Guan, Synthesis of gallic acid-loaded chitosan-grafted-2-acrylamido-2-methylpropane sulfonic acid hydrogels for oral controlled drug delivery: in vitro biodegradation, antioxidant, and antibacterial effects, Gels 8 (12) (2022) 806, https://doi.org/10.3390/gels8120806.
[38] H. Dai, Y. Huang, H. Huang, Enhanced performances of polyvinyl alcohol films by introducing tannic acid and pineapple peel-derived cellulose nanocrystals, Cellulose 25 (8) (2018) 4623–4637, https://doi.org/10.1007/s10570-018-1873-5.
[39] C.S. Kumar, A.M. Soloman, R. Thangam, R.K. Perumal, A. Gopinath, B. Madhan, Ferulic acid-loaded collagen hydrolysate and polycaprolactone nanofibres for tissue engineering applications, IET Nanobiotechnol. (2020) 202–209, https://doi.org/10.1049/iet-nbt.2019.0281. Institution of Engineering and Technology.
[40] L. Zhang, L.-N. Yue, Y.-L. Sui, Y. Zhao, X. Ding, Q. Li, C. Zhang, C. Wu, C. Gao, J.-Y. Qian, Regulating the mechanical properties and microporous structures of hydroxypropyl methylcellulose based microporous photophobic films by adjusting the l-ethyl-3-methylimidazolium acetate content, Prog. Org. Coat. 155 (2021), 106226, https://doi.org/10.1016/j.porgcoat.2021.106226.
[41] H. Wu, Y. Lei, J. Lu, R. Zhu, D. Xiao, C. Jiao, R. Xia, Z. Zhang, G. Shen, Y. Liu, S. Li, M. Li, Effect of citric acid induced crosslinking on the structure and properties of potato starch/chitosan composite films, Food Hydrocoll. 97 (2019), 105208, https://doi.org/10.1016/j.foodhyd.2019.105208.
[42] J. Promsorn, N. Harnkarnsujarit, Oxygen absorbing food packaging made by extrusion compounding of thermoplastic cassava starch with gallic acid, Food Control 142 (2022), 109273, https://doi.org/10.1016/j.foodcont.2022.109273.
[43] D. Zhang, W. Zhou, B. Wei, X. Wang, R. Tang, J. Nie, J. Wang, Carboxyl-modified poly(vinyl alcohol)-crosslinked chitosan hydrogel films for potential wound dressing, Carbohydr. Polym. 125 (2015) 189–199, https://doi.org/10.1016/j.carbpol.2015.02.034.
[44] A.D. Štiglic, F. Gürer, F. Lackner, D. Bračič, A. Winter, L. Gradišnik, D. Makuc, R. Kargl, I. Duarte, J. Plavec, U. Maver, M. Beaumont, K.S. Kleinschek, T. Mohan, Organic acid cross-linked 3D printed cellulose nanocomposite bioscaffolds with controlled porosity, mechanical strength, and biocompatibility, iScience 25 (5) (2022), 104263, https://doi.org/10.1016/j.isci.2022.104263.
[45] N. Goudar, V.N. Vanjeri, S. Dixit, V. Hiremani, S. Sataraddi, T. Gasti, S.K. Vootla, S. P. Masti, R.B. Chougale, Evaluation of multifunctional properties of gallic acid crosslinked poly (vinyl alcohol)/Tragacanth gum blend films for food packaging applications, Int. J. Biol. Macromol. 158 (2020) 139–149, https://doi.org/10.1016/j.ijbiomac.2020.04.223.
[46] M.R. Khan, S. Volpe, E. Salucci, M.B. Sadiq, E. Torrieri, Active caseinate/guar gum films incorporated with gallic acid: physicochemical properties and release kinetics, J. Food Eng. 335 (2022), 111190, https://doi.org/10.1016/j.jfoodeng.2022.111190.
[47] M. Zhang, B. Yang, Z. Yuan, Q. Sheng, C. Jin, J. Qi, M. Yu, Y. Liu, G. Xiong, Preparation and performance testing of corn starch/pullulan/gallic acid multicomponent composite films for active food packaging, Food Chem. X 19 (2023), 100782, https://doi.org/10.1016/j.fochx.2023.100782.
[48] S. Huang, X. Chen, R. Yan, M. Huang, D. Chen, Isolation, identification and antibacterial mechanism of the main antibacterial component from pickled and dried mustard (Brassica juncea Coss. var. foliosa Bailey), Molecules 27 (8) (2022), https://doi.org/10.3390/molecules27082418.

[49] L.H. Yang, S.C.K. Lau, O.O. Lee, M.M.Y. Tsoi, P.Y. Qian, Potential roles of succinic acid against colonization by a tubeworm, J. Exp. Mar. Biol. Ecol. 349 (1) (2007) 1–11, https://doi.org/10.1016/j.jembe.2007.03.016.
[50] R. Kumar, B. Chandar, M. Parani, Use of succinic & oxalic acid in reducing the dosage of colistin against New Delhi metallo-β-lactamase-1 bacteria, Indian J. Med. Res. 147 (1) (2018) 97–101, https://doi.org/10.4103/ijmr.IJMR_1407_16.
[51] T.J. Gutiérrez, P.G. Seligra, C.M. Jaramillo, C.M. Jaramillo, L. Famá, S. Goyanes, Effect of filler properties on the antioxidant response of thermoplastic starch composites, Handbook of Composites From Renewable Materials, pp. 337–369. doi:https://doi.org/10.1002/9781119441632.ch14.
[52] K.M. Zepon, M.M. Martins, M.S. Marques, J.M. Heckler, F. Dal Pont Morisso, M. G. Moreira, A.L. Ziulkoski, L.A. Kanis, Smart wound dressing based on κ–carrageenan/locust bean gum/cranberry extract for monitoring bacterial infections, Carbohydr. Polym. 206 (2019) 362–370, https://doi.org/10.1016/j.carbpol.2018.11.014.